A SOUTH POLAR VIEW OF LATE PALEOZOIC GLACIATION: PHYSICAL SEDIMENTOLOGY AND PROVENANCE OF GLACIAL SUCCESSIONS IN THE TASMANIAN AND TRANSANTARCTIC BASINS

by

Libby R.W. Ives

A Dissertation Submitted in

Partial Fulfillment of the

Requirements for the Degree of

Doctor of Philosophy

in Geosciences

at

The University of Wisconsin – Milwaukee

December 2021

ABSTRACT

A SOUTH POLAR VIEW OF LATE PALEOZOIC GLACIATION: PHYSICAL SEDIMENTOLOGY AND PROVENANCE OF GLACIAL SUCCESSIONS IN THE TASMANIAN AND TRANSANTARCTIC BASINS

by

Libby R.W. Ives

The University of Wisconsin – Milwaukee, 2021

Under the Supervision of Distinguished Professor Dr. John L. Isbell

The Late Paleozoic Ice Age (LPIA; ~ 374 – 256 Ma) is the longest Phanerozoic icehouse interval. this interval in Earth's history was largely defined by extensive glaciation of the southern hemisphere at both polar and temperate latitudes. Glaciers are powerful climatic and geologic actors, especially during icehouse periods, and widespread glaciation can have a significant influence on both regional and global climate and geology. Therefore, constraining the characteristics of LPIA glaciers is essential to developing a global-scale understanding of this key climatic event in Earth's history. The manuscripts in this dissertation examine the sedimentology, transport directions, stratigraphy, and detrital zircon provenance of the Pennsylvanian – Permian glacigenic succession from the LPIA at locations in the Transantarctic (Antarctica) and Tasmanian (Australia) basins.

The Transantarctic and Tasmanian basins share many characteristics that make them interesting and important places to study LPIA glacigenic rocks. In both basins, sediments were deposited during a ~ 14 Myr icehouse interval spanning the Pennsylvanian-Permian boundary during which time glaciation is thought to have been the most extensive of the LPIA. During this interval, both basins were located at high (> 60°) southern latitudes along the Panthalassan margin of southeastern Gondwana. The similarities in paleogeographic, geologic, and temporal contexts between the Transantarctic and Tasmanian basins mean that characterizing and comparing LPIA glaciations in

both areas is critical to understanding the late Paleozoic glacial maximum at polar latitudes. The works presented in this dissertation demonstrate that building an accurate, nuanced understanding of global glaciations during the LPIA, requires beginning at the local scale and building outward.

Chapter 2 examines the Pagoda Formation of the Transantarctic Basin at four locations in the Shackleton Glacier Region of Antarctica. The dominant lithology in the Pagoda Fm at those locations is a massive, sandy, clast-poor diamictite. Depositional processes governing these diamictites were proglacial, subaqueous glacial processes, likely a combination of mass transport, iceberg rain-out, iceberg scouring, plume sedimentation, and subglacial till deposition. Some of the deposits are part of grounding-line fan systems. All glacigenic sediments in the Pagoda Fm at these locations were likely deposited during the retreat phase of a single, up to 90 m thick glacial sequence. Flow directions from these successions support the hypothesis that an ice center was present toward the Panthalassan margin of East Antarctica (Marie Byrd Land) during the LPIA.

Chapter 3 describes the basal 415 m of the type section of the Wynyard Formation of the Tasmanian Basin, which outcrops along the coast of northwestern Tasmania. Facies associations in this succession include muddy massive diamictite, sandy massive diamictite, and rhythmically laminated fine-grained facies. Respectively, these sediments were deposited as a grounding-zone wedge, proglacial, proximal grounding line fan or morainal bank, and proglacial, glacier-distal cyclopelites. In this succession, the basal Wynyard Fm was deposited in glacier-proximal to glacier-distal, marine environments on a continental shelf at water depths below storm wave base. All facies associations contain mass transport and turbidite deposits that could have been driven by slope instability due to rapid deposition. The "Wynyard Glacier" was most likely an outlet glacier or ice stream draining a large ice cap or ice sheet.

Chapter 4 is a detrital zircon geochronology provenance study of sandstones from the Wynyard Formation. These data represent the first such measurements from the Wynyard Formation anywhere in the basin. With these data, and using a "local first" approach, we demonstrated that all measured detrital zircon dates from the Wynyard Fm can be attributed to zircon sources that occur within 33 km of the sample location along the glacier's flow path. Therefore, while the detrital zircon provenance signature of the Wynyard Fm also supports the hypothesis that the Wynyard Glacier flowed from south to north, this information does not impart insight into where the ice center was nucleated.

This dissertation is dedicated to all of those who gave me opportunities, took chances on me, and allowed me to try, stumble, and try again. I only hope I can pay that grace forward.

TABLE OF CONTENTS

LIST OF FIGURES

LIST OF TABLES

ACKNOWLEDGEMENTS

All science is a thoroughly human endeavor that blossoms from collective efforts built by communities through the exchange of ideas, knowledge, and curiosity. While this dissertation has one name on the cover page, the work it stems from would not have been possible without the efforts and support of many people and organizations.

I must first and foremost acknowledge the supervisor, instigator, and coauthor of this work, John Isbell. I am grateful for the opportunities you have given me and your support throughout this process. Thank you for taking on this physical geographer and teaching me how to be a sedimentologist and geologist – a process that started in your Stratigraphy and Sedimentology class back in 2014.

I am also tremendously thankful to others who have acted as mentors to me throughout this process. These people include my dissertation committee, who shepherded me through the preliminary, proposal, and writing stages of this dissertation; Elmo Rawling, who created the opportunity for, and led me through the process of creating my first surficial geologic map on the landscape that originally inspired my curiosity about glaciers; and Kathy Licht, for lending her expertise to this dissertation, especially Chapter 4, and for inviting me to be a part of the remarkably supportive community of student scholars she has created at IUPUI.

I am also grateful to the Department of Geoscience faculty, lecturers, and staff for providing wonderful courses and other educational opportunities, and for all your work keeping the wheels of bureaucracy grinding along.

The research in this dissertation and professional development opportunities I participated in during this Ph.D. were made possible by numerous generous funders through grants and scholarships. Major funders include the National Science Foundation, the Department of Geosciences through

their Chancellor's and Lukowicz Memorial scholarships, the University of Wisconsin – Milwaukee Graduate School for the Distinguished Fellowships and Conference Travel Awards Program, UWM Center for Latin American and Caribbean Studies Tinker Research Grant, International Association of Sedimentologists, Geological Society of America Graduate Students Grants, Geological Society of America Energy Division, the Wisconsin Geological Society, POLENET, AGU, and SEPM.

I am especially grateful to Bernice McCloskey of Milwaukee who, as a member of the Kettle Moraine Geological Society and American Federation of Mineralogical Societies, selected me for a very generous scholarship that allowed me to spend a semester at UNIS in Longyearbyen, Svalbard. That special gratitude also extends to the wonderful women of the P.E.O. chapter in Mankato, Minnesota (including my grandma and aunt; Sue Scott & Amy Kolb) who successfully nominated me for the P.E.O Scholar's Award, which funded the third year of my Ph.D. P.E.O. is a philanthropic organization where women celebrate the advancement of women, educate women through scholarships, grants, awards, loans, and stewardship of Cottey College, and motivate women to achieve their highest aspirations.

It is an open secret that graduate students often have to take on jobs outside of the University, myself included. I am indebted to the employers who took me on despite my sporadic availability and school priorities, including Bière de Mac Brew (Mackinaw City, MI), the Hiawatha National Forest (St. Ignace, MI), the United States Postal Service (Petoskey, MI), the Wisconsin Geological and Natural History Survey, and the United States Geological Survey.

Money may make the world go round, but friends are the flowers in the garden of life. I am thankful for all the geo-friends I made at UWM and in the short courses I've participated in. A special shout out is owed to my comrades in sedimentology, including Nick Fedorchuck, Scott Litwin, Eduardo Rosa, Natalie McNall, Miles Harbury, Allison Kusick, and especially Kate Pauls, my pre-pandemic

officemate who has been both a fount of advice and shoulder to lean on during the writing phase of this dissertation. While UWM has been my academic home, my roots for the last five years have been in the "northern lower peninsula" of Michigan, and the friends we have made here. Though the whole community up here is amazing, I am grateful especially for Jon, Laura, Pat, and Kelly who have been the greatest friends in farming, pandemic letter-writing, seasonal depression, and late-night laughs. As far as support networks go, for the last six months one of the things I've looked forward to most every week is meetings with students at IUPUI – and their willingness to share not only their science, but their experiences. So, thank you also to Eiríka, Chris, Sarah, Hannah, Connor, Gianina, and Hamna for welcoming me.

Of course, this whole process would have been impossible without my family. Thank you to my parents, Mark and Katie, who gave me every opportunity to make my own way and find my own happiness. To my siblings and their significant others, Molly, Tim, Milada, Brad, and Phonsuda for their support and for being constant sources of both inspiration and joy. I especially want to thank Molly for being my daily G-chat buddy, belay partner, and occasional roommate. Life in Bliss, Michigan wouldn't be the same with the constant support of my in-laws, Dave and Gail, and my aunt- and uncle-in-laws, Jane and Mac.

Though he will never read these acknowledgements thanks also go out to my canine well-being supervisor, Esau, who can be relied upon to remind me that the day is incomplete without breakfast, dinner, treats, play time, belly rubs, and walks in the woods.

Finally, I am full of a lifetime's gratitude for my husband, Patrick. You have been nothing but a source of support, comfort, and thoughtfulness throughout this whole Ph.D. process. I'm so proud of everything you have accomplished with Bliss Valley Farm, and how you've grown as a farmer and entrepreneur.

It would feel odd to finish this thesis without acknowledging how tumultuous the last two years have been. Like many of us, I have spent the COVID-19 pandemic working alone in my home office, interfacing with colleagues through a computer. It's been a surreal experience, and hopefully whatever future we build after this will be kinder. My gratitude extends toward those working to make the world fairer and more just:

Black Lives Matter.

Biden Won.

Climate Change is Real.

COVID is Real. Get Vaccinated.

[this page is intentionally left blank]

CHAPTER 1: INTRODUCTION

1.1. Motivation and Context

The Late Paleozoic Ice Age (LPIA; ~ 374 – 256 Ma) is the longest Phanerozoic icehouse interval. It is the only icehouse that included complex, land-based life prior to the Cenozoic. The LPIA was therefore likely the icehouse most similar to in terms of global bio-geo-chemical systems. Extensive glaciation of the southern hemisphere at both polar and temperate latitudes were hallmarks of this interval, as were low pCO^2, high pO^2, generally low eustatic levels with large magnitude fluctuations, low solar luminosity, and increased $\delta^{18}O$ and $\delta^{13}C$ values relative to the rest of the Phanerozoic (Gastaldo et al., 1996; Raymond and Metz, 2004; Montañez and Soreghan, 2006; Fielding et al., 2008b; Montañez and Poulsen, 2013; Frank et al., 2015). The existence and characteristics of glaciers of any age are controlled by global, regional, and local climatic and geologic conditions (Isbell et al., 2012, 2021; Pauls et al., 2021). Therefore, constraining the characteristics of LPIA glaciers is essential to developing a global-scale understanding of this key climatic event in Earth's history, its impacts on the evolution of life, and the extent it can be used to predict future climate change. The characteristics of glaciers that can potentially be constrained by their geologic records are largely physical characteristics (e.g., size and thermal regime), distribution, and age/timing. The geochemical (e.g., Chemical Index of Alteration; Nesbitt and Young, 1982) and biologic records of glacigenic sediments can also be used to understand local climate and environmental conditions at the time of deposition.

Glaciers are powerful climatic and geologic actors, especially during icehouse periods. They are both controlled by and exert influence over the distribution of regional and global temperatures, precipitation, and oceanic and atmospheric circulation patterns (Saltzmam, 2003). These effects can go far beyond the ability of glaciers to reshape landscapes (both terrestrial and sub-aqueous) through

extensive erosion and deposition. During icehouse periods changes in glacier volume compel significant and relatively rapid changes in eustatic sea level (Isbell et al., 2003, 2021; Heckel, 2008; Rygel et al., 2008; Eros et al., 2012). Additionally, the mass of glaciers isostatically depresses the Earth's crust, which can have dramatic near-field effects on sedimentation as well as drive far-field changes in isostacy/apparent eustacy (Mitrovica et al., 2009; Whitehouse, 2018). Because wide-spread glaciation can have a significant influence on both regional and global climate and geology, constraining glacier behavior during the LPIA is critical to understanding the geologic and climatic records from that period.

Despite glaciers' ties to the global climate system, reconstructing and relating the physical characteristics of glaciers (physical characteristics and distribution) to global climate trends (timing) through their sedimentary records is not a straightforward task. This is largely due to the unique nature of glacial depositional systems.

1. The combination of depositional processes of glacigenic systems are unique, but the resulting lithologies are not (Isbell et al., 2021). This means that any certainty about the glacigenic origin of a facies or succession is difficult to ascertain.

2. How glacial sediments accumulate and are eroded through time (the stratigraphy) is unlike any other sedimentary system in that the glacier's shifting grounding line and physical characteristics (basal temperature), and not a shoreline, acts as the fulcrum between areas of erosion and sedimentation (Powell and Cooper, 2002).

3. The sedimentary records of glaciers are also strongly biased towards glaciers with certain physical properties and depositional regimes (Eyles et al., 1985; Kurjanski et al., 2020). Specifically, glaciers with temperate (warm-based) thermal regimes are much more likely to be preserved in the sedimentary record because they are more effective at subglacially

eroding the records of prior glaciations and because they are more effective at depositing large volumes of pro-glacial sediment than glaciers with "cooler" thermal regimes.

4. The ages of glacial strata are often difficult to constrain. Many glacigenic depositional environments, especially glacier-proximal environments, are fossil poor. In both sedimentary basins studied in this dissertation, there was no known volcanic activity providing detritus to the basins concurrent to glaciation so radiometric ages are currently not an option for determining age.

The works in this dissertation examine the sedimentology, transport directions, stratigraphy, and detrital zircon provenance of glacigenic successions from the LPIA at locations in the Transantarctic and Tasmanian basins. While the diamictites and other glacigenic strata are often enigmatic, useful characterizations of these units can be made through lithofacies descriptions, thoughtful provenance analyses, and robust, processes-informed interpretations of this data.

1.2. Geologic Setting

The glacigenic strata in both basins were likely deposited sometime during at 14 Myr interval spanning the late Carboniferous – early Permian, which is when glaciation during the LPIA is thought to have been most extensive (Isbell et al., 2003, 2012; Fielding et al., 2008; Montañez and Poulsen, 2013). Not only were these southeastern Gondwanan basins glaciated at similar times, both basins were located at high (> 60°) southern latitudes. Records of glaciations in polar and sub-polar regions are especially important for constraining climatic trends during the LPIA. High-latitude regions will have the longest-lived glacial episodes during icehouse events but remain sensitive to climatic changes. For example, as Earth transitions from Cenozoic icehouse conditions to a period of increased average global temperatures and pCO^2, temperatures at high latitudes have increased

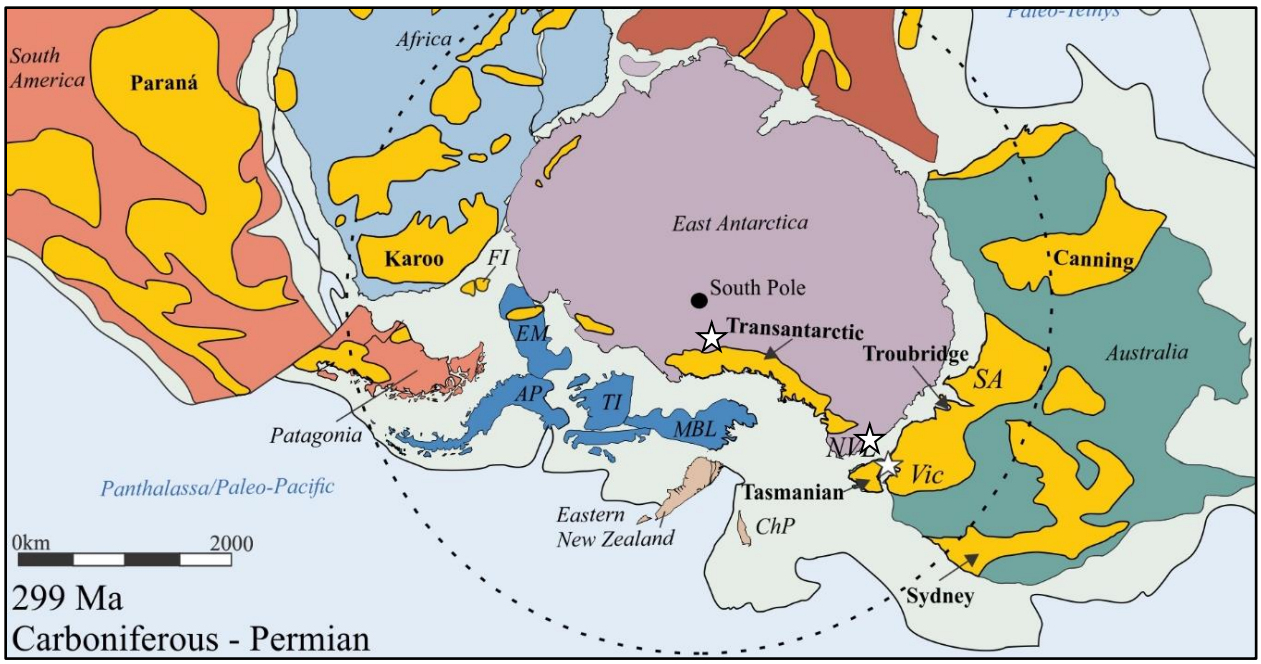

Figure 1-1. Paleogeographic reconstructions of Gondwana near the Pennsylvanian-Permian Boundary. Stars indicates the approximate location of the study areas in the Tasmanian and Transantarctic basin study locations. Continent distributions are based on Lawver et al. (2011) and are copied from (Isbell et al. 2012). The south pole position is from Meredith et al. (2021). Yellow regions indicate the modern extent of sedimentary basins containing late Paleozoic Ice Age strata. Abbreviations include: Falkland Islands/Malvinas (FI), Ellsworth Mountain block (EM), Antarctic Peninsula (AP), Thurston Island (TI), Marie Byrd Land (MBL), and the Challenger Plateau/western New Zealand (ChP). Dashed line indicates 60˚S. Basins adapted from Isbell et al. (2012).

more rapidly than at mid or low latitudes, driving global changes to atmospheric and ocean circulation (Steig et al., 2009; Francis and Vavrus, 2015; Turner et al., 2016; Choi and Kim, 2018). Unlike at mid-latitudes, glaciers at high latitudes do not reflect climate primarily by their presence or absence, but rather (to a greater degree) by their thermal regime and extent (Pollard and DeConto, 2009; Landvik et al, 2014).

The Transantarctic and Tasmanian basins share many characteristics that make them interesting and important places to study LPIA glacigenic rocks. As previously mentioned, glacial strata in these basins are from the Permo-Carboniferous and were located at polar latitudes during that time (

Figure 1-1). Additionally, both basins were located along the Panthalassan margin of southeastern Gondwana. This margin has a long history of subduction and orogenies, beginning in at least the early Cambrian and continuing to the Mesozoic break up of Gondwana (Veevers and Powell, 1994; Elliot, 2013). The similarities in paleogeographic, geologic, and temporal contexts between the Transantarctic and Tasmanian basins mean that characterizing and comparing LPIA glaciations in both areas may offer insight into the late Paleozoic glacial maximum at polar latitudes.

Since the Transantarctic Basin and Tasmanian Basin are both situated along the Panthalassan margin of Gondwana, they have experienced similar tectonic histories. These parallel geologic events have resulted in similar basin structure and stratigraphy. The shared geologic history of these basins likely began in the Neoproterozoic, but clear geologic connections between eastern Australia and the Transantarctic Mountains start in the early Paleozoic when they were subjected to the early Cambrian Ross-Delamerian Orogeny. This orogeny was the product of continental arc tectonism and resulted in the emplacement of extensive intrusions, significant syn-orogenic sediment accumulation, and related deformation and metamorphism (Bodger and Miller, 2004; Foden et al., 2006). Post-orogenic sedimentation persisted in both basins at least into the Devonian, and possibly the early Carboniferous. During the Devonian, sedimentation in both areas consisted of dominantly non-marine and shallow marine siliciclastic successions; the Wurawina Supergroup in Tasmania (Banks and Williams, 1986) and the Taylor Group in the Transantarctic Mountains (Barrett et al., 1986; Barrett, 1991). The deposition of these units ceased around the time the Panthalassan margin of Gondwana was subjected to another orogenic event: the late Devonian – early Carboniferous

Lachlan Orogen in Australia (Gray and Foster, 2004) and its corollary orogenies in Antarctica, as evidenced by granitoid magmatism and metamorphism of the same age in Marie Byrd Land (Elliot, 2013; Jordan et al., 2020;

Figure 1-1). This orogeny was similar to the Ross-Delamerian Orogeny in that the event resulted in the emplacement of extensive intrusions, significant syn-orogenic sediment accumulation, and related deformation and metamorphism. However, in this case the area that was to become the Transantarctic Basin in the Central Transantarctic Mountains (Chapter 2; Ives and Isbell, 2021) was located significantly inboard of an orogenic front, and does not contain any syn-orogenic strata, related intrusions, or deformation (Elliot, 2013). This period is represented in Transantarctic Basin stratigraphy as an erosional disconformity of Permian sediments with the Devonian Taylor Group or an unconformity with pre-Devonian rocks (Collinson et al., 1994; Isbell, 1999). The Lachlan Orogeny volcanic arc passed through Tasmania, and is represented there by widespread granitic intrusions (Black et al., 2010). The youngest of these granites have ages of 350 Ma (Hong et al., 2017). These intrusions were exposed at the surface prior to the initiation of Permo-Carboniferous glacial sedimentation in the Tasmanian Basin around 300 Ma. The dramatic uplift that resulted in the exposure of these rocks may have been a regional phenomenon (Rolland et al., 2019).

The similarities between the two basins continued once sedimentation began. Permo-Carboniferous glacigenic sediments make up the basal strata of both the Transantarctic (Pagoda Formation and equivalent units) and Tasmanian (Wynyard Formation and equivalent units) basins. In both basins these strata were deposited on top of erosional surfaces with significant topographic relief on the order of hundreds of meters (Hand, 1993; Isbell, 1999). The underlying crystalline basement and Devonian strata sometimes show evidence for glacial erosion and/or deformation (Hand, 1993; Isbell et al., 2008a; Chapter 2). The ages of glacigenic strata in both basins are constrained primarily

through palynomorph biostratigraphy. Interestingly, the palynomorph zones that constrain the ages of both units are the same (*cf.* Kyle, 1997; Truswell, 1978), but the interpretations of their absolute ages are slightly different due to geologic context and a limited invertebrate record (Figure 1-2). The Pagoda Fm is interpreted to be from the early Permian (Asselian – Sakmarian; Masood et al., 1994; Askin, 1998), and the Wynyard Fm is interpreted as late Carboniferous to early Permian (Gzhelian – Asselian; Chapter 2). The Pagoda and Wynyard formations are both noteworthy for their thick successions of dominantly massive diamictites. These diamictites led to relatively early interpretations of these strata as glacigenic (*cf.* David, 1907; Grindley, 1963; Pinet et al., 1967).

Even though the diamictites of these two basins have long been considered glacigenic (and those interpretations have withstood evolving paradigms of diamictite interpretation), extracting information on the type, timing, and extent of late Paleozoic glaciers in these basins has been challenging (e.g., Isbell et al., 2008a; Fielding et al., 2010). This is largely because unlike larger and

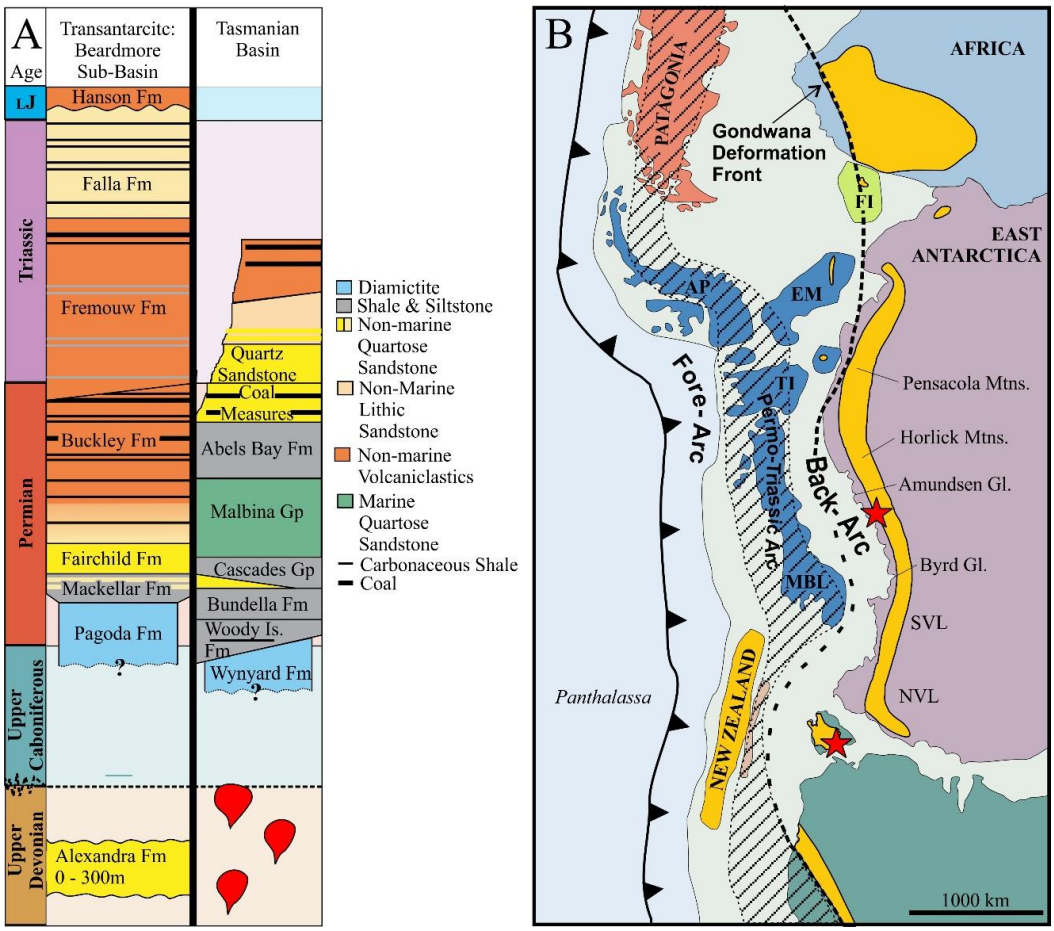

Figure 1-2. Regional geologic context and tectonic setting of the Transantarctic and Tasmanian basin during the early Permian A. Stratigraphy of the Beacon Supergroup of the Transantarctic Basin. Adapted from Elliot (2013); Cornamusini (2017); Elliot et al. (2017), and Parmeener Supergroup in the Tasmanian Basin. Adapted from Fielding et al., 2010 and Reid et al., 2014. Uppermost units are not named, and are absent in western Tasmanian Basin/Dundas Trough (Reid et al., 2014). **B.** Tectonic setting of southern Gondwana during the Permian, adapted from Elliot (2013). Regions of sedimentary deposition are shaded yellow. Note that there are differences in the positioning of some crustal blocks (e.g., Patagonia and New Zealand) between this reconstruction and

Figure **1-1**.

higher accommodation basins such as the Karoo (Isbell et al., 2008b) or Paraná (Vesely and Assine, 2006), the Transantarctic and Tasmanian basins do not contain any "interglacial" or "deglaciation" sediments preserved within glacigenic successions that can be used as correlative sequence boundaries. Such deglaciation units often span large swaths of a basin, are typically composed of stratified, fine-grained sediment, and are much more likely to contain fossils than glacigenic units.

Without interglacial deposits, the only temporal control available for the Pagoda Fm and Wynyard Fm is the age of the overlying strata and the rare fossil record, sometimes recycled, that is present in the glacial units. Such limited chronological constraints make temporally relating the deposits from the same lithostratigraphic unit within these basins almost impossible. For example, it is difficult to discern whether the striations that underlie the Pagoda Fm in one location from the same glacial advance as the striae that underlie the Pagoda Fm 50 km away? In Chapter 3, we identify several stratigraphic sequences within the Wynyard Fm. Despite their local importance, these sequences are likely a local phenomenon and cannot be correlated to similar patterns anywhere else in the Tasmanian Basin. Ultimately the Transantarctic and Tasmanian basins contain glacigenic strata from a keystone time and place of the LPIA, but those records remain relatively inscrutable due to their geologic setting.

1.3. Research Question and Objectives

Research Question: To what extent can the physical characteristics, size, distribution, and timing of LPIA glaciers in high-latitude Gondwanan basins be constrained, and how does this knowledge inform our understanding of regional and global climate change during that time?

The manuscripts in this dissertation attempt to demonstrate that while the diamictites and other glacigenic strata of the Pagoda Fm and Wynyard Fm are enigmatic, useful characterizations of these units can be made through lithofacies descriptions, thoughtful provenance analyses, and robust, processes-informed interpretations of this data. These works demonstrate that the best way to address these challenges and build an accurate, nuanced understanding of global glaciations during the LPIA is to begin at the local scale and build outward. In the lithofacies-based manuscripts (Chapter 2 and Chapter 3), the aim is to build on our current understanding of the physical characteristics of LPIA glaciations in the Transantarctic and Tasmanian basin. These works argue

that LPIA glacigenic deposits like the Pagoda and Wynyard formations must be understood in detail on a local level before they can be tied to basinal, regional, or global patterns of climate change. These works also demonstrate what kind of details about the physical characteristics and extent of LPIA glaciers can be derived from sedimentological data (Objective 1). In the manuscript that addresses detrital zircon provenance of the Wynyard Fm (Chapter 4), the overall aim is to improve understanding of the scale of past ice sheets. Understanding of the LPIA has shifted from one of a single, persistent, super-continent-sized ice sheet (e.g., Frakes, 1979), to one of multiple ice centers (ice sheets or ice caps) that were distributed across Gondwana, and that grew and shrank asynchronously (Fielding et al. 2008; Isbell et al. 2012; Montañez and Poulsen 2013). Thus, locally-focused studies have increased in importance. The work in Chapter 4 shows that provenance studies of glacial sediments should also be approached by first comparing provenance indicators to local sediment sources, and specifically tests whether the detrital zircon provenance of the Wynyard Fm reflects local (< 100 km) detrital zircon along the Wynyard Glacier's proposed flow path.

Objective 1: Characterize the types of glaciations in South Polar regions during the LPIA

Hypothesis 1.1: In the Shackleton Glacier Region of the Transantarctic Basin, LPIA glacigenic strata were deposited in a "basin-marginal", marine setting by a warm-based glacier (Isbell et al., 2008a). This hypothesis is based on the lithofacies model for glacigenic deposition in the Transantarctic Basin proposed by Isbell et al. (2008). This hypothesis proposes that basin-margin successions are thin (< 100 m) and contain lithofacies that are likely to have evidence for subglacial deposition and deformation.

Hypothesis 1.2: Glacigenic sediments in the Tasmanian Basin were deposited by multiple advances of temperate glaciers (Hand, 1993; Henry et al., 2012). Specifically, the Wynyard Fm was deposited

by north-flowing glaciers, sourced from the south and east, that occupied a 40 km-wide, NNE-SSW trending bedrock valley (Hand, 1993).

Objective 2: Infer the extent of glaciers contributing to sedimentation in polar basins through provenance studies

Hypothesis 2.1: Glaciers contributing to deposits in the Tasmanian Basin could have come from ice centers nucleated in North Victoria Land (Antarctica), eastern Australia, or locally. Measured flow directions in Tasmania, Antarctica, and mainland Australia indicate glacier motion both into the Tasmanian basin from either the north (Australia; Fielding et al., 2010) or the south, (Antarctica; e.g., Cornamusini, 2017), and out of the Tasmanian Basin, to the north and east (e.g., Hand, 1993).

1.4. Dissertation Structure

This dissertation consists of three manuscripts written for publication in peer-reviewed journals. The manuscripts are followed by a conclusions chapter summarizing the findings of this dissertation and how the proposed objectives of this dissertation were addressed by these works. The citation style of each chapter is consistent with the scientific journal that the journal was or will be submitted to.

Chapter 2: A lithofacies analysis of a south polar glaciation in the early Permian: Pagoda Formation, Shackleton Glacier Region, Antarctica

This chapter is a lithofacies analysis of the Pagoda Fm in the Shackleton Glacier Region of the Central Transantarctic Mountains and evaluates the sedimentology, stratigraphy, and flow directions of the glacigenic strata from four localities in that area. This work establishes that glacigenic sediments of the Pagoda Fm were deposited during a single glacier retreat phase. Evidence from this study does not preclude prior or later glacier advance-retreat cycles preserved elsewhere in the basin. Additionally, ice flow directions from this study indicate that the glacier responsible for this

sedimentation was likely flowing off of an upland on the side of the Transantarctic Basin closer to the Panthalassan/Gondwanide margin, which supports the hypothesis that two different ice centers contributed glacigenic sediments to the Transantarctic Basin. This chapter has been published in the *Journal of Sedimentary Research* (Ives and Isbell, 2021).

Chapter 3: Contrasting styles of glacial sedimentation and glacier thermal regimes in the lower Wynyard Formation (Permo-Carboniferous, Tasmanian Basin)

This chapter is a lithofacies analysis of the basal 415 m Wynyard Fm at its type section in northwestern Tasmania. This work evaluates the sedimentology, stratigraphy, and flow directions of the glacigenic strata from that site. Paleotransport directions in this succession support the hypothesis that the 'Wynyard Glacier' flowed from south to north through the structural element and paleotopographic low in western Tasmania. Deposition of the Wynyard Fm at its type section was initiated when the margin of the Wynyard Glacier had a dominantly cold subpolar thermal regime (muddy diamictite facies association), but that thermal regime shifted to temperate (sandy diamictite facies association) for most of the depositional succession. This succession was all likely deposited during the same overall glacier retreat event, and the glacier's grounding line was likely never more than a few kilometers in either direction of the measured sedimentary sections while deposition was occurring. This chapter is formatted for submission to the International Association of Sedimentologists' open access journal, *The Depositional Record.*

Chapter 4: Glacigenic sediment provenance should be determined through a "local first" approach

This chapter uses newly-measured detrital zircon U-Pb ages from the Wynyard Fm and a Monte-Carlo unmixing models of pre-Permian lithologies from western Tasmania to test whether all of the detrital zircons in the Wynyard Fm could have been derived from proximal sources along the inferred Wynyard Glacier. To this aim, we employ a "local first" approach. In this approach,

provenance indicators are first compared to local source lithologies, and if the indicator cannot be attributed to a proximal source, only then are progressively distal sources investigated. We propose that a "local first" approach should be applied to the interpretation of provenance indicators in glacigenic sediments, especially where the glacier flow path is poorly constrained and the records of potential source lithologies are incomplete (like the LPIA). This approach is more consistent with current understandings of glacial processes, and is essentially the opposite of the approach taken by many studies of LPIA zircon provenance (e.g., Griffis et al., 2019; Craddock et al., 2019). Such studies assume that similar detrital zircon provenance signals between geographically dispersed glacigenic sediments of equivalent depositional age are evidence that they were deposited by the same large mass (i.e., large glaciers such as ice sheets, and ice caps), but do not account for variations in the geology underlying a proposed ice center or the physical realities of how glaciers move, entrain, and distribute sediment. All measured Wynyard Fm dates can be attributed to zircon sources within 33 km of the sample location along the glacier's flow path. This chapter is formatted for submission to *Nature Geoscience*.

References

Banks, M.R. and Williams, E. (1986). Wurawina Supergroup, Late Cambrian to Early Devonian, Tasmania. Papers and Proceedings of the Royal Society of Tasmania, 120, 95-96. https://doi.org/10.26749/rstpp.120.95

Barrett, P. J. (1991). The Devonian to Jurassic Beacon Supergroup of the Transantarctic Mountains and correlatives in other parts of Antarctica. in Tingey, R.J. (ed), The Geology of Antarctica, Oxford Monographs on Geology and Geophysics. Oxford University Press, Oxford, 17, 120-152.

Barrett, P. J., Elliot, D. H., & Lindsay, J. F. (1986). The Beacon Supergroup (Devonian-Triassic) and Ferrar Group (Jurassic) in the Beardmore Glacier Area, Antarctica. Geology of the central Transantarctic Mountains, 36, 339-428.

Black, L.P., Everard, J.L., McClenaghan, M.P., Korsch, R.J., Calver, C.R., Fioretti, A.M., Brown, A.V. and Foudoulis, C. (2010). Controls on Devonian–Carboniferous magmatism in Tasmania, based on inherited zircon age patterns, Sr, Nd and Pb isotopes, and major and trace element geochemistry. Australian Journal of Earth Sciences, 57(7), 933-968.

Boger, S. D., & Miller, J. M. (2004). Terminal suturing of Gondwana and the onset of the Ross–Delamerian Orogeny: the cause and effect of an Early Cambrian reconfiguration of plate motions. Earth and Planetary Science Letters, 219(1-2), 35-48.

Choi, W., and Kim, K. Y. (2018). Physical mechanism of spring and early summer drought over North America associated with the boreal warming. Scientific reports, 8(1), 7533.

Clarke, M.J. (1977) 'Paleontology' in Gee, R.D. (ed.) Geological atlas 1 mile series. Zone 7, Sheet 28 (8015N). Burnie, Explanatory Report of the Geological Survey, Tasmania Department of Mines, 53-54.

Collinson, J. W., Isbell, J. L., Elliot, D. H., Miller, M. F., Miller, J. M., & Veevers, J. J. (1994). Permian-Triassic Transantarctic basin. Geological Society of America Memoirs, 184, 173-222.

Craddock, J.P., Ojakangas, R.W., Malone, D.H., Konstantinou, A., Mory, A., Bauer, W., Thomas, R.J., Affinati, S.C., Pauls, K., Zimmerman, U. and Botha, G. (2019). Detrital zircon provenance of Permo-Carboniferous glacial diamictites across Gondwana. Earth-Science Reviews, 192, 285-316.

David, T.W.E. (1907) The Permo-Carboniferous glacial beds at Wynyard, near Table Cape, Tasmania. Australian Association for the Advancement of Science, XI, 274 – 279. Available at: https://www.biodiversitylibrary.org/item/50730

Elliot, D. H. (2013). The geological and tectonic evolution of the Transantarctic Mountains: a review. Geological Society, London, Special Publications, 381(1), 7-35.

Eros, J. M., Montañez, I. P., Osleger, D. A., Davydov, V. I., Nemyrovska, T. I., Poletaev, V. I., & Zhykalyak, M. V. (2012b). Sequence stratigraphy and onlap history of the Donets Basin, Ukraine: insight into Carboniferous icehouse dynamics. Palaeogeography, Palaeoclimatology, Palaeoecology, 313, 1-25.

Eyles, C. H., Eyles, N., & Miall, A. D. (1985). Models of glaciomarine sedimentation and their application to the interpretation of ancient glacial sequences. Palaeogeography, Palaeoclimatology, Palaeoecology, 51(1-4), 15-84.

Fielding, C. R., Frank, T. D., & Isbell, J. L. (2008). The late Paleozoic ice age—a review of current understanding and synthesis of global climate patterns. Geological Society of America Special Papers, 441, 343-354.

Fielding, C. R., Frank, T. D., Isbell, J. L., Henry, L. C., & Domack, E. W. (2010). Stratigraphic signature of the late Palaeozoic Ice Age in the Parmeener Supergroup of Tasmania, SE Australia, and inter-regional comparisons. Palaeogeography, Palaeoclimatology, Palaeoecology, 298(1-2), 70-90.

Foden, J., Elburg, M. A., Dougherty-Page, J., & Burtt, A. (2006). The timing and duration of the Delamerian Orogeny: correlation with the Ross Orogen and implications for Gondwana assembly. The Journal of Geology, 114(2), 189-210.

Frakes, L.A. (1979). Climates throughout geologic time. Elsevier, Amsterdam, 310 p.

Francis, J. A. and Vavrus, S. J. (2015). Evidence for a wavier jet stream in response to rapid Arctic warming. Environmental Research Letters, 10(1), 014005.

Frank, T. D., Shultis, A. I., & Fielding, C. R. (2015). Acme and demise of the late Palaeozoic ice age: A view from the southeastern margin of Gondwana. Palaeogeography, Palaeoclimatology, Palaeoecology, 418, 176-192.

Gastaldo, R. A., DiMichele, W. A., & Pfefferkorn, H. W. (1996). Out of the icehouse into the greenhouse: a late Paleozoic analogue for modern global vegetational change. GSA Today.

Gray, D. R., & Foster, D. A. (2004). Tectonic evolution of the Lachlan Orogen, southeast Australia: historical review, data synthesis and modern perspectives. Australian Journal of Earth Sciences, 51(6), 773-817.

Griffis, N.P., Montañez, I.P., Fedorchuk, N., Isbell, J., Mundil, R., Vesely, F., Weinshultz, L., Iannuzzi, R., Gulbranson, E., Taboada, A. and Pagani, A. (2019). Isotopes to ice: Constraining provenance of glacial deposits and ice centers in west-central Gondwana. Palaeogeography, palaeoclimatology, palaeoecology, 531, 108745.

Grindley, G.W. (1963). The geology of the Queen Alexandra Range, Beardmore Glacier, Ross Dependency, Antarctica. New Zealand Journal of Geology and Geophysics, 6, 307 – 347.

Hand, S. J. (1993). Palaeogeography of Tasmania's Permo-Carboniferous glacigenic sediments. Gondwana Eight: Assembly, Evolution and Dispersal, 459-469.

Heckel, P. H. (2008). Pennsylvanian cyclothems in Midcontinent North America as far-field effects of waxing and waning of Gondwana ice sheets. Resolving the Late Paleozoic Ice Age in Time and Space; Fielding, CR, Frank, TD, Isbell, JL, Eds, 275-290.

Hong, W., Cooke, D.R., Huston, D.L., Maas, R., Meffre, S., Thompson, J., Zhang, L. and Fox, N. (2017). Geochronological, geochemical and Pb isotopic compositions of Tasmanian granites (southeast Australia): Controls on petrogenesis, geodynamic evolution and tin mineralisation. Gondwana Research, 46, 124-140.

Isbell, J. L. (1999). The Kukri Erosion Surface; a reassessment of its relationship to rocks of the Beacon Supergroup in the central Transantarctic Mountains, Antarctica. Antarctic Science, 11(2), 228-238.

Isbell, J. L., Miller, M. F., Wolfe, K. L., & Lenaker, P. A. (2003). Timing of late Paleozoic glaciation in Gondwana: Was glaciation responsible for the development of Northern Hemisphere cyclothems?. Special papers-geological society of America, 5-24.

Isbell, J. L., Koch, Z. J., Szablewski, G. M., & Lenaker, P. A. (2008a). Permian glacigenic deposits in the Transantarctic Mountains, Antarctica. Resolving the late Paleozoic ice age in time and space: Geological Society of America Special Paper, 441, 59-70.

Isbell, J. L., Cole, D. I., Catuneanu, O. and Fielding, C. R. (2008b). Carboniferous-Permian glaciation in the main Karoo Basin, South Africa: Stratigraphy, depositional controls, and glacial dynamics. In Resolving the Late Paleozoic ice age in time and space (Vol. 441, pp. 71-82). Geological Society of America Special Paper.

Isbell, J.L., Henry, L.C., Gulbranson, E.L., Limarino, C.O., Fraiser, M.L., Koch, Z.J., Ciccioli, P.L. and Dineen, A.A. (2012) Glacial paradoxes during the late Paleozoic ice age: Evaluating the equilibrium line altitude as a control on glaciation. Gondwana Research, 22(1), pp.1-19.

Isbell, J.L., Vesely, F.F., Rosa, E.L., Pauls, K.N., Fedorchuk, N.D., Ives, L.R., McNall, N.B., Litwin, S.A., Borucki, M.K., Malone, J.E. and Kusick, A.R. (2021). Evaluation of physical and chemical proxies used to interpret past glaciations with a focus on the late Paleozoic Ice Age. Earth-Science Reviews, p.103756.

Ives, L. R., and Isbell, J. L. (2021). A lithofacies analysis of a South Polar glaciation in the Early Permian: Pagoda Formation, Shackleton Glacier region, Antarctica. Journal of Sedimentary Research, 91(6), 611-635. https://doi.org/10.2110/jsr.2021.004

Jordan, T. A., Riley, T. R., & Siddoway, C. S. (2020). The geological history and evolution of West Antarctica. Nature Reviews Earth & Environment, 1(2), 117-133.

Kurjanski, B., Rea, B. R., Spagnolo, M., Cornwell, D. G., Howell, J., & Archer, S. (2020). A conceptual model for glacigenic reservoirs: from landsystems to reservoir architecture. Marine and Petroleum Geology, 115, 104205.

Landvik, J. Y., Alexanderson, H., Henriksen, M., & Ingólfsson, Ó. (2014). Landscape imprints of changing glacial regimes during ice-sheet build-up and decay: a conceptual model from Svalbard. Quaternary Science Reviews, 92, 258-268.

Masood, K.R.; Taylor, T.N., Horner, T., and Taylor, E.L. (1994). Palynology of the Mackellar Formation (Beacon Supergroup) of East Antarctica: Review of Palaeobotany and Palynology, 83, 329–337.

Mitrovica, J.X., Gomez, N. and Clark, P.U., 2009. The seal-level fingerprint of West Antarctic Collapse. Science, 323: 753.

Montañez, I., & Soreghan, G. S. (2006). Earth's fickle climate: lessons learned from deep-time ice ages. Geotimes, 51(3), 24.

Montañez, I. P., & Poulsen, C. J. (2013). The Late Paleozoic ice age: an evolving paradigm. Annual Review of Earth and Planetary Sciences, 41, 629-656.

Nesbitt, H., & Young, G. M. (1982). Early Proterozoic climates and plate motions inferred from major element chemistry of lutites. Nature, 299(5885), 715-717.

Pauls, K.N., Isbell, J.L., Limarino, C.O., Alonso-Murauga, P.J., Malone, D.H., Schencman, L.J., Colombi, C.E. and Moxness, L.D. (2021). Constraining late paleozoic ice extent in the Paganzo basin of western Argentina: Provenance of the lower Paganzo group strata. Journal of South American Earth Sciences, 106, p.102899.

Pinet, P.R., Matz, D.B., Hayes, M.O (1967). Petrology of the upper division of the Beacon Sandstone. Antarctic Journal of the U.S., 2, 108 – 109.

Pollard, D., & DeConto, R. M. (2009). Modelling West Antarctic ice sheet growth and collapse through the past five million years. Nature, 458(7236), 329.

Raymond, A., & Metz, C. (2004). Ice and its consequences: glaciation in the Late Ordovician, Late Devonian, Pennsylvanian-Permian, and Cenozoic compared. The Journal of Geology, 112(6), 655-670.

Rolland, Y., Bernet, M., van der Beek, P., Gautheron, C., Duclaux, G., Bascou, J., Balvay, M., Héraudet, L., Sue, C. and Ménot, R.P. (2019). Late Paleozoic ice age glaciers shaped East Antarctica landscape. Earth and Planetary Science Letters, 506, 123-133.

Rygel, M. C., Fielding, C. R., Frank, T. D., & Birgenheier, L. P. (2008). The magnitude of Late Paleozoic glacioeustatic fluctuations: a synthesis. Journal of Sedimentary Research, 78(8), 500-511.

Saltzman, M. R. (2003). Late Paleozoic ice age: Oceanic gateway or pCO_2?. Geology, 31(2), 151-154.

Steig, E. J., Schneider, D. P., Rutherford, S. D., Mann, M. E., Comiso, J. C., & Shindell, D. T. (2009). Warming of the Antarctic ice-sheet surface since the 1957 International Geophysical Year. Nature, 457(7228), 459.

Truswell, E.M. (1978) Palynology of the Permo-Carboniferous in Tasmania: and interim report. Bulletin of the Geological Survey of Tasmania, 56, 1-39.

Turner, J., Lu, H., White, I., King, J. C., Phillips, T., Hosking, J. S., Bracegirdle T.J., Marshall G.J., Mulvaney R., & Deb, P. (2016). Absence of 21st century warming on Antarctic Peninsula consistent with natural variability. Nature, 535(7612), 411 - 415.

Veevers, J. J., and Powell, C. McA. (1994). Permian-Triassic Pangean Basins and foldbelts along the Panthalassan Margin of Gondwana. Geological Society of America Memoir vol. 184, 368 p.

Vesely, F. F. and Assine, M. L. (2006). Deglaciation sequences in the Permo-Carboniferous Itararé Group, Paraná Basin, southern Brazil. Journal of South American Earth Sciences, 22(3-4), 156-168.

Whitehouse, P. L. (2018). Glacial isostatic adjustment modelling: historical perspectives, recent advances, and future directions. Earth surface dynamics, 6(2), 401-429.

CHAPTER 2.

A LITHOFACIES ANALYSIS OF A SOUTH POLAR GLACIATION IN THE EARLY PERMIAN: PAGODA FORMATION, SHACKLETON GLACIER REGION, ANTARCTICA

This chapter is published as:

Ives, L. R., & Isbell, J. L. (2021). A lithofacies analysis of a South Polar glaciation in the Early Permian: Pagoda Formation, Shackleton Glacier region, Antarctica. *Journal of Sedimentary Research, 91*(6), 611-635. DOI: 10.2110/jsr.2021.004

Abstract

The currently favored hypothesis for late Paleozoic Ice Age glaciations is that multiple ice centers were distributed across Gondwana and that these ice centers grew and shrank asynchronously. Recent work has suggested that the Transantarctic Basin has glacigenic deposits and erosional features from two different ice centers, one centered on the Antarctic Craton and another located over Marie Byrd Land. To work towards an understanding of LPIA glaciation that can be tied to global trends, these successions must be understood on a local level before they can be correlated to basinal, regional, or global patterns. This study evaluates the sedimentology, stratigraphy, and flow directions of the glacigenic, Asselian – Sakmarian (early Permian) Pagoda Formation from four localities in the Shackleton Glacier region of the Transantarctic Basin to characterize late Paleozoic Ice Age glaciation in a South Polar, basin-marginal setting. These analyses show that the massive, sandy, clast-poor diamictites of the Pagoda Fm were deposited in a basin-marginal subaqueous setting through a variety of glacigenic and glacially-influenced mechanisms in a depositional environment with depths below normal wave base. Current-transported sands and stratified diamictites that occur at the top of the Pagoda Fm were deposited as part of grounding-line fan systems. At least 100 m of topographic relief on the erosional surface underlying the Pagoda Fm strongly influenced the thickness and transport-directions in the Pagoda Fm. Uniform subglacial striae orientations across 100 m of paleotopographic relief suggest that the glacier was significantly thick to "overtop" the paleotopography in the Shackleton Glacier region. This pattern suggests that the glacier was likely not alpine, but rather an ice cap or ice sheet. The majority of the Pagoda Fm in the Shackleton Glacier region was deposited during a single retreat phase. This retreat phase is represented by a single glacial depositional sequence that is characteristic of a glacier with a temperate or mild subpolar thermal regime and significant meltwater discharge. The position of the glacier margin likely experienced minor fluctuations (readvances) during this retreat. Though

sediment in the Shackleton Glacier region was deposited during a single glacier retreat phase, evidence from this study does not preclude prior or later glacier advance-retreat cycles preserved elsewhere in the basin. Ice flow directions indicate that the glacier responsible for this sedimentation was likely flowing off of an upland on the side of the Transantarctic Basin closer to the Panthalassan/Gondwanide margin (Marie Byrd Land), which supports the hypothesis that two different ice centers contributed glacigenic sediments to the Transantarctic Basin. Together, these observations and interpretations provide a detailed local description of Asselian – Sakmarian glaciation in a South Polar setting that can be used to understand larger-scale patterns of regional and global climate change during the late Paleozoic Ice Age.

2.1. Introduction

Strata of the Transantarctic Basin (TAB) contain a complete South Polar sedimentary record of the global "icehouse" to "greenhouse" transition during the early Permian (Collinson et al. 1994; Collinson et al. 2006; Isbell et al. 2008b). Sedimentation in the TAB was dominated by glacigenic processes during the Asselian-Sakmarian (Isbell et al. 2008c). This interval was part of the Late Paleozoic Ice Age (LPIA, ~374 – 256 Ma) (Fielding et al. 2008c; Montañez and Poulsen 2013). Widespread glaciation across Gondwana characterized the LPIA, as did low pCO2, high pO2, generally low eustatic levels with large magnitude fluctuations, low solar luminosity, and increased δ18O and δ13C values relative to the rest of the Phanerozoic (Gastaldo et al. 1996; Raymond and Metz 2004; Montañez and Soreghan 2006; Fielding et al. 2008d; Rygel et al. 2008; Montañez and Poulsen 2013).

The currently favored hypothesis for LPIA glaciations is that multiple ice centers (ice sheets or ice caps) were distributed across Gondwana, and that these ice centers grew and shrank asynchronously over the LPIA's ~80 Myr duration (Fielding et al. 2008c; Isbell et al. 2012; Montañez and Poulsen 2013; López-Gamundí et al. 2021; Rosa and Isbell 2021). The character, distribution, and resulting sedimentary records of these glaciers would have been driven by global, regional, and local climatic and geologic influences (Isbell et al. 2012; Montañez and Poulsen 2013; López-Gamundí et al. 2021). The potential for local and regional heterogeneity of LPIA glacigenic strata is therefore extremely high. To work towards an understanding of LPIA glaciation that can be tied to global trends, these successions must be understood on a local level before they can be correlated to basinal, regional, or global patterns.

In this paper, we evaluate the sedimentology, stratigraphy, and flow directions of four glacigenic (Pagoda Fm) successions in the Shackleton Glacier region of the TAB (Fig. 2- 1B). The Pagoda Fm

in the Shackleton Glacier region has not previously been described and analyzed at the level of detail reported in this study. The Shackleton Glacier region can offer a different perspective to better-studied areas of the TAB (e.g., the Beardmore Glacier region) because it was located in a basin marginal position on the non-cratonic (or, "Panthalassan proximal") side of the basin during the deposition of the Pagoda Fm (Fig. 2- 1).

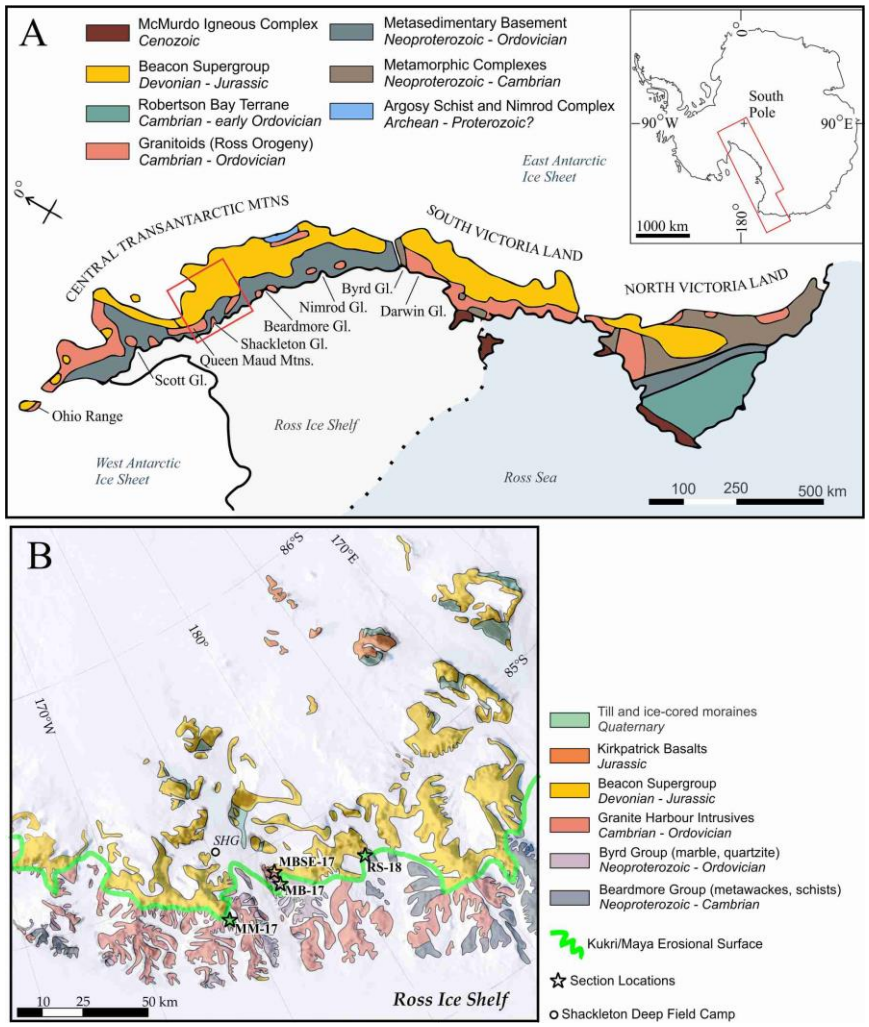

Figure 2-1. Generalized geologic maps of study area. Maps are South Polar projections. A. Geologic map of the Central Transantarctic Mountains and Victoria Land, with relevant outlet glaciers and mountain ranges labeled. Modified after Elliot (2013), Goodge (2016), and Estrada et al. (2016). Box on inset map indicates extent of this geologic map. Red box on geologic map indicates the extent of "map B". B. Regional geologic map of the Shackleton Glacier area, noting the locations of sections described in this study. MM-17 is Mt. Munson, MB-17 is Mt. Butters 1, MBSE-17 is Mt. Butters 2, and RS-18 is Reid Spur. Geology adapted from McGregor and Wade (1969); Mirsky (1969), aerial photos from LIMA Landsat imagery (Bindschadler 2008).

2.2. Geological Setting

Asselian-Sakmarian glacigenic strata of the Transantarctic Basin (TAB) occur in discontinuous outcrops along the margin of the East Antarctic Craton from Victoria Land, near Australia, to Dronning Maud Land, near southern Africa (Frakes et al. 1971; Collinson et al. 1994; Isbell et al. 2008c) (Fig. 2- 2A). During the lower Cisuralian, the TAB was a narrow (~100 – 200 km-wide), trough-shaped basin that formed parallel and proximal to the Gondwanide margin of the East Antarctica Craton, but inboard of the Panthalassic margin (Fig. 2- 3B) (Collinson et al. 1994; Elliot 2013; Isbell 2015; Elliot et al. 2017). In the central Transantarctic Mountains and Victoria Land, glacigenic strata occur within four sub-basins; the Ohio Range to the Scott Glacier (Horlick Sub-basin), the Amundsen Glacier to the Darwin Glacier area (Beardmore Sub-basin), south Victoria Land (SVL), and north Victoria Land (NVL) (Figs. 1B, 3) (Frakes et al. 1966; Isbell et al. 2008c; Isbell 2010; Cornamusini 2017). The Shackleton Glacier region is located near the southern edge of the Beardmore Sub-basin.

The origin and nature of the TAB during the lower Permian is not well understood. Hypotheses include intracratonic and extensional settings (Collinson et al. 1994; Isbell 2015; Elliot et al. 2017). Regardless of what processes drove basin formation at that time, the TAB was a narrow, trough-shaped basin, with Proterozoic and early Paleozoic basement shoulders, that paralleled the Panthalassan margin of the East Antarctic Craton during the deposition of the Pagoda Fm (Fig. 2-3) (Isbell et al. 1997b). Though there is no evidence for upper Carboniferous to Sakmarian orogenic activity in the central Transantarctic Mountains or adjacent Marie Byrd Land, volcanic arcs and tectonic compression were occurring elsewhere along Gondwana's Panthalassan margin during that time, including in eastern Australia, the Andean margin of South America and Patagonia, the Ellsworth Mountains, Thurston Island, and the Antarctic Peninsula (Fielding et al. 2001; Elliot 2013;

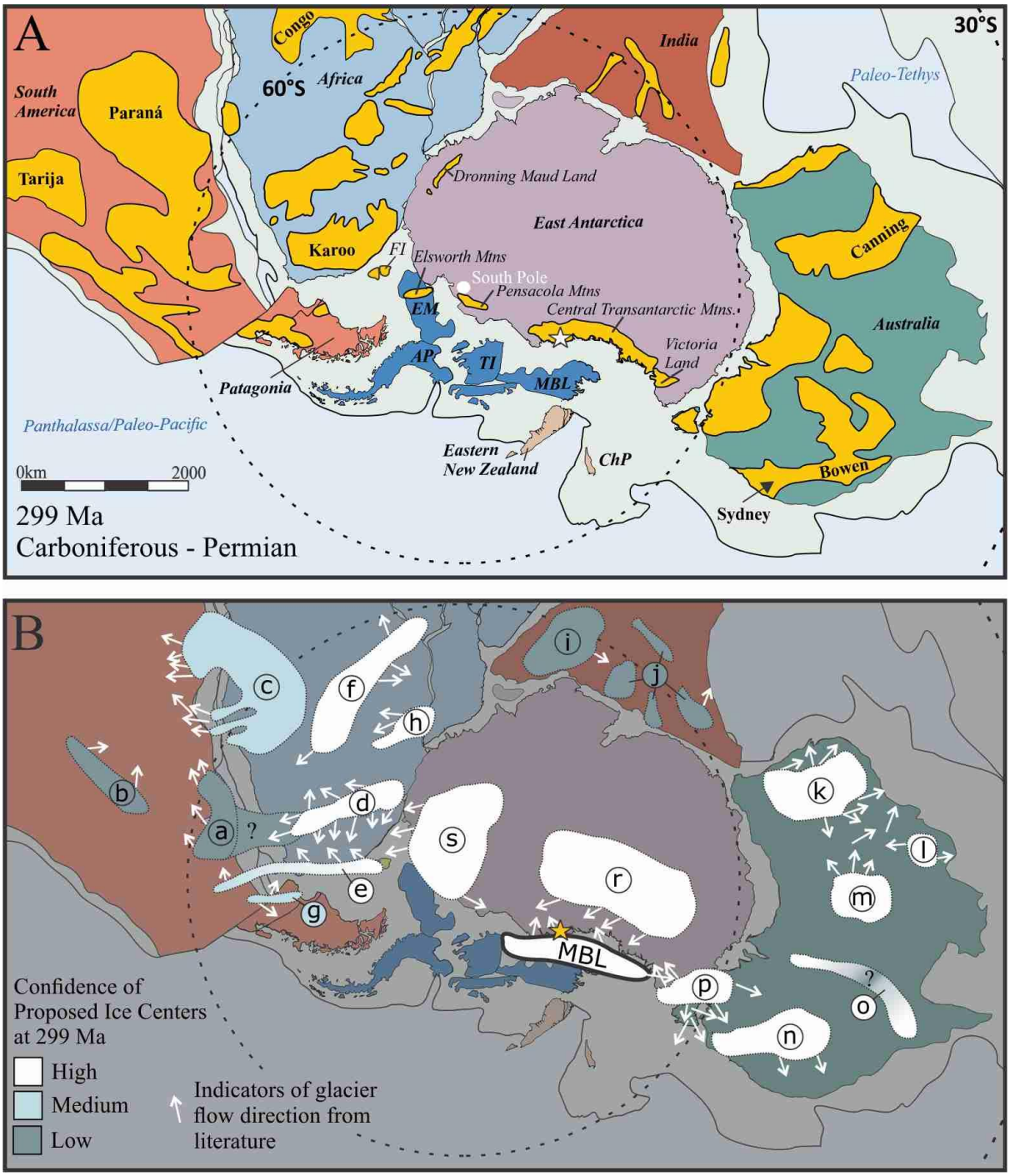

Figure 2-2. Paleogeographic reconstructions of Gondwana near the Carboniferous-Permian Boundary. All maps are south-polar projections. Star indicates the approximate location of the Shackleton Glacier area. Continent distributions and paleolatitudes are based on Lawver et al. (2011) and copied from (Isbell et al. 2012). Note that there are differences in the positioning of some crustal blocks (e.g., Patagonia and New Zealand) between this reconstruction and Figure 3, which is modified after Elliot (2013). **A.** Yellow regions indicate the modern extent of sedimentary basins containing late Paleozoic Ice Age strata. Abbreviations include: Falkland Islands/Malvinas (FI), Ellsworth Mountain block (EM), Antarctic Peninsula (AP), Thurston Island (TI), Marie Byrd Land (MBL), and the Challenger Plateau/western New Zealand (ChP). Basins adapted from Isbell et al. (2012). **B.** Proposed positions of glacial centers during the early Permian based on flow directions and position of basins and "highlands". Illustrated ice centers are not

(Fig. 2-2 continued) meant to represent the whole possible extent of each proposed glacier, but where proposed glaciers were likely to be nucleated. The arrows reflect field measurements of flow directions reported in the studies cited for each ice center. However, flow directions of glaciers are highly variable, both spatially and temporally, and the true flow paths of these ancient ice centers were likely much more variable than the arrows on this map. Confidence is based on abundance of available lithologic data, and both relative and absolute ages. Ice centers are as follows: MBL. The proposed Marie Byrd Land ice-center, discussed in this study as the most likely source for the glacigenic sediments of the Pagoda Fm in the Shackleton Glacier region (Isbell et al. 1997b; Isbell 2010) a. Uruguay (Crowell and Frakes 1975; Assine et al. 2018; Fedorchuk et al. 2019), b. Asunsción (Frakes and Crowell 1969; Franca and Potter 1988; Limarino et al. 2014), c. Windhoek/ Koakoveld Highlands (Martin 1981; Visser 1987; Franca et al. 1996; Rosa et al. 2016; Tedesco et al. 2016; Assine et al. 2018; Dietrich et al. 2019; Fallgatter and Paim 2019) , d. Cargonian Highlands (Crowell and Frakes 1972; Visser 1997; Isbell et al. 2008a; Dietrich et al. 2019), e. Cape-Ventana Fold Belt (Visser 1997; Isbell et al. 2008a; Wopfner 2012), f. East African Thermal Rise (Rust 1975; Wopfner 2012), g. Patagonian Western Magmatic Arc (Pauls 2014; Survis 2015; Marcos 2018), h. Zimbabwe (Wopfner 2012; Dietrich et al. 2019), i. Madagascar-SW India (Veevers and Tewari 1995; Isbell et al. 2012), j. Chotanagpur & Chhattisgarh (Veevers and Tewari 1995; Dasgupta 2006; Isbell et al. 2012), k. Pilabra-Yilgarn, l. Kimberly (see Mory et al. (2008); Martin (2019), and references therein), m. Arunta-Musgrave (Mory et al. 2008; Martin 2019) and references therein, n. Bowen-Gunnedah-Sydney (Fielding et al. 2008a; Fielding et al. 2008b; Fielding et al. 2010), o. Galilee (Fielding et al. 2008a; Fielding et al. 2008b; Fielding et al. 2010; Isbell et al. 2012), p. Wilson (Hand 1993; Rocchi 2011; Jordan 2013), r. East Antarctic (Isbell et al. 1997a; Isbell 2010), s. Ellsworth (Frakes et al. 1971; Ojakangas and Matsch 1981; Matsch and Ojakangas 1992; Visser 1997).

Vizán et al. 2017). This same margin was extremely active and subject to repeated, complex accretion events throughout the Paleozoic (Veevers et al. 1994; Domeier and Torsvik 2014; Goodge 2020). As a result of this activity, the TAB evolved into a foreland basin later in the Permian (Collinson et al. 1994; Elliot et al. 2017). During the Lower Jurassic, strata in the central Transantarctic Mountains were pervasively intruded by sills associated with Ferrar Group volcanism and the break-up of Gondwana (Elliot 1992).

2.3. Sedimentology and Stratigraphy of the Pagoda Formation

The Pagoda Fm is the basal unit in the Permian – early Jurassic Victoria Group (upper Beacon Supergroup) in the Beardmore Sub-basin of the TAB. Rare palynomorphs and conchostracans suggest that the Pagoda and Mackellar fms are Asselian - Sakmarian (Masood et al. 1994; Askin 1998; Babcock et al. 2002). The Pagoda Fm overlies both the Kukri and Maya regional erosional surfaces (Figs. 1B, 3) (Collinson et al. 1994; Isbell 1999; Elliot 2013). The Maya Erosional Surface is a disconformity that separates Devonian(?) clastics of the lower Beacon Supergroup from the

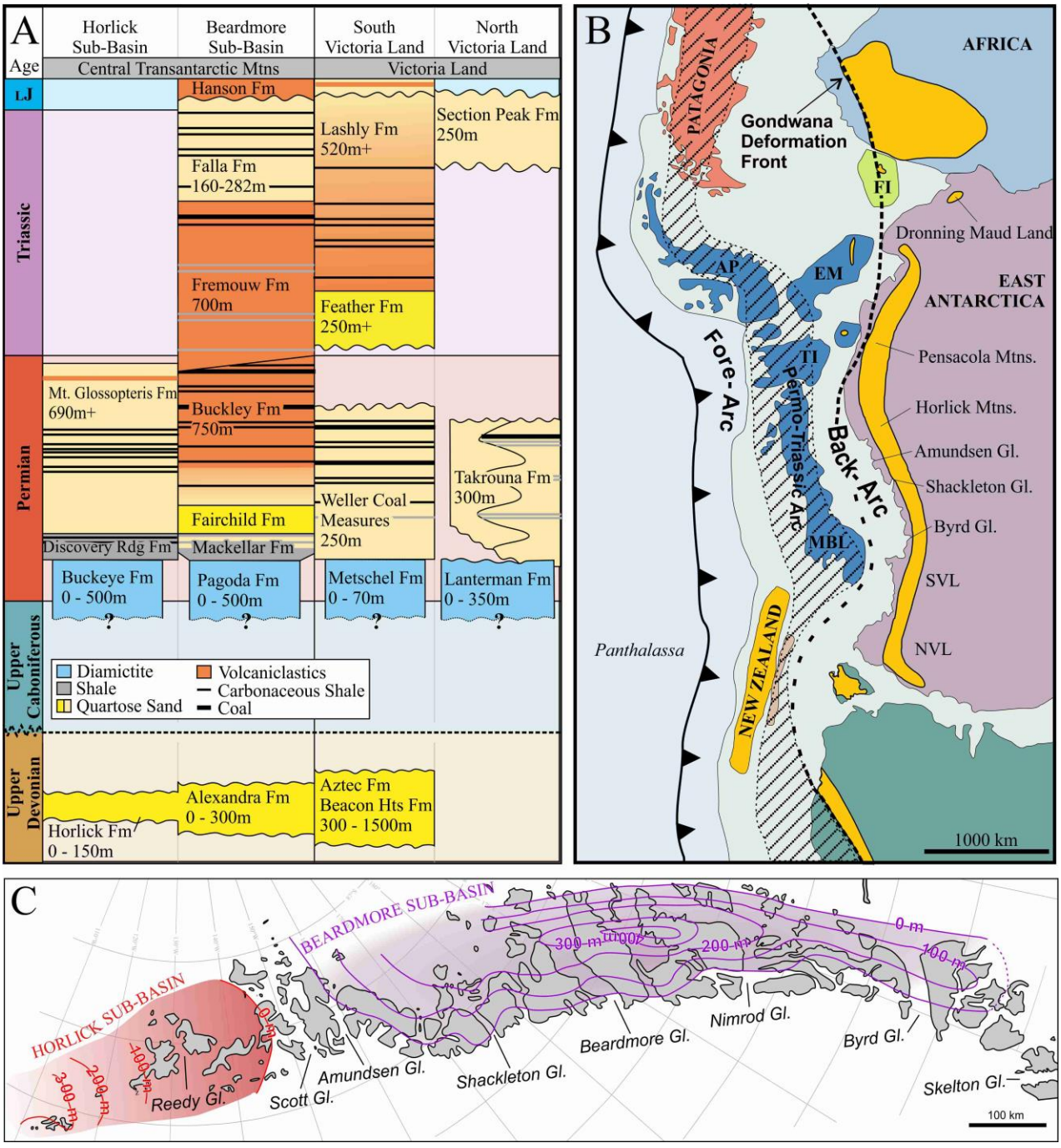

Figure 2-3. Regional geologic context and tectonic setting of the Transantarctic Basin during the Asselian - Sakmarian. A. Stratigraphy of the Beacon Supergroup across different regions of the Transantarctic Basin. Adapted from Elliot (2013); Cornamusini (2017); Elliot et al. (2017). B. Tectonic setting of southern Gondwana during the Permian, adapted from Elliot (2013). Regions of sedimentary deposition are shaded yellow. Note that there are differences in the positioning of some crustal blocks (e.g., Patagonia and New Zealand) between this reconstruction and Figure 2. C. Modern extent and isopach map of the Asselian - Sakmarian glacigenic facies (Pagoda Fm and equivalents) in the Horlick Sub-Basin and Beardmore Sub-basin in the Transantarctic Mountains. Grey areas are outcrops/ nunatuks. Lines show isopachs of the Pagoda Fm (Beardmore Sub-basin) and Buckeye Fm (Horlick Sub-basin) from Isbell et al. (2008c).

Victoria Group (Isbell 1999). The Kukri Erosional Surface separates the Beacon Supergroup from underlying Ross Orogeny intrusions and associated metasediments. Significant relief of at least 150 m occurs on these unconformities (Fig. 2- 4) (Isbell et al. 1997a; Isbell 1999; Isbell et al. 2008c). Both the Pagoda Fm, and the overlying, post-glacial Mackellar Fm, lap onto the erosional surfaces, indicating that the Pagoda Fm and its equivalents in other sub-basins often did not overtop the relief (Isbell et al. 1997a). The lower Beacon Supergroup units are not present in the Shackleton Glacier region. The erosional surface underlying the Pagoda Fm is consists of two, merged regional unconformities, the Maya and Kukri erosional surfaces (Isbell et al. 2008c). At all sites in this study, the Pagoda Fm overlies Ross Orogeny granites.

Since their discovery, the Pagoda Fm and its equivalents throughout the Transantarctic Mountains have been unanimously interpreted as glacigenic or glacially-influenced because their predominant lithologies are massive and laminated, sandy and silty diamictites (Long 1964a; Lindsay 1970a; Coates 1985; Barrett et al. 1986; Collinson et al. 1994; Isbell et al. 2008c). Minor lithologies of the Pagoda Fm include conglomeratic sandstones, sandstones, mudrocks, and lonestone-bearing mudrocks (Isbell et al. 2008c). Besides diamictites and lonestones, evidence for a glacial origin for the Pagoda Fm includes striated and polished basement surfaces, the prevalence of striated and faceted clasts, and a clear relationship between local basement composition and lithologies of large clasts within the diamictites (Lindsay 1969; Coates 1985). Detailed interpretations of depositional environments have been made for a few Pagoda Fm localities (Lindsay 1970a; Waugh 1988; Miller 1989; Isbell et al. 2001; Lenaker 2002; Long et al. 2008-2009; Koch 2010; Koch and Isbell 2013) and its equivalents in Victoria Land (Askin et al. 1971; Barrett 1972; Barrett and McKelvey 1981; Isbell 2010; Cornamusini 2017), Horlick Mountains (Frakes et al. 1966; Aitchison et al. 1988), and Ellsworth Mountains (Ojakangas and Matsch 1981; Matsch and Ojakangas 1991). With few exceptions, these analyses have invoked sub-aqueous, glacial-proximal depositional settings. This

contrasts with early surveys that interpreted diamictites as subglacially-deposited "tillites" (Lindsay 1970a; Coates 1985; Miller 1989; Isbell et al. 1997b).

Isbell et al. (2008c) separated the Permian glacigenic units in the Transantarctic Mountains into basin-margin and basinal facies associations. Basin-margin successions are predicted to occur near basement highs and along basin margins, are relatively thin (<100 m), contain evidence for subglacial deformation and erosion, have deformation resulting from proglacial glaciotectonism, and small (m-scale) gravity-driven deposition. Basinal successions are thicker (100 - 500 m), have little-to-no evidence for subglacial processes, and are more likely to contain stratified diamictites, lonestone-bearing mudrocks, mudrocks, and larger (up to 10's of meters) mass-transport deposits. Evidence of grounded ice and grounding-line processes have been identified in both basinal (e.g., Koch and Isbell (2013)) and basin-margin (e.g. Isbell (2010)) facies associations. Based on its paleogeographic position and Pagoda Fm thickness, the Shackleton Glacier area is here predicted to contain the basin-margin facies.

In the Shackleton Glacier region, the glacigenic facies of the Pagoda Fm are underlain by a non-glacial, lacustrine facies association at a single site on Mt. Butters (site MB-17). This facies and its depositional environment are described in detail by Isbell et al. (2001). Below this contact, the fine-grained lacustrine facies are pervasively sheared, likely subglacially (Isbell et al. 2001). Lonestones, interpreted to be iceberg-rafted debris, occur in the lower post-glacial Mackellar Fm in the Shackleton Glacier region (Seegers 1996; Seegers-Szablewski and Isbell 1998). This suggests that glaciers were still present in the Transantarctic Basin even after glacigenic sedimentation was no longer dominant.

2.4. Study Area and Methods

The sedimentary sections described in this paper were examined as part of the US Antarctic Program's helicopter-supported Shackleton Glacier Deep-Field Camp during the 2017 – 2018 austral summer (Table 2-1; Fig. 2- 1B). These sections are located on the Mt. Butters Massif (MB-17; MBSE-17) on the west side of the Shackleton Glacier, on the east face of Reid Spur (RS-18) of the Ramsey Glacier, and Mount Munson (MM-17) at the head of Barrett Glacier. The two sections at Mt. Butters are separated by approximately 2 km.

Table 2-1. Names and locations of sedimentary sections described in this paper.

Location Name	Section Name	Geographic Coordinates	Thickness of Pagoda Fm
Mt. Butters 1	MB-17	S84° 51.029' W177° 25.216'	90 m
Mt. Butters 2	MBSE-17	S84° 53.003' W177° 22.354'	77 m
Reid Spur	RS-18	S84° 47.035' E178° 46.680'	> 62 m
Mt. Munson	MM-17	S84° 45.359' E173° 41.118'	5 m

Sites were selected for section descriptions based on accessibility, continuity of exposure, and preliminary observations from previous expeditions to the area. At MB-17 several shorter sections were measured to capture lateral variability. Sedimentological data (texture, grain shape, sedimentary structures, etc.) as well as paleotransport indicators (including cross stratification, primary current lineations, striae, slickensides, fold hinge lines, and thrust plane orientation) were logged in each section. Measured sections were placed in context using outcrop-scale photographs taken from helicopters (Fig. 2- 4).

Structural and sedimentary orientations were measured using a Brunton compass, with the azimuth set to 000°. Measurements were corrected for magnetic declination using the NOAA Magnetic Declination Estimated Value Calculator (NOAA 2019). Orientations were corrected for structural dip and aggregate orientations calculated using Stereonet (v.11) software (Allmendinger et al. 2011; Cardozo and Allmendinger 2013). Some measurements from Mt. Munson were collected by JLI during the 1997-1998 field campaign to the Shackleton Glacier region. New flow direction measurements are in Table 2 and site descriptions are in Appendix A

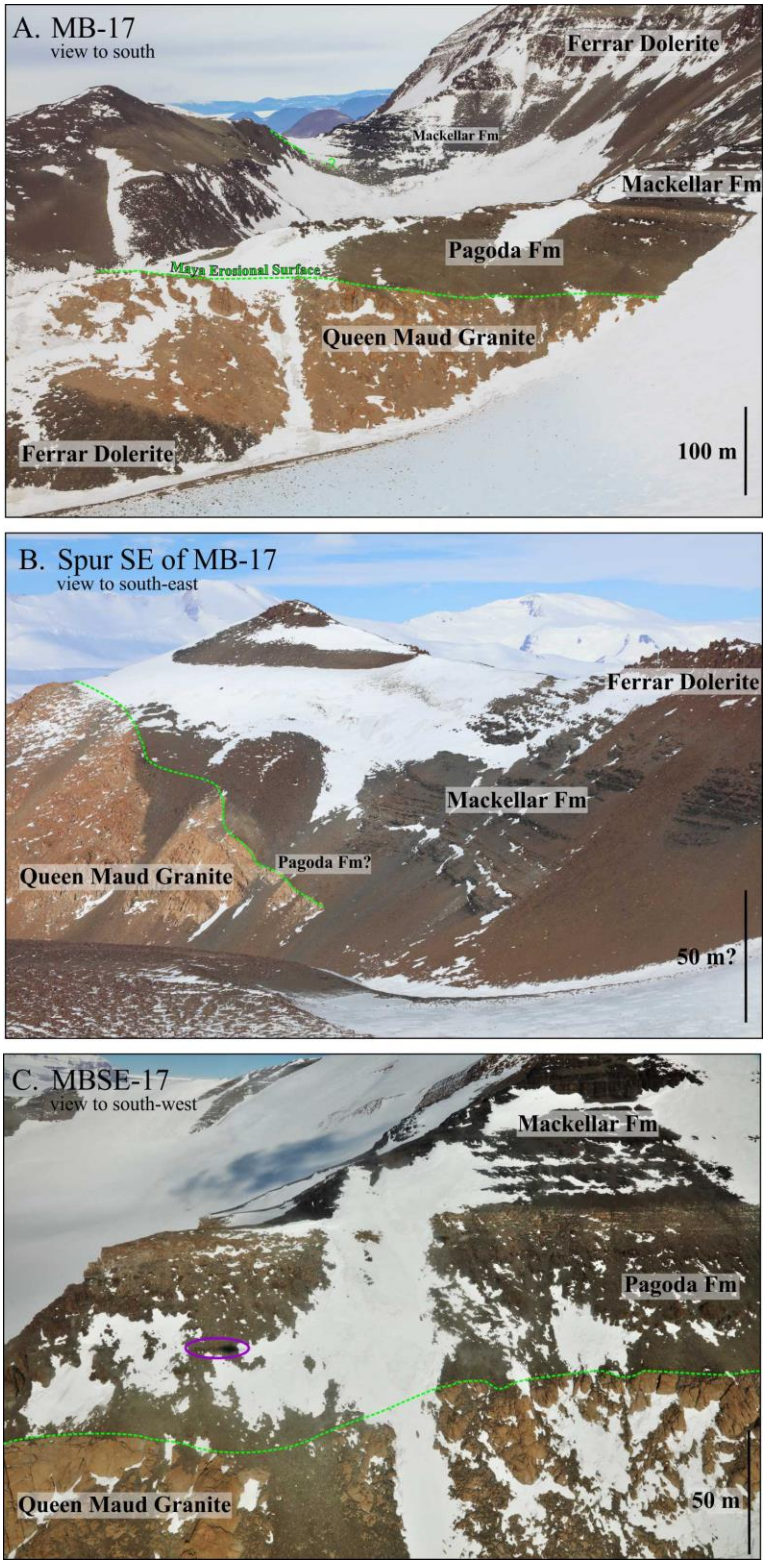

Figure 2-4. Photographs of Mt. Butters outcrops showing the stratigraphy of the Pagoda Fm and post-glacial Mackellar Fm, as well as the relief of the Maya Erosional Surface, in this area. Formations are labeled and the Maya Erosional Surface is marked by a green, dashed line. **A.** Is a photograph of section MB-17 taken from a helicopter, view to the south. This saddle in the background of this photo is approximately halfway between section MB-17 and MBSE-17. **B.** This is an outcrop that is part of the Mt. Butters Massif, and occurs on a spur located south-east of section MB -17. View is toward the south-east from MB-17. This site has never been visited on foot, so the scale is not certain. Note the dip of the granitic basement towards the south-west, which is consistent with basement dip measurements at site MB-17 and MBSE-17 in this study. This exposure is the same as Figure 4 in (Isbell et al. 2001). **C**. Photograph of section MBSE-17, view toward the SW. Purple oval shows to helicopter's shadow.

Table 2-2. Summary of Paleo-transport measurements from this study (mean = Fisher mean ± a99). Note that due to the proximity of the study locations to the south pole that the orientation of compass directions are not the same across the basin. Mack = Mackellar Fm, L. Pag = lower Pagoda lacustrine facies (Isbell et al., 2001); T = Trend, P = Plunge, D = Dip angle, DD = Dip Direction, S = strike, * = measured during 1997 field season

Section (height)	Facies/Fm	Feature	Measurement	Orientation	N
Site MW-18					
10 m above basement	Mack	Asymmetrical ripples	Transport	T: 322˚, 312˚, 002˚	3
Site MM-17					
0 m	-	Striae on basement	Lineation	T: 180˚	1
*0 m	-	Striae on basement	Lineation	T: 095˚ ± 3.7˚	8
*4 m above base of Mackellar	Mack	Asymmetrical ripples	Transport	T: 157˚ ± 28.5˚	7
13-17.5 m	Mack	Highly-deformed slump features	Vergence	T: 109˚, 104˚, 114˚	3
*4 - 48 m of Mackellar Fm	Mack	Asymmetrical ripples	Transport	T: 109˚ ± 20.0˚	10
Site MB-17					
0 m	-	Dip and dip direction of basement	Mean pole to plane Plane from mean pole	T: 262˚ P: 79˚ S: 352˚± 12˚ D: 11˚ **DD: 262˚**	5
MB-17A/B	L. Pag	Symmetrical Ripple Crest Axes	Mean lineation	T: 346˚ ± 6.0 ˚	17
MB-17B	L. Pag	Slickenside lineation	Mean	T: 006 ˚	1
MB-17C (12 m)	MSD	Fold axes and small thrust faults	Mean Vergence	T: 220˚± 31˚	7
MB-17C (20 m)	MSD	Plane of thrust faults	Vergence	T: 256˚, 251˚	2
MB-17C (58 m)	MSD	Slide/slump plane	Planes Plane from mean pole	DD: 243˚, 191˚ D: 15˚, 35˚ S: 117˚ D: 23˚ DD: 206 ˚	2
MB-17C/D (73 – 81m)	HA	Asymmetrical ripples	Mean transport Spread	T: 325˚ 236˚ - 055˚	30
MB-17C/D	HA	Cross beds	Transport	T: 346˚, 356˚, 356˚ 226˚, 221˚	5
MB-17D	HA	Climbing Ripples	Transport	T: 221˚, 256˚	2
MB-17C (84 m)	HA	Grooves (iceberg keel marks?)	Direction of shallowing	T: 253˚ ± 24 ˚	5
MB-17C (18 m above Pagoda)	Mack	Asymmetrical ripples	Mean Transport	T: 219˚ ± 39 ˚	7
Site MBSE-17					
0 m	-	Striae on Basement	Lineation	T: 311˚, 316˚	2
MBSE-17 (29 m)	MSD	Sheath Fold Hing	Orientation Vergence	T: 016˚, P: 20 ˚ 286 ˚??	1
MBSE-17 (31 – 32 m)	MSD	Thrust faults	Mean pole to plane Plane from mean pole Vergence:	T: 263˚ P: 69˚ S: 353˚ D: 21˚ DD: 083˚ T: 263˚	7
MBSE-17 (54 m)	HA	Crenulations under slump/slide	Lineation	T: 241˚, 251˚	2
MBSE-17 (61 – 68 m)	CBS	Cross beds and asymm. ripples	Mean transport	T: 208˚± 29 ˚	7
MBSE-17 (21 – 26 m above Pagoda)	Mack	Asymmetrical Ripples	Mean transport	T: 298˚± 6 ˚ 23	
Site RSP-18					
24 – 48 m	LS	Cross beds, asymm. ripples, & PCL	Mean transport	T: 176˚± 29 ˚	18
68 – 70 m	Mack	Asymmetrical Ripples	Transport	T: 261˚, 241˚, 211˚ 281˚	4

Table 2-3. Facies and Facies Association Descriptions.

Facies Association	Facies Name	Thickness	Lithology	Structures	Formative Process	Depositional Environment
Massive Sandy Diamictite (MSD)	--	5 – 75 m (at least)	Clast-poor to clast-rich, sandy diamictite; muddy sand matrix; minor amounts of discontinuous sand and gravel bodies	Diamictites are massive to crudely bedded and ungraded, sands are generally massive, and sometime laminated, but always highly deformed	Glacigenic, subaqueous processes; likely a combination of mass-transport, iceberg-rainout, iceberg scouring, plume sedimentation, and subglacial till deposition	Glacier-proximal to glacier-intermediate, continental shelf
Laminated Sands (LS)	--	~17 m	Coarse to fine-grained, well-sorted sandstones; quartz-rich; sub-angular to rounded	Fine- to medium-grained sands that occur in thin, planar beds with primary current lineations; coarse-grained sandstones are trough cross-bedded; Fine- to very-fine grained sandstones are laminated, or thinly-bedded with unidirectional ripples	High-density turbidites and/or a transitional concentrated density flow (Mulder and Alexander 2001)	Distal or medial portion of an ice-contact fan or delta
Heterogenous Sandy (HS)	**HS1:** Bedded diamictite	1 – 10 m	Clast-rich, sandy diamictite; matrix is moderately well-sorted	3 – 7 cm beds that are massive with sharp, horizontal, and laterally discontinuous contacts; soft sediment deformation associated with facies HA2	Glacigenic, subaqueous processes; likely a combination of iceberg-rainout and plume sedimentation	Subaqueous glacier-proximal and grounding-line fan system
	HS2: Chaotic sandstones	0 – 15 m	Conglomerates to very fine-grained sandstones	Bedding is usually massive, soft-sediment deformation is pervasive; few primary sedimentary structures preserved; secondary structures include fold noses, boudinage, faulting, shear structures above and below contacts, and ruck structures	Mass-transport, gravity-driven processes in the form of slides, slumps, and/or mass transport deposits.	
	HS3: Stratified sandstones	0 – 15 m	Coarse- to very fine-grained sandstones	Medium- to coarse-grained sandstones are thickly laminated to bedded with	Current-dominated transport and deposition, with	

				planar cross beds, trough cross beds, climbing ripples, 3D ripples that are asymmetrical or climbing, hummocky and swaley cross stratification, and symmetrical ripples with bundled upbuilding; Very-fine and fine sandstones are laminated or thinly bedded include uni-directional ripples, some flaser ripples and climbing ripples; occasional, small-scale soft-sediment deformation occurs in all lithologies	some slumping; Unconfined flow; Poorly-sorted sediment source; large variations in current velocities; occasional wave re-working	
---	**Cross bedded Sandstone** (CBS)	10 – 30 m	Well-sorted, medium- to very coarse-grained quartz arenite sandstone; rare pebbles, cobbles, and conglomerates	Low-angle and trough crossbeds; Crossbed sets range in thicknesses from ~15 cm to ~1.5 m; rare thin beds with asymmetrical ripples; Occur within amalgamated channels in multi-storied, multi-lateral sand sheet <2 km wide	Strong tractive flow confined to a series of amalgamated channels; subaqueous	Unconfined, distributive flow; likely glacial-proximal subaqueous fan/ grounding-line fan

2.5. Facies Associations

The following descriptions are of glacigenic facies associations (FA) that comprise the Pagoda Fm in the Shackleton Glacier region (Table 3). We use the term glacigenic to refer to sedimentary systems whose components are dominantly derived from glacial erosion and/or transport, and whose depositional processes are glacier-driven. For example, a succession that is the result of a plume from a subglacial jet would be glacigenic, but largely non-glacially-derived deep water sediments with the occasional outsized clast would instead be considered "glacially influenced". The characteristics of distinct sediment grain sizes are consistent throughout these successions. Very-fine grained sandstones and shales are black in color. Fine- to medium-grained sandstones are generally quartz-rich with some lithic and potassium feldspar grains. Cobble and boulder-sized clasts are sourced from local basement lithologies (Fig. 2- 1B), and include predominately phaneritic granitoids, with some gneiss, quartzite, and grey, fine-grained meta-sedimentary rocks. All sand-sized and coarser-grained material in the Pagoda Fm occurs in all categories of particle roundness (angular to well rounded), although finer-grained sands are typically better-rounded than medium- and coarse-grained sands. Striations occur on large clasts throughout the Pagoda Fm but are not common. The lack of striations is possibly due to the hardness of individual clasts, which are primarily composed of granite, quartz, and feldspar (Dowdeswell et al. 1985; Bennett et al. 1997).

2.5.1. Massive Sandy Diamictite Facies Association (MSD)

2.5.1.1. MSD Description

This diamictite is the dominant FA of the Pagoda Fm. Similar lithologies occur throughout the Transantarctic Basin. In the Shackleton Glacier region, the thickness of this FA ranges from 3 m at Mt. Munson (MM-17) to 73 m at Mt. Butters (MB-17C). Since this diamictite is almost wholly massive, there is no clear way to further sub-divide these successions. Where exposed, the lower

contact overlies either a striated and polished unconformity with the Queen Maud Batholith (MM-17 and MBSE-17) or subglacially-deformed lacustrine sediments (Isbell et al., 2001; MB-17C). The upper contact of this FA is sharp or erosive with current-transported facies, including Cross Bedded Sandstone (CBS) facies association, Heterogenous Sandy (HS) facies association, and the Mackellar Fm. The contact between this FA and the HS facies association is also gradational where facies HS1 (stratified diamictite) is present above the contact. Upper portions of this FA are intercalated with turbidites (see LS facies' interpretation), and may interfinger with stratified diamictites and mass transport deposits (see HS facies' association interpretation).

Approximately 90% of this FA is clast-poor to clast-rich diamictite (Hambrey and Glasser 2003; Hambrey and Glasser 2012) with minor amounts of sorted sands and gravels (Fig. 2- 5). Clast abundances fluctuate throughout the succession. Some intervals are sufficiently clast-poor that they could be classified as muddy sandstones with dispersed clasts (<1% clasts) (Fig. 2- 5F) (Moncreiff 1989; Hambrey 1994; Hambrey and Glasser 2012). Most clast-rich portions of this diamictite contain 10 – 15% clasts (Fig. 2- 5A, Fig. 2-5E), but some very limited areas contain up to ~30% clasts (Fig. 2- 5C). Clasts range from pebble-sized to 4 m in diameter. Clast compositions includes granite, feldspar, vein quartz, gneiss, and fine-grained meta-sandstone. Clast shapes ranges from rounded to angular. Faceted clasts are common, but bullet-shaped and striated clasts are rare. The matrix is very poorly sorted, with sizes ranging from muds through granule-sized grains. Matrix grain-size distributions remain constant within and between outcrops of this facies, though mean matrix grain size increases slightly in clast-rich sections relative to clast-poor sections.

The diamictite in this FA is massive, with very rare exceptions. However, broadly-defined zones of clast-poor or clast-rich diamictites do occur. These zones are anywhere from 1 – 30 m thick. While we tracked these changes in clast abundance vertically through the measured sections, it was not our

impression that these "zones" have any sort of horizontal organization as might be implied by the terms "layers" or "horizons", and that there are no distinct bounding surfaces between these zones. The transitions between these zones are gradational. These gradational transitions occur on the decimeter- to meter-scale. There was no clear relationship between transition thickness and any other property of these rocks. Zones of diamictites with similar clast concentrations cannot be correlated between outcrops; the distribution of clast-poor and clast-rich diamictites appears to be unique to each locality.

Crude and chaotic bedding occur very occasionally within the otherwise massive diamictite. Where bedding can be discerned, the beds are 2 -10 cm thick, laterally discontinuous, and internally massive. Rare sedimentary structures include ruck structures beneath large clasts (Fig. 2- 5D) and thinning of beds over large clasts (Fig. 2- 5H). Rare beds of boulders and cobbles occur in the lower portion of this facies at both Mt. Butters sites (Fig. 2- 5G). In all "boulder beds" the clasts were not striated, polished, or uniformly oriented.

Sandstone and/or conglomerate bodies are also rare within this FA. These bodies occur within the diamictite and are poorly- to moderately -sorted. The grain compositions within these bodies are similar to sand- to gravel-sized grains in the diamictite. Most sand bodies are massive but can contain layers of discrete grain sizes. However, these layers are often highly deformed. Bodies of sorted sand and/or gravel occur in two distinct sizes. Small bodies consist of sorted sediments that most often occur as irregularly-shaped, horizontally elongate lenses, "whisps", and boudinage-like bodies that are up to 20 cm thick and 100 cm long (Figs. 5A, B, E, F). Such structures may occur alone or, more frequently, within bands and zones up to 1 m thick. Occasionally, diapir-like structures made of sand and/or gravel, 1 to 2 m thick are also present. These structures project upward into the diamict, but are not associated with other sand or gravel bodies. Larger bodies of

well-sorted sand or gravel range in thickness from 1 to 3 m and are laterally discontinuous. These bodies have the same grain size distributions as the smaller bodies. Large sand bodies are typically massive, but where stratification does exist in the sands and/or gravels the beds are largely deformed and display water-escape structures. The large sand bodies thin laterally and have over-turned folds on their thicker ends. In one instance, the main sand body was accompanied by smaller sand bodies that trailed off away from its thick end (comet-like structure) (Fig. 2- 5F; Sandstone with dispersed clasts). The lower contact between the comet-like bodies and the surrounding diamictite has a slope of 30° to 35° above horizontal, and the underlying diamictite sometimes has a fissile structure, indicating shearing. Occasionally such contacts overlie smaller sand lenses, sheath folds, "whisps", and boudins.

2.5.1.2. MSD Interpretation

This FA is most likely glacigenic or glacially influenced. Evidence for glacial transport of sediment in this FA includes striations and polish on basement granites where diamictites rest directly on granite (MBSE-17 and MM-17), the very poor sorting of sediment in the system, and the presence of angular to rounded grains of all sizes, faceted and striated clasts, and large boulders composed of local basement lithologies. In glacial settings, massive diamictites, like the facies described here, may be the result of subglacial till deposition (Evans et al. 2006), settling from suspension of a meltwater plume (Visser 1994), settling from suspension and rain-out from icebergs and iceberg scouring (Dowdeswell et al. 1994; Lisitzin 2002), mass-transport deposits (Rodrigues et al. 2019), or debris flows (Powell and Molnia 1989). Glacial depositional environments that include these processes are subglacial, proglacial proximal (but outside the influence of the grounding zone), and grounding-zone-environments including ground-zone wedges (Batchelor and Dowdeswell 2015; Demet et al. 2019; Dietrich and Hoffmann 2019), morainal banks (Eidam et al. 2020), and ice-contact fans

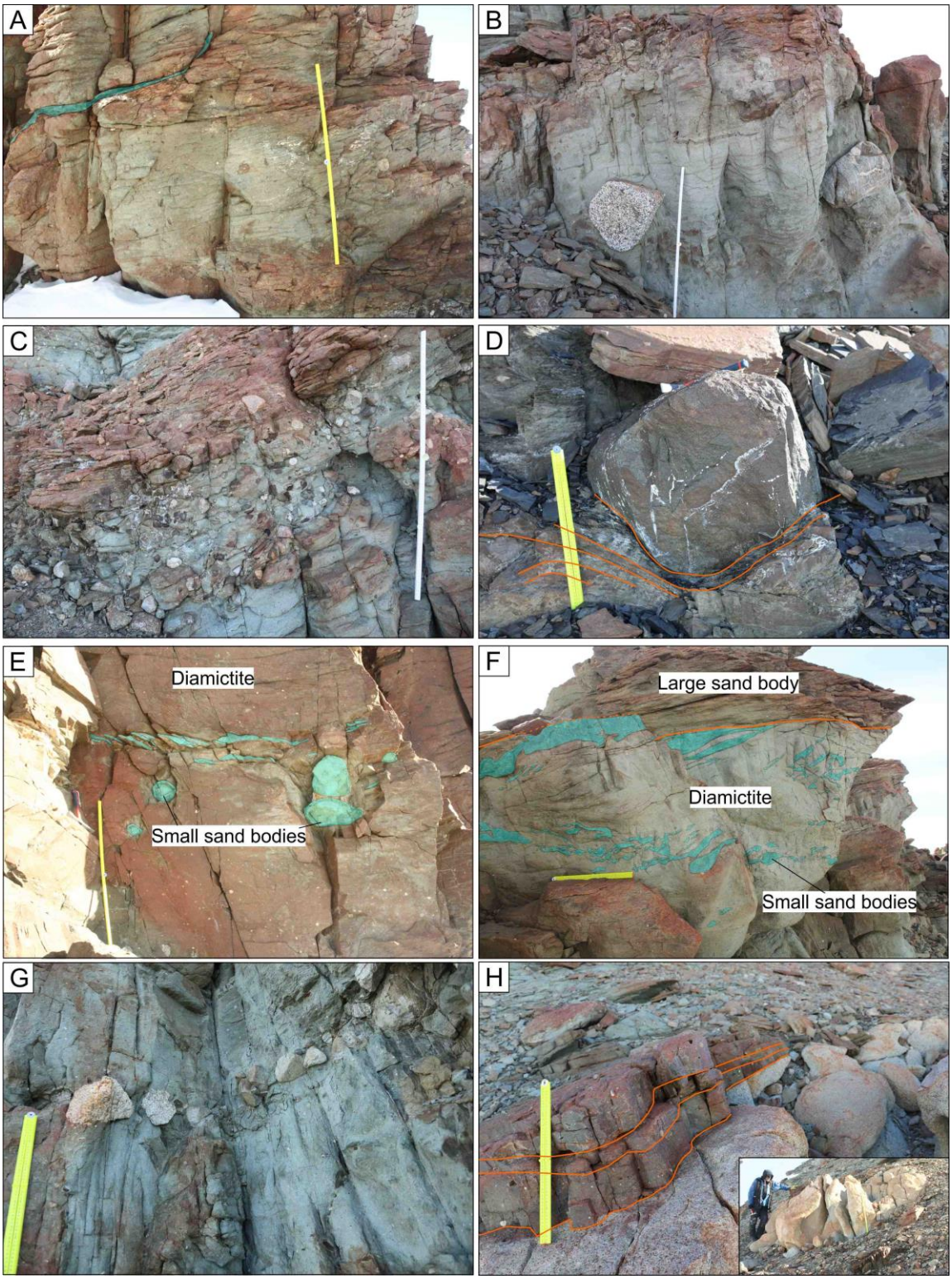

Figure 2-5. Photographs of the Massive Sandy Diamictite (MSD) facies association. Rulers are 50 cm long when folded in half and 1 m long when unfolded. Marks on rulers are in cm. The weathered color of the diamictite is grey to beige and tend to be redder when the matrix has a higher percentage of sand in the matrix. Small sand bodies are highlighted by blue where present and orange lines indicate important bedding planes. A. A characteristic clast poor section of the MSD facies association with a sand "whisp" (MB-17C). B. A section of this facies' diamictite that is very

(Fig. 2-6, continued) clast poor, yet contains several large boulders (MB-17C). C. A clast rich section of the MSD diamictite (MB-17C). D. A ruck structure within the diamictite made by a boulder (MM-17). E. Examples of small sand bodies within the MSD diamictite that had experienced simple shear strain, result in sheath fold, "stringers", boudinage, and en echelon structures. (MBSE-17). F. Example of small sand body bands within an otherwise massive, clast-poor diamictite. (MB-17C). G. A boulder and cobble bed in an otherwise massive diamictite (MBSE-17). H. Diamictite beds onlapping on to a large, 4m boulder within the diamictite. Inset picture shows the whole, ~4 m diameter boulder in outcrop, with person for scale.

(Powell 1990; Benn 1996). The most likely depositional processes and environments for the MSD facies can be inferred by considering the unique features of this facies.

The subglacial deposition of this FA is not likely to be the dominant process, but cannot be wholly ruled out. A tillite interpretation for the MSD FA is supported by the massive, poorly-sorted nature of the diamictites. However, there is no strong evidence for glacier grounding (for example, striated pavements or continuous erosional surfaces) above the base of this facies. Boulder/cobble beds in this FA do not contain uniform oriented, bulleted, or striated clasts. This suggests that the boulder beds are lags; that they formed due to winnowing (Eyles 1988), not subglacial processes.

This FA was more likely deposited subaqueously than subaerially. In most of the sections measured in this study, the upper contact of the diamictite is conformable with, and in some cases, gradationally transitions into, subaqueous facies' (HS Facies Association). At section RSP-18, the massive diamictite is interstratified with turbidites, a subaqueous process (see LS facies interpretation). Additionally, there are no characteristics in this FA that suggest subaerial exposure (e.g. paleosols, desiccation features, wind-transported sediments).

The lack of clear or laterally continuous stratification, as well as a wide range of grain sizes in the matrix throughout this diamictite, indicate that the deposition of these sediments was not principally controlled by "sorting" processes such as currents and/or low-density flows. The massive nature of beds may be a primary depositional feature, as is the case in subglacial deposits, supraglacial debris,

or subaqueous plume sedimentation. Alternatively, this facies may also be the result of secondary processes, such as re-deposition by mass-transport and high-density gravity-driven processes/flows (Wright and Anderson 1982; Vesely et al. 2018) or homogenization due to iceberg scour (Dowdeswell et al. 1994), dewatering (Collinson and Mountney 2019), or bioturbation (Svendsen and Mangerud 1997; Murray et al. 2013). Where crude stratification does occur, there are indicators that settling from suspension may be a key depositional process. Ruck structures beneath large clasts suggest those clasts were dropped into the surrounding diamictite from ice rafted debris (Fig. 2- 5D) (Thomas and Connell 1985). The thinning of diamictite beds over large clasts suggests that there was some component of settling from suspension in their depositional process (Fig. 2- 5H). In glaciomarine settings, this most often occurs as meltwater plume sedimentation.

Small, deformed, sorted sediment bodies occur in many depositional settings alongside diamictites, including in till (Kessler et al. 2012) and proximal glaciomarine sediments (Domack 1983; Sheppard et al. 2000). Depending on their depositional context, small sand bodies are proposed to be sourced from iceberg dumps, winnowing due to de-watering, or from incorporating subglacial sediment into till through freeze-on. The small sand and gravel bodies all indicate pervasive simple shear (whisps/stringers, boudinage, and sheath folds) or loading (diapir structures). In at least one case, shearing was associated with an overlying, thicker sandstone body (Fig. 2- 5F). If the diamictite experienced similar strain conditions, representative structures would likely be impossible to observe in outcrop, due to the homogenous natures of the diamictite. The large sand bodies are most likely mass-transport deposits that underwent slumping or non-turbulent flow (Posamentier and Martinsen 2011; Rodrigues et al. 2019).

The combination of processes (subglacial till deposition, iceberg rain-out, plume sedimentation, iceberg scouring, and mass-transport) that potentially contributed to the deposition of the massive

diamictite and related facies are most likely to occur in a glacier-proximal to glacier-intermediate (not distal or proximal) setting, with water depths below storm wave base (i.e. offshore-transition to offshore) (Licht et al. 1999; Powell and Cooper 2002; Powell et al. 2009). In the Cenozoic, comparable depositional models have been proposed for similar successions in the Yakataga Fm, Alaska (Eyles and Lagoe 1990), Weddell Sea, Ross Sea, and George V regions of Antarctica (Anderson et al. 1980; McKay et al. 2009), as well as St. George's Bay, Newfoundland (Sheppard et al. 2000). Of these examples, St. George's Bay is likely the most analogous to the Shackleton Glacier region during the Permian, since it is not an open shelf setting, but an embayment whose topography is controlled by much-older basement rocks (Batterson and Sheppard 2000; Shaw 2016).

Plumes emitted from subglacial and englacial meltwater jets were likely the primary sources of sediments in this system. Plume sedimentation is not likely to occur where the glacier meltwater is denser than the ambient water in the depositional environment; a condition associated with lacustrine conditions and resulting hyperpycnal flows. Therefore, the deposition of this facies most likely occurred in marine or estuarine conditions (Powell 1990). Variations in iceberg calving, fluctuating glacial hydraulic systems, and minor movement of the ice margin, may explain the variation of matrix grain size and clast abundance throughout the facies. Glacial hydraulic systems and icebergs capable of producing sufficient sediment to create this FA are characteristic of temperate to "mild" subpolar glaciers (Matsch and Ojakangas 1991; Hambrey and Glasser 2012; Dowdeswell et al. 2016; Kurjanski 2020).

The time frame in which the deposition of this facies occurred is difficult to infer, especially without any evidence within the facies for glacier grounding above its lower contact. Sedimentation rates in glaciomarine settings are highly variable, even for the same glacier, and strongly depend on glacier conditions and proximity to the ice front (Hallet et al. 1996). Rates of accumulation will also depend

on physiography of the depositional area (e.g. fjord vs. open shelf). Accumulating ~100 m of glaciomarine diamictite could take anywhere from a few years (Cowan and Powell 1991) to a few millennia (Partin and Sadler 2016; Domack and Powell 2018). The lack of non-glacigenic deposits (see LS and HS facies descriptions for glacial interpretations) interstratified with the MSD facies, suggest that the deposition of this facies occurred on the shorter end of this time scale.

2.5.2. Laminated Sands Facies Association (LS)

2.5.2.1. LS Description

This is a sandstone FA that occurs only at site RS-18 and is interstratified with facies MSD. This succession is ~17 m thick and laterally continuous across the outcrop. Its lower contact is erosional above MSD and its upper contact was covered. Internally, this FA consists of fining-upward packages 3-5 m thick (Fig. 2- 6). This FA consists of coarse- to fine-grained, well-sorted sandstones. The dominant lithology in this FA is fine- to medium-grained sands that occur in thin, horizontally laminated beds with primary current lineations. Coarse-grained sandstones at the base of some packages are trough cross-bedded. Fine- to very-fine grained sandstones are laminated, or thinly-bedded with unidirectional cross-laminations and/or ripples. The sandstone is quartz-rich and grains are sub-angular to rounded. Pebbles up to 8 cm in diameter occur at the base of some cross-beds. The uppermost portions of fining-upward packages sometimes include fine- to very-fine-grained black-colored sandstone.

2.5.2.2. LS Interpretation

This FA is most likely the result of a series of non-cohesive density flow events, either in the form of high-density turbidites and/or a transitional concentrated density flows (Mulder and Alexander 2001). Fining upward sequences such as these could also be formed in a fluvial or shallow marine setting, where bedload-dominated currents are common. However, a fluvial setting is inconsistent

with the lack of channelization or indication of surface exposure in the RSP-18 succession. Similarly, a shoreface setting is unlikely because there is no evidence of emergence or wave action in the succession. The current directions measured in this unit are unidirectional, which is also not indicative of a shoreface. Since these turbidites are interstratified with facies MSD, they are most likely the distal or medial portion of an ice-contact fan or delta (Lønne 1995; Dowdeswell et al. 2015).

Figure 2-6. Photograph of the Laminated Sands (LS) facies association at site RS-18 (Reid Spur). Triangles show fining-upward packages separated by erosional surfaces. Reddish lithologies are medium sandstone to coarse-grained sandstone, and have planar laminar and low-angle cross-stratification. Black lithologies are fine-grained sandstones.

2.5.3. Heterogenous Sandy Facies Association (HS)

2.5.3.1. HS Stratigraphy

This FA (Fig. 2- 7) occurs at both Mt. Butters sites above a gradational contact with the massive diamictite (MSD), and below a sharp, erosional contact with the cross-bedded sands facies (CBS) at MBSE-17 and a sharp, horizontal contact with the Mackellar Fm at MB-17 (Fig. 2- 8). The lower part of the facies association begins as interbedded, discontinuous bodies of deformed, sorted sands and gravels (facies HS2) within stratified diamictites (facies HS1). Undeformed, moderately- sorted, stratified sandstone bodies with a range of grain-sizes (facies HS3) occur in the middle of the succession and eventually become the dominant facies near the top of the succession. This FA ranges in thickness from 1 – 15 m. Lithologies in this facies are inter-stratified.

2.5.3.2. Facies HS1: Stratified diamictite

Description

This facies is a clast-rich, sandy diamictite (Figs. 7D, G, I, 8). This diamictite facies is similar to the massive diamictite facies (MSD), but is consistently stratified, is more clast-rich, and the matrix is better sorted. The matrix in this facies is moderately- to well-sorted. Matrix grain sizes range from medium to very-fine sand. The mean matrix grain size varies between beds. Most beds have a mean matrix grain size of medium-sand, but some beds have a dominantly very-fine-grained sand matrix. Clasts in this facies are angular to sub-rounded, and have a similar size range as MSD, granule to 1 m boulders. The beds in this facies are 3-7 cm thick, are horizontal, laterally discontinuous, and have sharp contacts. The distribution of clasts is random and unrelated to bedding planes. Larger clasts often punctuate bedding planes. This facies has a gradational lower contact overlying the massive diamictite (MSD) facies. Vertical and lateral contacts with other facies in this FA (HS3 and HS2) are most often sharp, sometimes loaded, deformed, or erosional. This bedded diamictite is frequently

interbedded with facies HS2. Strata in this facies adjacent to contacts with facies HS2 often display soft-sediment deformation, including load structures and sheared contacts.

Interpretation

Similar to facies MSD, this facies was likely deposited in a glacier-proximal glaciomarine setting, but was dominated by plume sedimentation and iceberg rainout (Eyles 1987; Licht et al. 1999; Powell and Domack 2002; McKay et al. 2009). The consistency of the stratification in this facies compared to the MSD facies suggests that the sediment in this facies was not as frequently subject to remobilization, either through gravity-driven transport or iceberg scour. The better sorting of the matrix in this facies relative to the massive diamictite facies indicate that sediment-sorting processes were more active than during the deposition of MSD. In a glacial-proximal setting, this likely means that turbulence kept fine-grained sediment suspended in the water column and did not allow it to settle out. The clast-rich composition and thin nature of the beds also suggest that depositional processes were relatively constant, compared to the high variability of clast-contents in facies MSD. Loaded, deformed, and erosional contacts within this facies, and with other facies in this FA, indicate that this facies was rheologically "weak", or experienced ductile deformation at low strains. Therefore, during and shortly following deposition, facies HS1 was likely water-saturated. This also suggests that that sedimentation was rapid, that this facies was subject to gravity-driven processes, and that these sediments were deformed by gravity-driven deposits (Figs. 7D, 7F, 8) (Visser 1994).

2.5.3.3. Facies HS2: Chaotic Sandstones

Description

This facies is comprised of very fine- to coarse-grained sandstones (Figs. 7A-C). Beds in this facies are laterally discontinuous (Figs. 7G, 8). The thicknesses of sandstone bodies are laterally inconsistent and range in thickness from 0.5 m – 2 m. Widths of sandstone bodies range from ~1 m

to outcrop scale. Sandstone beds may be interbedded with one another, but are dominantly interbedded with the surrounding either massive (MSD FA) of stratified (HS1) diamictite facies. Sandstone bodies are irregularly shaped, but generally have planar to lenticular shapes. Lower and lateral contacts are deformed, sharp, or erosional, and often show evidence of soft-sediment deformation (Figs. 7D, F). Upper contacts are sharp and conformable. Contacts between sandstone bodies are erosional or loaded/deformed.

Beds in this facies are often internally massive and soft-sediment deformation is pervasive (Figs. 7E, F). Primary sedimentary structures are sometimes preserved, but this is rare and only occurs in a small area of any given bed. Secondary structures in this facies include fold noses (Fig. 2- 7E), boudins, faults, and other simple shear structures above and below contacts (Figs. 7D – G), and ruck structures associated with rare outsized clasts (Fig. 2- 7I). Grain size in this facies ranges from conglomerate to very-fine-grained sandstone. Fine- to medium-grained sandstones tend to be well-sorted, while coarse-grained sandstones and conglomerates are poorly sorted. The medium- and coarse-grained sandstones occur more frequently than finer-grained lithologies.

Interpretation

The sandstone bodies in this facies are most likely the result of mass-transport, gravity-driven processes (Posamentier and Martinsen 2011; Sobiesiak et al. 2018; Rodrigues et al. 2019). Preserved primary sediment structures in some of these bodies indicate that sediment sorting due to current transport likely occurred before the remobilization and final deposition of these sediments. Irregular lateral contacts between this facies and the two diamictite facies (HS1 and MSD) indicate that mass-transported bodies were sandstone rafts deposited into pre-existing diamictites by gravity driven processes. The deposition of mass transport deposits (MTD) into the diamictite indicates that diamictite deposition was contemporaneous with MTD emplacement. This also suggests that the

diamictite was weak (highly susceptible to deformation), likely due to high pore-water pressures/lack of consolidation.

2.5.3.4. Facies HS3: Stratified Sandstones

Description

This facies is comprised of very fine- to coarse-grained sandstones (Figs. 7A-C). Medium- to coarse-grained sandstones are thickly laminated to bedded. Common sedimentary structures in medium- to coarse-grained sandstones include planar cross beds, trough cross beds, climbing ripples, 3D ripples that are asymmetric or climbing (Fig. 2- 7A). Rare sedimentary structures include hummocky and swaley cross stratification and symmetrical ripples with bundled upbuilding (Figs. 7B, 7C). Lateral and vertical variations in sedimentary structures within a unit of the same lithology/grain-size is common. Coarser sands are occasionally massive or contain laterally discontinuous sand or gravel lenses. Trough cross-beds occasionally have pebbles at the bases of troughs. Very fine- and fine-grained sandstones are laminated or thinly bedded. Sedimentary structures in fine-grained and very fine-grained sandstones include uni-directional cross-laminations/ripples, planar and wavy laminations, some flaser bedded cross-laminated units, climbing-ripple laminations, and rare outsized clasts with ruck structures. Lithologies of all grain sizes also have minor amounts of soft-sediment deformation, including dewatering structures, minor folds, and loading.

At the upper contact of the Heterogenous Sandy FA with the Mackellar Fm in section MB-17 (Fig. 2- 10), these sandstones had at least five large, shallow, east-west oriented grooves (Table 2) that occur within a massive, well-sorted sandstone (Fig. 2- 7H). All grooves were ~1-2 m wide and 10 cm deep. Berms ~10 - 20 cm high bound the grooves on their long sides. All of the grooves gradually shallow towards the west (215°), and two of the groves had prow-like berms at their eastern terminus.

Strata in this facies are laterally continuous across the outcrop. Sandstone bodies are generally wedge-shaped and thicken in the direction of flow. Erosional surfaces are common within the facies. This facies has an erosional lower contact with both diamictite facies (MSD and HS1), and a sharp, conformable contact with overlying UFG facies association.

Interpretation

This facies was likely deposited rapidly in an unconfined, sub-aqueous setting with limited reworking by waves and icebergs. The sedimentary structures in this facies indicate that current-dominated transport and deposition occurred, followed by syn- or post-depositional slumping of some deposits. The wide range of grain sizes and sedimentary structures indicate a sediment source with a wide range of grain sizes and huge variations in current velocities during deposition. Common sedimentary structures, such as planar cross beds, trough cross beds, and asymmetrical ripples suggest unidirectional, relatively high-velocity currents. Climbing ripples suggest decrease in flow velocity downcurrent, which is characteristic of unconfined flows, which is supported by the lack of channelized deposits. Flaser bedding, as well as abrupt changes in grain size and sedimentary structures within and between beds, indicates that current velocities were highly variable and fluctuated. Rare soft-sediment deformation suggests high pore-water-pressure during rapid deposition. Rare hummocky and swaley cross-stratification and symmetrical ripples form under oscillatory flow conditions created by surface waves, possibly during reworking by storms (Reineck and Singh 1980; Dumas and Arnott 2006; Collinson and Mountney 2019). Their rare occurrence and inter-stratification with fine-grained sediments suggest that these wave features formed below normal wave base. The shape of the grooves on the upper contact of this FA at site MB-17, their position in the upper contact of a massive (homogenized) sandstone, and immediately below the contact with the dropstone-bearing lower Mackellar Fm suggest that these features are iceberg keel

marks (Dowdeswell et al. 1994; Vesely and Assine 2014). These massive sandstones were likely deposited in a similar way to other sandstones in this facies, but were homogenized by iceberg actions.

2.5.3.5. HS Depositional Environment

The three facies in this FA represent a complex depositional environment that is characteristic of subaqueous, glacier-intermediate to -proximal settings in front of the terminus of temperate to "mild" subpolar glaciers. Evidence for the glacigenic origin of this FA includes pebbles with ruck structures (representing ice-rafted debris), iceberg keel marks (facies HS3), the very poor sorting of sediment in the system, and the wide range of sedimentary grain shapes in the Pagoda Fm sandstones, which are described at the beginning of the facies section.

The stratified diamictite (facies HS1) was deposited primarily through plume sedimentation in a glacier-proximal setting, and is the dominant, or "background", sedimentation type in this FA. The gradational contact separating MSD (massive diamictite) and facies HS1 suggests a gradual shift in depositional environments between the two. Sediment composition is consistent between the two diamictite facies, suggesting that the sediment source did not change, but that the depositional environment shifted from glacier-intermediate to glacier-proximal. The deposition of both diamictites was likely controlled by the same processes (i.e. plume sedimentation, iceberg rain-out, iceberg scouring, and mass-transport) but to different degrees. This shift from glacier-intermediate to glacier-proximal was most likely driven by a minor re-advance of the glacier margin, but it may have also been an apparent effect caused by the progradation of the overlying grounding-line fan system (HS2 and HS3).

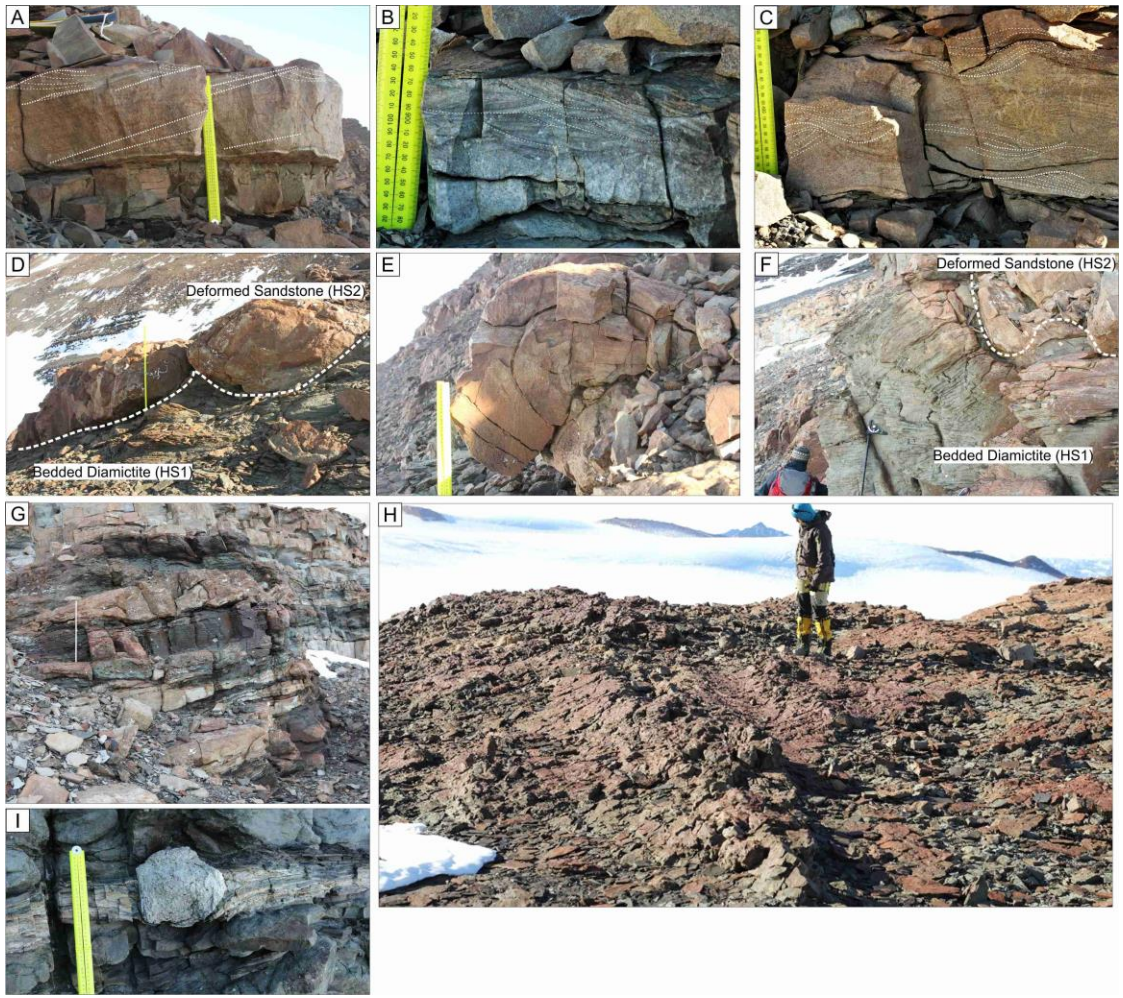

Figure 2-7. Photographs of the Heterogenous Sandy (HS) facies association at Mt. Butters in section MB-17 and MBSE-17. Marks on all rulers are in cm. Rulers are 50 cm when folded in half, and 1 m long when unfolded. White dashed lines have been used to highlight contacts and important bedding surfaces. **A.** Medium-grained sandstone layer in facies HS3. Sandstone body composed mostly of climbing dunes (cross beds) and capped by asymmetrical ripples. Note sharp contact with black-colored, bedded diamictite (facies HS1) in lower part of image (MB-17) **B.** Fine- to – medium grained sandstone in facies HS3 with up-building symmetrical ripples (MB-17)**. C.** Swaley and hummocky cross-stratification in sandstone layer of facies HS3 (MB-17). **D.** Loaded, possibly boudinage, contact between a massive sandstone (HS2) and bedded diamictite (HS3) (MB-17). **E.** Sandstone with a soft-sediment recumbent fold nose in facies HS2, likely at the front of a slump. (MB-17). **F.** Deformed contact between facies HS2 and HS3. Jacob's staff for scale – marking every 10 cm. (MB-17) **G.** Outcrop showing inter-fingering between facies in this facies association. Black-colored sediments are bedded diamictites (facies HS1), other lithologies show sand and gravel of facies HS2. (MB-17) **H.** Groove structures on top of facies HS1. View approximately toward north (down the Shackleton Glacier). **I.** Granitic outsized clast punctuating inter-laminated sandstone beds within the bedded diamictite facies HS1. (MB-17).

The sandstone facies in this FA (facies HS2 and HS3) most likely represent the medial portion of a subaqueous grounding-line fan(s) system (Powell 1990; Lønne 1995; Dowdeswell et al. 2015). In facies HS3, the high-velocity, unidirectional current transport combined with abrupt changes in grain size (i.e. current velocity), unconfined flow, and interstratification with the bedded diamictite (facies HS1) are characteristic of grounding-line fans (Powell 1991). The gravity-driven transport of facies HS2 sandstone bodies were likely derived from deposits similar to (or the same as) facies HS3. "Shedding" of sediments is characteristic of the rapid sedimentation in grounding-line fan systems (Benn 1996; Powell and Alley 1997; Lønne et al. 2001). Intense, ductile deformation and loading along contacts throughout this FA indicate that all facies were water-saturated, unconsolidated, and generally had the consistency of soup, suggesting rapid deposition and that they were therefore prone to resedimentation (Fig. 2- 8B).

The wave reworking of some sandstone beds, as indicated by hummocky and swaley cross-stratification and wave-ripple stratification (symmetrical ripples) in facies HS3 suggest that this depositional environment was occasionally subjected to surface-wave activity (below normal wave base). These features indicate that there was not perennial ice cover during the deposition of this FA. This evidence for wave reworking may also suggest a similar, wave-winnowing origin for the boulder beds in facies MSD.

Where this FA is well-developed in outcrops at Mt. Butters (sites MB-17 and MBSE-17), the succession has a general coarsening and increase in sorting trends upward. This trend indicates the increase in the proximity of the energy and sediment source, either through progradation of the grounding-line system and/or advance of the glacial front.

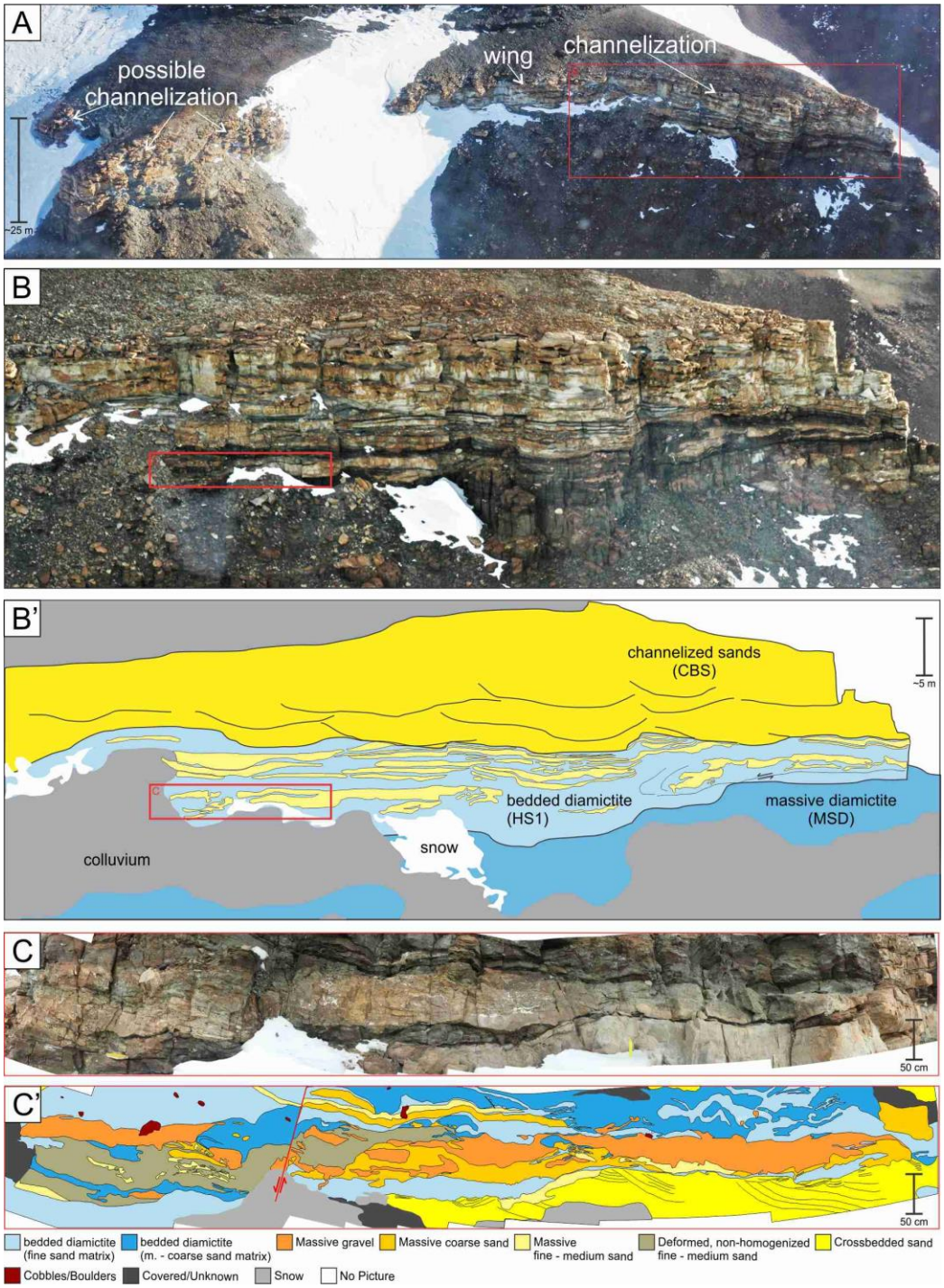

Figure 2-8. Photo mosaics (A, B, and C) and interpretive sketches (B' and C') of the upper portion of section MBSE-17 at Mt. Butters. Mosaics A and B were taken from a helicopter, and mosaic C from the ground. This is the opposite side of the outcrop shown in Figure 2-4C. View is to the north, and the ridge runs roughly east-west. Figure **A** shows lateral variations in the architecture of the cross bedded sandstone (CBS) facies. Figures B and B' highlight the stratigraphic relationships between Massive Diamictite (MSD) facies association, Heterogenous Sandy (HS) facies association, and the CBS facies association. Black lines in CBS denote channel erosional surfaces. Black lines in HS3 indicate soft-sediment deformation. The part of this outcrop highlighted by **C** and **C'** is located within the red box on **B.** Figure **C** shows a portion of the outcrop is characteristic of the HS facies association, and was selected to illustrate the pervasive nature of soft-sediment deformation within this facies association.

2.5.4. Cross Bedded Sandstone Facies (CBS)

2.5.4.1. CBS Description

This facies occurs at Mt. Butters section MBSE-17, and consists of an erosive-based, laterally extensive, channel-form, sandstone body 10-30 m thick and several hundred m wide that cuts into and through a laterally continuous thick sandstone sheet at the top of a coarsening upward succession of the HS (1-3) facies association (Figs. 8, 9). The sandstone body is laterally continuous across outcrop MBSE-17 but is not present at section MB-17, which is ~2 km north (Fig. 2- 1B). The basal CBS erosional surface has a relief of up to 10 m, and lower contacts with all HS facies and the MSD facies. This facies' upper contact with the overlying Mackellar Fm is sharp and horizontal.

This facies occurs within multi-storied, multi-lateral sand-filled channel-form bodies displaying non-sequential, lateral compensational stacking patterns (Fig. 2- 9). Individual channels are m-scale thick and 10s of m wide, trough-shaped in cross section, and are filled by either vertical or downstream accretion dipping in an easterly direction. Channels are truncated by the base of overlying channel bodies. Channel stacking is non-sequential and disorganized, with some aggradation. This facies is comprised of well-sorted, medium- to very coarse-grained quartz sandstone, with minor occurrences of conglomerate lenses and beds (Fig. 2- 9). Mudrocks were not observed within the sandstone bodies. Very rare pebble- and small-cobble-sized clasts occur throughout the sandstones. Those clasts have similar lithologies to clasts observed in both diamictite facies (HS1 and MSD). Sedimentary structures are almost exclusively 0.15 to 1.5 m thick sets of low-angle stratification and trough cross-beds (Fig. 2- 9A). Thin beds with asymmetrical ripples also occur but are rare.

Adjacent to the described section (MBSE-17), the edge of the channel-form body appears to extend across the top of the underlying strata as a wing-like extension (Fig. 2- 8A). Channel-form sandstone bodies occur within the wing. These bodies appear to transition laterally into other thick sandstones

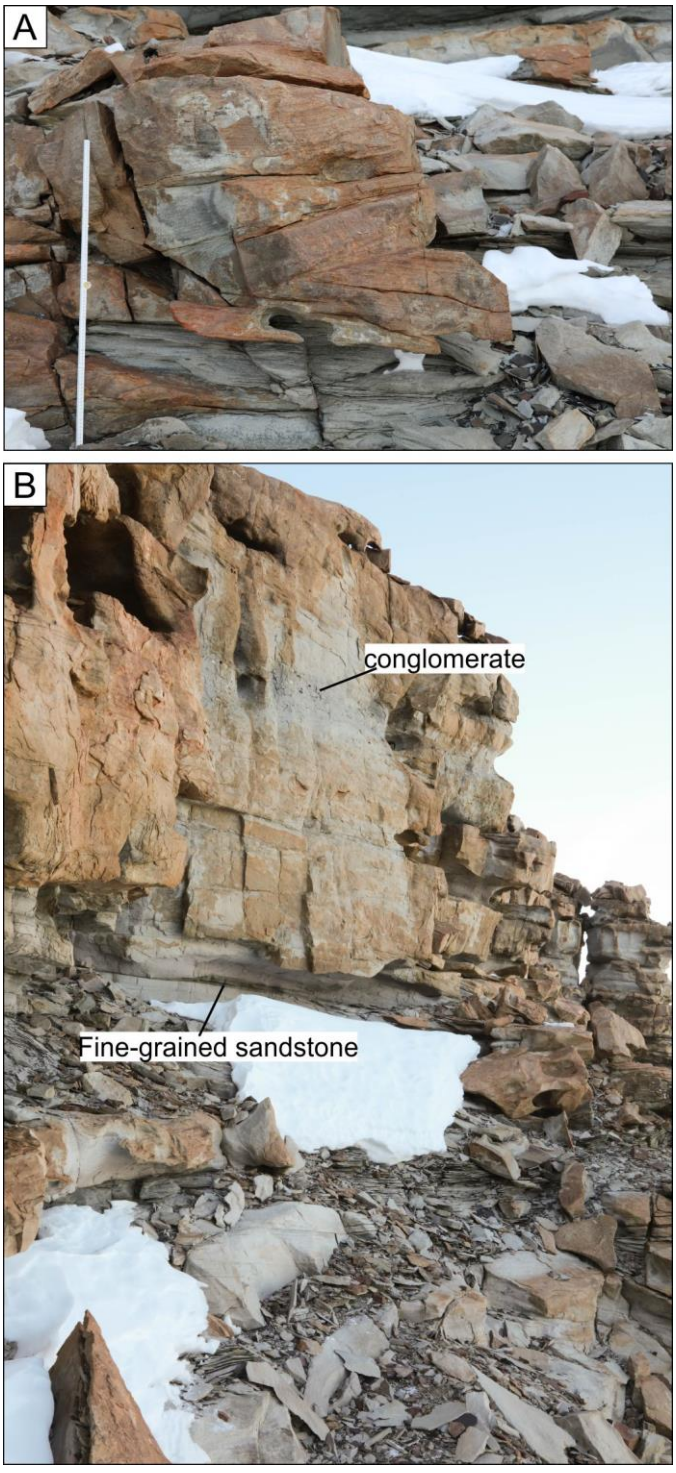

Figure 2-9. Photographs of the Cross Bedded Sandstone (CBS) facies at section MBSE-17 on Mt. Butters.
A. An example of low angle and trough cross-bed sets in this facies. Measuring stick in 1m long. **B.** Photograph of facies in outcrop noting occurrences of minor lithologies.

with channelized bases. Most notably, the contact between the channelized sandstones in the wing and the underlying HS facies appears to be sharp.

2.5.4.2. CBS Interpretation

The CBS facies in the Pagoda Fm was deposited by strong, tractive, confined flow as indicated by the occurrence of the basal erosion surface and the internal channel bodies filled by down-stream accreting bar forms and cross-stratification. The trough-shape of the internal sandstone-filled channels and their multistoried and multilateral characteristics suggest that the channels were stationary during flow within the channels and that they did not migrate until channel switching occurred and new channels formed as older channels filled and were abandoned (Friend 1983). The occurrence of low angle stratification and m-scale trough cross beds organized into down-stream accreting bodies with massive bedded to lenticular gravels suggest high

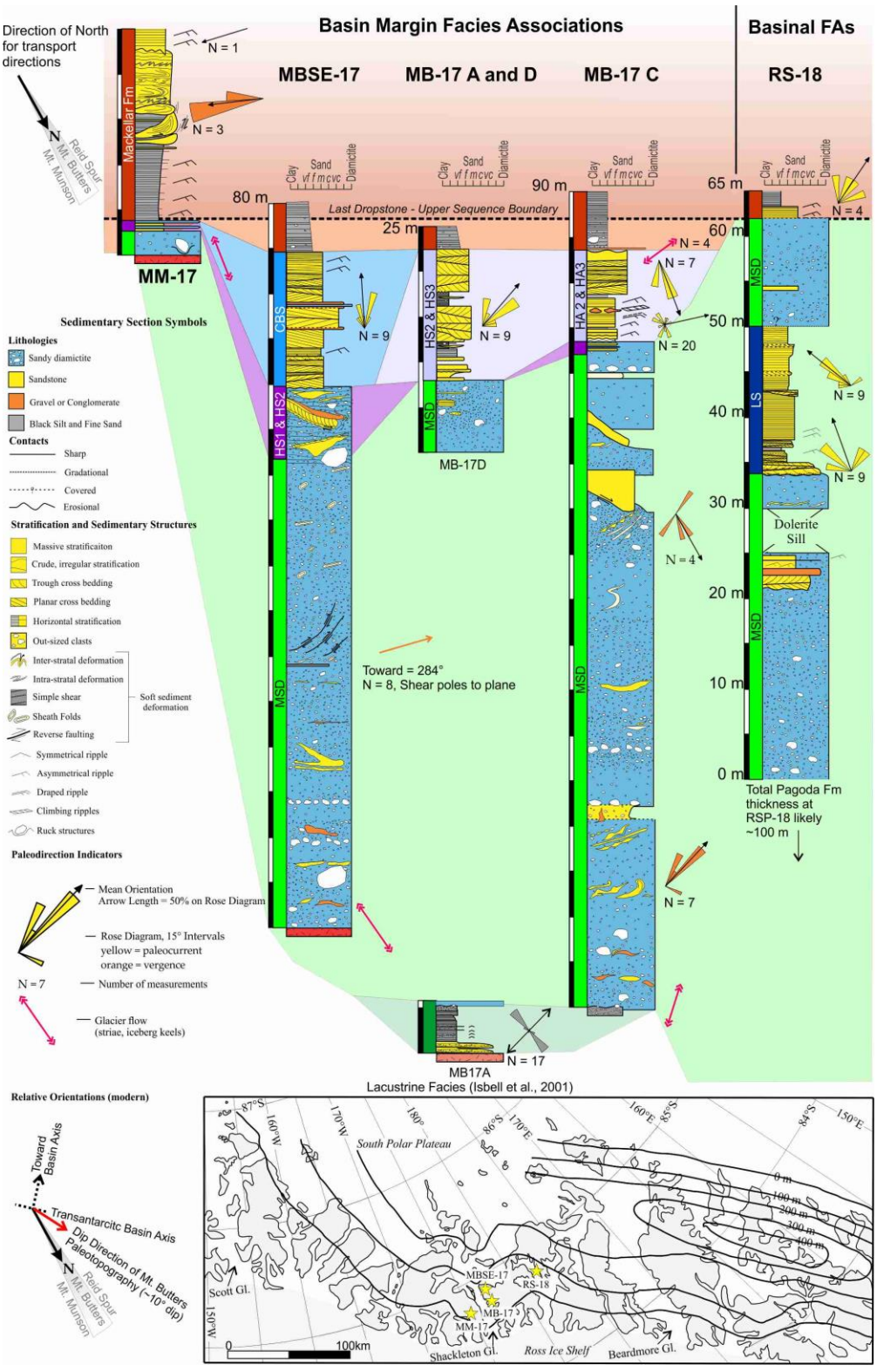

Figure 2-10. Sedimentary logs and paleotransport directions from sites described in this study. Paleotransport directions are plotted to align with the maps of modern Transantarctic Mountains presented in this study, so that north is toward the bottom of the page and varies by geographic position (see inset map). Details of paleotransport measurements are available in Table 2. MM-17 is Mt. Munson, MB-17(A-C) is Mt. Butters 1, MBSE-17 is

(figure 2-11, continued) Mt. Butters 2, and RS-18 is Reid Spur. Lithologies are grouped by their interpreted facies or facies association. Colored bars next to each log are used to indicate the distribution facies associations in these sections, and colored areas in between sections show interpretation of each facies extent outside the section. Dark green corresponds to the localized lacustrine facies of the Pagoda Fm at Mt. Butters described by Isbell et al., (2001). Bright green represents the Massive Sandy Diamictite (MSD) facies association. Different shades of purple represent grouping of the Heterogenous Sandy facies association (HS1 – stratified diamictite, HS2 – chaotic sandstones, HS3- stratified sandstones). The inset map shows the location of each section and isopachs of the Pagoda Fm in the Beardmore Sub-basin from Isbell et al. (2008c). Light blue represents the Cross Bedded Sandstone facies (CBS). Dark blue represents the Laminated Sandstone facies association (LS). Red represents the Mackellar Fm. The datum for these columns were chosen using the last evidence for glacigenic sediments, either the uppermost outsized clast or diamictite, which is a marker that also serves as an upper sequence boundary.

flow velocities. Such features are characteristic of highly dynamic systems where aggradation within channels likely forced channel switching to adjacent areas on the depositional surface. The occurrence of this facies association on top of unconfined coarsening-upward HS (1-3) facies association and the occurrence of wings that appear as a continuation of the HS (1-3) coarsening upward succession suggest that the CBS facies formed as part of a HS-CBS larger-scale dispersal system. The presence of wings also suggests that parts of the CBS system were unconfined and represent "overbank" deposition on surfaces in areas between channels. Together, these patterns are most characteristic of an unconfined, distributive setting (Funk et al. 2012). This unit is similar to some grounding-line fan systems that authors have called sub-aqueous outwash fans (Visser et al. 1987; Thomas and Chiverrell 2006; Rose 2018).

Whether this facies was deposited subaerially or subaqueously is unclear. However, the CBS sandstone body does not contain evidence for shallow water wave reworking, pedogenesis, or subaerial exposure; whereas, facies both below and above this facies represent subaqueous deposition below normal wave base, and likely below storm wave base. Therefore, a subaqueous setting seems likely.

2.6. Depositional Model

The majority of the Pagoda Fm in the Shackleton Glacier Area is composed of massive diamictites (facies MSD) that likely formed in glacier-proximal to glacier-intermediate environments, at depths largely below normal wave base, through a variety of glacigenic and glacially-influenced processes. These massive diamictites are also conformably overlain by, and interstratified with, grounding line fan deposits (facies associations LS, HS, and CBS). These glacially derived lithologies are conformably succeed by pro-deltaic, fine-grained facies of the Mackellar Fm.

Evidence for the grounded advance of a glacier(s) in the Shackleton Glacier region is present at the base of the MSD facies at both Mt. Butters' sites (MB-17 and MBSE-17) and at Mt. Munson (MM-17). The lower contact of the MSD facies is not exposed at Reid Spur, so similar inferences cannot be made for that locality. No conclusive evidence for subglacial deformation or erosion was observed higher in the Pagoda Fm at any site examined, though a subglacial origin for the MSD facies cannot be wholly ruled out. This advance was likely made by a glacier whose thickness exceed 100 m and flowed from north to south across the Shackleton Glacier region; from the direction of the present Ross Sea crossing basins margins perpendicular to the elongate trend of TAB (See discussion in prior section; Fig. 2- 11D). This observation, along with other data from the TAB strongly suggest that there were at least two ice centers in Antarctica during the Permian, one located on the East Antarctica craton and one in present day West Antarctica (Isbell 2010).

When the glacier margin retreated from the Mt. Butters, Mt. Munson, and Reid Spur sites, the deposition of glacier-proximal deposits was initiated. The massive diamictite (MSD) facies that dominated the Pagoda Fm at Mt. Butters and Reid Spur (RSP-18) was likely deposited through a combination of glacigenic depositional processes characteristic of (*sensu lato*) glaciomarine settings; a combination of settling from suspension of neritic sediments, plume sedimentation from subglacial

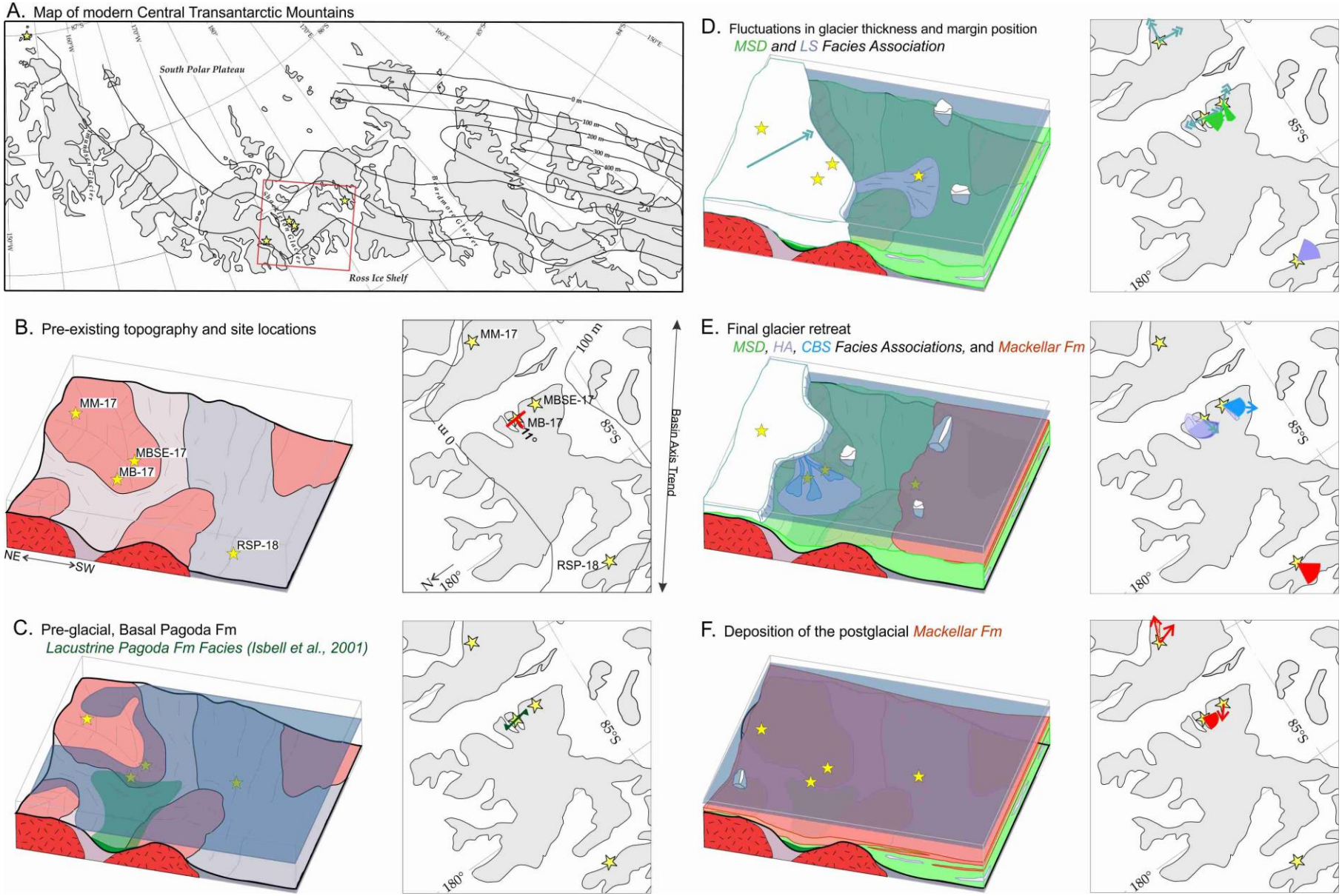
A. Map of modern Central Transantarctic Mountains
South Polar Plateau
Ross Ice Shelf
B. Pre-existing topography and site locations
MM-17
MBSE-17
MB-17
RSP-18
NE
SW
100 m
0 m
111°
85°S
180°
N
Basin Axis Trend
C. Pre-glacial, Basal Pagoda Fm
Lacustrine Pagoda Fm Facies (Isbell et al., 2001)
D. Fluctuations in glacier thickness and margin position
MSD and LS Facies Association
E. Final glacier retreat
MSD, HA, CBS Facies Associations, and Mackellar Fm
F. Deposition of the postglacial Mackellar Fm

Figure 2-11. Box diagrams showing progressive phases of the depositional model for the Pagoda Fm and lower-most, glacially-influenced Mackellar Fm in the Shackleton Glacier region, alongside maps showing the modern locations of the sites described in this study with transport orientations related to each part of the depositional model See Table 3 for flow directions. **A.** Map of the modern central Transantarctic Mountains. Grey areas are approximate locations of nunatuk regions. Solid black lines are isopachs of the Pagoda Fm, copied from Isbell et al. (2008c). Red square indicates map area in parts B – F. Note that the smaller map areas are rotated relative to the larger "map A". Yellow stars show site locations described in this study. **B.** Paleotopography of the Shackleton Glacier Area prior to deposition of the Pagoda Fm. Map shows strike and dip of granite surface underlying the Pagoda Fm at Mt. Butters site MB-17, corrected for modern structural conditions. This map also includes the Isbell et al. (2008c) isopach lines and derived basin axis orientation for reference **C.** Proposed depositional conditions for the lacustrine facies at the base of the Pagoda Fm at site MB-17 (Isbell et al., 2001). The green, double-sided arrow shown on the map shows the orientation of symmetrical (wave) ripple crests, which parallels the strike of the underlying basement. **D.** Proposed depositional conditions for Massive Sandy Diamictite (MSD) facies and Laminated Sands (LS) facies during retreat of the glacier out of the Shackleton Glacier area. On the map, purple wedge indicates range of flow direction in the LS facies, green wedges indicate down-slope transport direction in the MSD facies. Blue double-headed arrows show glacier flow directions measured in this study. **E.** Proposed conditions during the deposition of the grounding-line fan represented by facies associations MSD, Heterogenous Sandy (HS), Cross-bedded Sands (CBS), and Mackellar Fm. The red wedge shows range of flow directions in the Mackellar Fm, blue and purple show the range of flow direction for the CBS and HS flow directions, respectively and the blue arrow indicates the mean flow direction of the CBS facies at site MBSE-17. **F.** Proposed conditions during the deposition of the lower Mackellar Fm.

and englacial jets, as well as iceberg sedimentation and mixing. The prevalence of plume sedimentation and lack of hyperpycnal (under-) flow, indicate that the water within the TAB was likely either marine or brackish. It should be noted that the TAB did not have a shelf, in the formal sense, as it was a trough-shaped basin that was not directly connected to the open ocean.

The Shackleton Glacier region during the Cisuralian was not an open shelf, but a near-coastal setting with ample topographic relief, and water depths below normal wave base, such as St. George's Bay, Newfoundland (Sheppard et al. 2000). Ultimately, many of these sediments were likely remobilized by gravity-driven slides, slumps, and flows. This is especially true at the Mt. Butters site, where the vergence of soft-sediment deformation features in the MSD facies follow the local paleotopographic slope (Figs. 11B, E). Soft sediment deformation caused by mass-transport deposits (facies HS) within bedded diamictites at Mt. Butters shows that the diamictites were unconsolidated, water-saturated, and subject to resedimentation, suggesting relatively rapid deposition.

At Mt. Butters and Reid Spur, massive diamictites are inter-stratified with and overlain by grounding line fan deposits in the form of the LS, HS, and CBS facies associations. The stacked density flows (facies LS) at Reid Spur represent the medial to distal portion of a fan, likely in relatively deep water. Flow directions in these sediments are towards the basin axis (Fig. 2- 11D), suggesting the basin geometry controlled topography in this area. On the other hand, the fan deposits at Mt. Butters are more proximal to the glacier margin. The laminated diamictites, reactivation surfaces, and storm-wave deposits in the fan at the top of the Mt. Butters section (MB-17 and MBSE-17) suggest this fan was built gradually along a relatively stable margin and not during a single, catastrophic drainage event (Dowdeswell et al. 2016). The successions at Mt. Butters from the HS facies association through the CBS facies association represents either the progradation of one of these fans, a minor readvance associated with the deposition of the fan, or a combination of the two (Fig. 2- 11E). The dispersed flow directions within the HS facies are characteristic of a fan, though their orientation broadly toward the north is away from the basin axis and opposed to glacier flow directions. Flow directions in the CBS facies are well clustered toward the south-west (Table 2, Fig. 2- 11E). Influence of the paleotopographic slope at Mt. Butters and the radial nature of fan geometries are the most likely cause for these seemingly antagonistic flow directions (Fig. 2- 11E). The orientation of the ice front would have also likely been influenced by this topography.

2.7. Stratigraphic Framework

2.7.1. Basin Margin vs. Basinal Facies Associations

Isbell et al. (2008c) described two generalized facies associations of the Pagoda Fm; one that occurs in basinal settings and another that occurs along the basin margins. The sites described in this study from Mt. Munson and Mt. Butters in the Pagoda Fm are characteristic of the Basin Margin FA, because they are relatively thin successions (<100 m) and have evidence for subglacial erosion in the

form of polished and striated bedrock (MBSE-17 and MM-17), and subglacially sheared lacustrine sediments (MB-17; Isbell et al. 2001). The site at Reid Spur (RSP-18) is also most characteristic of the Basin Margin FA, because diamictite facies there are thick, unstratified, and have a poorly-sorted matrix, suggesting plume sedimentation and gravity-driven redeposition. However, this section also likely represents a transition between the two facies associations. This is indicated by the LS facies at this site, which is attributable to the mid to distal portion of a grounding-line fan, and by the inferred thickness of the Pagoda Fm at Reid Spur (~100 m), which is the same as the transition thickness between Isbell et al. (2008c)'s two FAs.

2.7.2. Effects of Topography

The transport directions within these successions strongly suggest that paleotopography (relief on the Maya Erosional Surface) played a significant role in the deposition of the Pagoda in the Shackleton Glacier region. The influence of topography is particularly evident in the section MB-17 (Fig. 2- 11). The surface of the basement at MB-17 dips toward the west at 11° (Figs. 4, 11B; Appendix A). Wave ripple crests in facies BFG are parallel to the strike of the basement surface at MB-17 (Fig. 2- 11C), suggesting that the paleotopography created by this surface was sufficient to affect and orient wave action. The transport directions of slumping and other gravity-driven processes within facies MSD at both sites MB-17 and MBSE-17 are also generally towards the west (Figs. 10, 11D), following the same slope. Flow directions in the grounding-line fan facies associations (HS and CBS) have a wide spread ranging from the south-west toward the east. However, within the HS facies association at MBSE-17, gravity-driven transport is still towards the west (Figs. 10, 11E). The south-south-east flow directions in the turbidite facies (LS) at site RSP-18 do not align with the flow direction at Mt. Butters, suggesting that those facies have a separate origin from the Mt. Butter's grounding line fan(s) (Figs. 10, 11D).

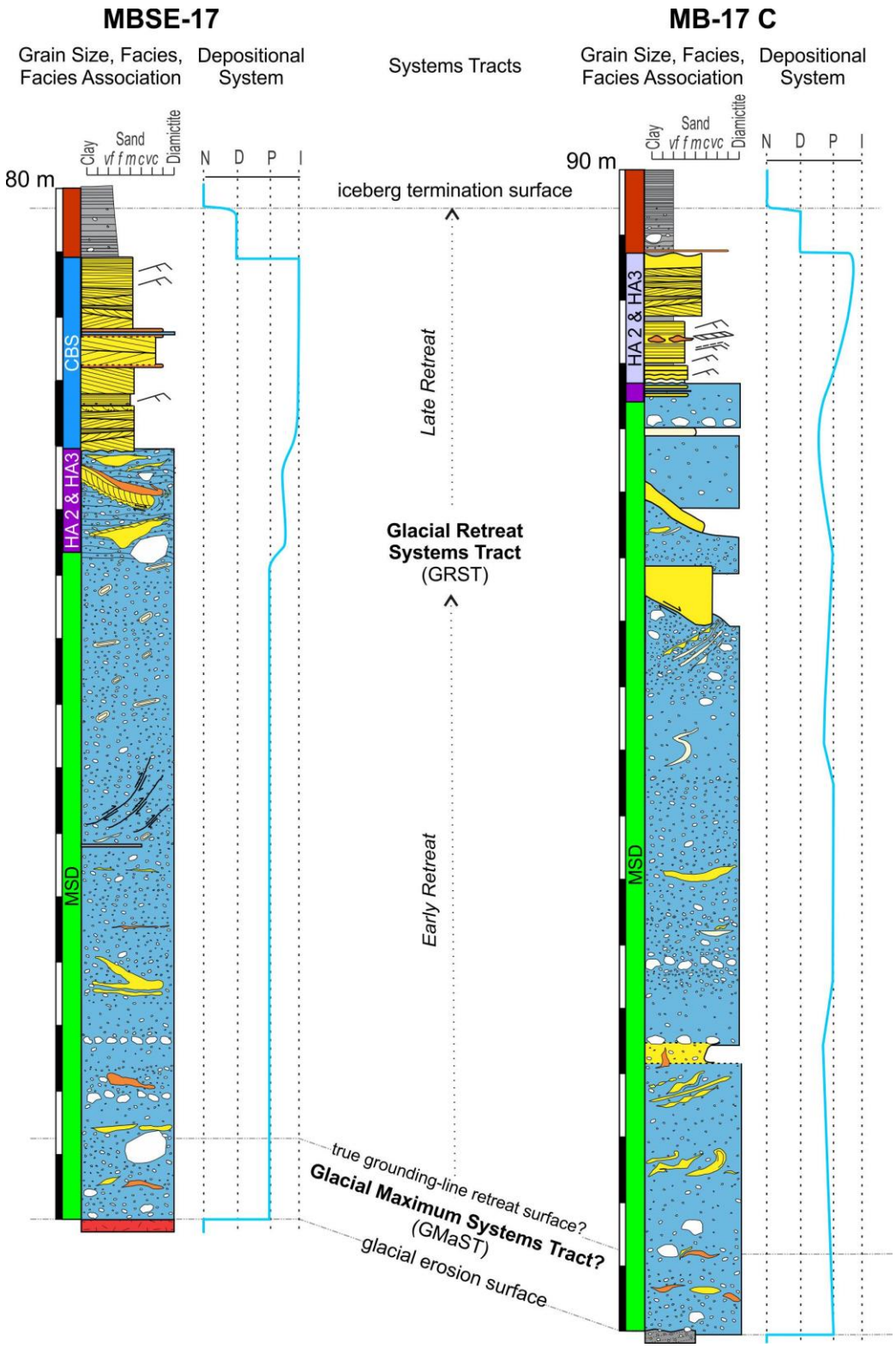

Figure 2-12. Glacial sequence stratigraphy of the Mt. Butters sections, after Powell and Cooper (2002) and Roseblume and Powell (2019). The depositional systems are defined as N = non-glacial, D = glacier distal, P = glacier proximal, and I = ice-contact.

Paleotopographic control on the deposition of Pagoda Fm and Mackellar Fm has been noted by authors throughout the TAB (Lindsay 1970b; Barrett 1972; Isbell et al. 1997a; Isbell et al. 2008c; Cornamusini 2017). In previous studies, ice-flow directions (usually striae on bedrock or clast pavements) have often been combined with other transport directions in the Pagoda Fm to infer a generalized transport direction. However, recent work in modern, high-relief, glaciated landscapes has shown that the relationship between glacier flow directions, other transport directions, and topography can be used to infer the thickness of the glacier relative to the magnitude of relief on the landscape (Landvik et al. 2014). In other words, whether a glacier "follows" the underlying topography is a function of the glacier's thickness. Therefore, indicators of glacier flow should be considered separately from other transport directions.

The ice-flow directions below the Pagoda Fm in the Shackleton Glacier region are oriented generally north-west to south-east at Mt. Butters and Mt. Munson (Fig. 2- 11D). Though none of the striae observed during this study had uni-directional indicators, previous workers in this area have found glacially-carved features in the basement underlying the Pagoda Fm that show glacier flow was basin-ward (toward the south) or along the basin axis (toward the south-east) (Appendix A). These uniform flow directions on both a paleo-topographic high (MM-17) and paleo-topographic low (MB-17 and MBSE-17) suggest that the glacier, when it created these striae, was sufficiently thick to "overtop" the pre-existing topography in the Shackleton Glacier Area. Based on the difference in Pagoda Fm thickness, the local relief between site MB-17 (Mt. Butters) and MM-17 (Mt. Munson) was at least 85 m, and the onlapping of the Mackellar Fm onto basement in this area suggest that localized relief may have exceeded 100 m (Seegers 1996; Isbell et al. 1997a; Seegers-Szablewski and Isbell 1998). This scale of relief is on the scale of large hills. The topographic prominence of subglacial features on the scale of 100 m is considered negligible in studies of modern ice sheet

margins (e.g., Lindbäck and Pettersson (2015); Cooper et al. (2019)), but would likely perturb or redirect the flow of relatively thin glaciers.

This discussion is all to say that the thickness of the glacier that created these striae more likely than not greatly exceeded the thickness of local topographic relief (~100 m), and that flow was most likely toward the center of the TAB. This inference suggests that the glacier was more likely an ice cap or ice sheet than an alpine glacier.

2.7.3. Glacial Systems Tracts

In this study, the sequence stratigraphy of the Pagoda Fm in the Shackleton Glacier region can only be considered at Mt. Butters, because that is the only location where the authors were able to measure complete sections. Since the Mt. Butters locations are basin-marginal successions (Fig. 2-11), this analysis of glacial sequence stratigraphy should not be considered applicable to basinal successions of the Pagoda Fm. The Pagoda Fm at Mt. Butters is unique within the TAB because it contains only a single glacial sequence as defined by Powell and Cooper (2002) and Rosenblume and Powell (2019) (Fig. 2- 12). The sequence described in this paper is bounded at its base by a surface of glacial erosion (defined by striae on bedrock and the deformation of underlying lacustrine sediments (see Isbell et al. 2001)), and at its top by an iceberg termination surface (defined by the final outsized clast in the section). Since the Pagoda Fm in this location is overlain by the non-glacial Mackellar Fm, there is no true maximum retreat surface beyond the iceberg termination surface (i.e., the last dropstone in the lower Mackellar Fm). Most of the succession likely represents a glacial retreat systems tract, though there is likely some fraction of the massive diamictite facies above the erosional surface that is more likely to have been subglacially deposited and would therefore represent a glacial maximum systems tract. The transition between those two systems tracts would be defined by a grounding-line retreat surface.

This sequence is most consistent with Rosenblume and Powell (2019)'s Type I "idealized glacial sequence", which is a model developed to reflect a sedimentation sequence deposited during the retreat of a relatively warm subpolar glacier with a glacial erosion surface as a lower sequence boundary and sufficient meltwater for grounding-line fan development. This sequence model was developed based on Upper Miocene sediments from the Ross Sea region of Antarctica (Rosenblume and Powell 2019), whose climate and geology were likely reasonably similar to the TAB during the Permian. The Type I idealized sequence is interpreted to represent a dynamic climatic glacial system with very high erosional rates and debris fluxes, which is consistent with the depositional model presented for the Pagoda Fm in this paper.

2.8. Discussion

This study finds that most sediments in the Pagoda Fm in the Shackleton Glacier region were deposited during the retreat of a temperate to "mild" subpolar glacier. The key indicators for this retreat include the presence of grounding-line fan systems, ample evidence for plume sedimentation and rapid deposition, as well as abundant glacially-transported clasts with a wide size range made of local basement lithologies. This glacier had a subaqueous terminus during the deposition of the Pagoda Fm in the Shackleton Glacier area, either in a marine or brackish setting.

One of the ultimate goals of the study of LPIA glacigenic sediments is to infer the "type" and distribution of glaciation experienced in any given basin. Glacier "type" typically refers to the glacier's thermal regime and its size (i.e. ice sheet, ice cap, or ice field). Such characteristics of glaciers are controlled by many factors, but generally tie back into climate and geologic setting. Glacigenic sedimentary deposits are often used to infer the thermal regime of their parent glacier (Dowdeswell et al. 2016; Kurjanski 2020). Recent studies all agree that glacigenic deposits in the TAB are most likely the result of transport and deposition by temperate or "mild" subpolar glaciers,

largely because grounding line fans are common in the Pagoda Fm and its equivalents, which suggest the TAB glaciers released an abundance of meltwater (Isbell et al. 2008c; Isbell 2010; Koch and Isbell 2013; Cornamusini 2017).

The presence of sub-aqueous fan deposits interspersed within the massive diamictite facies of the Pagoda Fm in the Shackleton Glacier area suggests that the glacier had an active, persistent, and organized subglacial hydrologic system, and that during its retreat the glacial margin was stationary for at least a few years at a time to create grounding-line fans (Cowan and Powell 1991; Hunter et al. 1996; Dowdeswell et al. 2015; Dowdeswell et al. 2016). These inferences are also supported by the succession's stratigraphy, which is characteristic of a "Type I" ("mild" subpolar glacier with grounding-line fan development) glacial systems tract (Rosenblume and Powell 2019). Whether the glacier responsible for the deposition of the Pagoda Fm in the Shackleton Glacier Region had more of a "mild subpolar" thermal regime, similar to modern glaciers in eastern Svalbard, or more of a truly "temperate" thermal regime, like modern glaciers of southern Alaska, is difficult to discern. To clarify the likely thermal regime, additional glacigenic successions and non-glacial paleoclimate indicators in the TAB should be examined. In either case, glaciers with mild thermal regimes and developed subglacial hydrological systems are far-and-away the more prolific producers and transporters of sediments, and that the sedimentary record is therefore biased towards them. The presence of deposits from temperate or mild subpolar glaciers does not mean the thermal regime of the glaciers were never cold-based or that there was not lateral variation in glacier thermal regime.

The unidirectional orientation of subglacial flow indicators, along with evidence to topographic relief exceeding ~100 m in the Shackleton Glacier region, suggest that glacier thickness also exceeded 100 m during its maximum. Such observations do not allow for an inference of maximum possible ice thickness. However, we can infer that the glacier was more likely part of an ice sheet or ice cap, than

an ice field or alpine glacier. The glacier also may have thinned substantially during its retreat and subsequent deposition of the Pagoda Fm in this area.

Throughout the TAB, Asselian - Sakmarian glacigenic depositional environments were locally and regionally variable in part due to the inherent complexity of glacial processes and preservation potential, but also due to the topography of the pre-existing landscape. Most studies of glacigenic rocks in the TAB note up to several hundred meters of topographic relief on the underlying basement that is not wholly "filled" by glacial sediments and continued to influence post-glacial sedimentary deposition (Isbell et al. 1997a). Studies of both modern (e.g. Lawson (1979)) and ancient (e.g. Cornamusini (2017)) glacial sedimentary systems have observed how topographic effects can result in seemingly contradictory flow directions. This study is another example. Transport directions at all the sites in this study appear contradictory, unless paleotopography and the processes that created each feature are considered (Fig. 2- 11). For example, at Mt. Butters the flow directions of Permian glaciers in the TAB appears to be from north to south, while the transport directions of gravity-driven deposits and flow directions within the grounding line fan are perpendicular to that (Figs. 11D, E). If averaged together, these flow directions would imply general transport toward the south-west, when the most likely scenario was that the mass- and current-transported deposits followed a paleotopographic slope and the glacier did not.

The Pagoda Fm in the Shackleton Glacier region likely represents a single glacial-interglacial cycle, stratigraphically represented by a single glacial sequence. In this context, the phrase "glacial-interglacial cycle" refers to the advance of a glacier into the basin and its whole retreat out of the basin, which is stratigraphically defined by a surface of glacial retreat. This is not to say that the position of the glacier margin did not fluctuate during that cycle, but that only one grounded erosional surface is present in the study area and only one surface of glacier retreat (Powell and

Cooper 2002; Rosenblume and Powell 2019). No instances of a grounded re-advance over any of the sections examined in this study were observed beyond the basal erosional surfaces. As previously discussed, the processes and environments responsible for the extensive deposition of the massive, glacigenic diamictite facies were likely diverse and largely subaqueous. The preservation of such sediments is most probable if deposited during the final retreat phase with no subsequent advances over the area (Kurjanski 2020). This is especially true in a basin-marginal position in a basin like the TAB that was trough-shaped and not exposed to open marine conditions. Evidence for glacier readvance above the basal erosional surface of the Pagoda Fm does exist at other Pagoda Fm outcrops in the TAB, including within the Beardmore Sub-basin (Lindsay 1970a; Miller 1989; Koch and Isbell 2013). This evidence typically occurs in thicker, basinal facies association which are likely areas with higher accommodation than the basin margins.

The flow-directions and facies analyses from this study strongly support the hypothesis that an ice center was positioned inboard of the Panthalassan margin of Antarctica (an area that is now Marie Byrd Land) during the Asselian - Sakmarian (Fig. 2- 2B, ice center "q"). The presence of such an ice sheet is a relatively new hypothesis that was first proposed by Isbell (2010) and Isbell et al. (2008c) based on transport directions in South Victoria Land. In recent publications, this proposed ice center on the Panthalassan side of the TAB has been inconsistently included (Fielding et al. 2008c; Isbell et al. 2012; Montañez and Poulsen 2013) and excluded (Fielding et al. 2010; Craddock et al. 2019) from LPIA ice center reconstructions. Evidence from this study and Isbell (2010) shows that an ice center should be included on the non-cratonic edge of the TAB in reconstructions including the Gzhelian - Sakmarian, an interval also referred to as "Event 5" (López-Gamundí et al. 2021), and Australian "P1" (Fielding et al. 2008b). Ice-flow directions elsewhere in the TAB clearly indicate that glaciers also flowed into the TAB off of the East Antarctic Craton and along the TAB's basin axis toward the Wisconsin and Ohio Ranges (Fig. 2- 2B, ice center "r"). The multiple ice centers

contributing to sedimentation in the TAB may not have been synchronous in their advances and retreats throughout the LPIA. This additional evidence for an ice center over Marie Byrd Land is important because it helps to explicate the hypothesis that glaciation during the LPIA consisted of asynchronous, discrete ice centers and not a single, large ice sheet centered over Antarctica (Isbell et al. 2012; Montañez and Poulsen 2013) (Fig. 2- 2B). Inferences made from glacigenic and glacially-influenced sediments ("near-field" records) can be tied to global and "far-field" records of climate change from the ~80 myr of the LPIA to approach a holistic understanding of the effects that the onset, duration, and ultimate collapse of a global icehouse influenced Earth, both geologically and biologically (Montañez et al. 2007; Rygel et al. 2008; Soreghan et al. 2019).

2.9. Conclusions

The Pagoda Fm in the Shackleton Glacier region is glacigenic and was deposited in a basin-marginal subaqueous setting, by a glacier with a temperate or mild subpolar thermal regime. The dominant lithology in the Pagoda Fm here is massive, sandy, clast-poor diamictite. The depositional processes governing these diamictites were subaqueous glacial processes in a marine or brackish setting; likely a combination of mass-transport, iceberg-rainout, iceberg scouring, plume sedimentation, and subglacial till deposition. Current-transported sands and stratified diamictites within the Pagoda Fm were deposited as part of grounding-line fan systems. In the Shackleton Glacier region, all glacigenic sediments in the Pagoda Fm were likely deposited during the retreat phase of a single glacial sequence. The transport directions and thicknesses of strata along the TAB margin were strongly controlled by topographic relief on the underlying erosional surface. Glacier flow directions (towards the south and south-east) and trends in Pagoda Fm thicknesses in the Shackleton Glacier Area support the hypothesis that an ice center was present toward the Panthalassan/Gondwanan margin of East Antarctica (Marie Byrd Land) during the LPIA.

Acknowledgements

This work would have been impossible without the hard work of all the people who made the 2017 - 2018 Shackleton Deep Field Camp such a success, including the talented people of the National Science Foundation, Antarctic Support Contract, Ken Borek Air, Petroleum Helicopters, Inc., New York Air National Guard, and the U.S. Air Force. Special thanks are owed to Edith Taylor and Rudolf Serbet for aiding in the field planning, Danny Uhlmann and Ted Grosgebauer for keeping us from tumbling off of cliffs, and to Patty Ryberg, Rudolf Serbert, Brian Atkinson, and Erik Gulbranson for their companionship and cooking in the deep field. Thanks also to Kate Pauls and Eduardo Rosa for their feedback on the manuscript. Funding for this research came from National Science Foundation OPP-1443557, EAR-1729219, and OISE-1559231 grants, the University of Wisconsin – Milwaukee Graduate Fellowships programs, the P.E.O. Scholar Awards Program, The American Federation of Mineralogical Societies, The Wisconsin Geological Society, University of Wisconsin-Milwaukee (RGI grant), and the University of Wisconsin-Milwaukee Department of Geosciences. And finally, thanks are due to Fernando Vesely and an anonymous reviewer for their thoughtful comments and suggestions that improved this manuscript.

References

Aitchison, J.C., Bradshaw, M.A., and Newmann, L., 1988, Lithofacies and origin of the Buckeye Formation: Late Paleozoic glacial and glaciomarine sediments, Ohio Range, Transantarctic Mountains, Antarctica: Palaeogeography, Palaeoclimatology, Palaeoecology, v. 64, p. 93-104.

Allmendinger, R.W., Cardozo, N., and Fisher, D.M., 2012, Structural Geology Algorithms: Vectors and Tensors in Structural Geology, Cambridge University Press. 302 p.

Anderson, J.B., Kurtz, D.D., Domack, E.W., and Balshaw, K.M., 1980, Glacial and glacial marine seidment of the Antarctic continental shelf: Journal of Geology, v. 88, p. 399-414.

Askin, R.A., 1998, Floral trends in the Gondwana high latitudes: palynological evidence from the Transantarctic Mountains: Journal of African Earth Sciences, v. 27, p. 12-13.

Askin, R.A., Barrett, P.J., Kohn, B.P., and Mcpherson, J.G., 1971, Stratigraphic sections of the Beacon Supergroup (Devonian and older(?) to Jurassic) in south Victoria Land, *in* Barrett, P.J., ed., Antarctic Data Series No. 2: Wellington, Victoria University.

Assine, M.L., De Santa Ana, H., Veroslavsky, G., and Vesely, F.F., 2018, Exhumed subglacial landscape in Uruguay: Erosional landforms, depositional environments, and paleo-ice flow in the context of the late Paleozoic Gondwanan glaciation: Sedimentary Geology, v. 369, p. 1-12.

Babcock, L.E., Isbell, J.L., Miller, M.F., and Hasiotis, S.T., 2002, New late Paleozoic conchostracan (Crustacea: Branchiopoda) from the Shackleton Glacier Area, Antarctica: Age and paleoenvironmental implications: Journal of Paleontology, v. 76, p. 70-75.

Barrett, P.J., 1972, Late Paleozoic glacial valley at Alligator Peak, Southern Victoria Land, Antarctica: New Zealand Journal of Geology and Geophysics, v. 15, p. 262-268.

Barrett, P.J., Elliot, D.H., and Lindsay, J.F., 1986, The Beacon Supergroup (Devonian-Triassic) and Ferrar Group (Jurassic) in the Beardmore Glacier area, Antarctica, *in* Turner, M.D., and Splettstoesser, J.F., eds., Geology of the central Transantarctic Mountains: Washington, D.C., Antarctic Research Series, American Geophysical Union, p. 339-428.

Barrett, P.J., and Mckelvey, B.C., 1981, Permian tillites of southern Victoria Land, Antarctica, *in* Hambrey, M.J., and Harland, W.B., eds., Earth's pre-Pleistocene Glacial Record: Cambridge, Cambridge University Press, p. 233-236.

Batchelor, C.L., and Dowdeswell, J.A., 2015, Ice-sheet ground-zone wedges (GZWs) on high-latitude continental margines: Marine Geology, v. 363, p. 65-92.

Batterson, M., and Sheppard, K., 2000, Deglacial history of northern St. George's Bay, western Newfoundland: Current Research, v. 1, Newfoundland Deparment of Mines and Energy, Geological Survey of Newfoundland, p. 33-47.

Benn, D.I., 1996, Subglacial and subaqueous processes near a glacier grounding line: Sedimentological evidence from a former ice-dammed lake, Achnasheen Scotland: Boreas, v. 25, p. 23-36.

Bennett, M.R., Hambrey, M.J., and Huddart, D., 1997, Modification of clast Shape in high artic glacial environments: Journal of Sedimentary Research, v. 67, p. 550-559.

Bindschadler, R., Vornberger, V., Fleming, A., Fox, A., Mullins, J., Binnie, D., Paulsen, S.J., Granneman, B., and Gorodestzky, D., 2008, The Landsat image mosaic of Antarctica: Remote Sensing of Environment, v. 112, p. 4214-4226.

Cardozo, N., and Allmendinger, R.W., 2013, Spherical projections with OSXStereonet: Computers & Geosciences, v. 51, p. 193-205.

Coates, D.A., 1985, Late Paleozoic glacial patterns in the central Transantarctic Mountains, Antarctica, *in* Turner, M.D., and Splettstoesser, J.F., eds., Geology of the Central Transantarctic Mountains: Washington, D.C., Antarctic Research Series, American Geophysical Union, p. 325-338.

Collinson, J.D., and Mountney, N., 2019, Sedimentary Structures: Edinburgh, Dunedin, Academic Press Ltd, 340 p.

Collinson, J.W., Hammer, W.R., Askin, R.A., and Elliot, D.H., 2006, Permian-Triassic boundary in the central Transantarctic Mountains, Antarctica: Geological Society of America, Bulletin, v. 118, p. 747-763.

Collinson, J.W., Isbell, J.L., Elliot, D.H., Miller, M.F., and Miller, J.M.G., 1994, Permian-Triassic Transantarctic basin, *in* Veevers, J.J., and Powell, C.M., eds., Permian-Triassic Pangean basins and Foldbelts along the Panthalassan Margin of Gondwanaland: Boulder, Colorado, Geological Society of America Memoir 184, p. 173-222.

Cooper, M.A., Jordan, T.M., Schroeder, D.M., Siegert, M.J., Williams, C.N., and Bamber, J.L., 2019, Subglacial roughness of the Greenland Ice Sheet: relationship withcontemporary ice velocity and geology: The Cryosphere, v. 13, p. 3093-3115.

Cornamusini, G., Talarico, R.M., Simonette, C., Spine, A., Olivetti, V., and Woo, J., 2017, Upper Paleozoic glacigenic deposits of Gondwana: Stratigraphy and paleoenvironmental significance of a tillite succession in Northern Victoria Land (Antarctica): Sedimentary Geology, v. 358, p. 51-69.

Cowan, E.A., and Powell, R.D., 1991, Ice-proximal sediment accumulation rates in a temperate glacial fjord, south-eastern Alaska, *in* Anderson, J.B., and Ashley, G.M., eds., Glacial Marine Sedimentation; aleoclimatic Significance: Geological Society of America, Special Paper 261, Boulder, Colorado, p. 61-73.

Craddock, J.P., Ojakangas, R.W., Malone, D.H., Konstantinou, A., Mory, A.J., Bauer, W., Thomas, R.J., Affinati, S.C., Pauls, K.N., Zimmerman, U., Botha, G., Rochas-Campos, A., Dos Santos, P.R., Tohver, E., Riccomini, C., Martin, J., Redfern, J., Horstwood, M., and Gehrel, G., 2019, Detrital zircon provenance of Permo-Carboniferous glacial diamictites across Gondwana: Earth-Science Reviews, v. 192, p. 285-316.

Crowell, J.C., and Frakes, L.A., 1972, Late Paleozoic glaciation: Part V, Karoo Basin, South Africa: Geological Society of America, Bulletin, v. 83, p. 2887-2919.

Crowell, J.C., and Frakes, L.A., 1975, Late Paleozoic glaciaition, *in* Campbell, K.S.W., ed., Gondwana Geology: Papers Presented at the Third Gondwana Symposium Canberra, Australia, 1973: Canberra, Australia, Australian National University Press, p. 313-331.

Dasgupta, P., 2006, Facies characteristics of Talchir Formation, Jharia Basin, India: implications for initiation of Gondwana sedimentation: Sedimentary Geology, v. 185, p. 59-78.

Demet, B.P., Nittrouer, J.A., Anderson, J.B., and Simkins, L.M., 2019, Sedimentary processes at ice sheet grounding-zone wedges revealed by outcrops, Washington State (USA): Earth Surface Processes and Landforms, v. 44, p. 1209-1220.

Dietrich, P., Franchi, F., Setlhabi, L., Prevec, R., and Bamford, M., 2019, The nonglacial diamictite of Toutswemogala Hill (lower Karoo Supergroup, central Botswana): Implications of the extent of the late Paleozoic Ice Age in the Kalahari-Karoo Basin: Journal of Sedimentary Research, v. 89, p. 1-15.

Dietrich, P., and Hoffmann, A., 2019, Ice-margin fluctuation sequences and grounding zone wedges: The record of the Late Palaeozoic Ice Age in the eastern Karoo Basin (Dwyka Group, South Africa): The Depositional Record, v. 5, no. 2, p. 247-271.

Domack, E.W., 1983, Facies of Late Pleistocene glacial-marine sediments on Whidbey Island, Washington: An isostatic glacial-marine sequence., *in* Molina, B.F., ed., Glacial-Marine Sedimentation: Boston, MA, Springer, p. 535-570.

Domack, E.W., and Powell, C.M., 2018, Modern Glaciomarine Environments and Sediments, *in* Menzies, J., and van der Meer, J.J.M., eds., Past Glacial Environments: Elseveir, p. 105 - 158.

Domeier, M., and Torsvik, T.H., 2014, Plate tectonics in the Late Paleozoic: Geoscience Frontiers, v. 5, no. 3, p. 303-350.

Dowdeswell, J.A., Canals, M., Jakobsson, B.J., Todd, B.J., Dowdeswell, E.K., and Hogan, K.A., 2016, The variety and distribution of submarine glacial landforms and implications for ice-sheet reconstruction, *in* Dowdeswell, J.A., Canals, M., Jakobsson, B.J., Todd, B.J., Dowdeswell, E.K., and Hogan, K.A., eds., Atlas of Submarine Glacial Landforms: Modern, Quaternary and Ancient: Geological Society of London, Memoir 46, p. 519-552.

Dowdeswell, J.A., Hambrey, M.J., and Wu, R., 1985, A comparison of clast fabric and shape in Late Precambrian and modern glacigenic sediments: Journal of Sedimentary Petrology, v. 55, p. 691-704.

Dowdeswell, J.A., Hogan, K.A., Arnold, N.S., Mugford, R.I., Wells, M., Hirst, J.P.P., and Decalf, C., 2015, Sediment-rich meltwater plumes and ice-proximal fans at themargins of modern and ancient tidewater glaciers: Observations and modeling: Sedimentology, v. 62, p. 1665-1692.

Dowdeswell, J.A., Whittington, R.J., and Marienfeld, P., 1994, The origin of massive diamicton facies by iceberg rafting and scouring, Scoresby Sund, East Greenland: Sedimentology, v. 41, p. 21-35.

Dumas, S., and Arnott, R.W.C., 2006, Origin of hummocky and swaley cross-stratification--the controlling influence of unidirectional current strength and aggradation rate: Geology, v. 34, p. 1073-1076.

Eidam, E.F., Sutherland, D.A., Duncan, D., Kienholz, C., Amundson, J.M., and Motyka, R.J., 2020, Morainal bank evolution and impact on terminus dynamics during a tidewater glacier stillstand: Journal of Geophysical Research: Earth Surface, v. 125, no. 11, e2019JF005359.

Elliot, D.H., 1992, Jurassic magmatism and tectonism associated with Gondwanaland break-up: an Antarctic perspective, *in* Storey, B.C., Alabaster, T., and Pankhurst, R.J., eds., Magmatism and the Causes of Continental Break-up: Geological Society of London, Special Publication 68, p. 165-184.

Elliot, D.H., 2013, The geological and tectonic evolution of the Transanatarctic Mountains: a review, *in* Hambrey, M.J., Barker, P.F., Barrett, P.J., Bowman, V., Davies, B., Smellie, J.L., and Tranter, M., eds., Antarctic Palaeoenvironments and Earth-Surface Processes: Geological Society of London, Special Publication 381, p. 7-35.

Elliot, D.H., Fanning, C.M., Isbell, J.L., and Hulett, S.R.W., 2017, The Permo-Triassic Gondwana sequence, central Transantarctic Mountains, Antarctica: Zircon geochronology, provenance, and basin evolution: Geosphere, v. 13, p. 155-178.

Estrada, S., Läufer, A., Eckelmann, K., Hofmann, M., Gärtner, A., and Linnemann, U., 2016, Continuous Neoproterozoic to Ordovician sedimentation at the EastGondwana margin—Implications from detrital zircons of the RossOrogen in northern Victoria Land, Antarctica: Gondwana Research, v. 37, p. 426-448.

Evans, D.J.A., Phillips, E.R., Hiemstra, J.F., and Auton, C.A., 2006, Subglacial till: Formation, sedimentary characteristics and classification: Earth-Science Reviews, v. 78, p. 115-176.

Eyles, C.H., 1987, Glacially influenced submarine-channel sedimentation in the Yakataga Formation, Middleton Island, Alaska: Journal of Sedimentary Petrology, v. 57, p. 1004-1017.

Eyles, C.H., 1988, A model for striated boulder pavement formation on glaciated, shallow-marine shelves; an example from the Yakataga Formation, Alaska: Journal of Sedimentary Petrology, v. 58, p. 62-71.

Eyles, C.H., and Lagoe, M.B., 1990, Sedimentation patterns and facies geometry on a temperate glacially-influenced continental shelf: the Yakataga Formation, Middleton Island, Alaska, *in* Dowdeswell, J.A., and Scourse, J.D., eds., Glacimarine Environments: Processes and Sediments: Geological Society of London, Special Publication 53, p. 363–386.

Fallgatter, C., and Paim, P.S.G., 2019, On the origin of the Itararé Group basal nonconformity and itsimplications for the Late Paleozoic glaciation in the Paraná Basin, Brazil: Palaeogeography, Palaeoclimatology, Palaeoecology, v. 531, 108225.

Fedorchuk, N.D., Isbell, J.L., Griffis, N.P., Montañez, I.P., Vesely, F.F., Iannuzzi, R., Mundil, R., Yin, Q.-Z., Pauls, K.N., and Rosa, E.L., 2019, Origin of paleovalleys on the Rio Grande do Sul Shield (Brazil): Implications for the extent of late Paleozoic glaciation in west-central Gondwana: Palaeogeography, Palaeoclimatology, Palaeoecology, v. 531, 108738.

Fielding, C.R., Frank, T.D., Birgenheier, L.P., Rygel, M.C., Jones, A.T., and Roberts, J., 2008a, Stratigraphic imprint of the late Palaeozoic ice age in eastern Australia: a record of alternating glacial and nonglacial climate regime: Geological Society of London, v. 165, p. 129-140.

Fielding, C.R., Frank, T.D., Birgenheier, L.P., Rygel, M.C., Jones, A.T., and Roberts, J., 2008b, Stratigraphic record and facies associations of the late Paleozoic ice age in eastern Australia (New South Wales and Queensland), *in* Fielding, C.R., Frank, T., and Isbell, J.L., eds., Resolving the Late Paleozoic Ice Age in Time and Space: Boulder, Geological Society of America, Special Paper 441, p. 41-57.

Fielding, C.R., Frank, T.D., and Isbell, J.L., 2008c, The late Paleozoic ice age--A review of current understanding and synthesis of global climate patterns, *in* Fielding, C.R., Frank, T.D., and Isbell, J.L., eds., Resolving the Late Paleozoic Ice Age in Time and Space: Boulder, CO, Geological Society of America, Special Publication, p. 343-354.

Fielding, C.R., Frank, T.D., and Isbell, J.L., eds., 2008d, Resolving the Late Paleozoic Ice Age in Time and Space: Boulder, CO, Geological Society of America, Special Publication 441, 354 p.

Fielding, C.R., Frank, T.D., Isbell, J.L., Henry, L.C., and Domack, E.W., 2010, Stratigraphic signature of the late Palaeozoic Ice Age in the Parmeener Supergroup of Tasmania, SE Australia, and inter-regional comparisons: Palaeogeography, Palaeoclimatology, Palaeoecology, v. 298, p. 70-90.

Fielding, C.R., Sliwa, R., Holcombe, R.J., and Jones, A.T., 2001, A new palaeogeographic synthesis for the Bowen, Gunnedah and Sydney basins of eastern Australia, *in* Hill, K.C., and Bernecker, T., eds., Eastern Australasian Basins Symposium: A Refocused Energy Perspective for the Future: Victoria, Australia, Petroleum Exploration Society of Australia, Special Publication, p. 269-278.

Frakes, L., Matthews, J., Neder, I., and Crowell, J., 1966, Movement directions in Late Paleozoic glacial rocks of the Horlick and Pensacola Mountains, Antarctica: Science, v. 153, p. 746-749.

Frakes, L.A., and Crowell, J.C., 1969, Late Paleozoic glaciation: I, South America: Geological Society of America, Bulletin, v. 80, p. 1007-1042.

Frakes, L.A., Matthews, J.L., and Crowell, J.C., 1971, Late Paleozoic glaciation: Part III, Antarctica: Geological Society of America, Bulletin, v. 82, p. 1581-1604.

França, A.B., and Potter, P.E., 1988, Estratigrafia, ambiente deposicional e analise de reservatorio do Grupo Itarare (Permocarbonifero), Bacia do Parana (Parte 1): Boletim de Geociencias da PETROBRAS, v. 2, p. 147-191.

França, A.B., Winter, W.R., and Assine, M.L., 1996, Arenitos Lapa-Vila Velha; um modelo de trato de sistemas subaquosos canal-lobos sob influencia glacial, Grupo Itarare (C-P), Bacia do Parana: Revista Brasileira de Geociencias, v. 26, p. 43-56.

Friend, P.F., 1983, Towards the field classification of alluvial architecture or sequence, *in* Collinson, J.D., and Lewin, J., eds., Modern and Ancient Fluvial Systems, International Association of Sedimentologists, Special Publication 6, p. 345-354.

Funk, J.E., Slatt, R.M., and Pyles, D.R., 2012, Quantification of static connectivity between deep-water channels and stratigraphically adjacent architectural elements using outcrop analogs: American Association of Petroleum Geologists, Bulletin, v. 96, p. 277-300.

Gastaldo, R.A., Dimichele, W.A., and Pfefferkorn, H.W., 1996, Out of the icehouse into the greenhouse; a late Paleozoic analog for modern global vegetational change: GSA Today, v. 6, no. 10, p. 1-7.

Goodge, J.W., 2020, Geological and tectonic evolution of the Transantarctic Mountains, fromancient craton to recent enigma: Gondwana Research, v. 80, p. 50-122.

Goodge, J.W and Fanning, M. C., 2016, Mesoarchean and Paleoproterozoic history of the Nimrod Complex,central Transantarctic Mountains, Antarctica: Stratigraphic revisions andrelation to the Mawson Continent in East Gondwana: Precambrian Research, v. 285, p. 242-271.

Hallet, B., Hunter, L., and Bogen, J., 1996, Rates of erosion and sediment evacuation by glaciers: a review of field data and their implications: Global and Planetary Change, v. 12, p. 213-235.

Hambrey, M.J., 1994, Glacial Environments: Vancouver, University of British Columbia Press, 296 p.

Hambrey, M.J., and Glasser, N.F., 2003, Glacial sediments: processes, environments and facies, *in* Middleton, G.V., ed., Encyclopedia of Sediments and Sedimentary Rocks: Dordrecht, Kluwer Academic Publishers, p. 316-331.

Hambrey, M.J., and Glasser, N.F., 2012, Discriminating glacier thermal and dynamic regimes in the sedimentary record: Sedimentary Geology, v. 251-252, p. 1-33.

Hand, S.J., 1993, Palaeogeography of Tasmania's Permo-Carboniferous glacigenic sediments, *in* Findlay, R.H., Unrug, R., Banks, M.R., and Veevers, J.J., eds., Gondwana Eight: Assembly, Evolution and Dispersal: Rotterdam, A.A. Balkema, p. 459-469.

Hunter, L.E., Powell, R.D., and Lawson, D.E., 1996, Flux of debris transported by ice at three Alaskan tidewater glaciers: Journal of Glaciology, v. 42, p. 123-135.

Isbell, J.L., 1999, The Kukri Erosion Surface; a reassessment of its relationship to rocks of the Beacon Supergroup in the central Transantarctic Mountains, Antarctica: Antarctic Science, v. 11, p. 228-238.

Isbell, J.L., 2010, Environmental and paleogeographic implications of glaciotectonic deformation of glaciomarine deposits within Permian strata of the Metschel Tillite, southern Victoria Land, Antarctica, *in* López-Gamundí, O.R., and Buatois, L.A., eds., Late Paleozoic Glacial Events and Postglacial Transgressions in Gondwana: Boulder, CO, Geological Society of America, Special Publication 468, p. 81-100.

Isbell, J.L., 2015, Permian and Triassic sedimentation in the central Transantarctic mountains, southern Victoria Land and Northern Victoria Land: a south polar view of Gondwanan during the Paleozoic-Mesozoic transition, The 21st Internation Symposium on Polar Science: Polar Region as a Key Observatory for the Changing Globe and Beyond: Incheon, Republic of Korea, Korea Polar Institute.

Isbell, J.L., Seegers, G.M., and Gelhar, G.A., 1997b, Upper Paleozoic glacial and postglacial deposits, central Transantarctic Mountains, Antarctica, *in* Martini, I.P., ed., Late Glacial and Postglacial Environmental Changes: Quaternary, Carboniferous-Permian, and Proterozoic: Oxford, U.K., Oxford University Press, p. 230-242.

Isbell, J.L., Miller, M.F., Babcock, L.E., and Hasiotis, S.T., 2001, Ice-marginal environment and ecosystem prior to initial advance of the late Paleozoic ice sheet in the Mount Butters area of the central Transantarctic Mountains, Antarctica: Sedimentology, v. 48, p. 953-970.

Isbell, J.L., Cole, D.I., and Catuneanu, O., 2008a, Carboniferous-Permian glaciation in the main Karoo Basin, South Africa: stratigraphy, depositional controls, and glacial dynamics, *in* Fielding, C.R., Frank, T.D., and Isbell, J.L., eds., Resolving the Late Paleozoic Ice Age in Time and Space: Boulder, CO, Geological Society of America, Special Publication 441, p. 71-82.

Isbell, J.L., Fraiser, M.L., and Henry, L.C., 2008b, Examining the complexity of environmental change during the late Paleozoic and early Mesozoic: Palaios, v. 23, p. 267-269.

Isbell, J.L., Gelhar, G.A., and Seegers, G.M., 1997a, Reconstruction of preglacial topography using a postglacial flooding surface: Upper Paleozoic deposits, central Transantarctic Mountains, Antarctica: Journal of Sedimentary Research, v. 67, p. 264-273.

Isbell, J.L., Koch, Z.J., Szablewski, G.M., and Lenaker, P.A., 2008c, Permian glacigenic deposits in the Transantarctic Mountains, Antarctica, *in* Fielding, C.R., Frank, T.D., and Isbell, J.L., eds., Resolving the Late Paleozoic Ice Age in Time and Space: Boulder, CO, Geological Society of America, Special Publication 441, p. 59-70.

Isbell, J.L., Henry, L.C., Gulbranson, E.L., Limarino, C.O., Fraiser, M.L., Koch, Z.J., Ciccioli, P.L., and Dineen, A.A., 2012, Glacial paradoxes during the late Paleozoic ice age: Evaluating the equilibrium line altitude as a control on glaciation: Gondwana Research, v. 22, p. 1-19.

Jordan, T.A., Ferraccioli, F., Armadillo, E., and Bozzo, E., 2013, Crustal architecture of the Wilkes Subglacial Basin in East Antarctica, as revealed fromairborne gravity data: Tectonophysics, v. 585, p. 196-206.

Kessler, T.C., Klint, K.E.S., Nilsson, B., and Bjerg, P.L., 2012, Characterization of sand lenses embedded in tills: Quaternary Science Reviews, v. 53, p. 55-71.

Koch, Z.J., 2010, reevaluation of the late Paleozoicglacigenic deposits of the Pagoda Formation at Tillite Glacier, central Transanatarctic Mountains, Antarctica [unpublished Ph.D. Dissertation thesis]: University of Wisconsin-Milwaukee, Milwaukee, 145 p.

Koch, Z.J., and Isbell, J.L., 2013, Processes and products of grounding-line fans from the Permian Pagoda Formation, Antarctica: Insight into glacigenic conditions in polar Gondwana: Gondwana Research, v. 24, p. 161-172.

Kurjanski, B., Rea, B.R., Spagnolo, M., Cornwell, D.G., Howell, J., and Archer, S., 2020, A conceptual model for glacigenic reservoirs: From landsystems to reservoir architecture: Marine and Petroleum Geology, v. 115, 104205.

Landvik, J.Y., Alexanderson, H., Henriksen, M., and Ingólfsson, Ó., 2014, Landscape imprints of changing glacial regimes during ice-sheetbuild-up and decay: a conceptual model from Svalbard: Quaternary Science Reviews, v. 92, p. 258-268.

Lawson, D.E., 1979, Sedimentological analysis of the western terminus region of the Matanuska Glacier, Alaska: Hanover, New Hampshire, U.S. Army Cold Regions Research and Engineering Laboratory, 122 p.

Lawver, L.A., Dalziel, I.W.D., Norton, I.O., and Gahagan, L.M., 2011, The Plates 2011 Atlas of Plate Reconstructions (500 Ma to Present Day): University of Texas, Technical Report 198: Austin, Texas, 189 p.

Lenaker, P.A., 2002, Sedimentology of Permian glacial deposits in the Darwin Glacier region, Antarctica [unpublished M.S. thesis]: University of Wisconsin-Milwaukee, Milwaukee, 173 p.

Licht, K.J., Dunbar, N.W., Andrews, J.T., and Jennings, A.E., 1999, Distinguishing subglacial till and glacial marine diamictons in the western Ross Sea, Antarctica: Implications for a last glacial maximum grounding line: Geological Society of America, Bulletin, v. 111, p. 91-103.

Limarino, C.O., Alonso-Muruaga, P.J., Ciccioli, P.L., Loinaze, V.S.P., and Césari, 2014, Stratigraphy and palynology of a late Paleozoic glacial paleovalley in the Andean Precordillera, Argentina: Palaeogeography, Palaeoclimatology, Palaeoecology, v. 412, p. 223-240.

Lindbäck, K., and Pettersson, R., 2015, Spectral roughness and glacial erosion of a land-terminating section of the Greenland Ice Sheet: Geomorphology, v. 238, p. 149-159.

Lindsay, J.F., 1969, Stratigraphy and sedimentation of Lower Beacon rocks in the central Transantarctic Mountains, Antarctica: Institute of Polar Studies, Report 33: Research Foundation and the Institute of Polar Studies, The Ohio State University, Columbus, 58 p.

Lindsay, J.F., 1970a, Depositional environment of Paleozoic glacial rocks in the central Transantarctic Mountains: Geological Society of America, Bulletin, v. 81, p. 1149-1172.

Lindsay, J.F., 1970b, Paleozoic cave deposit in the central Transantarctic Mountains: New Zealand Journal of Geology and Geophysics, v. 13, p. 1018-1023.

Lisitzin, A.P., 2002, Sea-Ice and Iceberg Sedimentation in the Ocean: Berlin, Springer-Verlag, 800 p.

Long, W.E., 1964a, The stratigraphy of the Horlick Mountains, *in* Adie, R.J., ed., International Symposium on Antarctic Geology: Amsterdam, North Holand Publiching, p. 352-363.

Long, W.E., 1964b, The stratigraphy of the Ohio Range, Antarctica [unpublished Ph.D. thesis]: The Ohio State University, Columbus, Ohio, 340 p.

Long, W.E., Mclell, D., Collinson, J.W., and Elliot, D.H., 2008-2009, Geology of the Nilsen Plateau, Queen Maud Mountains, Transantarctic Mountains: Terra Antarctica, v. 15, p. 239-253.

Lønne, I., 1995, Sedimentary facies and depositional architecture of ice-contact glaciomarine systems: Sedimentary Geology, v. 98, p. 13-43.

Lønne, I., Nemec, W., Blikra, L.H., and Lauritsen, T., 2001, Sedimentary architecture and dynamic stratigraphy of a marine ice-contact system: Journal of Sedimentary Research, v. 71, p. 922-943.

López-Gamundí, O., Limarino, C.O., Isbell, J.L., Pauls, K.N., Césari, S.N., and Muruaga, P.A., 2021, The Late Paleozoic Ice Age along the southwestern margin of Gondwana: facies models, age constraints, correlation and sequence stratigraphic framework: Journal of South American Earth Sciences, v. 107, 103056.

Marcos, P, Gregori, D.A., Benedini, L., Barros, M. Strazzere, L., and Pivette, C.P.,, 2018, Pennsylvanian glacimarine sedimentation in the CushamenFormation, western North Patagonian Massif: Geoscience Frontiers, v. 9, p. 485-504.

Martin, H., 1981, The late Palaeozoic Gondwana glaciation: Geologische Rundschau, v. 70, p. 480-496.

Martin, J.R., Redfern, J., Horstwood, M.S.A., Mory, A.J., and Williams, B.P.J., 2019, Detrital zircon age and provenance constraints on late Paleozoic ice-sheet growth and dynamics in Western and Central Australia: Australian Journal of Earth Sciences, vol. 66, no. 2, p. 183 - 207.

Masood, K.R., Taylor, T.N., Horner, T., and Taylor, E.L., 1994, Palynology of the Mackellar Formation (Beacon Supergroup) of East Antarctica: Review of Palaeobotany and Palynology, v. 83, p. 329-337.

Matsch, C.L., and Ojakangas, R.W., 1991, Comparison in depositional style of "polar" and "temperate" glacial ice: late Paleozoic Whiteout Conglomerate (West Antarctica) and late Proterozoic Mineral Fork Formation (Utah), *in* Anderson, J.B., and Ashley, G.M., eds., Glacial Marine Sedimentation; Paleoclimatic Significance: Boulder, Colorado, Geological Society of America, Special Publication 261, p. 191-206.

Matsch, C.L., and Ojakangas, R.W., 1992, Stratigraphy and sedimentology of the Whiteout Conglomerate - a late Paleozoic glacigenic sequence in the Ellsworth Mountains, West

Antarctica, *in* Webers, G.F., Craddock, G.F., and Splettstoesser, J.F., eds., Geology of the Ellsworth Mountains, Antarctica: Boulder, Colorado, Geological Society of America Memoir 170, p. 37-62.

Mcgregor, V.R., and Wade, F.A., 1969, Geologic Map of Antarctica Sheet 16, Western Queen Maud Mountains: American Geographical Society of New York.

McKay, R., Browne, G., Carter, L., Cowan, E., Dunbar, G., Krissek, L., Naish, T., Powell, R., Reed, J., Talarico, F., and Wilch, T., 2009, The stratigraphic signature of the late Cenozoic Antarctic Ice Sheets in the Ross Embayment: Geological Society of America, Bulletin, v. 121, p. 1537-1561.

Miller, J.M.G., 1989, Glacial advance and retreat sequences in a Permo-Carboniferous section, central Transantarctic Mountains: Sedimentology, v. 36, p. 419-430.

Minshew, V.H., 1967, Geology of the Scott Glacier and Wisconsin Range areas, central Transantarctic Mountains, Antarctica [unpublished Ph.D. thesis]: The Ohio State University, Columbus, Ohio, 268 p.

Mirsky, A., 1969, Geologic Map of Antarctica Sheet 17, Ohio Range to Liv Glacier: American Geographical Society.

Moncreiff, A.C.M., 1989, Classification of poorly sorted sediments: Sedimentary Geology, v. 65, p. 191-194.

Montañez, I., and Soreghan, G.S., 2006, Earth's fickle climate; lessons learned from deep-time ice ages: Geotimes, v. 51, p. 24-27.

Montañez, I.P., Tabor, N.J., Niemeier, D., Dimichele, W.A., Frank, T., D., Fielding, C.R., Isbell, J.L., Birgenheier, L.P., and Rygel, M.C., 2007, CO_2-forced climate and vegetation instability during late Paleozoic deglaciation: Science, v. 315, p. 87-91.

Montañez, I.P., and Poulsen, C.J., 2013, The late Paleozoic ice age: an evolving paradigm: Annual Review of Earth and Planetary Sciences, v. 41, p. 1-28.

Mory, A.J., Martin, J.R., and Redfern, J., 2008, A review of Permian-Carboniferous glacial deposits in Western Australia, *in* Fielding, C.R., Frank, T.D., and Isbell, J.L., eds., Resolving the Late Paleozoic Ice Age in Time and Space: Boulder, CO, Geological Society of America, Special Publication 441, p. 29-40.

Mulder, T., and Alexander, J., 2001, The physical character of subaqueous sedimentary density flows and their deposits: Sedimentology, v. 48, p. 269-299.

Murray, K.T., Miller, M.F., and Bowser, S.S., 2013, Depositional processes beneath coastal multi-year sea ice: Sedimentology, v. 60, p. 391-410.

NOAA, 2019, NCEI Geomagnetic Calculators, National Geophysical Data Center, National Oceanic and Atmospheric Administration (NOAA), p. NOAA's National Centers for Environmental Information (NCEI), formerly the National Geophysical Data Center, and the collocated World Data Service for Geophysics, Boulder, operated by NOAA/NESDIS/NCEI, archive and make available geomagnetic data and information relating to Earth's magnetic field and Earth-Sun environment, including current declination, geomagnetic field models and magnetic indices, geomagnetic observatory data, and geomagnetic surveys.

Ojakangas, R.W., and Matsch, C.L., 1981, The late Paleozoic Whiteout Conglomerate: a glacial and glaciomarine sequence in the Ellsworth Mountains, West Antarctica, *in* Hambrey, M.J., and Harland, W.B., eds., Earth's pre-Pleistocene Glacial Record: Cambridge, Cambridge University Press, p. 241-244.

Partin, C.A., and Sadler, P.M., 2016, Slow net accumulation sets snowball Earth apart from all younger glacial episodes: Geology, v. 44, p. 1019-1022.

Pauls, K.N., 2014, Sedimentology and paleoecology of fossil-bearing, high-latitude marine and glacially influenced desposits in the Tepuel Basin, Patagonia, Argentina: University of Wisconsin - Milwaukee, M.S. Thesis.

Posamentier, H.W., and Martinsen, O.J., 2011, The character and genesis of submarine mass-transport deposits; insights from outcrop and 3D seismic data, *in* Shipp, R.C., Weimer, P., and Posamentier, H.W., eds., Mass-Transport Deposits in Deepwater Settings: Society for Sedimentary Geology, Special Publication 96, p. 7-38.

Powell, R., and Domack, E., 2002, Modern glaciomarine environments, *in* Menzies, J., ed., Modern and Past Glacial Environments: Oxford, Butterworth-Heinemann Ltd., p. 361-389.

Powell, R.D., 1990, Glacimarine processes at grounding-line fans and their growth to ice contact deltas, *in* Dowdeswell, J.A., and Scourse, J.D., eds., Glacimarine Environments: processes and sediments: Geological Society of London, Special Publication 53, p. 53-73.

Powell, R.D., 1991, Grounding-line systems as second-order controls on fluctuations of tidewater termini of temperate glaciers, *in* Anderson, J.B., and Ashley, G.M., eds., Glacial Marine Sedimentation; Paleoclimatic Significance: Geological Society of America, Special Publication 261, p. 75-93.

Powell, R.D., and Alley, R.B., 1997, Grounding-line systems: processes, glaciological inferences and the stratigraphic record, *in* Barker, P.F., and Cooper, A.C., eds., Geology and Siesmic Stratigraphy of the Antarctic Margin, 2: American Geophysical Union, Antarctic Research Series 71, p. 169-187.

Powell, R.D., and Cooper, J.M., 2002, A glacial sequence stratigraphic model for temperate, glaciated continental shelves: Geological Society Special Publication, p. 215-244.

Powell, R.D., and Molnia, B.F., 1989, Glacimarine sedimentary processes, facies and morphology of the south-southeast Alaska shelf and fjords: Marine Geology, v. 85, p. 359-390.

Raymond, A., and Metz, C., 2004, Ice and Its Consequences: Glaciation in the Late Ordovician, Late Devonian, Pennsylvanian-Permian, and Cenozoic Compared: Journal of Geology, v. 112, p. 655-670.

Reineck, H.E., and Singh, I.B., 1980, Depositional Sedimentary Environments: Berlin, Springer-Verlag, 551 p.

Rocchi, S., Bracciali, L., Di Vincenzo, G., Gemelli, M., Ghezzo, C., 2011, Arc accretion to the early Paleozoic Antarctic margin of Gondwana in Victoria Land: Gondwana Research, v. 19, no.3, p. 594-607.

Rodrigues, M.C.N.dL., Trzakos, B., Alsop, G.I., Vesely, F.F., 2019, Making a homogenite: An outcrop perspective into the evolution of deformation within mass-transport deposits: Marine and Petroleum Geology, v. 112, 104033.

Rosa, E.L.M., and Isbell, J.L., 2021, Late Paleozoic Glaciation: Reference Module in Earth Systems and Environmental Sciences, p. 534-545.

Rosa, E.L.M., Vesely, F.F., and França, A.B., 2016, A review on late Paleozoic ice-related erosional landforms in the Paraná Basin: origin and paleogeographical implications: Brazilian Journal of Geology, v. 46, n. 2, p. 147-166.

Rose, P., Byerley, G., Vaughan, O., Cater, J., Rea, B.R., Spagnolo, M. and Archer, S., 2018, Aviat: a Lower Pleistocene shallow gas hazard developed as a fuel gas supply for the Forties Field, *in* Bowman, M. and Levell, B, eds., Petroleum Geology of NW Europe: 50 Years of Learning – Proceedings of the 8th Petroleum Geology Conference: Geological Society of London, Petroleum Geology Conference Series 8, p. 485 - 505.

Rosenblume, J.A., and Powell, R.D., 2019, Glacial sequence stratigraphy of ANDRILL-1B core reveals adynamic subpolar Antarctic Ice Sheet in Ross Sea during thelate Miocene: Sedimentology, v. 66, p. 2072–2097.

Rust, I.C., 1975, Tectonic and sedimentary framework of Gondwana basins in southern Africa, *in* Campbell, K.S.W., ed., Gondwana Geology: Canberra, Australian National University Press, p. 537-564.

Rygel, M.C., Fielding, C.R., Frank, T.D., and Birgenheier, L.P., 2008, The magnitude of late Paleozoic glacioeustatic fluctuations: a synthesis: Journal of Sedimentary Research, v. 78, p. 500-511.

Seegers, G.M., 1996, Sedimentology of the Permian Mackellar Formation, Centratl Transantarctic Mountains, Antarctica: University of Wisconsin - Milwaukee, M.S. Thesis, 106 p.

Seegers-Szablewski, G., and Isbell, J.L., 1998, Stratigraphy and depositional environments of Lower Permian post-glacial rocks exposed between the Byrd and Nimrod Glaciers, Antarctica: Journal of African Earth Sciences, v. 27, p. 175-176.

Shaw, J., 2016, Paraglacial landscapes in St George's Bay, Newfoundland, Canada, *in in* Dowdeswell, J.A., Canals, M., Jakobsson, B.J., Todd, B.J., Dowdeswell, E.K., and Hogan, K.A., eds., Atlas of Submarine Glacial Landforms: Modern, Quaternary and Ancient: Geological Society of London, Memoir 46, p. 97-98.

Sheppard, K., Bell, T., and Liverman, D.G.E., 2000, Late Wisconsinan stratigraphy and chronology at Highlands, southern St. George's Bay, southwest Newfoundland: Quaternary International, v. 68-71, p. 275-283.

Sobiesiak, M.S., Kneller, B., Alsop, G.I., and Milana, J.P., 2018, Styles of basal interaction beneath mass transport deposits Marine and Petroleum Geology, v. 98, p. 629-639.

Soreghan, G.S., Soreghan, M.J., and Heavens, N.G., 2019, Explosive volcanism as a key driver of the late Paleozoic ice age: Geology, v. 47, p. 600-604.

Survis, S.R., 2015, Sedimentology and stratigraphy of high-latitude, glacigenic deposits from the Late Paleozoic Ice Age in the Tepuel-Genoa Basin, Patagonia, Argentina: University of Wisconsin - Milwaukee, M.S. Thesis, 104 p.

Svendsen, J.I., and Mangerud, J., 1997, Holocene glacial and climatic variations on Spitsbergen, Svalbard: The Holocene, v. 7, p. 45-57.

Tedesco, J., Cagliari, J., Coitinho, J.D.R., Lopes, R.D.C., and Lavina, E.L.C., 2016, Late Paleozoic paleofjord in the southernmost Parana Basin (Brazil): Geomorphology and sedimentary fill: Geomorphology, v. 269, p. 203-214.

Thomas, G.S.P., and Chiverrell, R.C., 2006, A model of subaqueous sedimentation at the margin of the Late Midlandian Irish Ice Sheet, Connemara, Ireland, and its implications for regionally high isostatic sea-levels: Quaternary Science Reviews, v. 25, p. 2868-2893.

Thomas, G.S.P., and Connell, R.J., 1985, Iceberg drop, dump, and grounding structures from Pleistocene glacio-lacustrine sediments, Scotland: Journal of Sedimentary Petrology, v. 55, p. 243-249.

Veevers, J.J., Powell, C.M., Collinson, J.W., and López-Gamundí, O.R., 1994, Synthesis, *in* Veevers, J.J., and Powell, C.M., eds., Permian-Triassic Pangean basins and foldbelts along the Panthalassan Margin of Gondwanaland: Boulder, Colorado, Geological Society of America, Memoir 184, p. 331-353.

Veevers, J.J., and Tewari, R.C., 1995, Gondwana master basin of Peninsular India between Tethys and the interior of the Gondwanaland province of Pangea: Geological Society of America, Memoir 187, 72 p.

Vesely, F., and Assine, M.L., 2014, Ice-keel scour marks in the geologic record: evidence from Carboniferous soft-sediment striated surfaces in the Paraná Basin, southern Brazil: Journal of Sedimentary Research, v. 84, p. 26-39.

Vesely, F.F., Rodrigues, M.C.N.L., Da Rosa, E.L.M., Amato, J.A., Trzaskos, B., Isbell, J.L., and Fedorchuk, N.D., 2018, Recurrent emplacement of non-glacial diamictite during the late Paleozoic ice age: Geology, v. 46, p. 615-618.

Visser, J.N.J., 1987, The palaeogeography of part of southwestern Gondwana during the Permo-Carboniferous glaciation: Palaeogeography, Palaeoclimatology, Palaeoecology, v. 61, p. 205-219.

Visser, J.N.J., 1994, The interpretation of massive rain-out and debris-flow diamictites from the glacial marine environment, *in* Deynoux, M., Miller, J.M.G., Domack, E.W., Eyles, N., Fairchild, I.J., and Young, G.M., eds., Earth's Glacial Record: Cambridge, Cambridge University Press, p. 83-94.

Visser, J.N.J., 1997, A review of the Permo-Carboniferous glaciation in Africa, *in* Martini, I.P., ed., Late Glacial and Postglacial Environmental Changes: Quaternary, Carboniferous-Permian, and Proterozoic: Oxford, U.K., Oxford University Press, p. 169-191.

Visser, J.N.J., Loock, J.C., and Colliston, W.P., 1987, Subaqueous outwash fan and esker sandstones in the Permo-Carboniferous Dwyka Formation of South Africa: Journal of Sedimentary Petrology, v. 57, p. 467-478.

Vizán, H., Prezzi, C.B., Geuna, S.E., Japas, M.S., Renda, E.M., Franzese, J., and Van Zele, M.A., 2017, Paleotethys slab pull, self-lubricated weak lithospheric zones, poloidal and toroidal plate motions, and Gondwana tectonics: Geosphere, v. 13 , n. 5, 1541 - 1554.

Waugh, B.J., 1988, Sedimentology and petrology of sandstones from the Permo-Carboniferous Pagoda Formation, central Transantarctic Mountains, Antarctica: Vanderbilt University, M.S. Thesis, 146 p.

Wopfner, H., 2012, Late Palaeozoic-Early Triassic deposition and climates between Samfrau and Tethys: a review: *in* Gąsiewicz, M. and Słowakiewicz, M., eds., Paleozoic Climate Cycles: Their Evolutionary and Sedimentological Impact: Geological Society of London, Special Publication 376, p. 5-32.

Wright, R., and Anderson, J.B., 1982, The importance of sediment gracity flow to sediment transport and sorting in glacial marine environment, Eastern Weddell Sea, Antarctica: Geological Society of America, Bulletin, v. 93, p. 951-963.

CHAPTER 3.
CONTRASTING STYLES OF GLACIAL SEDIMENTATION AND GLACIER THERMAL REGIMES IN THE LOWER WYNYARD FORMATION (PENNSYLVANIAN – EARLY PERMIAN, TASMANIAN BASIN)

To be submitted to *The Depositional Record* by Ives, L.R.W. and Isbell, J.L.

Abstract

The Late Paleozoic Ice Age (LPIA) was an ~ 118-million-year interval in earth's history with extensive high-latitude glaciation. There is mounting evidence that intervals of widespread glaciation can be attributed to multiple, dispersed ice centers that grew and shrank asynchronously across polar Gondwana due to local, regional, and global climatic and geologic drivers. To understand the complex interaction between glaciers and climate during this time, LPIA glacigenic deposits must be understood in detail on a local level before they can be tied to basinal, regional, or global patterns of climate change. This study evaluates the sedimentology and stratigraphy of the basal portion (415 m) of the glacigenic, Permo-Carboniferous (Gzhelian – Asselian) Wynyard Fm (Tasmanian Basin) at its type section in northwestern Tasmania. In this succession, the Wynyard Fm contains three facies associations: a muddy, clast-rich diamictite, a sandy clast-rich diamictite, and a rhythmically interstratified unit. All three facies associations contain mass transport deposits and turbidites, and were likely deposited below storm wave base. The lowermost 58 m of the succession is composed of the muddy diamictite facies association, which was likely deposited as a proglacial, glacier-proximal and possibly the subglacial portions of a grounding zone wedge. Grounding zone wedges are associated with fast-flowing (i.e., ice streams) glaciers that have polythermal subglacial thermal regimes. The rest of the succession is dominated by the sandy diamictite facies association, which was likely deposited as the proglacial, glacier-proximal portion of a grounding-line fan and/or morainal bank. The rhythmically interstratified facies association makes up ~ 15 m of the succession and was likely deposited by the same glacial system as the sandy diamictite, but in a proglacial glacier-intermediate or glacier-distal position as cyclopelites. Grounding-line fans, morainal banks, and cyclopelites are typically associated with glaciers that have mild subpolar to temperate thermal regimes. Paleotransport directions in this succession support the hypothesis that the "Wynyard Glacier" flowed from south to north through the Dundas Trough, a structural element and

paleotopographic low in western Tasmania. Together, the sedimentology, sequence stratigraphy, and transport directions allow some inferences to be made about the "Wynyard Glacier". The glacier was most likely a fast-flowing part of a large ice cap or ice sheet that was nucleated somewhere to the modern south of Tasmania. Deposition of the Wynyard Fm at its type section was initiated when the margin of the "Wynyard Glacier" had a dominantly cold subpolar thermal regime (muddy diamictite facies association), but that thermal regime shifted to temperate (sandy diamictite facies association) for most of the depositional succession. This entire succession was all likely deposited during the same overall glacier retreat event, and the glacier's grounding line was likely never more than a few kilometers in either direction of the measured sedimentary sections while deposition was occurring. A possible reason why this portion of the Wynyard Fm type section is lithologically homogenous and thick relative to its correlates throughout Tasmania is that this was a location of a glacial pinning point that forced the glacier's grounding line to stay in this location for relatively extended periods, allowing for the buildup of a thick, proglacial, glacier-proximal succession. The grounding zone wedge in this succession likely took decades to centuries to create, while the cyclopels, grounding-line fan, or morainal bank deposits were likely created on the order of years to decades. The question remains how the glacigenic sediment and "Wynyard Glacier" relate to similarly-aged glacigenic deposits elsewhere in the Tasmanian Basin, southern and eastern Australia, and North Victoria Land (Antarctica).

3.1. Introduction

The Pennsylvanian - Permian Wynyard Fm in the Tasmanian Basin is a classic example of glacigenic strata from the Late Paleozoic Ice Age (LPIA; ~ 374 -256 Ma) (Isbell et al., 2003, 2012; Fielding et al., 2008a; Rosa and Isbell, 2021; Isbell et al., 2021; **Error! Reference source not found.**). The L PIA was an interval of widespread glaciation across Gondwana, and was characterized by globally low pCO_2, high pO_2, generally low eustatic levels with large magnitude fluctuations, low solar luminosity, and increased $\delta^{18}O$ and $\delta^{13}C$ values relative to the rest of the Phanerozoic (Montañez and Poulsen, 2013). The Wynyard Fm was originally interpreted as glacigenic in the 1860's (Stephens, 1869) due to the thick successions of massive diamictites containing an abundance of striated and faceted clasts in a wide range of sizes. The Wynyard Fm's glacigenic interpretation has stood the test of time (see Ahmad, 1957; Banks, 1962, 1981; Hand, 1993; Henry et al., 2012), but the massive and homogenous nature of the diamictite has meant that the strata have been relatively opaque to interpretations of glacial depositional environments (Fielding et al., 2010).

In this paper, we evaluate the sedimentology, sequence stratigraphy, and flow directions of the basal 415 m of the Wynyard Fm type section in northwestern Tasmania (**Error! Reference source not f ound.**). The succession described in this study begins at the basal unconformity of the Wynyard Fm and continues to the base of sections described in a similar way by Henry et al. (2012). This assessment includes sub-dividing the massive diamictite of the Wynyard Fm based on its matrix composition. From this information we infer physical characteristics of the glacier responsible the deposition of these sediments (the "Wynyard Glacier") including its size and thermal regime.

This detailed, lithofacies-based assessment of the Wynyard Fm (and similar successions throughout Gondwana) is critical to our understanding of the LPIA. The emerging view of glaciation during the LPIA is that multiple ice centers (ice caps and ice sheets) were distributed across Gondwana, and

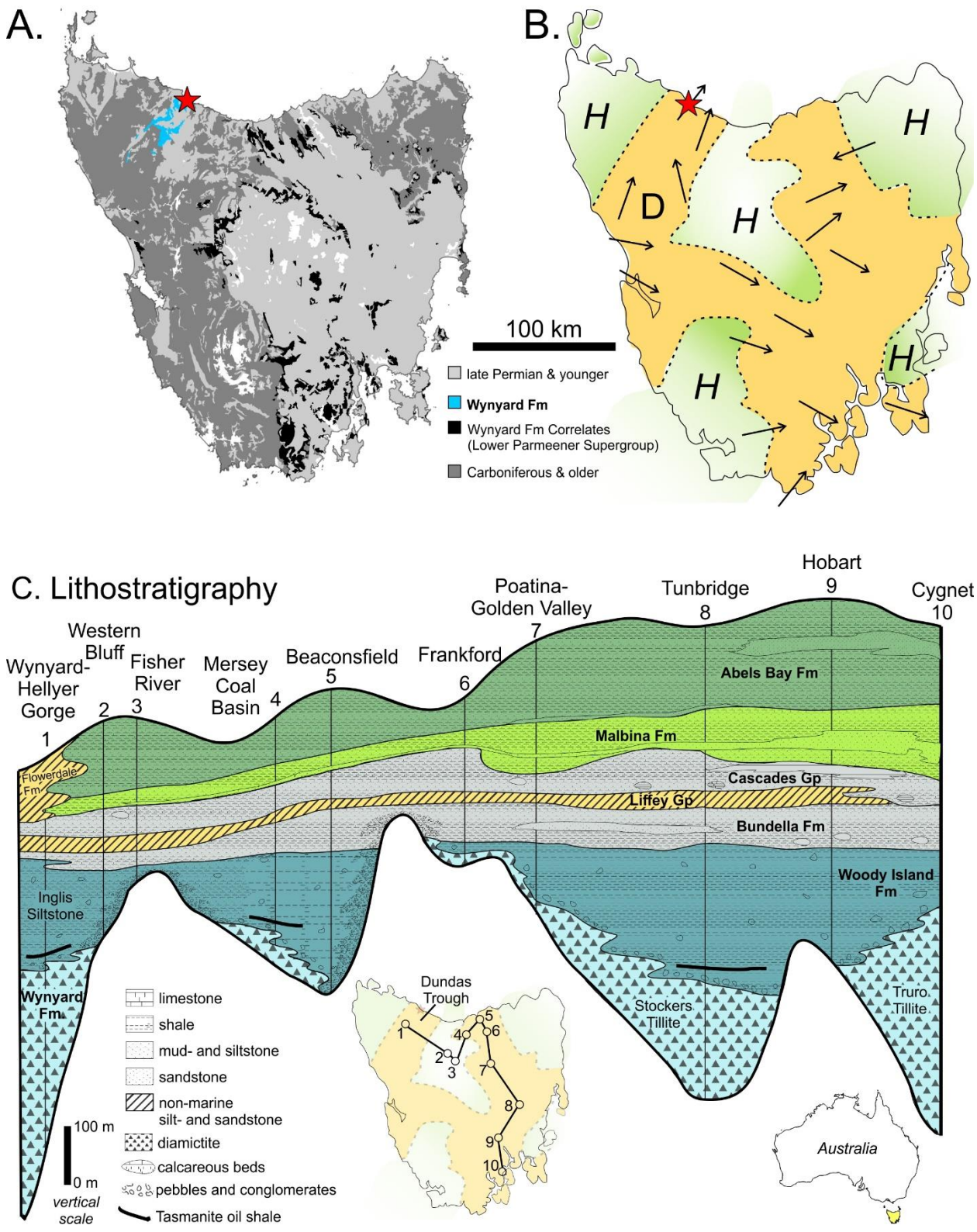
A.
B.
H
D
H
H
H
H
100 km
late Permian & younger
Wynyard Fm
Wynyard Fm Correlates
(Lower Parmeener Supergroup)
Carboniferous & older
C. Lithostratigraphy
Wynyard-
Hellyer
Gorge
1
Western
Bluff
2
Fisher
River
3
Mersey
Coal
Basin
4
Beaconsfield
5
Frankford
6
Poatina-
Golden Valley
7
Tunbridge
8
Hobart
9
Cygnet
10
Abels Bay Fm
Malbina Fm
Flowerdale
Fm
Cascades Gp
Liffey Gp
Bundella Fm
Woody Island
Fm
Inglis
Siltstone
Wynyard
Fm
Stockers
Tillite
Truro
Tillite
limestone
shale
mud- and siltstone
sandstone
non-marine
silt- and sandstone
diamictite
calcareous beds
pebbles and conglomerates
Tasmanite oil shale
100 m
0 m
vertical
scale
Dundas
Trough
1
2
3
4
5
6
7
8
9
10
Australia

Figure 3-1. Geologic and paleogeographic maps of the Wynyard Formation, Tasmania and lithostratigraphy of the Tasmanian Basin A. A reproduction of the Tasmanian portion of the 1:1 million scale Surface Geology of Australia Map GIS dataset (Raymond et al., 2012). The Wynyard Formation is indicated by the black and white horizontal stripes, correlates of the Wynyard Fm throughout Tasmania are indicated in black, rocks younger than the Wynyard Formation (mid Permian and younger) are indicated in light grey, rocks older than the Wynyard Formation (late Carboniferous and older) are indicated by dark grey, and water bodies are white. The location of this study is indicated by a red star. B. Tasmanian paleogeography during the time of the Wynyard Formation deposition (late Carboniferous to early Permian) inferred from previous studies. Green areas are inferred highlands (H) and orange areas are inferred glaciated lowlands. The "D" specifically indicated the Dundas Trough, which is the structural and topographic low that trends northeast to southwest across western Tasmania. The Dundas Trough defines the suggested flow path for the "Wynyard Glacier". Arrows show measured ice flow directions from previous studies (Hand, 1993; Henry et al., 2012). The location of this study is indicated by a red star. Map after Hand (1993), Henry et al. (2012), and Reid (2014). C. Cross section of the Tasmania Basin showing lithostratigraphic units, showing the Pennsylvanian – Cisuarlian strata (Lower Parmeener Supergroup). Lithostratigraphic names used in this diagram (in bold) are those most often used when discussing basin stratigraphy (see part B of this figure). Readers should note that lithostratigraphic names for units of similar age and depositional environment depend on location within the basin. Un-bold lithostratigraphic names are those mentioned in the text. Map of Tasmania showing cross section locations is from Figure 1B. This figure is modified from Clarke and Forsyth (1989), Henry et al. (2012), and Reid et al. (2014).

that those ice centers grew and shrank asynchronously in response to local, regional, and global climatic and geologic drivers (Isbell et al., 2012; Montañez and Poulsen, 2013). Local and regional heterogeneity in the lithofacies and timing of glacial successions like the Wynyard Fm have the potential to be very high. Therefore, LPIA glacigenic deposits must be understood, in detail, on a local level before they can be tied to basinal, regional, or global patterns of climate change (e.g., Rygel et al., 2008; Chen et al., 2016; Soreghan et al., 2019).

3.2. Sedimentology and Stratigraphy

The Wynyard Formation consists of Permo-Carboniferous, diamictite-rich strata that outcrop in northwestern Tasmania (**Error! Reference source not found.**; Figure 3-3). This succession has long been interpreted as glacigenic (Stephens, 1869; Kitson, 1902; Twelvetrees, 1905; David, 1907; Howchin, 1912) and many authors agree that the depositional environment of the Wynyard Fm was most likely proglacial, glacier-proximal marine conditions created by a temperate glacier (Banks et al., 1955; Ahmad, 1957; Carey and Ahmad, 1961; Clarke and Banks, 1975; Banks, 1981; Powell, 1990; Hand,1993; Henry et al., 2012; Reid et al., 2014). Most successions of the Wynyard Fm and its correlates throughout Tasmania are composed predominantly of massive and crudely stratified

diamictites, but many locations also include stratified conglomerates and sandstones, turbidites, and significant thicknesses of rhythmically laminated fine-grained deposits with dropstones (up to 145 m; Banks et al., 1955; Williams and Lennox, 1989). All these lithologies are often redeposited through mass transport (Banks et al., 1955; Crowell and Frakes, 1971; Banks, 1981; Hand, 1993). Erosional unconformities, which have been interpreted as glacial advance surfaces, occur within the Wynyard Fm where diamictites units overlie and deform rhythmically laminated units (Banks, 1962).

The diamictites of the Wynyard Fm are often discussed and treated as a singular unit. This is mostly because massive diamictites are relatively inscrutable (Fielding et al., 2010). While previous workers have used some features of these diamictites, such as sedimentary structures (Henry et al. (2012) and clast composition (Banks 1962; 1981) to interpret depositional environment, little interpretive consideration has been paid to other characteristics. Specifically, little attention has been paid to variations in diamictite lithology. Variability in matrix grain size of diamictites is an important characteristic to consider because it is key in discriminating between glacigenic depositional environments (Hambrey and Glasser, 2012). Consideration of matrix composition may be very useful for more specific interpretations of the Wynyard Fm and its correlates because a wide range of matrix grain sizes has been described in Tasmanian diamictites. For example, the matrix of diamictites in the Wynyard Fm have been described as clay (David, 1907), 'calcareous and argillaceous matrix of clay grade' (Clarke, 1968), silty clay (Ahmad, 1957; Gulline and Bravo, 1977; this study), "grey sandy mudstone" (Powell, 1990; Henry et al., 2012), "comminuted fragments of the Ordovician shales and quartzites" (David, 1907), "dark grey arenite" (Jago, 1972), "poorly cemented angular chips of quartzite and slate" (Gee, 1971), and sandy (this study). In this study we provide an example of how dividing diamictite facies based on matrix grain size may lead to a better understanding of the depositional environments represented by glacigenic successions in Tasmania.

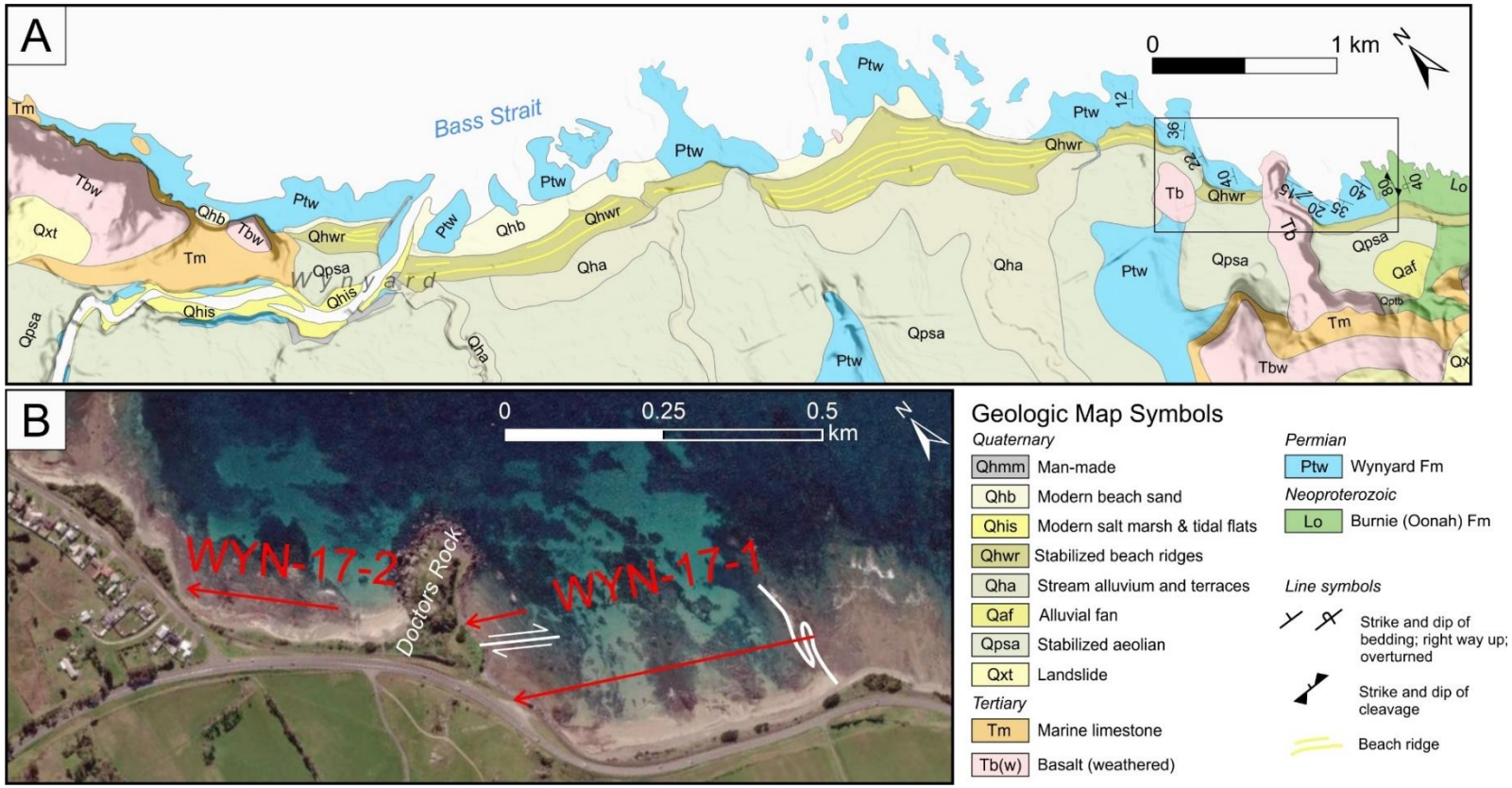

Figure 3-3. Geologic map of Wynyard Fm type section and aerial photograph of study location. A. Geologic map over a hillshade of the Wynyard area, with emphasis on the Wynyard Fm (Ptw) type section, which outcrops along the coast. Geologic map polygons from the 1:25k digital geology of Tasmania (Mineral Resources Tasmania, 2020). Structural information from this study and from 1:25,000 scale maps of the Wynyard (Everard and Calver, 2011) and Calder (Everard, 2011) areas. Hillshade was derived from 1 m digital elevation model (ELVIS). The extent of figure 3-2B is indicated by the black box. B. Satellite imagery of study area, with the vertical extents of sections WYN17-1 and WYN17-2 indicated by red arrow. The lower contract of the Wynyard Fm with the underlying Burnie Fm is indicated by a white line, the fault in WYN17-1 is indicated by a white line with directional arrows, and Doctors Rock is labeled. Satellite imagery was obtained from the ESRI ArcGIS "World Imagery" Basemap layer. The image was sourced from Maxar Vivid Imagery Basemap Layer, and is dated from 29 August 2018.

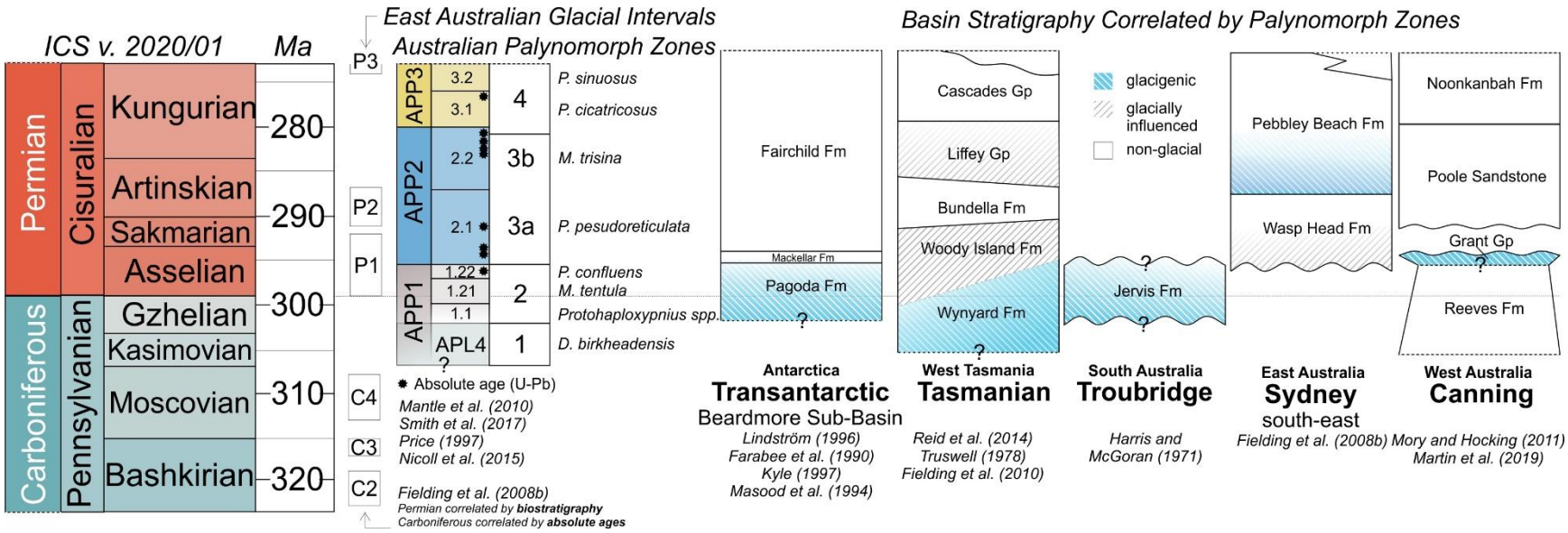

Figure 3-4. Biostratigraphy of the Tasmanian Basin and other regionally significant basins with glacigenic strata of similar age. Palynomorph-based biozones are related to the geologic time scale through U-Pb zircon ages from eastern Australian Basins (Nicoll et al., 2016).

94

The Wynyard Fm and its correlates across Tasmania make up the basal strata of the Parmeener Supergroup, a Pennsylvanian to Late Triassic sedimentary succession within the Tasmanian Basin (Clarke et al. 1989; Fielding et al. 2010; **Error! Reference source not found.**C). These glacial s uccessions, which can exceed 500 m in thickness, are mostly confined to structural lows within the Tasmanian Basin (Banks and Clarke 1987; Hand 1993; **Error! Reference source not found.**C). T here are large variations in Wynyard Fm thickness in northeastern Tasmania (e.g., Reid et al., 2014). Many successions of the Wynyard Fm are much thinner (5 – 150 m), which is consistent observations of relief on the sub-Permian surface throughout the Dundas Trough (e.g., Gee, 1977; Williams and Lennox, 1989; Hand, 1993). Across the basin, these sediments are separated into several different formations (Truro Tillite, Stockers Tillite, and Zeehan Tillite; **Error! Reference s ource not found.**C) that all unconformably overlie Proterozoic to late Devonian metamorphosed basement. The Wynyard Fm, Truro Tillite, and Stockers Tillite all conformably underlie lower Permian, marine, black shales (Banks 1981; Banks and Clarke 1987; Domack et al. 1993). Following the deposition of the Wynyard Fm and its correlates, sedimentological records indicate that the Tasmanian Basin alternated between marine and freshwater conditions throughout the Permian and into the Triassic (Banks, 1962; Banks and Clarke, 1987; Fielding et al., 2010; Reid et al., 2014; **Error! R eference source not found.**).

3.3. Geologic Context

3.3.1. Biostratigraphy and Age

Deposition of the Wynyard Fm likely spans the Pennsylvanian-Permian boundary from the late Pennsylvanian (Kasimovian) through the early Permian (Asselian) (**Error! Reference source not f ound.**). The age of the Wynyard Fm and its correlates have been inferred through biostratigraphy.

No absolute ages have been measured. The age of the Wynyard Fm in the Wynyard area has been constrained by palynomorphs and macrofloral remains that were recovered from rare, laminated, siltstone and mudstone rhythmites that are intercalated with the diamictite. Fossils have been studied at such successions within the Wynyard Fm type section at Doctors Rock (Banks et al. 1955; Clarke and Banks, 1975) and at Hellyer Gorge ~ 33 km south-southwest of Wynyard (Clarke and Banks, 1975). Palynomorphs from these locations are typical of Australian palynomorph Stage 1, which is characterized by *Diatomozonotrietes birkheadensis* (Clarke and Banks, 1975; Truswell, 1978; **Error! Reference source not found.**). This zone is now referred to as palynomorph zone APL4 (Price, 1997) or the lowermost part of APP1 (Mantle et al., 2010).

Absolute ages obtained using U-Pb zircon dates measured using CA-IDTIMS and interpreted to represent the deposition age of the unit, place the minimum age of APP1 in eastern Australian basins as 295.5 Ma (early Permian, Asselian Stage) (Smith et al., 2017). This age suggests that APP1 spans the Permian-Carboniferous boundary (Smith et al., 2017; Mantle et al., 2010; **Error! Reference source not found.**). The biostratigraphy of the Wynyard Fm broadly correlates to, but may have partially preceded, the "P1" glacial interval in eastern Australia, which was the time of the most extensive glaciation in eastern Australia (Fielding et al., 2008b; Fielding et al., 2010; Frank et al., 2015; **Error! Reference source not found.**).

3.3.2. Structural Setting

The Wynyard Fm occurs within a topographic and structural low called the Dundas Trough, which is ~50 km wide, 100 km long, has several hundred meters of paleotopographic relief below the Permian, and trends northeast-southwest across western Tasmania (**Error! Reference source not found.**B; Clarke, 1968; Banks, 1981; Hand, 1993; Reid et al., 2014). The glacial paleoflow directions associated with the Wynyard Fm and its correlates indicate that the "Wynyard Glacier(s)" likely

flowed north through the Dundas Trough (Hand 1993). In many places throughout Tasmania, the Wynyard Fm and its correlates are structurally horizontal (e.g., Gulline and Bravo, 1977). However, the type section of the Wynyard Fm that outcrops along Tasmania's northeast coast includes minor folds and faults (Ahmad, 1957; Gee, 1971). In this study, one small fault (Figure 3-3) as well as changes in structural strike and dip orientations were observed and accounted for in measuring the section thickness and paleo-transport directions.

3.3.3. Paleogeography and Paleoclimate

The Tasmanian Basin was likely located at high polar latitudes (> 60°S) during the Kasimovian through Asselian and drifted slightly southward during that time (Meredith et al., 2021; Figure 3-5). During that interval, the Tasmanian Basin was located continent-ward of the convergent Panthalassan margin of southeastern Gondwana between North Victoria Land (Antarctica) and eastern Australia (Veevers, 2006). Glacial deposits of similar age to the Wynyard Fm occur in the paleogeographically adjacent areas of North Victoria Land in Antarctica (Collinson and Kemp, 1983; Cornamusini et al., 2017; Zurli et al., 2021) as well as the Australian states of Victoria (Webb and Spence, 2008) and South Australia (Normington, 2017). Flow directions measured in these successions suggest that the same ice center may have been responsible for glacial deposits in North Victoria Land and Tasmania (Veevers, 2006). This same ice center may have extended into South Australia (Normington, 2017).

3.4. Study Area and Methods

The succession described in this study is the base of the Wynyard Fm type section. The Wynyard Fm type section is exposed along ~ 6.5 km of coast in the intertidal zone around the town of Wynyard on the shoreline of the Bass Strait in northwestern Tasmania (**Error! Reference source n**

ot found.; Figure 3-2). Most authors agree that the Wynyard Fm repeats several times through the whole length of the type section, and have pervasive folds and faults that appear to be relatively minor in magnitude (best

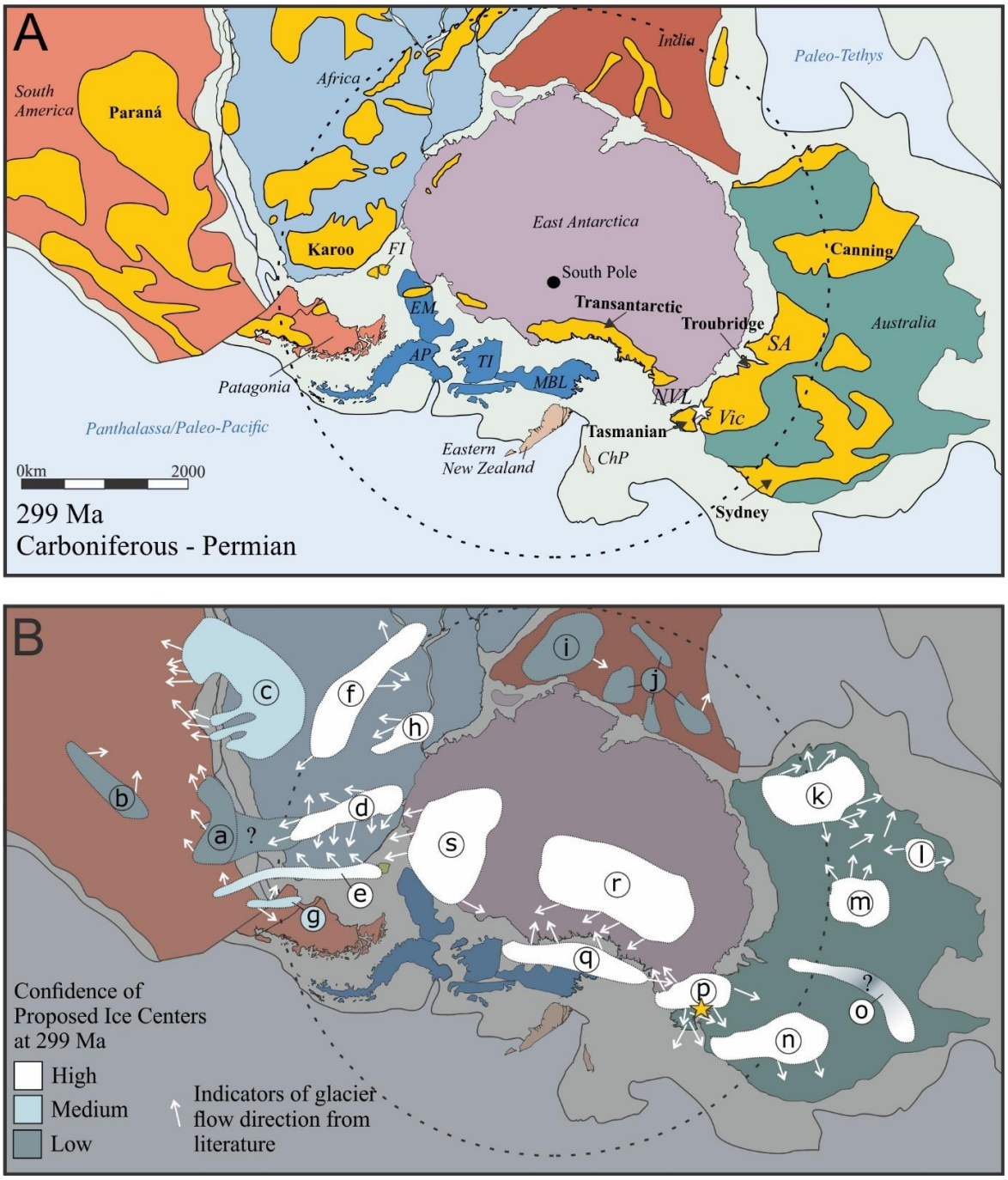

Figure 3-5. Paleogeographic reconstructions of Gondwana near the Pennsylvanian-Permian Boundary. All maps are south-polar projections. Star indicates the approximate location of the Shackleton Glacier area. Continent distributions are based on Lawver et al. (2011) and copied from (Isbell et al. 2012), and south pole position is from Meredith et al. (2021). **A.** Yellow regions indicate the modern extent of sedimentary basins containing late Paleozoic Ice Age strata. Abbreviations include: Falkland Islands/Malvinas (FI), Ellsworth Mountain block (EM), Antarctic Peninsula (AP), Thurston Island (TI), Marie Byrd Land (MBL), and the Challenger Plateau/western New Zealand (ChP). Basins adapted from Isbell et al. (2012). **B.** Proposed positions of glacial centers during the early Permian based on flow

(Figure 3-4, continued) directions and position of basins and "highlands". Illustrated ice centers are not meant to represent the whole possible extent of each proposed glacier, but where proposed glaciers were likely to be nucleated. The arrows reflect field measurements of flow directions reported in the studies cited for each ice center. However, flow directions of glaciers are highly variable, both spatially and temporally, and the true flow paths of these ancient ice centers were likely much more variable than the arrows on this map. Confidence is based on the abundance of available lithologic data, and both relative and absolute ages. Ice centers are as follows: a. Uruguay, b. Asunsción, c. Windhoek/ Koakoveld Highlands, d. Cargonian Highlands, e. Cape-Ventana Fold, f. East African Thermal Rise, g. Patagonian Western Magmatic Arc, h. Zimbabwe, i. Madagascar-SW India, j. Chotanagpur & Chhattisgarh, k. Pilabra-Yilgarn, l. Kimberly, m. Arunta-Musgrave, n. Bowen-Gunnedah-Sydney, o. Galilee, p. Wilson, r. East Antarctic, s. Ellsworth. References for ice centers in Figure 2-2 captions.

described by Gee, 1971). Estimates of the succession's thickness are far less than the extent of the exposure, and have included 370 m (David, 1907), 180 m (Ahmad, 1957), 600 m (Banks, 1962), and 550 m (Reid et al., 2014). The thickest observed succession of the Wynyard Fm after the type section is located at the confluence of the Arthur and Hellyer rivers, ~ 35 km southwest of Wynyard, and measures ~ 350 m (Gulline and Bravo, 1977). The lack of clear stratigraphic surfaces makes estimating the succession's thickness difficult. This area has been the focus of several studies including mapping reports (Gee, 1971; Gulline and Bravo, 1977; Everard and Calver, 2011) and detailed sedimentological studies (Banks et al., 1955; Ahmad, 1957; Banks, 1962; Powell, 1990; Henry et al., 2012).

The section described in this study is made up of the lowermost ~ 415 m of this succession. This succession has not been specifically described in its entirety, though portions of it are included in Ahmad (1957) and Banks et al. (1955). One fault was identified in this field study that resulted in 20 m of repeated section. The repeated section is not included in the reported thickness. The succession described in this study begins at the basal unconformity of the Wynyard Fm, and ends where sections described by Henry et al. (2012) begin. Sedimentological data (texture, grain shape, sedimentary structures, etc.) as well as paleotransport indicators (including cross stratification, striae, fold hinge lines, and thrust-plane orientation) were logged in these sections. Fieldwork was performed during low tide intervals of early November 2017. This was a period of relatively low

low-tides, which allowed the authors to examine more of the outcrop than is typically exposed. Two successive sedimentary sections were described in this study. Section WYN17-1 is stratigraphically 245 m thick, begins at the basal unconformity of the Wynyard Fm with the Proterozoic Burnie Fm, ~ 500 m east of Doctors Rock (an Oligocene - Miocene intrusion that juts out into the sea), and ends at the contact between the Wynyard Fm of Doctors Rock (Figure 3-1C). WYN17-2 is stratigraphically 170 m thick, begins on the western side of Doctors Rock, and ends ~ 350 m west of that location.

Rolling folds and minor faults occur in this succession (Figure 3-3). Structural dip direction and dip were measured where appropriate strata were available. In section WYN17-1 the structural dip direction and dip of the succession were 242˚/40˚ for 0 – 60 meters of section, 242˚/35˚ for 60 – 200 m, 248˚/20˚ for 200 – 210 m, and 248˚/15˚ for 210 – 245 m. The structural dip direction and dip for WYN17-2 was measured as 292˚/40˚. One minor fault was observed in this succession. The fault only outcropped in the uppermost 20 m of WYN17-1, east of Doctors Rock, and appears as a right lateral fault with about 20 m of stratigraphic offset and a trend of 300˚ -120˚. The two sides of the fault were correlated using the contact between a laminated, fine-grained facies association (facies association IsR) and the overlying massive diamictite (facies Dmm-s).

Structural and sedimentary orientations were measured using a Brunton compass, with the azimuth set to 000˚. Measurements were corrected for magnetic declination using the NOAA Magnetic Declination Estimated Value Calculator (NOAA 2019). Orientations were corrected for structural dip and aggregate orientations calculated using Stereonet (v. 11) software (Allmendinger et al., 2011; Cardozo and Allmendinger, 2013).

Table 3-1. Facies Associations

Facies Association Name	Section Name	Section Height Range (m)	Consituent Facies	Facies Thickness (m)	Portion of Facies Association (%)	Depositional Environment Interpretation	Glacier Characterisitcs
Muddy Diamictite (MDm)	WYN17 -1	0 - 58	Dmm-m	51	88%	grounding zone wedge; subglacial or glacier-proximal; subaqueous marine	polar or cold sub-polar thermal regime; distributed hydraulic system; ice shelf
			Cm	4	7%		
			Sc-vc	3	5%		
Sandy Diamictite (SDm)	WYN17-1	58 - 204, 207 - 220, 236 - 240	Dmm-s	281	88%	grounding-line fan and/or morainal bank; glacier-proximal; subaqueous marine	warm sub-polar or temperate thermal regime; organized hydraulic system; calving tidewater front
			Sc-fmc	10	3%		
	WYN17-2	0 - 174	Cm	15	5%		
			Cc(d)	14	4%		
Interstratified, Rhythmic (IsR)	WYN17-1	204 - 227, 240 - 246	Fs	6	17%	grounding-line fan and/or morainal bank; glacier-medial to glacier-distal; subaqueous marine	warm sub-polar or temperate thermal regime; organized hydraulic system; calving tidewater front
			Sc-fu	7	20%		
			Cc	2	6%		
			Dms-s	20	57%		

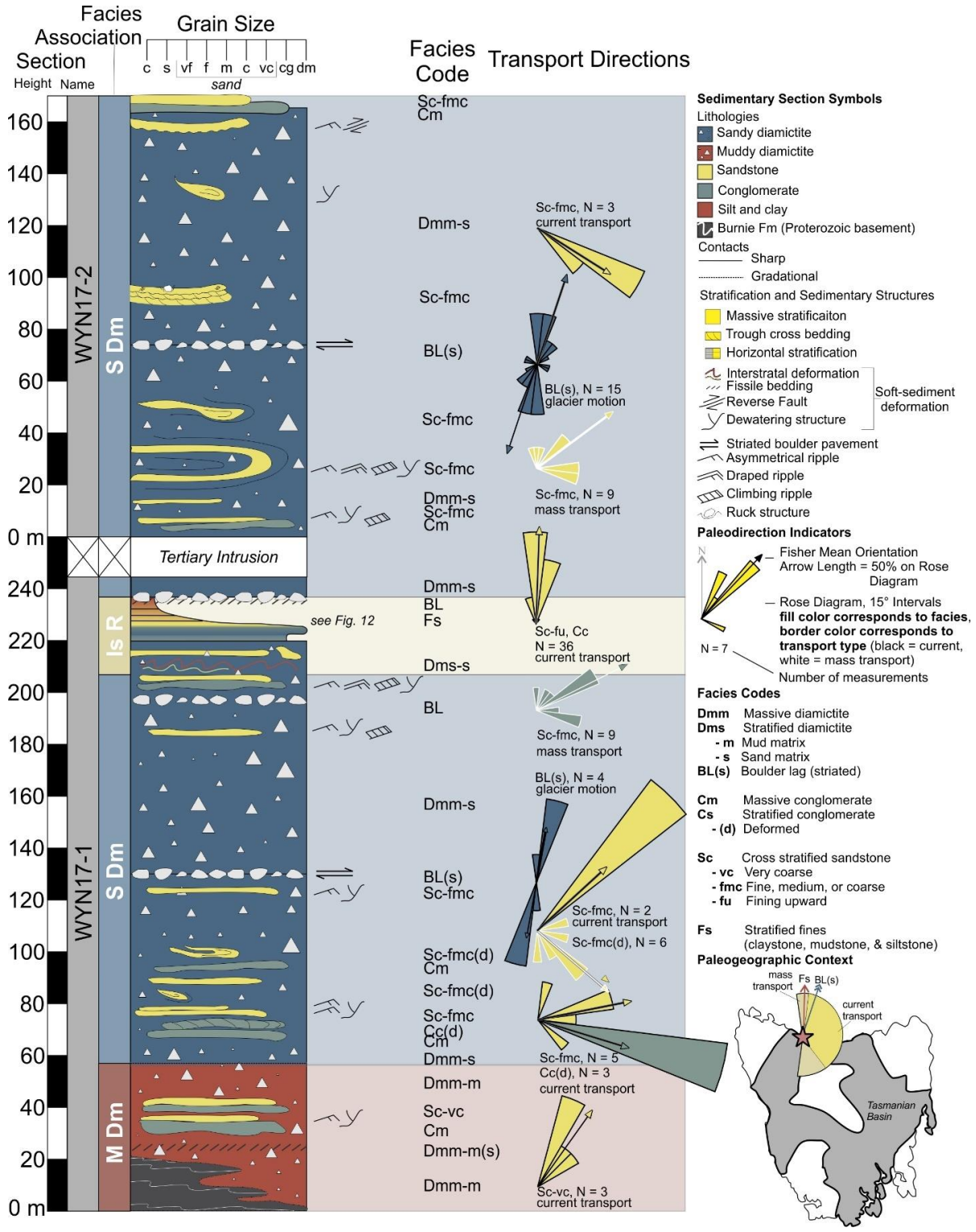

Figure 3-6. Sedimentary logs and paleotransport directions from the sites described in this study. Paleotransport directions are aligned so that the top of the page is modern north. MDm = Muddy Diamictite Facies Association, SDm = Sandy Diamictite Facies Association, IsR = Interstratified Rhythmic Facies Association.

Table 3-2. Facies descriptions

Facies Code	Facies Name	Texture	Grain Characteristics	Sedimentary Structures	Bounding Surfaces	Thickness	Geometry	Depositional Process Interpretation	Facies Associati-ons	References
Diamictites (D): Poorly Sorted Sediment Admixture										
Dmm-m	muddy, massive, matrix-supported, clast-rich	**matrix:** mud (fine silt and clay); **clasts:** granule (0.5 cm) to boulder (2 m), median size 1.5 cm	**matrix:** reddish-brown color; **clasts:** mostly angular, some sub-angular and sub-rounded; striated and faceted clasts common	massive	**lower:** sharp, undulating with (Proterozoic) Burnie Fm.; **lateral:** sharp, loaded, and/or sheared with Cm; **upper:** sharp to gradational (matrix coarsens) with Dmm-s	58 m (MDm), 1 m (SDm)	laterally continuous sheet	redeposition of muddy subglacial till or glacier-distal deposits through gravity-driven transport as cohesive debris flows	MDm	Mulder and Alexander (2001); McKay et al. (2009)
--- (s)	muddy, massive, matrix-supported, clast-rich (sheared)	*same as Dmm-m*	*same as Dmm-m*	0.1 - 1 m fissile zones, cm-scale lenticular structures	*same as Dmm-m*	0.1 - 1 m	*same as Dmm-m*	*same as Dmm-m*; deformation by simple shear (subglacial or sub-debris flow deformation)	MDm	
Dmm-s	sandy, massive, matrix supported, clast-rich	**matrix:** poorly- to moderately sorted fine sand with grain sizes from silt to coarse sand; **clasts:** granule (2 mm) to boulder (2 m), median clast size 1.5 cm	**matrix:** angular to sub-rounded, mostly sub angular; **clasts:** angular to sub-rounded, cobbles and boulder often striated, faceted, and polished	Massive; rare faint stratification, meter-scale coarsening upwards packages, and boulder pavements (striated and unstriated)	**lower:** sharp to gradational with Dmm-m, sharp and deformed with Fs; **internal:** sharp with Cm, Cs, Sc-fmc; **upper:** sharp	40 - 140+ m	laterally continuous sheet	combination of subglacial deposition, plume sedimentation, iceberg rain-out, and resedimentation through mass-transport in glacier-proximal setting	SDm	Eyles and Lagoe (1990); Powell and Cooper (2002); McKay et al. (2009); Ives and Isbell (2021)
Dms-s	sandy, stratified, matrix-supported, clast-rich	*same as Dmm-s*	*same as Dmm-s*	internally massive beds, 0.05 - 0.5, thick	sharp	0.25 - 5.5 m	*same as Dmm-s*	*same as Dmm-s,* but more distal or subject to less redeposition	IsR	

--- (d)	sandy, stratified, matrix-supported, clast-rich (deformed)	*same as Dmm-s*, and includes deformed lamina and thin beds from other stratified facies	*same as Dmm-s*	highly deformed through soft sediment folding	*same as Dmm-s*	*same as Dmm-s*	*same as Dmm-s*	*same as Dmm-s*, but more distal	IsR	
Conglomerates (C): Sorted Sediment Admixture										
Cm	massive, pebbly, clast supported	fine sand to boulders; pebbles and coarse sand most common; moderately- to very-poorly sorted	angular to sub-angular; similar to adjacent diamictite facies	massive, densely packed (very little void space), not imbricated	**upper and lower** sharp, loaded, and/or sheared with diamictites and other facies; occasional abrupt gradational contacts with Sc-vc	0.25 - 9 m	sheet-like, wedge-like, and lenticular bodies, laterally discontinuous	hyper-concentrated density flows or traction carpets	MDm, SDm, IsR	Mulder and Alexander (2001); Todd (1989); Sohn (1997)
--- (b)	massive, pebbly, clast supported (clast cluster)	*same as Cm*	*same as Cm*	*same as Cm*	*same as Cm*	*same as Cm*	stringers and "blobs" in diamictite	resedimented conglomerate bodies or as iceberg dump structures	MDm, SDm	Thomas and Connell (1985)
Cc	cross bedded conglomerate	coarse sand to small boulders (25 cm), pebbles and small cobbles most common; moderately-well-sorted	angular to sub-rounded	planar cross beds; cross bed sets (0.5 - 0.75 m thick)	**lower:** sharp, loaded (cm-scale flame and diapir structures); **upper:** sharp	0.2 - 2 m	laterally continuous sheet	non-channelized, down-current progradation of gravel bars; possibly reactivated Cm?	IsR	

--- (d)	cross bedded conglomerate (deformed)	*same as Cc*	*same as Cc*	soft sediment folding and water-escape structures of planar cross beds	*same as Cc*	*same as Cc*	discontinuous, maximum 10 m long and wide	resedimented Cc	SDm	

Sandstones (S): 0.063 - 2 mm Diameter										
Sc-vc	Very-coarse-grained, cross bedded	upper medium sand to granules, very coarse sand most common; moderately-well-sorted	angular to sub-rounded, similar composition to Cm	unidirectional cross beds; massive bedding; dewatering structures; beds 0.25 - 1 m thick	sharp upper, lower, and lateral contacts; rare abrupt gradational lower contacts with Cm	1 - 2 m	sheet-like, wedge-like, and lenticular bodies, laterally discontinuous	turbidite; likely resedimented in some places; turbid portion of a multiphase subaqueous flow, where facies Cm is the non-cohesive, high-density portion	MDm	Sohn et al., 2002; Henstra et al., 2016
Sc-fmc	Fine-, medium-, or coarse-grained, cross stratified	range of grain sizes from fine to very coarse, all moderately- to well-sorted in individual beds	angular to sub-rounded	cross stratified beds and laminae; planar and trough cross beds, unidirectional cross laminae, plane beds and laminae, climbing ripples, convoluted bed, flaser cross lamination	sharp, often with irregular or "loaded" surfaces, and in rare cases are erosional	0.25 - 1 m	laterally discontinuous, up to 5 m long, roughly lenticular	turbidites; deposited by sustained, but fluctuating and generally waning, sediment-rich, turbulent flows	SDm	Mulder and Alexander (2001); Winsemann et al., 2007

--- (d)	Fine-, medium-, or coarse-grained, cross stratified (deformed)	*same as Sc-fmc*	*same as Sc-fmc*	soft-sediment dewatering structures, normal faults, and folding	*same as Sc-fmc*	*same as Sc-fmc*	*same as Sc-fmc*	resedimented and rapidly consolidated Sc-fmc	SDm	
Sc-fu	Fining upward stratified sandstone	very coarse to very fine sand; medium-grained sandstones are moderately-well- to poorly-sorted, fine- and very-fine-grained sandstones are well- to very-well sorted; rare out-sized pebbles and cobbles	angular to sub-rounded	fining-upward successions of unidirectional 3D cross laminations, cross beds, climbing ripples, convolute bedding, and flaser cross laminations; water-escape structures; succession 0.1 - 0.25 m thick	sharp upper and lower contacts	0.1 - 0.5 m	laterally continuous or lenticular where relief present on bed	turbidites deposited by high-density turbidity currents ; outsized clasts from iceberg rain-out	IsR	Lowe, 1982; Nemec et al., 1999; Winsemann et al., 2007
Fine-grained (F): < 0.063 mm										
Fs	interlaminated claystone, mudstone, and siltstone	claystone, mudstone, and siltstone; rare out-sized pebbles and cobbles	claystones are dominantly red; mudstones are dominantly grey, but occasionally appear olive or dusky-green; siltstones are grey	laminae and rare thin beds; abrupt fining upward trend in some strata; water escape structures	**lower:** sharp; **internal**: sharp; **upper:** sharp, erosional, or sheared (fissile)	0.1 - 5 m	laterally continuous	settling from suspension; cyclopelites; outsized clasts from iceberg rain-out	IsR	Mackiewicz et al., 1984; Powell and Molina, 1989; Cowan and Powell, 1990; Ó Cofaigh and Dowdeswell, 2001

3.5. Facies and Facies Associations

3.5.1. Muddy Diamictite (MDm) Facies Association

The Muddy Diamictite Facies Association (MDm) makes up the lower 58 m of section WYN17-1 (Figure 3-6; Table 3-1). It is composed of 88% muddy, massive, matrix-supported diamictite (facies Dmm-m), 7% massive, clast-supported conglomerate (facies Cm) and 5% very-coarse-grained, cross bedded sandstone (facies Sc-vc). This facies association overlies an angular unconformity with the Neoproterozoic Burnie Fm (Figure 3-3) and has a gradational to sharp upper contact with overlying Sandy Diamictite facies association (SDm).

3.5.1.1. Dmm-m: Muddy, massive, matrix-supported, clast-rich diamictite

Dmm-m description

Muddy, massive, clast-rich, matrix-supported diamictite occurs at the base of section WYN17-1 (Figure 3-6; Figure 3-7; Table 3-2). This facies has a nonconformable, sharp, planar to irregularly-shaped lower contact with the underlying basement rocks (Neoproterozoic Burnie Fm; Figure 3-7A,B). Narrow protrusions of the Burnie Fm stick 10 – 20 cm into the diamictite's base (Figure 3-7B). Conversely, the diamictite sometimes protrudes into cm-scale, with vertical cracks and fissures in the basement rocks (Figure 3-7A). A continuous contact between the Wynyard Fm and the Burnie Fm was observed in outcrop up to 19 m above the base of the Wynyard Fm section indicating local relief on the unconformity (Figure 3-6). The authors did not observe any striations or polish on the Burnie Fm along this contact. This observation contradicts Ahmad (1957), who reported faint striations on this surface, but is consistent with the reports by other workers (e.g., Howchin, 1912). The upper contact of this facies is gradational to sharp with facies Dmm-s (sandy, massive, matrix supported diamictite; Table 3-1). The gradational contact occurs over less than a

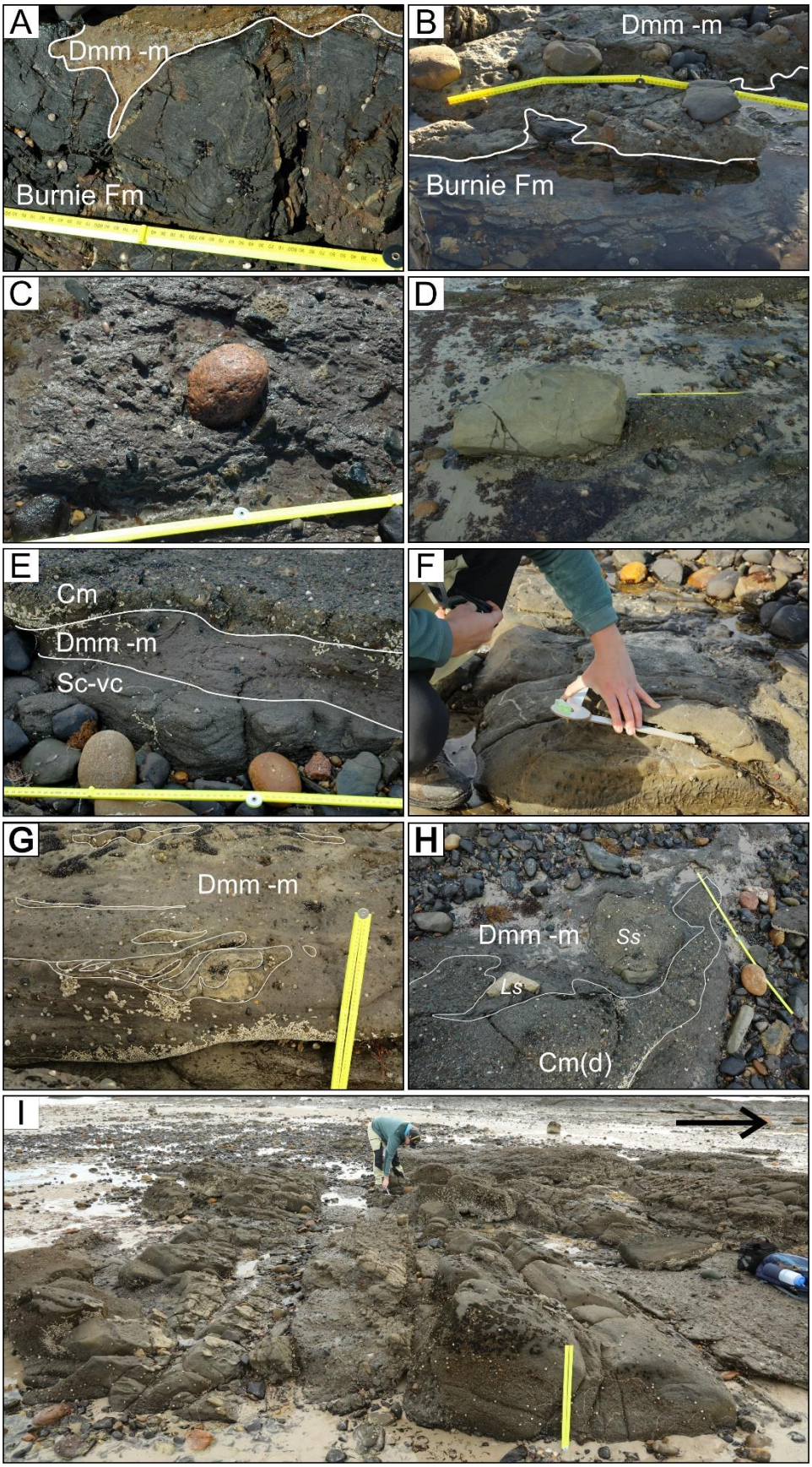

Figure 3-7. Representative photographs of the Muddy Diamictite (MDm) Facies Association. Marks on all rulers are in cm. Rulers are 50 cm when folded in half and 1 m long when unfolded. White dashed lines have been used to highlight contacts and important bedding surfaces. Cobbles were common in this inter-tidal zone, both derived from the Wynyard Fm and from the intrusion at Doctors Rock. Therefore, many of the cobbles in these photographs are not in situ and all the basaltic clasts are not from the Wynyard Fm. Some white "dots" on the rocks are modern barnacles. A. Basal unconformity where the Wynyard Fm (facies Dmm-m) overlies the Proterozoic Burnie Fm, and protrudes downward into cracks. B. Basal unconformity where the Wynyard Fm (facies Dmm-m) overlies the Proterozoic Burnie Fm, and the Burnie Fm protrudes upward. C. Characteristic massive, muddy diamictite (facies Dmm-m) with a wide variety of clast sizes. D. Meter-scale, faceted, bullet-shaped boulder in massive diamictite. E. Interbedded facies in this facies association with sharp, sometimes loaded contacts. F. Rare cross-stratified sandstone body in this facies association with dewatering structures. G. Sorted sand stringer within the massive to subtly stratified diamictite. Any apparent stratification is the result of sand lenses. H. Deformed, conglomeratic bodies (facies Cm) within the massive diamictite (facies Dmm-m). "Ss" labels sandstone clasts I. Succession of proposed bipartite flows (Cm and Sc-vc) interbedded with massive diamictite (facies Dmm-m) beds. Arrow points toward stratigraphic up.

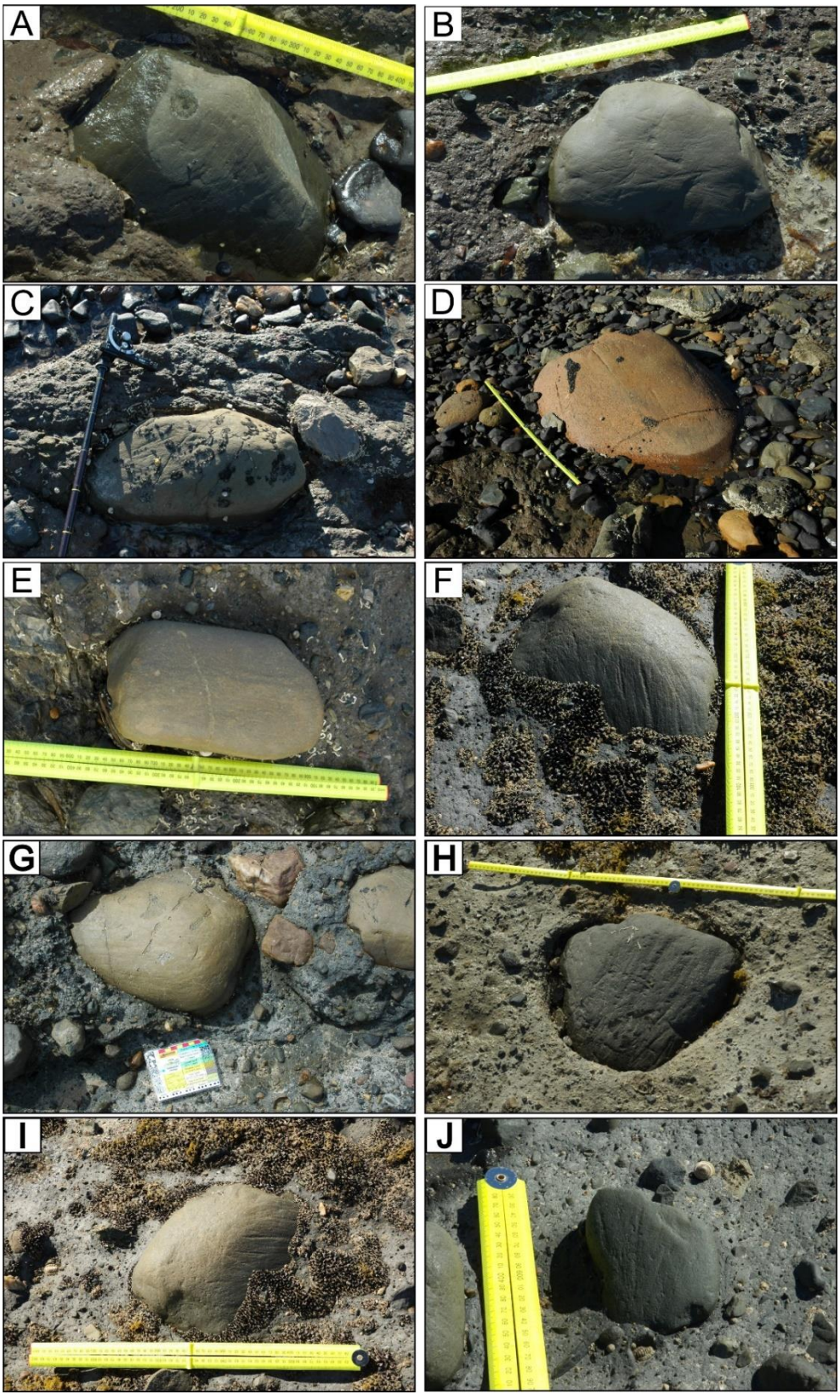

Figure 3-8. Examples of *in situ* striated and faced clasts in this succession. Marks on all rulers are in cm. Rulers are 50 cm when folded in half and 1 m long when unfolded. Cobbles were common in this inter-tidal zone, both derived from the Wynyard Fm and from the basaltic intrusion at Doctors Rock. Therefore, some of the black-colored cobbles in photographs A, C, and D are not *in situ*.

meter and is the result of a steady transition of the diamictite matrix from mudstone to muddy sandstone and an increase in clast content and size. Discontinuous conglomerate and sandstone bodies (facies Cm and Sc-vc) occur within and occasionally interfinger with this diamictite (Figure 3-7G,H,I). The sandstone and conglomerate bodies range in size from tens of meters wide and up to a meter thick to cm-scale sand stringers. Contacts between this facies and the conglomerate and sandstone bodies are mostly sharp and sometimes planar (Figure 3-7E), but more often appear to have been deformed or loaded into the underlying diamictite. For example, clasts from the conglomerate may protrude into the diamictites or the diamictites may inter-finger with the conglomerate along sharp contacts.

This muddy, massive, matrix-supported, clast-rich diamictite is ~ 58 m thick, laterally continuous in outcrop, homogenous, and massive except for occasional 0.1 - 1 m thick zones that appear to have a fissile, subtle stratification, or cm-scale lenticular structures (facies Dmm-m(s); Figure 3-6). The matrix of this diamictite is a reddish-brown, moderately well-sorted, mudstone (Figure 3-7C). Clasts range in size from granule (2 mm) to boulder (2 m). Median clast size (visual estimate) is 1.5 cm. Clasts are dominantly angular or sub-angular, with some rounded and sub-rounded clasts. Cobbles and boulders are much more likely to be rounded than granules and pebbles. Larger clasts, especially boulders, are also commonly faceted, polished, and striated (Figure 3-7D; Figure 3-8D). These textural observations are consistent with measurements made by Ahmad (1957) just above the Wynyard Fm basal unconformity at this same location.

The orientation of clasts in the diamictite appears to be random. This observation is confirmed by fabric measurements made by Ahmad (1957) (N = 100) near the base of the Wynyard Fm at this location. Unlike most clasts in this diamictite, larger, faceted faces of "bullet shaped" boulders (Figure 3-7D) in this succession (N = 3) face towards the north (Figure 3-7D).

Clasts larger than 1 cm were counted within 1 m^2 areas at 1 m (N = 26), 22 m (N = 26), and 49 m (N = 25) above the base of section WYN17-1 (Table 3-3).

Clastic sedimentary and metasedimentary rocks make up 74% of the total clasts. (Meta)sedimentary lithologies include black fine-grained sandstone, dark grey medium-grained sandstone, red fine-grained sandstone, red medium-grained sandstone, grey siltstone, grey sandstone, grey quartzite, and yellow fine-grained sandstone. Igneous clasts made up 13% of the total clasts. These clasts are equally parts red, phaneritic granitoid, and vein quartz. Chert, dolomite, and andesite each make up < 5% of total clasts.

Dmm-m interpretation

Previous sedimentological studies (e.g., Ahmad, 1957; Henry et al., 2012), as well as the characteristics of clasts (angular to subangular, frequently striated and faceted, wide range of sizes) in this facies, suggest that this diamictite was deposited in a glacigenic or glacially-influenced setting. The distinguishing characteristic of this lithology is the mudstone matrix. In a glacial environment, the most plausible depositional settings for a muddy, clast-rich diamictite are:

A. deposition as a subglacial till,

B. in a subaqueous, glacier-intermediate to -distal setting via rainout from a plume (matrix) and icebergs (clasts), or

C. through gravity-driven redeposition of either of the former (Kurjanski et al., 2019).

The non-redeposited, sub-aqueous, proglacial, glacier-distal scenario (B) is unlikely because of the absence of stratified intervals within this facies. In such a setting, one would expect stratified diamictites or stratified sorted sandstone, siltstone, and/or mudstone with evidence for dropstones

Table 3-3. Clast counts from 1 m² areas in facies Dmm-m.

Section	WYN17-1					
Section Height	1 m					
Clast type	Lithologic Class	Count	Percent	Lithologic Class	Count	Percent
black fine-grained sandstone	sedimentary	2	8%	clastic metased	23	88%
dark grey med-grains ss	sedimentary	14	54%	igneous	3	12%
fine grained burnie	sedimentary	5	19%			
Red, phaneritic granite	igneous	1	4%			
Vein Quartz (burnie?)	igneous	2	8%			
smooth, red fine-grained Ss	sedimentary	2	8%			
Total		26				

Section	WYN17-1					
Section Height	22 m					
Clast type	Lithologic Class	Count	Percent	Lithologic Class	Count	Percent
red, medium grained Ss	sedimentary	2	8%	clastic metased	17	65%
vein quartz	igneous	3	12%	igneous	5	19%
chert	sedimentary	3	12%	carbonate	1	4%
dolomite	sedimentary	1	4%	chert	3	12%
smooth, red fine-grained Ss	sedimentary	2	8%			
Grey quartzite	sedimentary	1	4%			
fine-grained burnie	sedimentary	9	35%			
Red, phaneritic granite	igneous	2	8%			
brown coarse Ss	sedimentary	2	8%			
yellow fine grained Ss	sedimentary	1	4%			
Total		26				

Section	WYN17-1					
Section Height	49 m					
Clast type	Lithologic Subclass	Count	Percent	Lithologic Class	Count	Percent
smooth, red fine-grained ss	sedimentary	4	15%	clastic metased	17	68%
Grey quartzite	sedimentary	5	19%	igneous	2	8%
chert	sedimentary	1	4%	chert	1	4%
greywacke	sedimentary	4	15%	volcanic	1	4%
vein quartz	igneous	2	8%			
Andesite w/ phenocrysts	volcanic	1	4%			
grey siltstone	sedimentary	3	12%			
fine grained burnie	sedimentary	3	12%			
Grey sandstone	sedimentary	1	4%			
yellow fine grained Ss	sedimentary	1	4%			
Total		25				

Summary

Lithologic Class	Count	Percent
clastic metasediments	57	74%
igneous	10	13%
carbonate	1	1%
chert	4	5%
volcanic	1	1%

(e.g., ruck structures). Therefore, this facies was either deposited as till (A) and/or as a mass-transport deposit (C). The massive nature of the diamictite could be the result of primary deposition (till) or secondary reworking during mass-transport (Rodrigues et al., 2020), either of till or of a glacier-distal subaqueous facies. Most characteristics of this facies could be the result of either depositional mechanism. The occasionally fissile nature of this diamictite is likely the result of simple shear deformation, which occurs both in subglacial settings as well as in and beneath mass-transport bodies. The ambiguous evidence for subglacial erosion or deposition at the Wynyard Fm's basal unconformity in this location means the nature of the contact should not be used to interpret this facies.

Several key characteristics of this diamictite suggest that it was more likely deposited as a series of mass-transport deposits than solely as a subglacial till. The partially gradational upper contact of this facies with Dmm-s suggests that the muddy massive diamictite was deposited in a similar environment to the sandy diamictite. Since the sandy diamictite (Dmm-s) was deposited in a sub-aqueous, proglacial, glacier-proximal setting (Henry et al., 2012; this study), this facies was also likely deposited, at least partially, in a sub-aqueous environment. Subglacial tills are much more likely to have sharp upper contacts with subaqueous sediments (e.g., Prothro et al., 2018; Robinson et al., 2021). Sediment flows tend to have disorganized clast orientations (fabrics), while clasts in subglacial tills are more likely to be strongly oriented (Dowdeswell et al., 1985; Bennett et al., 1999; McKay et al., 2009). The almost 60-meter accumulation of this homogenous facies is tens of meters thicker than most observed single-facies subglacial till units (e.g., Boulton, 1996; Evans and Ó Cofaigh, 2003), but is reasonable for accumulations of glacigenic debris flows and mass movements (McKay et al., 2009; Dietrich and Hofmann, 2019). An additional line of inference is the relationship between this diamictite (Dmm-m) and the sorted sediment bodies contained within it (facies Cm and Sc-vc). Mass-transport deposits (e.g., Sobiesiak et al., 2016; Ives and Isbell, 2021), glacial-marine

sediments, and subglacial tills (Ruszczyńska-Szenajch, 1987; Kessler et al., 2012) can all contain rafts, lenses, and stringers of sorted, stratified sediments. Many of the smaller sandstone and conglomerate bodies in this facies could have been deposited as part of a subglacial till, as iceberg dumps, or as part of a mass-transport deposit. However, the larger, intercalated sandstone and conglomerate bodies have roughly sheet-like geometries (are tens of meters across and less than a meter high), have sharp (non-erosional) contacts with overlying and underlying diamictites, do not appear to have been channelized, and often occur in stacked successions. Sheet-like bodies such as these are entirely uncharacteristic of sediment rafts in subglacial till but are characteristic of multiphase mass-transport deposits (see facies Cm and Sc-vc interpretations). The relationship between the massive diamictite with these sorted mass-transport deposits also suggests that the diamictite itself is the result of mass transport. Together, these characteristic facies Dmm-m suggest that this succession was most likely created through the redeposition of muddy subglacial till or proglacial glacier-distal deposits through gravity-driven transport as cohesive debris flows (scenario C; Mulder and Alexander, 2001).

The continuation of the lower contact of this facies with the Burnie Fm up to 19 m into the section indicates that there was at least 19 m of local relief on the basement prior to the deposition of the Wynyard Fm.

3.5.1.2. Cm: Massive, pebbly, clast-supported conglomerate

Cm description

Massive, clast-supported, conglomerate bodies (facies Cm) occur within facies Dmm-m (muddy, massive, matrix-supported diamictite) in section WYN17-1 from 21 – 58 m (Table 3-2; Figure 3-7E,H,I). Conglomerate bodies have sharp, irregular lower and upper contacts with muddy diamictites (Dmm-m), discontinuous sandstones, and other conglomerate bodies. Their lateral contacts with the muddy diamictites are also sharp and irregular.

The massive conglomerate bodies of this facies have two distinct geometries. The less common geometry is that of small "blobs" or "stringers" (Figure 3-7H). These irregular blobs occur sporadically from 20 – 29 m and from 55 – 58 m in section WYN17-1, and are 0.1 – 1 m wide and thick. Some of the small conglomerate bodies are nearly round, others are thin "stringers", and still others have complex shapes that suggest soft-sediment deformation of the gravel within the surrounding diamictite. The more common geometry is that of roughly sheet-like bodies (Figure 3-7E, I). The sheet-like bodies are common from 30 – 41m in section WYN17-1. The bodies are described as sheet-like, and not true sheets, because their thickness is variable across their width. These bodies are 0.25 – 1 m high and 0.5 – 10 m wide. From 30 – 33 m in the WYN17-1 section, such conglomerate bodies are chaotically interbedded with diamictite and sandstone bodies. In this interval, the bodies are more discontinuous, and have lenticular or wedge-like shapes. Wedge-shaped bodies thin toward the south. Above 33 m, the conglomerate bodies are interbedded with the same lithologies in a much more orderly way.

The conglomerates of this facies are massive. Some conglomerate bodies have hints of bedding and grading (Figure 3-7I), but the grain size distribution in a single conglomerate body is almost always too homogenous to discern any meaningful sedimentary structures. Where grading occurs in some of the thicker bodies, the bodies are normally graded. Conglomerates are moderately- to very-poorly-sorted. Grains range in size from fine sand up to small cobbles (5 cm). Pebbles and coarse sand are the most common grain sizes, and fine and medium sand are the rarest. Grains of all sizes are dominantly angular to sub-angular. Grains are packed together (very little void space), but do not appear to be imbricated. Clast lithologies and morphologies in this facies appear to be very similar to those in the surrounding diamictite, though no clast counts were made.

Cm interpretation

The larger, sheet-like conglomerate bodies were most likely deposited as relatively small hyper-concentrated density flows (Mulder and Alexander, 2001) or "traction carpets" (Todd, 1989) because of their massive, compacted, clast-supported nature, and their lack of cohesive particles. The absence of evidence for traction beneath these sandstone bodies, and lack of channel forms suggest that these sediments were not deposited as part of current-transported low-density flows, either as low-density turbidites or in a channel. Accumulation of gravel beds in this way is a well-documented depositional process in both subaerial and subaqueous proglacial environments (e.g., Zieliński and van Loon, 1996; Benn and Clapperton, 2000; Winsemann et al., 2007; Carrivick and Rushmer, 2009). In subaqueous systems, coarse-grained hyper-concentrated density flows are sometimes the lower portion of bi-partite flows where the upper portion is turbulent (low density) (Todd, 1989; Sohn, 1997; Sohn et al., 2002).

The smaller "blobs" and "stringer" bodies of this facies could have been deposited as resedimented parts of the larger conglomerate bodies or as iceberg dump structures (Thomas and Connell, 1985), represent materials loaded into underlying water saturated diamictites (pseudonodules/ ball-and-pillow structures; Owen, 2003), or be the result of mixing/shearing of materials by resedimentation processes (Rodrigues et al., 2020).

3.5.1.3. Sc-vc: Very-coarse-grained, cross bedded sandstone

Sc-vc description

This facies consists of cross bedded, very-coarse-grained sandstone (Figure 3-7E,I). This is a minor facies that occurs interstratified with facies Cm (massive, clast-supported conglomerate) within facies Dmm-m. Sediments of this facies were observed in section WYN17-1 from 30 – 39 m. Similar to the conglomerate (Cm) these sandstones occur as discontinuous bodies with sharp lower, upper, and

lateral contacts with facies Cm and facies Dmm-m. Lower contacts with Cm are occasionally gradational, but the transitions occur over ~ 1 cm. The sandstone bodies of this facies 0.25 – 1 m thick, 0.5 – 4 m long, and occur in 1 - 2 m-thick successions where they are interbedded with facies Cm. These sandstone bodies are most often organized as sheet-like bodies like Cm but will occur as rare "blobs" and "stringers" (Figure 3-7G).

These sandstone bodies are most often cross bedded, but several bodies were massive. Dewatering structures are common in stratified bodies (Figure 3-7F). The sandstones are moderately-well-sorted with grain sizes ranging from upper-medium sand to granules. The median grain size is very coarse sand. Grains are angular to sub-rounded, with a wide variety of lithologies, mirroring facies Cm.

Sc-vc flow directions

Flow directions were measured from cross beds in this facies from 30 – 32 m in section WYN17-1 (Figure 3-6). Out of seven cross bed orientation measurements, five had reasonable original dip angles (< 25°) once corrected for declination and structure. The dip directions of these features suggest depositional flow toward the northeast; current directions ranged from 051° to 025° with a mean vector of 036°. Two measurements had dip angles of 71° and 76°, with dip directions toward the east, 090° and 096°.

Sc-vc interpretation

This facies likely represents deposition from a more turbulent portion of a multiphase subaqueous flow, where facies Cm is the non-cohesive, high-density portion (e.g., Sohn et al., 2002; Henstra et al., 2016). The water-escape structures in the sandstones indicate rapid compaction (via loading) following deposition. The measured cross beds indicate flow towards the northeast, but several structures with very high dips suggest soft-sediment deformation or redeposition of at least some sandstone bodies.

3.5.1.4. MDm Facies Association Interpretation

The MDm facies association was most likely deposited as the subglacial or pro-glacial portion of a grounding-zone wedge (GZW). GZWs are asymmetric wedges of sediment that accumulate on continental shelves at the grounded, stable margins of marine-terminating ice sheets (Dowdeswell and Fugelli, 2012; Batchelor and Dowdeswell, 2015; Demet et al., 2019; Dietrich and Hofmann, 2019). These landforms range in size from 5 m – 200 m high and are up to 100 km long (Demet et al., 2019). Taller landforms are also longer, and size is related to duration of deposition and subglacial sediment flux during that time. The subglacial portions of GZWs are composed of long, shallowly upglacier-dipping slopes that are deposited subglacially as planar "topsets". Most of the volume of the landform is deposited as downglacier-dipping "foresets" that are deposited as mass-transport deposits of mainly resedimented subglacial debris (Simkins et al., 2017; Prothro et al., 2018). The "foresets" that gradually build the wedge portion of a GZW are often massive and homogenous, and individual mass transport events are usually indistinguishable from one another, both in seismic (e.g., Dowdeswell and Fugelli, 2012) and in outcrop (e.g., Dietrich and Hofmann, 2019). Where individual foresets are distinct, like in Pleistocene GZWs on Whidbey Island, Washington (western United States), the foreset dips range from 3-28˚ and individual foresets measured up to 15 m high (Demet et al., 2019). The boundary between the topset and foresets mark the glacier's grounding line. GZWs grow through the progradation and aggradation of these topset-foreset systems, a process that can take anywhere from decades to centuries (Batchelor and Dowdeswell, 2015; Simkins et al., 2017). During such extended time intervals (in glacial terms), the ice margin position fluctuates within the scale of the landform, resulting in subglacial erosion of GZWs and truncation of internal structure. At modern glacial margins where GZWs are forming, sediment flux to the glacier margin is most often dominated by high rates of (non-point-source transport of) deformation till and subglacially entrained sediments (Dowdeswell and Fugelli, 2012;

Batchelor and Dowdeswell, 2015), with occasional contributions from point-source sediment discharge in the form of channelized, subglacial meltwater (e.g., Simkins et al., 2017). The internal stratigraphy of GZWs is therefore largely homogenous; composed of subglacially-deposited diamicts or the same diamictite redeposited as mass transport or sediment gravity with occasional contributions of sorted sands and gravels from channelized meltwater flows. GZWs are most likely to form at the margins of ice streams or outlet glaciers in fjords or troughs (Demet et al., 2019) that are delivering glacially-entrained sediment to the glacier margin at relative high rates (Batchelor and Dowdeswell, 2015). Most often GZWs form at the margins of high-latitude ice sheets with polar or cold subpolar thermal regimes, which have dominantly distributed (unorganized/channelized; non-point-source) subglacial hydraulic systems. In modern settings, these landforms are most often observed at glaciers that have ice shelves (Batchelor and Dowdeswell, 2015; Smith et al., 2019) and are more likely to be deposited on or near topographic highs acting as "pinning points" which stabilize the glacier's margin (Batchelor and Dowdeswell, 2015; Simkins et al., 2018).

A GZW is the most likely setting for this facies association largely because it allows for the accumulation of homogenous, massive diamictites (facies Dmm-m) $\geq$ 58 m-thick that were deposited as subglacial diamicts redeposited as mass-transport deposits, and these diamictites be interbedded with mass-transport deposits. Multiphase, subaqueous flows composed of coarse-grained clastics (facies Cm and Sc-vc) are also consistent with re-sedimentation of subglacially channelized meltwater flow deposits that occur in GZWs. Additionally, the at least 20 m of relief on the unconformity underlying this facies suggests there may have been a bedrock "high" or slope that could have acted as a "pinning point" for a glacial margin. There is evidence for ridges as small as 30 m tall being effective pinning points on Pleistocene ice streams (Shackleton et al., 2020). A similar succession was described and interpreted by Dietrich and Hofman (2019) in the South African Dwyka Group.

The deposition of a GZW suggests several physical characteristics of the "Wynyard Glacier", including a cold subpolar thermal regime, a distributed hydraulic system with occasional channelized meltwater, relatively fast glacier flow, relatively high glacial sediment flux, and stabilization on or creation of a pinning point. GZWs are also strongly associated with flow of glaciers through fjords or troughs.

The clay-rich composition of the diamictite in this GZW does not conflict with the interpretation that this glacier had a relatively cold thermal regime. The clay component in tills with clay-rich matrices is most likely derived from a sediment source (i.e., lithified or unlithified fine-grained sediments and/or chemically-weathered, phyllosilicate-bearing or -producing rocks), and less likely to be created and concentrated in sufficient quantities purely through comminution (e.g., Haldorsen, 1981; Hart, 2017) or chemical weathering (i.e., Crompton et al., 2015; Graly et al., 2020) in a purely subglacial or englacial setting. Clay-rich subglacial sediments are common in subglacial environments, including those that occur at modern high-latitude glaciers that produce grounding zone wedges (e.g., Tulaczyk et al., 1998, Anandakrishnan et al., 2007).

Flow directions in facies Sc-vc indicate transport toward the northeast, which suggests that the glacier's grounding line was located somewhere to the southwest of this succession. Additionally, a southwest to northeast glacier paleoflow orientation is consistent with glacier flow directions inferred from striated boulder pavements in facies association SDm (see section 3.5.2).

3.5.2. Sandy Diamictite (SDm) Facies Association

The Sandy Diamictite (SDm) Facies Association is the most common in both section WYN17-1 and WYN17-2 (Table 3-1; Figure 3-6; Figure 3-9). This facies association is made up of 85% sandy, massive, matrix supported diamictite (facies Dmm-s), with ~ 5% each of the sorted sediment facies in this facies association (facies Sc-fmc, Cm, Cc(d)). This facies association is more-or-less the same

facies association as Henry et al. (2012)'s "Massive diamictite facies association", and is most often described as the characteristic lithofacies of the Wynyard Formation. This facies association differs from the previously discussed Muddy Diamictite Facies Association (MDm) because the dominant lithology is a sandy, mud-poor diamictite and the gravity-driven sand and gravel deposites are more likely to be stratified.

3.5.2.1. Dmm-s: Sandy, massive, matrix-supported diamictite

Dmm-s description

Sandy, massive, clast-rich, matrix-supported diamictite is the dominant facies in section WYN17-1 and WYN17-2 (Figure 3-9A,C; Table 3-2). This facies occurs in thick homogenous successions up to 140 m thick and is interstratified with the Sc-fmc, Cm, and Cc(d) facies in this facies association. The lowermost contact of this facies in section WYN17-1 is gradational to sharp with facies Dmm-m. The gradational contact occurs over less than a meter, and is the result of a gradual transition of the diamictite matrix from sandy mudstone to sandstone as well as an increase in clast content and size. Discontinuous conglomerate and sandstone bodies (facies Cm, Cc, and Sc-fmc) occur within this diamictite (Figure 3-9B, F, G, H). The sandstone and conglomerate bodies range in size from tens of meters wide and up to a meter thick to cm-scale sand stringers. Contacts between this facies and those non-diamictite bodies are sharp, but not planar, and often appear to have been deformed or have load structures. For example, clasts from the conglomerate may protrude into the diamictites or the diamictites may inter-finger with the conglomerate along sharp contacts (Figure 3-9F,G,H,). Upper contacts of this facies with conglomerates, sandstones, shales, and mudstones are most often sharp.

This diamictite facies is massive (Figure 3-9A). Within the diamictite, there are very rare bounding surfaces in the form of faint stratification, meter-scale coarsening upwards packages, and boulder

pavements. Boulder pavements are apparent bounding surfaces that contain a high concentration of boulders and cobbles (e.g., Eyles, 1988; Figure 3-10). Three boulder pavements were observed in this facies within sections WYN17-1 and WYN17-2. Boulders and cobbles in the pavements have shapes, sizes, and lithologies similar to those elsewhere in this facies – meaning that many of them are faceted and/or "bulleted" (Figure 3-9E). In one boulder pavement, there are no apparent shared orientations of the boulders and the boulders are mostly not striated (Figure 3-10B). In the other two pavements, many of the boulders have striae that point in a uniform direction (see Dmm-s flow directions). However, the orientation of these striae do not always align with the faceted ("plucked") faces on the boulders in the pavements (Figure 3-10A). The boulder pavements are not laterally extensive in outcrop, and are limited to ~ 2 m in width.

This facies is laterally and vertically homogenous (Figure 3-9A). The matrix is grey sandstone. The matrix grain size ranges from silt to coarse sand, is poor- to moderately-well-sorted, and the median grain size is dominantly fine sand. The median grain size of the matrix shifts gradually throughout the succession from coarse sand to silt. The reddish clay that makes up the bulk of the matrix in facies Dmm-m is absent from the matrix of this facies. The clast composition of this diamictite is very similar to facies Dmm-m. Clasts range in size from granule (2 mm) to boulder (2 m). Median clast size (visual estimate) is 1.5 cm. Clasts are dominantly angular or sub-angular, with some rounded and sub-rounded clasts. Cobbles and boulders are also commonly faceted, polished, and striated (Figure 3-8; Figure 3-9E). Clast abundance varies throughout these successions, but never becomes "clast poor" (< 5% clasts). Clasts appear to be randomly oriented except in boulder pavements.

In addition to the sorted and often stratified sand and gravel bodies that occur within this diamictite, this facies also contains "clast clusters" (Figure 3-9H). Clast clusters are poorly sorted mixtures of

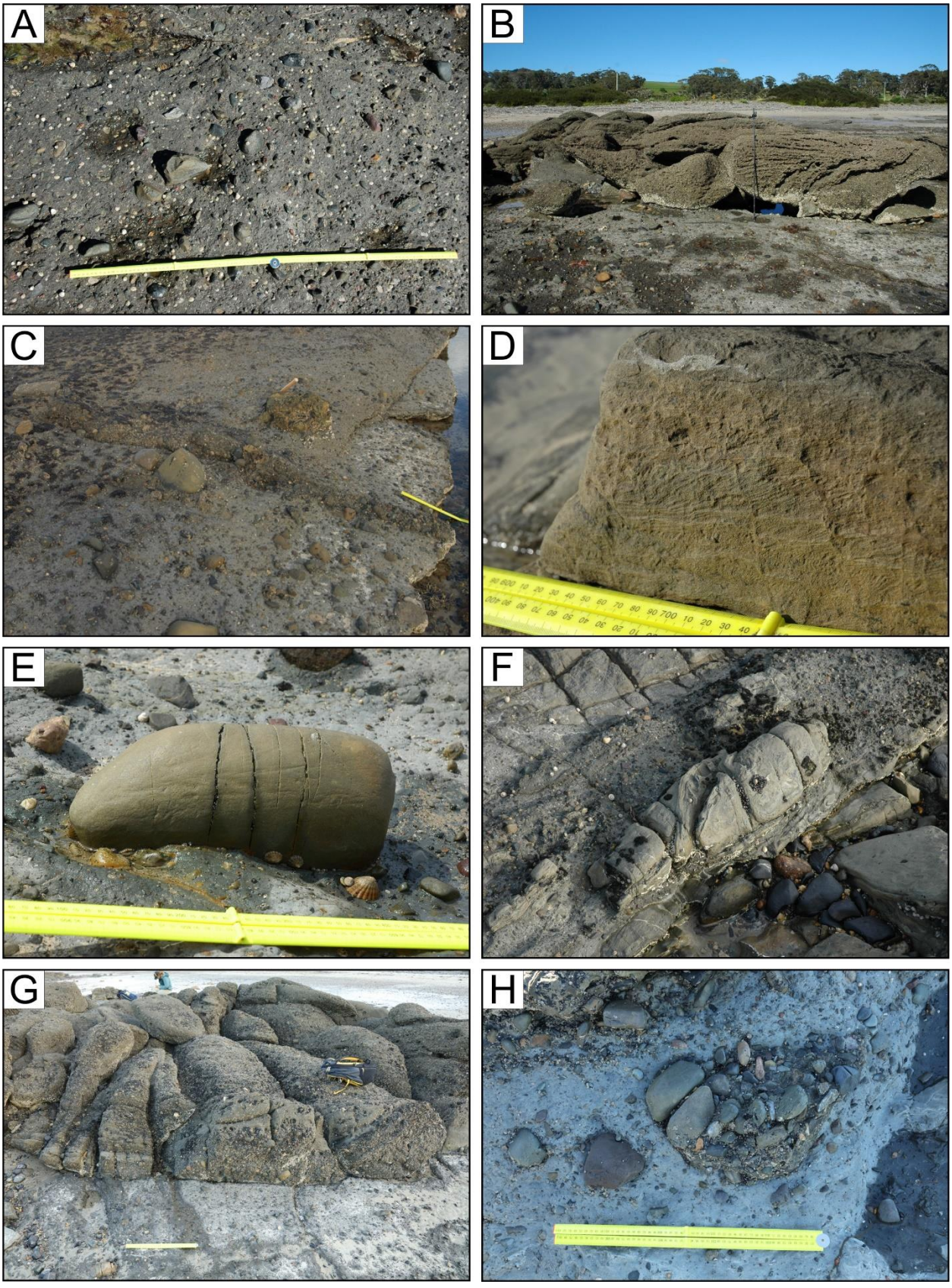
A
B
C
D
E
F
G
H

Figure 3-9. Representative photos of the Sandy Diamictite (SDm) Facies Association. Marks on all rulers are in cm. Rulers are 50 cm when folded in half and 1 m long when unfolded. Cobbles were common in this inter-tidal zone, both derived from the Wynyard Fm and from the intrusion at Doctors Rock. Therefore, many of the cobbles in these photographs are not in situ and all the basaltic clasts are not from the Wynyard Fm. Barnacles and bivalves are modern. A. Characteristic massive, sandy diamictite (facies Dmm-s). B. Deformed bedded conglomerates (facies Cc(d)) with sharp contact over massive diamictite. C. Massive diamictite with near-vertical conglomeratic, clastic dike (injectite). There is also a large clast cluster to the right of the dike. Stratigraphic up is to the left of the pictures. D. Cross laminated sandstone (facies Sm-fmc) with water escape structures. E. Striated and faceted, bullet-shaped clast within the massive diamictite. F. Small, deformed sand body (facies Sc-fmc), likely a sandstone boudin, within diamictite. G. Large, deformed conglomerate (facies Cm) with sharp contact over sandy diamictite (facies Dmm-s). H. Clast cluster in massive diamictite.

sand and gravel within the diamictite that do not occur in relationship to any larger sand or gravel bodies. These clusters are often round- or oval-shaped, and do not have any features indicating soft-sediment deformation.

Dmm-s flow direction: Boulder pavements

The orientation of striae in two boulder pavements were measured at 130 m in section WYN17-1 and 72 m in WYN17-2 (Figure 3-6; Figure 3-10A). At the WYN17-1 bed four measurements were taken, and the mean vector of the rotated measurements is 018°/198°. Fifteen measurements were taken from the second boulder pavement, and the mean vector of the measurements is also 018°/198°.

Dmm-s interpretation

Similar to the muddy diamictite facies (Dmm-m), the physical characteristics of clasts in this facies suggest that this diamictite was deposited in a glacigenic or glacially-influenced setting, which is an interpretation consistent with other studies of the Wynyard Fm and its correlates (e.g., Powell, 1990; Fielding et al., 2010; Henry et al., 2012). This facies is likely glacigenic because of the clast characteristics (i.e., wide variety of clast sizes and shapes, common striated and faceted clasts; Figure 3-7), as well as features like clast clusters (Figure 3-9H) and boulder pavements. Poorly-sorted, coarse-grained 'clast clusters' in this facies were likely deposited as 'rainout' of ice-cemented debris from icebergs (e.g., Eyles et al., 2005) or iceberg dump structures.

Massive, sandy, thick glacigenic diamictites like this facies are most characteristic of sub-aqueous, proglacial, glacier-proximal sedimentation (Eyles and Lagoe 1990; Powell and Cooper, 2002; McKay et al., 2009; Ives and Isbell, 2021). Such successions are created through a combination of subglacial deposition, plume sedimentation, iceberg rain-out, and resedimentation through mass-transport.

Striated boulder pavements may be deposited subglacially through the lodgment of boulders into a soft substrate or be created through winnowing in cold coastal environments (e.g., Hansom, 1983) or winnowing in a subaqueous glacier grounding zone (see discussions in Eyles, 1988 and López-Gamundí et al., 2016). In the subglacial scenario, deposition and striation of the boulders occurs simultaneously, while in the winnowing scenarios a boulder lag is formed first through winnowing and striations are created later by either sediment entrained in shore ice (coastal environments) or sediment entrained in subglacial ice (subaqueous grounding zone) (Eyles, 1988; López-Gamundí et al., 2016). The mismatch between striations and faceted faces in the boulder pavements observed in this study suggests that winnowing is a more likely formation mechanism than subglacial lodgment. Additionally, a winnowing process also allows the formation of the one non-striated boulder pavement that was observed in this succession. This winnowing likely did not take place in a coastal environment because no other lithologic indicators of a coastal setting are present in this succession of the Wynyard Fm. Subaqueous winnowing that results in boulder lags is most likely the result of wave activity or underflow currents (Eyles, 1988; López-Gamundí et al., 2016). The absence of other evidence for wave reworking in this succession suggests that underflow currents are the more likely cause. The uniform orientation of striae both within and between the two striated boulder pavements, separated by ~100 m of stratigraphy (Figure 3-6), suggest that the striae were created through subglacial erosion. The striated boulder pavements therefore suggest winnowing followed by periodic grounding of glacier ice over the study area.

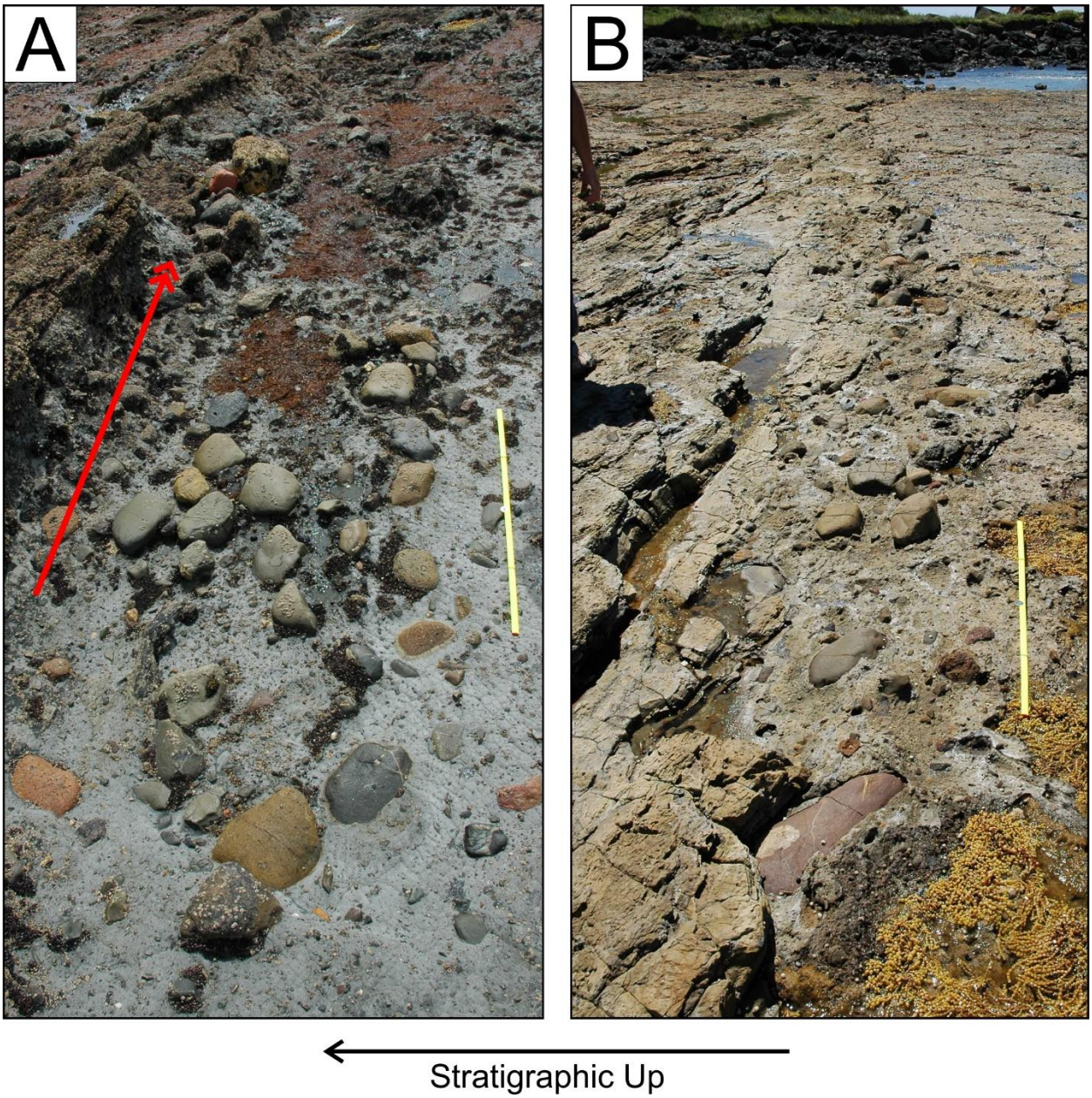

Figure 3-10. Examples of (A) striated and (B) non-striated boulder pavements (likely lags) within the massive sandy diamictite facies (Dmm-s). Stratigraphic up is the left in both photographs.

3.5.2.2. Sc-fmc: Fine-, medium-, or coarse-grained, cross stratified sandstone

Sc-fmc description

This facies consists of cross stratified sandstones that occur within the sandy diamictite (facies Dmm-s) (Figure 3-9D, H, F; Table 3-2). These sandstones are laterally discontinuous up to 5 m long and are 0.25 – 1 m thick. The lower contacts of these sandstone bodies with the diamictite are most often sharp, often with irregular or "loaded" surfaces, and in rare cases are erosional. They have sharp upper and lateral contacts with the surrounding diamictite. The shape of these sandstone bodies is roughly lenticular.

Sandstones of this facies range from undeformed to highly-deformed [sub-facies Sc(d)]. Sandstone bodies consist of 0.10 – 0.25 m-thick cross stratified sets. Where multiple sets occur, there is a fining upward trend from pebble conglomerate to fine-grained sandstone. The most common primary sedimentary structures are planar cross beds (in conglomerates and coarse-grained sandstones) or cross laminae (in medium-grained sandstones). Climbing ripples, convolute bedding, and flaser cross bedding also occurred in some sandstone bodies. Planar laminae of coarse-grained sandstones also occur between fine- and medium-grained beds. Secondary (deformation) structures most often included dewatering structures, normal (thrust) faults, and folding (Figure 3-8D, F).

The sandstones in this facies are moderately- to well- sorted, and include grain sizes from fine sand to pebbles. The sediment grains of all sizes are mixed lithics (similar to the clasts in the diamictites) and quartz, angular to sub-rounded, and imbricated.

Sc-fmc transport directions

Transport directions from primary and secondary sedimentary structures were measured in this facies in sections WYN17-1 and WYN17-2 (Figure 3-6). Both primary and secondary sedimentary

structures in this facies indicate transport directions generally toward the east WYN17-1 and toward the northwest in WYN17-2.

Primary transport directions were measured from cross beds, cross laminations, and primary current lineations. In section WYN17-1, these directions (N=8) ranged from 010° to 244°, with a mean orientation of 070°. This includes measurements from deformed and undeformed iterations of this facies. The sand body with the least soft sediment deformation in section WYN17-1 was at 75 m, and those measurements (N=5) have a mean orientation of 080°. The only primary transport directions in the WYN17-2 section from this facies were measured at 87 m from a series of cross bed sets (N=3). These measurements ranged from 014° to 041°, and have a mean orientation of 021°.

Secondary (soft sediment deformation) structures in this facies that indicate resedimentation direction include normal faults, fold nose axes, pressure ridge lineations, and en echelon sands in diamictite (Figure 3-9F, H). Vergence of these features (N = 10) in section WYN17-1 ranges from 048° to 171°, with a mean direction of 100°, and in section WYN17-2 (N = 5) ranges from 300° to 005° with a mean direction of 330°

Sc-fmc interpretation

This facies was most likely deposited from low density turbidity currents (Mulder and Alexander, 2001), and redeposited through mass transport. While much of this facies has been deformed through soft-sediment deformation, the primary structures in the less-pervasively deformed sandstone bodies help to constrain the initial depositional conditions. The cross stratification and planar bedforms in these sandstones indicate the downflow migration of 3D dunes and ripples and deposition of plane beds, suggesting that this facies was deposited in upper-lower and upper flow regime conditions. The fining upward nature of some sandstone bodies in this facies suggests

generally waning flow. There are several features that suggest flow velocities fluctuated during deposition of this facies, including intervals of interbedded coarse-grained (coarse sand to pebbles), planar beds with medium-grained sandstone cross laminated sets of sandstone and rare flaser bedding of cross laminae. Dominantly sharp basal contacts and roughly lenticular shape of the sand bodies are most consistent with non-channelized flow. Therefore, this facies was most likely deposited by sustained (i.e., the current did not turn "off" during deposition), but fluctuating and generally waning, sediment-rich, turbulent flows. These sandstone bodies were ultimately deformed through loading and consolidation (water-escape structures), and re-deposited through mass transport (e.g., slumping) with other facies in this facies association.

3.5.2.3. Cm: Massive, clast-supported conglomerate

This facies is the same as described in the MDm facies association, but only the small "blobs" and "stringers" occur in this facies association (Table 3-2; Figure 3-9G). The smaller "blobs" and "stringer" bodies of this facies could have deposited as resedimented parts of the larger conglomerate bodies or as iceberg dump structures. See section 3.5.1.2 for facies description and interpretation.

3.5.2.4. Cc(d): Cross bedded conglomerate (deformed)

Cc(d) description

Cross bedded, clast-supported, conglomerate bodies that have experienced soft sediment deformation occur within facies Dmm-s in section WYN17-1 from 67 – 73 m and 202 m (Figure 3-9B; Table 3-2). Conglomerate bodies have sharp and rare loaded lower contacts with sandy diamictites (facies Dmm-s), where flame-like structures or meter-scale diapirs of diamictite sometimes protrude into the conglomerate. Upper contacts are sharp and occur with the sandy

diamictite or other conglomerate bodies. Their lateral contacts with the sandy diamictites are sharp and irregular.

The deformed, cross bedded conglomerate bodies of this facies occur as 0.5 – 2m thick cross bed sets. These bodies are not more than 10 m long or wide, and are wholly contained within the sandy diamictite. The conglomerates have clear bedding planes that are often distorted and folded, most likely due to soft-sediment deformation. Conglomerates are moderately well-sorted. Grains range in size from coarse sand up to small cobbles (5 cm). Pebbles are the most common grain sizes. Grains of all sizes are angular to sub-rounded and appear imbricated. Clast lithologies and morphologies in this facies are very similar to those in the surrounding diamictite, though no clast counts were made.

Cc(d) transport directions

Cross bed sets in the Cc(d) bodies at 70 m in section WYN17-1 (N = 3) had dip directions of 105° - 109° with dips of 35°, 50°, and 90° (Figure 3-6). Slump folds in this facies at 202 m in section WYN17-1 have apparent vergence toward north.

Cc(d) interpretation

This facies was most likely deposited through the down-current progradation of large gravel dunes (Winsemann et al., 2007) that were resedimented through mass-transport along with the surrounding sandy diamictite. The sharp lower and upper contacts of these conglomerate bodies suggest non-channelized, subaqueous sedimentary density flow (Mulder and Alexander, 2001; Talling et al., 2012). The load structures at the basal contacts of conglomerate bodies may have formed during rapid deposition of this facies, due to differential compaction during burial, or as deformation during mass transport. The apparent vergence of folded bedding towards the north is consistent with other transport directions in sections WYN17-1 and WYN17-2, as are the apparent orientation of cross beds toward the east (Figure 3-6).

3.5.2.5. SDm Facies Association Interpretation

This facies association was most likely deposited in a proximal, pro-glacial subaqueous setting that was strongly influenced by subglacial or englacial meltwater discharge in the form of a jet (e.g., Powell, 1990). This type of sedimentation could have occurred as part of a grounding-line fan system or as a morainal bank (Henry et al., 2012). The processes of deposition for the massive diamictite facies (facies Dmm-s) were likely dominated by settling from suspension of sediments entrained in meltwater plumes (Powell, 1990) and deposition of iceberg-rafted sediments. Occasional advances of grounded glacier ice over the area are indicated by uniformed striated boulder pavements. Some of the diamictites may have been deposited or deformed subglacially, but, except in the case of striated boulder pavements, cannot be differentiated from those deposited in other ways. The massive structure of the diamictite in this facies association could be a depositional characteristic of the diamictites, could be due to homogenization by iceberg scouring (Dowdeswell et al., 1994), or resedimentation (Powell and Molnia, 1989; Rodrigues et al., 2019). The soft sediment deformation of stratified facies in this facies association, like folding and en echelon structures, suggest that resedimentation was common in this system. The presence of structures like "loaded" contacts and water escape structures throughout this facies association indicate the succession was water-saturated following deposition, which suggests that sedimentation was rapid. The deposition of turbidites (facies Sc-fmc) is common in proximal, pro-glacial settings (Lønne and Nemec, 2011; Dowdeswell et al., 2016). In such settings, sandy turbidites can be generated as hyperpycnal flows (usually in a fan or delta setting), or as a diluted portion of a debris flow (Sohn et al., 2002; Winsemann et al., 2007; Haughton et al., 2009).

The deposition of a grounding-line fan or morainal banks suggests several physical characteristics of the responsible glacier that differ from grounding zone wedge deposition. Grounding-line fan

systems with significant iceberg sedimentation, like the system described here, are most likely to occur at the margins of glaciers with organized subglacial hydraulic systems, high concentrations of entrained debris (sediment), high rates of sediment flux, and a calving, tidewater front. Glaciers with these characteristics usually have temperate or mild sub-polar thermal regimes.

3.5.3. Interstratified Rhythmic (IsR) Facies Association

This facies association occurs from 220 – 235.5 m in section WYN17-1 (Table 3-1; Figure 3-6; Figure 3-11; Figure 3-12; Figure 3-13; Figure 3-14). This facies association consists of ~ 57% stratified, sandy diamictite facies (Dms-s), ~ 19% of the interlaminated claystone, mudstone, and siltstone facies (Fs), ~ 19% of the fining-upward sandstone facies (Sc-fu), and ~ 6% of the cross-bedded conglomerate facies (Cc). Similar facies association in the Wynyard Fm have previously been described by Banks et al. (1955), Fielding et al. (2010) (facies A1 and A2), and Henry et al. (2012) (deformed mudstone and fine sandstone facies association). While prior works have described the fine-grained laminae and occasional interbeds of sandstone and diamictite in this facies association, its cross bedded conglomerate bodies (facies Cc) have not previously been described.

3.5.3.1. Fs: Interlaminated claystone, mudstone, and siltstone

Fs description

Inter-laminated layers of clay, mud, and silt are the characteristic facies of this facies association (Table 3-2; Figure 3-6). At the locality described in this study (Doctors Rock), Banks et al. (1995) described this facies as having a cyclic or rhythmic pattern. While we agree that there are frequent alterations in grain size at this locality, we were not convinced that there was a regular, rhythmic pattern to these interchanges. Laminae are parallel, horizontally continuous, and drape over relief created by sand and conglomerate bodies (such as bedforms is sandstone or large clasts in conglomerates) in this facies association (Figure 3-11; Figure 3-12B). Where relief is not present, the

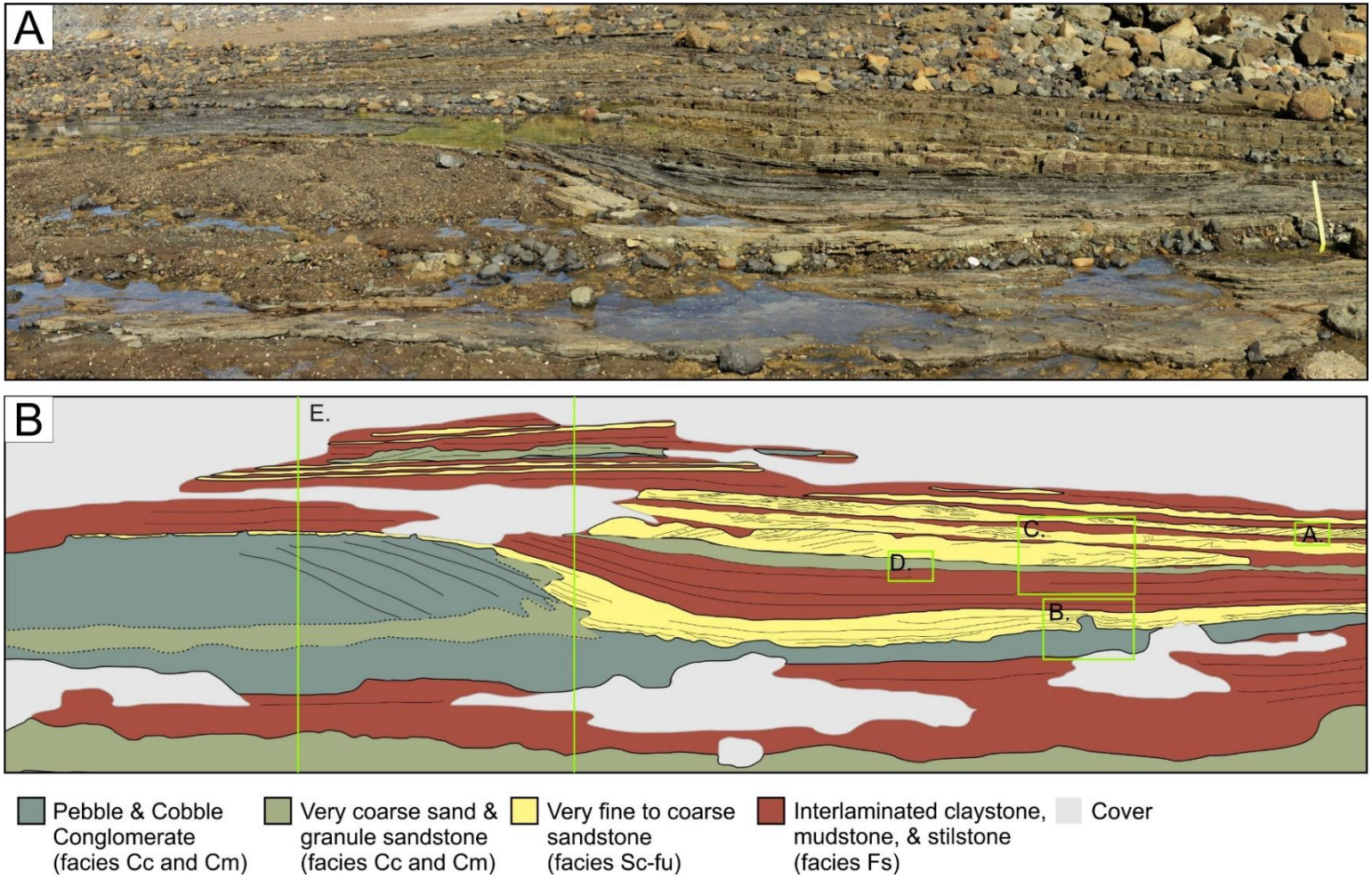

Figure 3-11. Photo mosaic (A) and interpretive sketch (B) of Interstratified Rhythmic (IsR) facies association in section WYN17-1. View is toward the west, and current transport directions are toward the north (right side of photo). Marks on all rulers are in cm. Rulers are 50 cm when folded in half and 1 m long when unfolded. Cobbles were common in this inter-tidal zone, both derived from the Wynyard Fm and from the intrusion at Doctors Rock. Therefore, many of the cobbles in these photographs are not in situ and all the basaltic clasts are not from the Wynyard Fm. Boxes A – E in B are outlines of reference photographs in Figure 3-12.

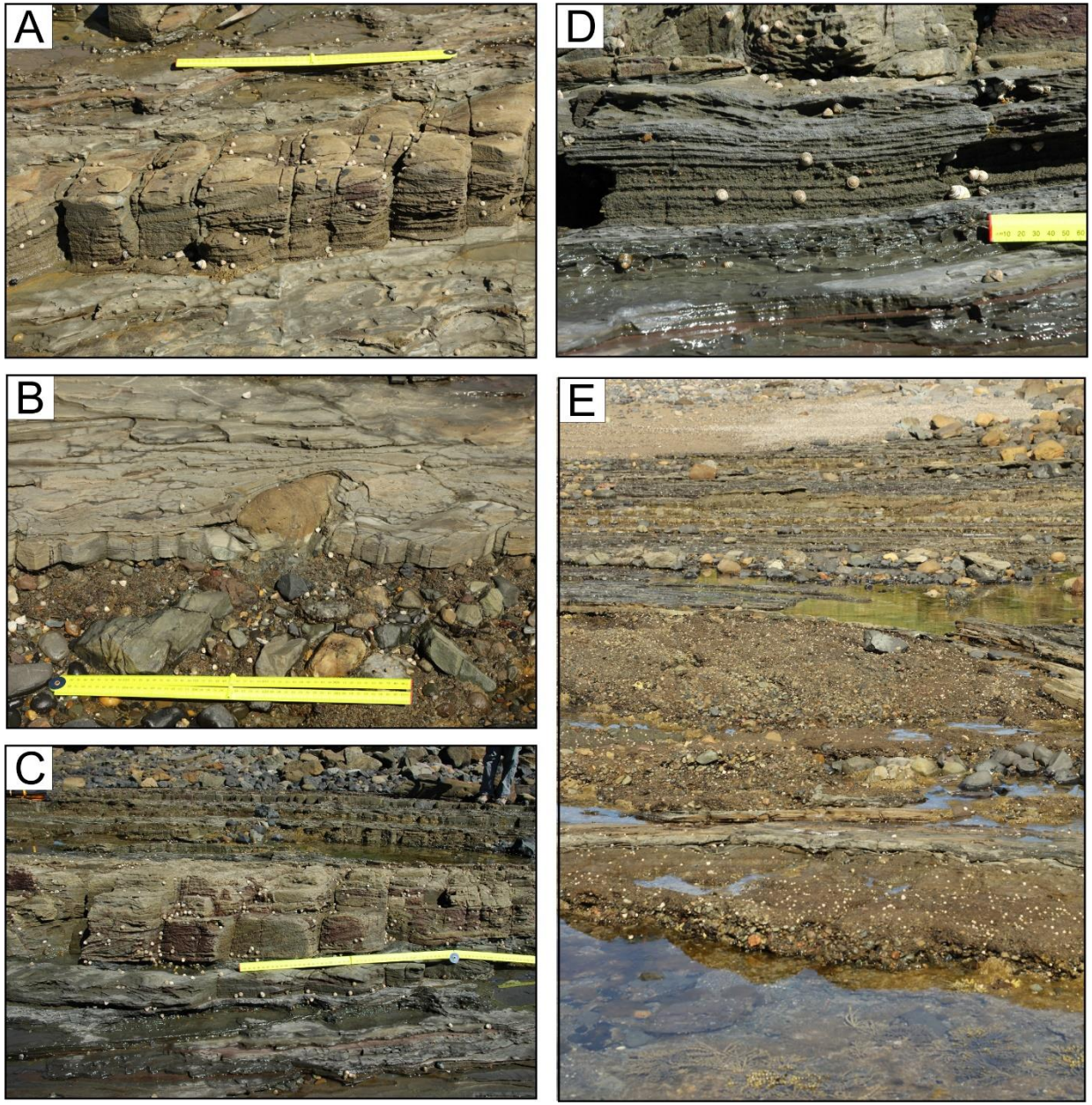

Figure 3-12. Reference photos for Figure 3-11. Marks on all rulers are in cm. Rulers are 50 cm when folded in half and 1 m long when unfolded. Cobbles were common in this inter-tidal zone, both derived from the Wynyard Fm and from the intrusion at Doctors Rock. Therefore, many of the cobbles in these photographs are not in situ and all the basaltic clasts are not from the Wynyard Fm. The little white dots are (modern) barnacles. A. Climbing ripples in coarse sand laminae (facies Sc-fu) with sharp upper and lower contacts with laminated fines (facies Fs). B. Conglomerate (facies Cc) covered with cross-laminated sandstone (facies Sc-fmc) and draped with laminated fines (facies Fs). Draped boulder is part of conglomerate bed. C. Interbedded laminated fine-grained sediments (facies Fs) with cross-laminated and plane bed sandstones (facies Sc-fu). Note the sharp contacts between facies, that bedforms are preserved on the upper surfaces of the sandstones, and the change in bedform type from the base (convolute, climbing ripples) to the top (thin cross laminations) of the sandstone body in the middle of the photograph. D. Laminated fine-grained sediments (facies Fs) overlain by upper plane bed very coarse sandstone that grades upward into cross laminated coarse-grained sandstone, and then medium-grained sandstone with dewatering structure. E. Portion of the Figure 3-11 photomosaic highlight the cross bedded conglomerate bodies (facies Cc).

laminae are planar. Lower contacts of this facies are sharp, as are the contacts between laminae. Upper contacts of this facies with coarser-grained inter-beds are usually sharp, but are rarely erosional. The uppermost contact of this facies is with facies Dmm-s (massive, clast-rich, sandy diamictite). The contact is sharp and undulating. The diamictite side of the contact consists of an unoriented boulder bed with some clasts protruding into the underlying mudstone. Additionally, the mudstone underlying the contact has a fissile texture and homogenized structure (Figure 3-13E). In this fissile zone, deformation appears to increase up over 10 – 20 cm. This facies is ~ 5 m thick, and fines upward over that distance, as sandstone interbeds transition from common (4 – 5 interbeds per meter of section) to absent.

This facies is composed of alternating claystone, mudstone, and siltstone laminae. Laminae are thin, except for rare siltstone layers that are thin beds (up to 1.5 cm). Claystones are dominantly red colored. Mudstones are dominantly grey, but occasionally appear olive or dusky-green. Siltstones are grey. Most laminae appear massive in the field, but some laminae are clearly couplets where the majority of the lamination is composed of grey siltstone or mudstone and the upper quarter to tenth of the lamination abruptly transitions or grades into red or olive-grey claystone or mudstone (Figure 3-12C, D). Banks et al. (1955) and Gee (1971), who both examined these laminae in thin section, also reported that normal grading was a common characteristic of laminae in this facies. Water-escape structures sometimes occur in this facies, including sand volcanos (Figure 3-13C). Some rare intervals of this facies have been pervasively folded through soft-sediment deformation. The folding events do not appear to have affected underlying laminae. Rare, pebble- and cobble-sized outsized clasts occur throughout this facies. These clasts penetrate laminae and often create ruck structures (Figure 3-13F).

These facies do not appear to have been significantly physically altered despite being within several meters of a Jurassic intrusion.

A mudstone sample from this facies was processed for palynomorphs and was found to be barren (Césari, *pers. comm.*)

Fs interpretation

This facies was most likely deposited through settling from suspension of fine-grained sediments, and can be considered cyclopelites (Mackiewicz et al., 1984). Hand (1993) made a similar interpretation. Coupled laminae are especially characteristic of cyclopels, which are couplets of silt and mud deposited from turbid over-flow and inter-flow plumes, often sourced from pro-glacial discharge in a marine environment (Mackiewicz et al., 1984; Powell and Molina, 1989; Cowan and Powell, 1990; Ó Cofaigh and Dowdeswell, 2001). Several other characteristics of this facies support this interpretation. The internal normal grading of laminae, variations in laminae thickness, and sharp contacts between laminae of different grain sizes and colors support that the deposition of these laminae was episodic and likely event-driven. The lack of bioturbation, dewatering structures, and soft-sediment deformation suggest that these sediments were deposited relatively rapidly. The inter-stratification of this facies with turbidity currents and other mass-transport facies is also characteristic of cyclopelites (Stewart, 1991; Ó Cofaigh and Dowdeswell, 2001; Batchelor et al., 2011)

Though originally studied in fjords (e.g., Mackiewicz et al., 1984), cyclopelites have also been identified from marine shelf settings such as McMurdo Sound, Antarctica (Powell et al., 2001) and the Hinlopen cross-shelf trough, Svalbard (Batchelor et al., 2011). The deposition of these couplets is largely driven and controlled by meltwater plume discharge, but when, why, and how cyclically settling from suspension occurs in these systems is also related to stratification of the marine

environment, which is commonly influenced by tides and wind shear (Powell and Molina, 1989). Cyclopelites are usually deposited between one and several kilometers from the meltwater plume discharge point (Mackiewicz et al., 1984), though they may be deposited within a kilometer of the discharge point during low flows (Powell and Molina, 1989). Cyclopelites may accumulate at rates of 9 m yr^{-1} in ice-proximal settings to 3.5 m yr^{-1} is ice-distal settings (Mackiewicz et al., 1984). Meltwater discharge plumes can occur at the front of any glacier with an organized hydraulic system, which includes temperate to subpolar glaciers (Dowdeswell et al., 2016).

If this facies of the Wynyard Fm is cyclopelites, we can infer some environmental characteristics of its deposition. This facies was most likely deposited > 1 km away from the meltwater plume discharge point (Mackiewicz et al., 1984). However, the interstratification of this facies with (facies Cm), and the absence of any marine mud facies from this succession, suggest that these cyclopelites were not deposited more than a few kilometers from the glacier margin. Rare outsized (likely ice-transported) clasts indicate that iceberg sedimentation in this facies was rare. Icebergs may have been kept out of the area by extensive sea ice (Ó Cofaigh and Dowdeswell, 2001; Fielding et al., 2010). This facies is 5 m thick and would have been thicker prior to compaction and lithification. Based on deposition rates at modern glaciers, this succession of cyclopelites could have been deposited in as little as a year (Mackiewicz et al., 1984).

The fissile upper contact of this facies beneath a boulder lag in facies Dmm-s, is likely due to subglacial deformation during a readvance of the glacier over the area.

3.5.3.2. Sc-fu: Fining upward stratified sandstone

Sc-fu description

This facies consists of laterally-continuous, fining-upward, stratified, lenticular packages of sandstone that are interstratified with facies Fs (Table 3-2; Figure 3-13G,H). These sandstone units

are 0.1 – 0.5 m thick and have sharp lower and upper contacts. The upper contacts of this facies follow the shape of the upper-most bedforms, which are often cross stratification. Sandstones of this facies become less common and fine from the stratigraphic bottom to the top of this facies association. The primary sedimentary structures in this facies include plane beds, unidirectional 3D cross laminations, cross beds, climbing ripples, convolute bedding, and flaser cross laminations. Water escape structures are common throughout this facies, some of which resulted in sand volcanoes. In thinner sandstone bodies (~ 0.1 – 0.25 m thick), grain size and bedform type are vertically constant. In successions thicker than ~ 0.25 m, the sandstone generally fines upward and transitions from relatively higher-energy bedforms at its base (e.g., plane beds) to lower-energy bedforms at their tops (e.g., 3D cross laminations or climbing ripples). Grain sizes in this facies range from very coarse- to very fine-grained sandstone. Relatively coarse lithologies are poorly sorted with grain sizes from very coarse- to fine-grained sandstone. Medium-grained bodies are moderately well-sorted with grain sizes from very coarse to very fine grained. Fine- and very-fine-grained sandstone bodies are well- to very-well sorted. Bed thickness is proportional to grain size. Well-sorted fine and very-fine-grained sandstones are quartz rich, and the medium- to coarse-grained sandstones, like most sandstones and conglomerates in this succession, are rich in a lithics. Sand grain shapes are angular to sub-rounded. Rare, pebble-sized outsized clasts occur throughout this facies. These clasts are more noticeable in fine- to medium-grained sandstones, where they punctuate sedimentary structures.

Sc-fu transport directions

Current orientations were measured from bedforms in these facies (N = 29; Figure 3-6). Measurements were clustered around north, and ranged from 355° to 026°. The mean current direction was 004° (toward north).

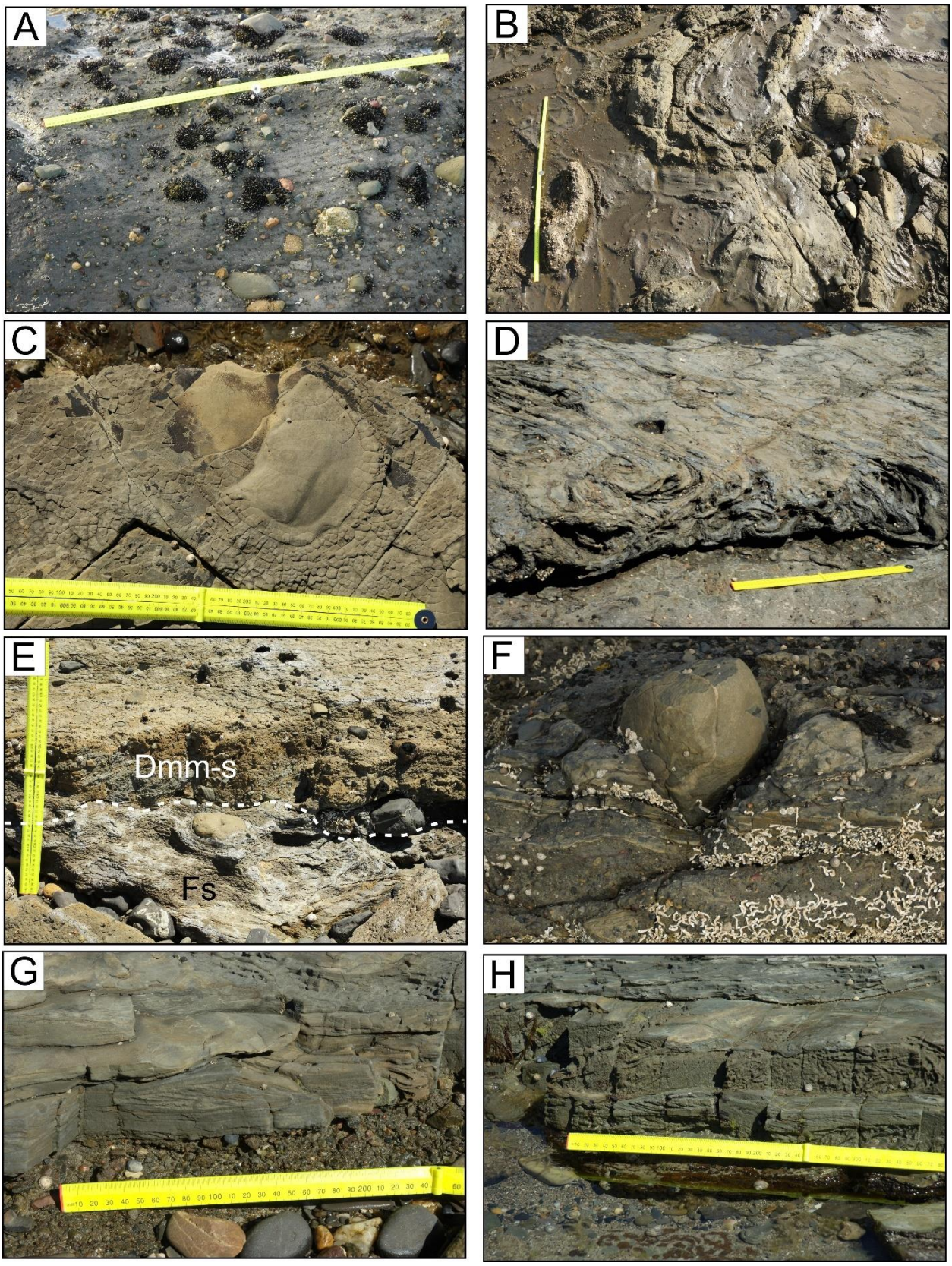
A
B
C
D
E
Dmm-s
Fs
F
G
H

Figure 3-13. Representative photos of features of the Interstratified Rhythmic (IsR) Facies Association not shown in Figure 3-12. Marks on all rulers are in cm. Rulers are 50 cm when folded in half and 1 m long when unfolded. Cobbles were common in this inter-tidal zone, both derived from the Wynyard Fm and from the intrusion at Doctors Rock. Therefore, many of the cobbles in these photographs are not in situ and all the basaltic clasts are not from the Wynyard Fm. A. Stratified, sandy diamictite (facies Dms-s). B. Deformed, interstratified diamictite (Dms-s) and laminated fine-grained sediments (facies Fs). C. Sand volcano on the upper surface of a fine-grained sandstone unit with dewatering structures. D. Folded laminated fine-grained sediments (Fs) with a sharp lower contact with the stratified diamictite facies (Dms-s). E. Upper contact of the IsR facies association with the sandy diamictite. Note fissile texture of the fine-grained sediments (Fs), and the protrusion of cobble-sized clasts from the diamictite into Fs. F. Outsized clasts and associated ruck structures punctuating laminated sediments. G. Flaser cross lamination in sandstone (facies Sc-fu). Note sharp contact between sandstone and underlying conglomerate. H. Example of climbing ripples and convolute cross laminations in sandstone units (facies Sc-fu). Note how fine-grained sediments (facies Fs) drapes over the sandstone bedforms.

Sc-fu interpretation

This facies was most likely deposited as non-cohesive, high-density turbidity currents (Lowe, 1982; Nemec et al., 1999; Winsemann et al., 2007). These currents were most likely distal portions a proglacial fan. Outsized clasts were likely sourced from iceberg rain-out, and not carried by a current.

3.5.3.3. Cc: Cross bedded conglomerate

Cc description

This facies consists of cross bedded conglomerates that are interbedded with other facies in this facies association (Table 3-2; Figure 3-11). These conglomerates have sharp, planar lower contacts. Evidence of loading (e.g., water-escape structures, small flame structures) of the underlying substrate are present at some locations. Upper contacts are also sharp. These conglomerate bodies can be 0.1 – 0.75 m thick, and the thickness changes along the direction of flow. The conglomerate bodies are thickest (0.5 – 0.75 m) where planar cross beds are present, and are thinner (0.1 – 0.5) upstream and downstream of the cross bedded sections where they appear massive or coarsen upward. The downstream change in thickness is abrupt, and upstream change is gradual.

Conglomerates in this facies are moderately well-sorted. Grains range in size from coarse sand up to small boulders (25 cm). Pebbles and small cobbles are the most common grain sizes. Grains are angular to sub-rounded and imbricated. Clast lithologies and morphologies in this facies appear to be very similar to those in the surrounding diamictite, though no clast counts were made.

Cc transport directions

Current orientations were measured from bedforms in this facies (N = 6; Figure 3-6). Measurements were clustered around north, and ranged from 353° to 002°. The mean current direction was 356° (toward north).

Cc Interpretation

The geometry of conglomerate bodies in this facies association indicate that they were deposited as migrating dunes (Winsemann et al., 2007; Figure 3-11) in non-channelized conditions. While gravel dunes and bars are common in proglacial settings, the non-channelized sharp lower contact of this dune and associated downstream conglomerates is very unusual, and somewhat problematic. A possible explanation for this phenomenon is that the deposition of the conglomerate and forming the conglomerate into a dune were two separate events. The conglomerate could have been deposited in a similar manner to facies Cm, as a hyper-concentrated density flow (Mulder and Alexander, 2001) or "traction carpet" (Todd, 1989). Then, in a similar manner to gravel bars in a river with variable flow regimes, the massive conglomerate was reformed into a dune by some subsequent, sufficiently strong current. Possible sources for a subaqueous flow of sufficient magnitude to rework gravel in a proglacial setting would be an outburst flood from a subglacial lake (e.g., Kirkham et al., 2019). This explanation is also problematic because there is no other indication of such an extreme event in this succession.

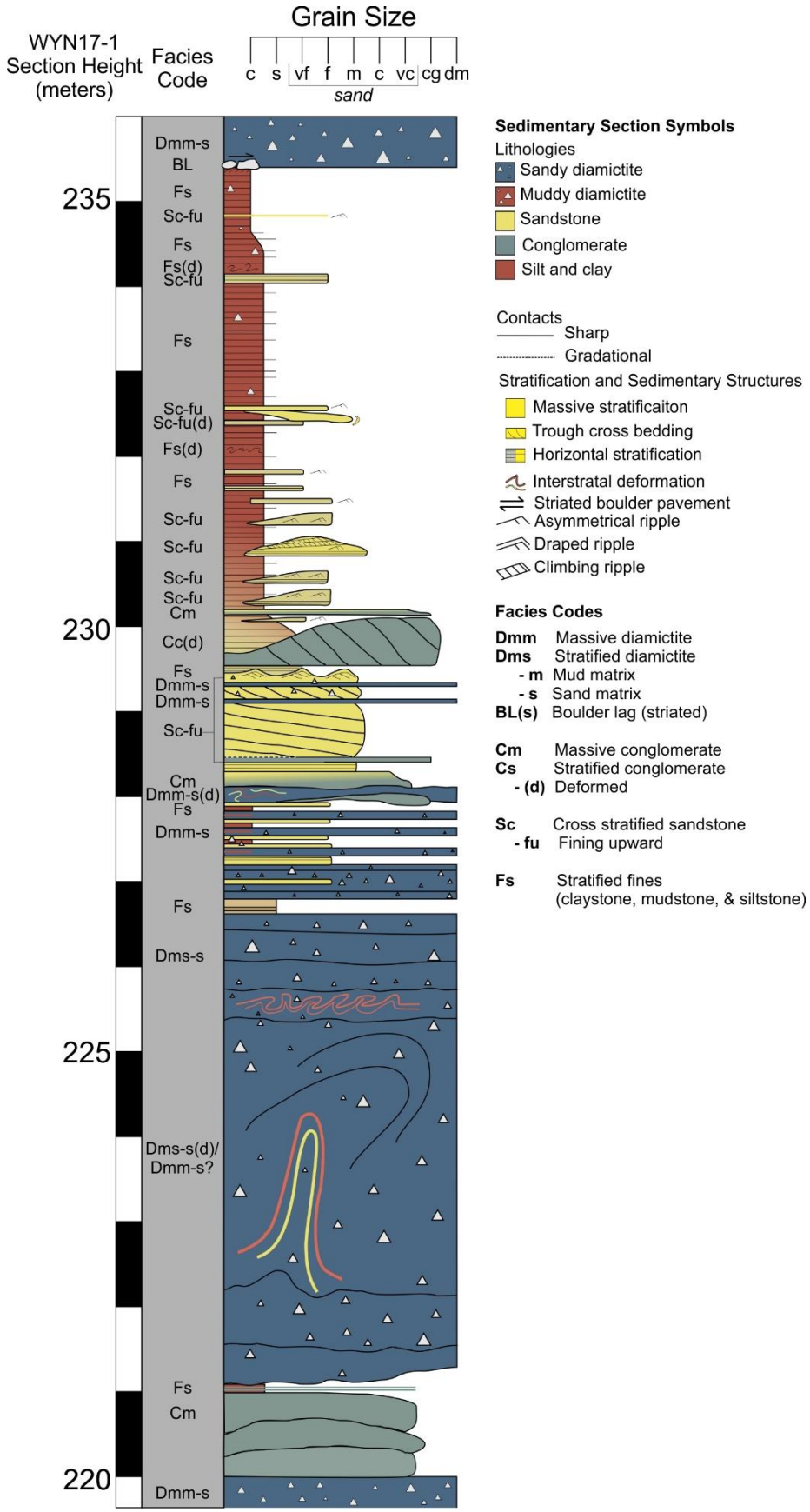

Figure 3-14. Sedimentary logs of the Interstratified Rhythmic (IsR) facies association.

3.5.3.4. Dms-s: Stratified sandy diamictite

Dms-s description

This diamictite facies has a similar composition to facies Dmm-s (massive, sandy diamictite), but is often stratified, interbedded with other facies in this facies association, and commonly deformed [facies Dms-s(d)] (Table 3-2; Figure 3-13A, B, D). The thickest continuous succession of this facies (5.5 m) occurs near the base of this facies association (Figure 3-14). Elsewhere the diamictite is interstratified with other facies in this association, and ranges in thickness from 0.25 - 1 m. The lower contacts of this facies are sharp and undulatory, and upper contacts are sharp. Beds of diamictite in these facies are 0.05 – 0.5 m thick and internally massive with planar contacts.

Where this facies is greater than one meter thick it is highly deformed through soft sediment folding [facies Dms-s(d)]. This deformation is only visible because of the presence of interstratified sorted facies, including claystone and siltstone laminae, as well as sandstone and conglomerate facies. Folded sandstones also contain dewatering structures. Folds composed of sorted facies are tight, often slightly overturned, and range in size from 0.1 m to 3 m long in outcrop. Fold vergence ranges from near-horizontal to near-vertical. There are also places where all lithofacies were chaotically intermixed, but not homogenized. Rare cobbles display ruck structures as deformed beds and laminae along the clast margins.

Dms-s transport directions

Measurable folds were rare in this facies (Figure 3-6). The vergence of folds in outcrop appeared to be generally toward the northwest. A single set of fold hinge orientations were measured (site fines fold figure), which has an orientation of 051˚/231˚, indicating transport toward 321˚.

Dms-s interpretation

This stratified diamictite was most likely deposited in a similar manner to facies Dmm-s (massive diamictite facies), in a sub-aqueous, proglacial, glacier-proximal setting. The stratification in this facies suggests that it was more likely to have been deposited through a combination of plume sedimentation, iceberg rain-out, and resedimentation through mass-transport and sediment gravity flow processes rather than subglacially. The interstratification of this facies with more glacially distal deposits suggests that the thinner nature of this diamictite (up to 5 m) than facies Dmm-s (up to 140 m) is the result of increased distance from a meltwater plume discharge point, likely due to retreat of the glacier front from this location.

The deformed parts of this facies were likely created through slumping. Paleoslope directional estimates from partial directional datasets of slumps can be inaccurate up to 90° (Alsop and Weinberger, 2020). Therefore, the paleoslope of this slump (or series of slumps) could be orientation anywhere between 051° and 231°.

3.5.3.5. IsR Interpretation

Stratified diamictite (Dms-s) and rhythmically laminated fines (Fs) are the two dominant facies in this facies association. The deposition of both of those facies was most likely driven by the settling of suspension from meltwater plumes in a proglacial, glacier-intermediate and glacier-distal setting (Mackiewicz et al., 1984; Powell and Molnia, 1989). The mass transport deposits (facies Sc-fu and Cc) that are interstratified with the meltwater plume derived facies are most likely the result of resedimentation from a glacier-proximal subaqueous fan.

The generally fining upward of this facies association indicates that it tracks the retreat of the glacier margin from the area. The subglacially-deformed upper contact of this facies that is stratigraphically

succeeded by more proglacial, glacier-proximal meltwater plume facies (Dmm-s) suggest a readvance of the ice front over the area.

This facies association was likely deposited as a relatively glacier-distal portion of the groundling-line fan and/or morainal bank system that is also responsible for the SDm (sandy diamictite) facies association (Mackiewicz et al., 1984). Grounding-line fan systems with significant iceberg sedimentation, like the system described here, are most likely to occur at the margins of glaciers with organized subglacial hydraulic systems, high concentrations of entrained debris (sediment), high rates of sediment flux, and a calving, tidewater front. Glacier with these characteristics usually have temperate or mild sub-polar thermal regimes.

3.6. Interpretation

3.6.1. Depositional Model

3.6.1.1. Sedimentary Environments

The basal succession of the Wynyard Fm described in this paper is composed of glacigenic sediments that were deposited in sub-aqueous, marine, and in predominantly proglacial, glacier-proximal and ice-contact environments (Figure 3-15). The basal muddy diamictite (MDm) facies association was likely deposited as the subglacial (topsets) and/or proglacial components (foresets) of a grounding zone wedge (GZW; Figure 3-15A). A GZW is the most likely setting for this facies association largely because it allows for the accumulation of homogenous, massive, clay-rich diamictites (facies Dmm-m) ≥ 58 m-thick that were deposited subglacially and redeposited as mass-transport deposits. Multiphase, subaqueous flows composed of coarse-grained clastics (facies' Cm and Sc-vc) are also consistent with re-sedimentation of channelized meltwater flow deposits that occur in GZWs. While the ~ 60 m thickness of the MDm facies association is a reasonable scale for a GZW (Batchelor and Dowdeswell, 2014; Demet et al., 2019), there is no way to tell where in the

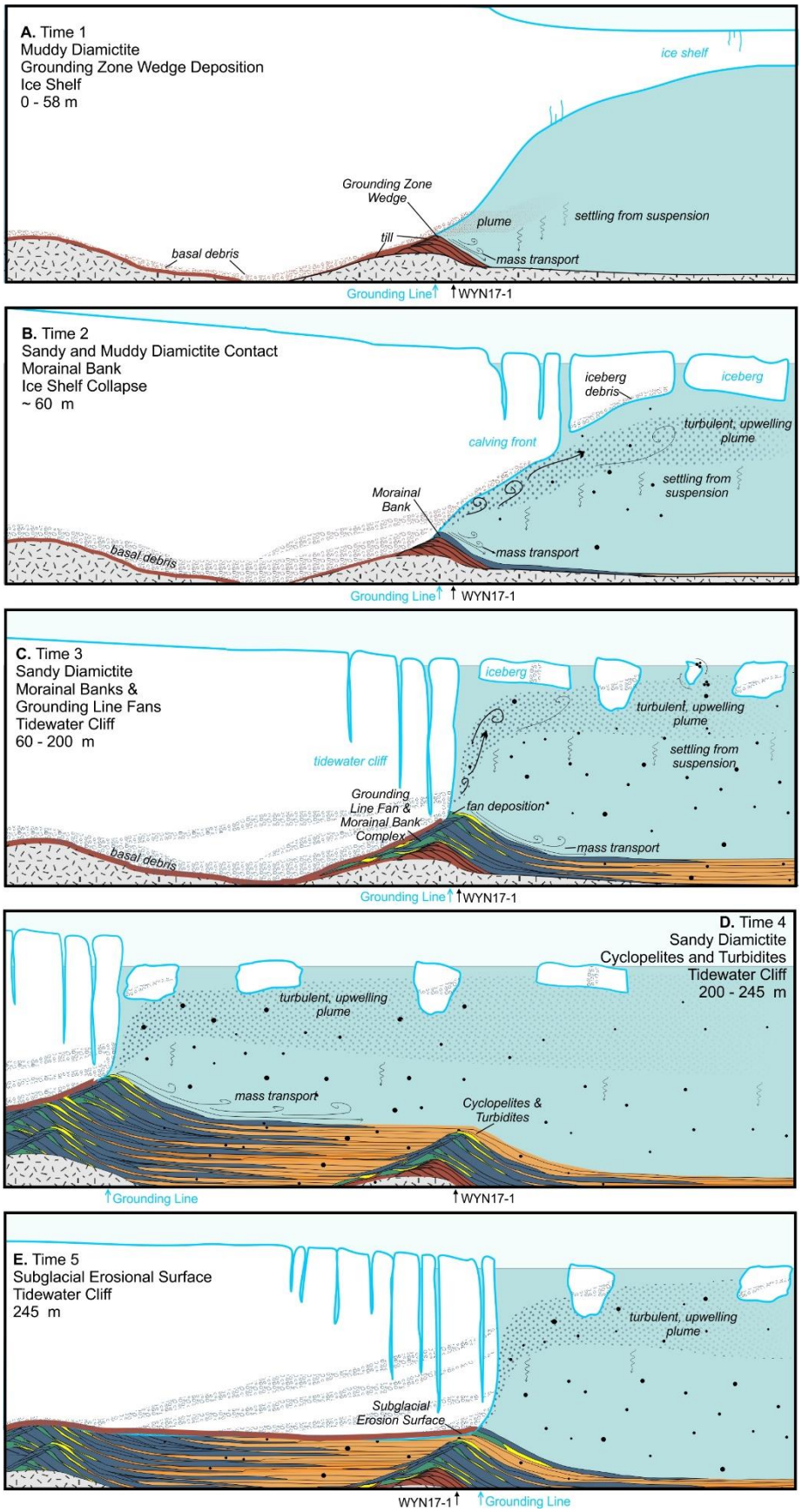

Figure 3-15. Model of proposed depositional environments for the Wynyard Fm in section WYN17-1.- Two- dimensional diagrams, perpendicular to glacier flow showing proposed depositional environments. Diagram concept and stratigraphic geometry after Powell and Cooper (2002).

wedge-form this section is located. Therefore, we cannot use that thickness in determine any characteristics of the 'Wynyard Glacier' thickness, buoyancy, or water depth.

The rest of the succession (facies associations SDm and IsR) was deposited as proglacial, glacier-proximal (SDm) and proglacial, glacier-intermediate or -distal (IsR) morainal bank and grounding-line fan deposits (Cowan and Powell, 1990; Henry et al., 2012; Figure 3-15B-D). The SDm facies association was most likely deposited in a proximal, proglacial subaqueous setting that was strongly influenced by subglacial or englacial meltwater discharge in the form of a jet (e.g., Powell, 1990). The processes of deposition for the massive diamictite facies (facies Dmm-s) were likely dominated by settling from suspension of sediments entrained in meltwater plumes (Powell, 1990) and deposition of iceberg-rafted sediments. Occasional advances of grounded glacier ice over the area are indicated by uniformed striated boulder pavements. The IsR facies association was likely deposited as a relatively glacier-distal portion of the groundling-line fan and/or morainal bank system that is also responsible for the SDm (sandy diamictite) facies association (Mackiewicz et al., 1984). Stratified diamictite (Dms-s) and rhythmically laminated fines (Fs) are the two dominant facies in the IsR facies association. The deposition of both of those facies was most likely driven by the settling of suspension from meltwater plumes in a proglacial, glacier-intermediate and glacier-distal setting (Mackiewicz et al., 1984; Powell and Molnia, 1989). Turbidites, other subaqueous sedimentary density flows, and mass-transport deposits are prevalent throughout this succession. Turbidity currents in proglacial, glacier-proximal systems can be generated by en-glacial or sub-glacial jet efflux or by slope failure instigated by rapid accommodation of sediments (e.g., Powell, 1990; Winsemann et al., 2007).

No unequivocal indicators of reworking of sediment by waves were observed in this succession. Boulder lags may be the result of rare winnowing by storm waves (Eyles, 1988; López-Gamundí et

al., 2016), but are not definitive. This observation suggests that this succession was deposited below storm wave base. A lack of wave-reworking in a proglacial, glacier-proximal environment could be due to depositional depth exceeding the normal and storm wave-base, or due to ice cover (sea ice or ice shelf) blocking wave energy (Hansom et al., 2014). An ice shelf may have been present for the deposition of the GZW (facies association MDm) at the base of the succession, but was unlikely present for most of the environments described here, since ice shelves are not typical of glaciers that produce grounding line fans/morainal banks of the thickness seen in this succession (Dowdeswell et al., 2015). Thick grounding line fan or morainal bank systems are most closely associated with temperate glaciers, because these systems require high-discharge (both water and sediment) from organized (channelized) subglacial hydraulic systems, where most of the water, by volume, is sourced from surface melt. Glaciers with those characteristics have tidewater fronts and don't create ice shelves. Additionally, iceberg deposition in both proglacial, ice-proximal (facies association SDm) and proglacial, ice-distal (facies association IsR) environments suggest that there was insufficiently "fast" sea ice to block iceberg movement over the area. Though the presence of an ice shelf may have inhibited wave reworking of sediments in a GZW (facies association MDm), the absence of wave-reworking for most of the succession (facies associations SDm and IsR) was likely the result of depositional depths exceeding wave base. This inference suggests that the Wynyard Fm at this location was deposited at significant depths, likely comparable to Pleistocene continental shelf depositional environments in the Ross Sea, Antarctica (e.g., Bart et al., 2018) or Hinlopen Trough across Svalbard's northern shelf (Batchelor et al., 2011).

3.6.1.2. Flow Directions and Topography

The transport directions in this succession of the Wynyard Fm can add detail to the depositional environment. It should be kept in mind when considering these transport directions, that directional

estimates from partial directional datasets are not accurate predictors of paleoslope, and can deviate from paleoslope by up to 090° (e.g., Alsop and Weinberger, 2020). Two striated clast pavements, stratigraphically separated by almost 200 m, both indicate glacier flow toward the NNE, which closely follows the trend of the Dundas Trough (Figure 3-1B; Figure 3-6). These uniform orientations support the hypothesis that the flow of the "Wynyard Glacier" was controlled by the topography of the trough (Hand, 1993). Throughout facies associations SDm and MDm (the diamictites), turbidity current flow directions and the vergence of soft-sediment deformation in resedimented bodies indicate transport generally toward the east (Figure 3-6). Individual turbidity current and mass transport directions in the diamictites do have a widespread that range from the NNW to the SSW (Figure 3-6). Turbidity current directions in these same facies associations are slightly more constrained around the ENE than mass transport directions. This spread is present throughout both section WYN17-1 and WYN17-2, and is characteristic of grounding line fan systems. The easterly flow direction in facies association MDm are likely parallel or near-parallel to the slope of the GZW, which may reflect the orientation of the glacier margin at this location or influence by the underlying bedrock topography.

In contrast to their diamictite-associated counterparts, glacier-distal turbidites that are interbedded with cyclopelites in facies association IsR have uniform current transport directions toward the north (Figure 3-6). This suggests that these turbidites were not influenced by the same topography as the underlying or overlying mass-transport and turbidites, and that the topography controlling the deposition of mass transport and turbidite deposits in the underlying succession was likely filled or over-topped before or during the deposition of the IsR facies association (Figure 3-15D). In glaciomarine systems, glacier-proximal systems like grounding line *fans* and morainal *banks* tend to create topographic relief, that relief can be filled by slope failure and proglacial, glacier-distal sedimentation (Figure 3-15). In the case of this succession, topographic relief was likely filled

through a combination of mass transport deposits (facies Dms-s) and glacier-distal deposits (facies Fs). This hypothesis could be reflected in successions of the Wynyard Fm outside this type section with significantly thicker proglacial, glacier-distal deposits. For example, the rhythmically laminated succession of the Wynyard Fm in Hellyer Gorge (30 km south of the Wynyard Fm type section) is 145 m thick (Williams and Lennox, 1989).

3.6.2. Glacial Sequence Stratigraphy

The portion of the lower Wynyard Fm described in this study contains two minor glacial (advance-retreat) sequences (Figure 3-15; Powell and Cooper, 2002; Rosenblume and Powell, 2019). Glacial sedimentary sequences are characterized by the proximity of the depositional environment to the glacier margin, and not accommodation, since the glacier is the primary source of sediment and cause of erosion in these systems (Powell and Cooper, 2002). The two sequences of the Wynyard Fm described in this study are dominated by proglacial, glacier-proximal and ice-contact sedimentation (facies association MDm and SDm), with rare proglacial, glacier-distal facies (facies association IsR). This suggests that the margin or grounding line of the 'Wynyard Glacier' was always within several kilometers (likely retreating to the south) of the section described in this study, and that the area was likely not ever open to non-glacial marine conditions during this time. Therefore, the advances and retreats of the glacier margin in this discussion likely refers to relatively minor fluctuations in the glacier margin position and not glacial-interglacial cycles. While the possibility exists that the erosional event between Sequences I and II removed open marine sediments that would have been deposited during a more extensive retreat of the "Wynyard Glacier", and/or that the sequence boundary represents more time than is proposed here, this is the less likely scenario for several reasons. First, the massive diamictite (facies Dmm-s) is indistinguishable above and below the sequence, suggesting there was no major change in

provenance or depositional style, and therefore no major reorganization of the glacier or ice center, between sequences. The detrital zircon provenance of sandstones (facies Sc-fmc) in the Sandy Diamictite (SDm) facies association is the same between the sequences (see Chapter 4, this dissertation), which supports the idea that the "Wynyard Glacier" was similarly organized while depositing both sequences. Additionally, no other workers have reported any open marine sediments in the Wynyard Fm or its correlates in western Tasmania (see references in section 3.2).

Sequence I is complete in outcrop and is ~ 245 m thick. This sequence is bounded at its base by the Wynyard Fm's basal unconformity, which we interpret to be a glacial advance surface (not a glacial erosion surface) since we saw no evidence for subglacial erosion of the underlying basement. The upper surface of Sequence I is the subglacial erosional surface between facies associations IsR and SDm at the top of section WYN17-1. Within this sequence there are several stratigraphic surfaces that bound different systems tracts. The glacial maximum systems tract (GMaST) occurs between the glacial advance surface (GAS) and the grounding line retreat surface (GLRS). Due to the homogenous nature of facies Dmm-m, the precise location of the GLRS, which denotes the boundary between subglacial and proglacial deposition, in this sequence is difficult to pin-point, but is likely in the lower 20 m of WYN17-1, below the first turbidite deposits (facies Cm, Cc(d), or Sc-vc). The glacial retreat system tract (GRST) in this sequence is bounded by the GLRS and the maximum retreat surface, which is in facies association IsR where the succession ceases to fine upward. In more glacier-distal depositional environments the top of the GRST is the iceberg termination surface (ITS). Since outsized clasts were observed throughout facies association IsR, this sequence does not contain an ITS. The uppermost system tract in this sequence is the glacial minimum system tracts (GMiST), which is bounded by the MRS and the top of the sequence.

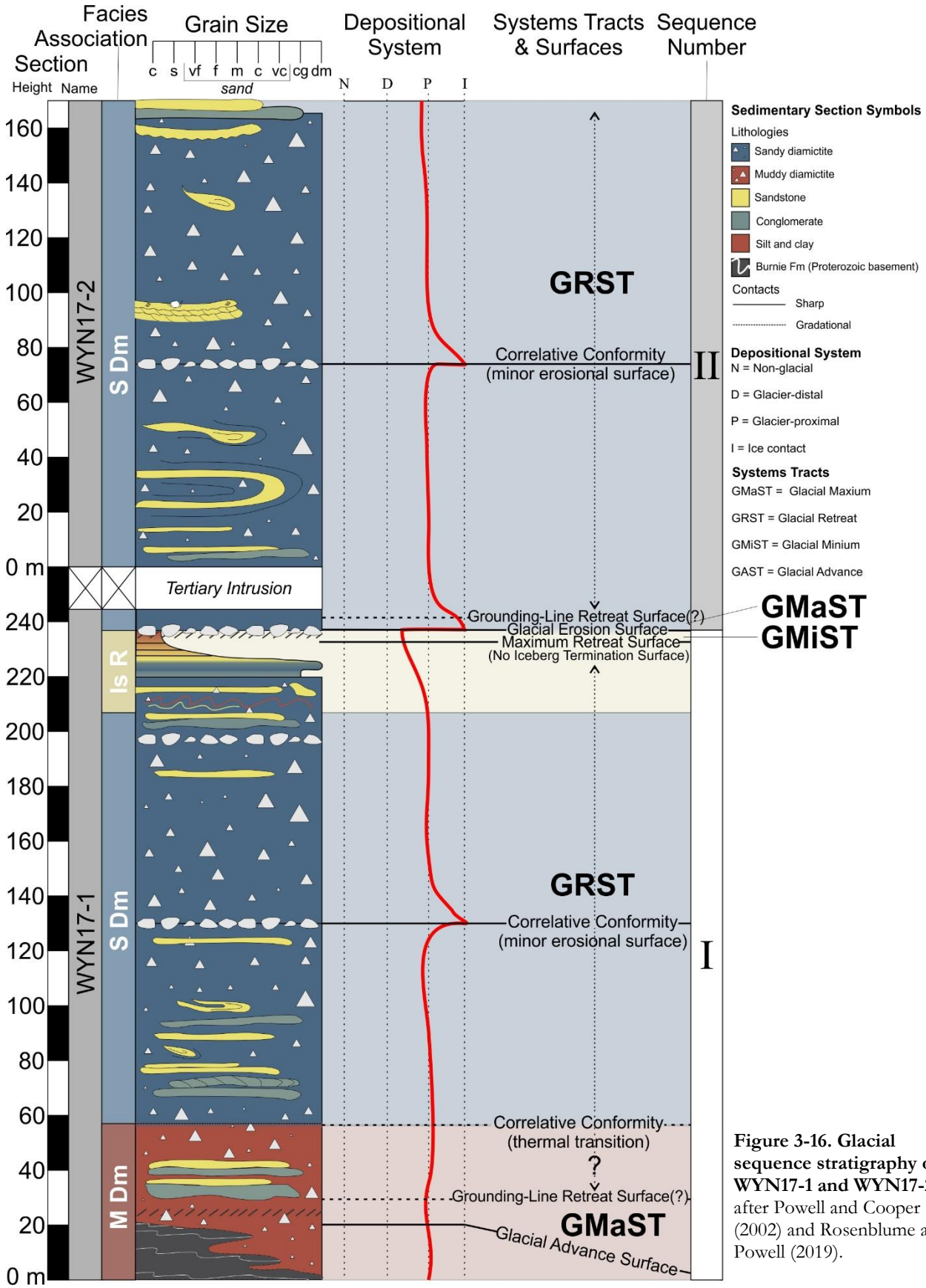

Figure 3-16. Glacial sequence stratigraphy of WYN17-1 and WYN17-2 , after Powell and Cooper (2002) and Rosenblume and Powell (2019).

Sequence I also includes several correlative conformities within its GRST. The contact between facies associations MDm and SDm likely represents a transition in glacier thermal regime, but not a significant change in glacier margin position. The striated boulder lag at 130 m in section WYN17-1 likely represents a minor readvance of an already proximal glacier margin. This surface is more correctly considered a correlative conformity than a system tract boundary because this readvance was likely relatively minor, did not result in significant incision into the underlying sediment, and does not mark a boundary between sedimentation styles in the upper and lower parts of the GRST of Sequence I.

Sequence II is not complete (the upper boundary of the sequence was not within the study area) and is > 170 m thick. The basal surface of this sequence is the GES that separates facies associations IsR and SDm at the top of section WYN17-1. The GMaST in facies is bounded by the lower sequence boundary (GES) and a GLRS. Like the GLRS in sequence I, the precise location of this surface is impossible to precisely locate, but is likely located below the lowest turbidite (facies Sc-fmc, Cm, or Cc) in the sequence, which occurs around 240 m in section WYN17-1. The rest of the succession is part of the GRST, which includes a correlative conformity in the form of a striated boulder lag.

Divided in this way, Sequence I is ~ 245 m thick and Sequence II is at least 170 m thick. These thicknesses are more consistent with sequences deposited by temperate glaciers, whose sequences are on the order to hundreds to thousands of meters thick (e.g., Zellers, 1995; Cowan et al., 2010; Henry et al., 2010), than polar or sub-polar glaciers, whose sequences are typically less than 100 m (e.g., Rosenblume and Powell, 2019; Ives and Isbell, 2021). Thick sequences at the margins of temperate glaciers are generally thought to be the result of their large sediment fluxes (Powell and Cowan, 1986), which allow for rapid accumulation of sediments that may drive subsidence due to loading, and the creation of additional accommodation space (Zellers, 1995). Therefore, the

sequence stratigraphy of the basal Wynyard Fm suggests that this succession is the result of the rapid deposition of thick, proglacial, glacier-proximal sediments by a temperate glacier. These inferences are consistent with the facies interpretation presented in this manuscript.

The interpretation that the basal strata of Sequence I (facies association MDm) were likely deposited by a glacier with a cold sub-polar thermal regime is not incongruous with this interpretation. The 'Wynyard Glacier' likely experienced a change in thermal regimes without a significant advance or retreat of the grounding line. Cenozoic examples of cold-to-warm thermal regime transition are rare (see discussion in section 3.6.4). The most analogous scenario the authors were able to identify has been inferred for a succession in the Whales Deep Basin of the Ross Sea, Antarctica, during the late Pleistocene (Bart et al., 2018). In this instance, the glacier's grounding zone remained in the same location for centuries following the collapse of the glacier's ice shelf (requiring major changes in glacier velocity), and was largely buttressed by the rapid aggradational stacking (~ 150 m) of GZW sediments.

3.6.3. A Pinning Point?

Pinning points are topographic constrictions, either relatively narrow or shallow areas, on a glaciated landscape that act to locally slow ice velocities, thereby leading to localized increases in ice volume and lateral friction that act to stabilize an otherwise retreating grounding line at that location (Warren and Glasser, 1992; Favier et al., 2012). Since pinning points create relatively stable glacier grounding lines, glacier-proximal landforms and sedimentary systems, like grounding line fans, morainal banks, and GZWs, will accumulate in these areas and increase the relief of the pinning point (e.g., Bart et al., 2018; Greenwood et al., 2018). When a marine-terminating glacier eventually retreats from a pinning point, it will retreat relatively rapidly until another stabilizing point in reached (Warren and Glasser, 1992; Powell et al., 2000). This behavior of glaciers means that proglacial,

glacier-proximal sedimentary successions are more likely to be deposited at pinning points than between pinning points, all other things being equal (Figure 3-15). The buildup of a positive-relief landform with a negative (upglacier) slope at the margin of a glacier during a period of a relatively stable grounding line, may also create a pinning point, independent of any pre-existing topography (e.g., Alley et al., 2007).

Several characteristics of this succession suggests that the basal section of the Wynyard Fm described in this manuscript may have been influenced by a pinning point for the "Wynyard Glacier". Though relatively small, the ~ 20 m of relief on the basal unconformity suggests that there may have been sufficient bedrock relief that could have created a pinning point. This is consistent with the large variation in thickness of the Wynyard Fm in northeastern Tasmania (e.g., Reid et al., 2014), and observations of relief on the sub-Permian surface throughout the Dundas Trough (e.g., Gee, 1977; Williams and Lennox, 1989; Hand, 1993). The initial deposition of a GZW, followed by a grounding line fan and/or morainal bank, could have created a positive feedback loop that resulted in continued aggradation of grounding line deposits in this location. The presence of a glacier pinning point at, and therefore the preference of the glacier grounding line for, the location of the Wynyard type section would also explain why the succession consists of primarily proglacial, glacier-proximal sedimentation (this study, Powell, 1990; Henry et al., 2012) when other part of the Wynyard Fm are dominantly glacier-distal facies (Williams and Lennox, 1985). Besides repeated section due to folding and faulting, the exceptional thickness of the Wynyard Fm type section may be due to the aggradation of grounding line fan and morainal bank successions (Powell, 1990; Henry et al., 2012) in a similar manner to the Pleistocene example in Whales Deep Basin of the Ross Sea, Antarctica (Bart et al., 2018).

3.6.4. Change in Glacier Thermal Regimes and Ice Shelf Collapse

The differences in depositional processes and inferred depositional environment between the muddy diamictite facies association (MDm) and the sandy diamictite facies association (SDm) imply that the 'Wynyard Glacier' experienced significant changes in thermal regime during the deposition of this succession.

The MDm facies association was likely deposited as a GZW. A GZW is the most likely setting for this facies association largely because it allows for the accumulation of homogenous, massive, clay-rich diamictites (facies Dmm-m) ≥ 58 m-thick that were deposited as subglacially and redeposited as mass-transport deposits. GZWs accumulate on cross-shelf troughs and fjords at the grounded, stable margins of marine-terminating ice sheets, often in ice streams (relatively fast-flowing portions of an ice-sheet whose bases are largely at the pressure melting point of the glacier, i.e., water is present), that have dominantly distributed, subglacial hydraulic systems and ice shelves (Dowdeswell and Fugelli, 2012; Batchelor et al., 2014; Batchelor and Dowdeswell, 2015; Simkins et al., 2017; Prothro et al., 2018; Demet et al., 2019). Ice shelves occur in high-polar settings at the margins of glaciers with polar thermal regimes. These wedges form where the glacier margin is relatively stable, and are built up on timescales from decades to centuries (Batchelor and Dowdeswell, 2015; Simkins et al., 2017).

The SDm facies association was likely deposited in a proglacial, glacier-proximal, subaqueous setting, such as a groundling-line fan or morainal bank, with occasional advances of grounded glacier ice over the area. Flow directions suggest that the succession described in this manuscript may have been on the flank of a grounding line fan. Depositional systems like the one suggested by the SDm facies association are created by glaciers with organized, high-discharge subglacial hydraulic systems and large sediment loads procured through high subglacial erosion rates (Dowdeswell et al., 2016).

Glaciers with these characteristics have mild-subpolar or temperate thermal regimes. Such glaciers do not have ice shelves because, all other things being equal, ice at its pressure melting point ("warm" ice) is more susceptible to crevassing, and therefore calving, than ice below its pressure melting point ("cold" ice) (Benn et al., 2007; Cuffey and Paterson, 2010).

The change in sedimentation styles between these two facies associations suggest a change in thermal regime from cold subpolar to mild subpolar or temperate, as well as possibly the collapse of an ice shelf.

3.7. Discussion

One of the proposed purposes of studying late Paleozoic ice age (LPIA) strata is to infer the type, timing, and extent of glaciations during this time. Ideally, those inferences about glacier characteristics can then be tied to other global and regional records of climate to better understand how these ancient glaciers interacted with those climate systems. Local and regional heterogeneity is common for both glaciers and their sedimentary deposits because a glacier's physical characteristics are ultimately a response to local, regional, and global climate, ocean conditions (in the case of marine-terminating glaciers), as well as local and regional physiography. Therefore, glacigenic sedimentary deposits must be understood on a local level before they can be correlated to basinal, regional, or local patterns (Isbell et al., 2012, 2021; Pauls et al., 2021). This is especially true in the "ancient" record, where temporal constraints are on the order of millions to tens of millions of years. This is all to say that the interpretations discussed here apply only to the lower Wynyard Fm at the described locality. How this succession relates to other glacigenic strata in both the Tasmanian, including the upper portion of the type section, and adjacent basins is another question.

The succession of the Wynyard Fm described in this study comprises the base of the Wynyard Fm type section, which, at an estimated 600 m (Banks, 1962; Reid et al., 2014), is the thickest known

accumulation of Permo-Carboniferous glacigenic sediments in Tasmania (Reid et al., 2014). Though these strata were described (certain features in detail) by early workers (i.e., Howchin, 1912; Banks et al., 1955; Ahmad, 1957), this study presents the first comprehensive lithofacies analysis and specific sequence-stratigraphic consideration of the succession.

The lowermost 415 m of this type section were described in this study. The described succession is dominated by a massive, sandy diamictite facies association (SDm), whose components are characteristic of proglacial, glacier-proximal, subaqueous, marine morainal bank and grounding line fan deposits. The rhythmically-laminated siltstones, mudstones, and claystones that are interbedded with coarse-grained turbidites (facies association IsR) are most likely cyclopelites, making them the proglacial, glacier-intermediate or glacier-distal component of the same depositional system responsible for the SDm facies association. The lack of fossils, bioturbation, or open-marine sediments in this succession indicate that the sediments in the IsR and SDm facies associations were deposited rapidly, an inference consistent with the conclusions of previous studies (Powell, 1990; Henry et al., 2012), as well as with the nature and pervasiveness of soft-sediment deformation and mass-transport bodies described in this study. The lack of evidence for wave reworking suggests these strata were deposited below normal and storm wave base, likely on a continental shelf. Depositional environments like the one interpreted from the IsR and SDm facies associations are created by glaciers with temperate or mild sub-polar thermal regimes, that have organized, high-discharge meltwater systems, have significant subglacial and englacial sediment loads, and create sediment-laden icebergs.

The thicknesses of the stratigraphic sequences described in this succession are ~ 245 m and > 170 m respectively. Glacimarine sequences that are > 100 m are more likely to be deposited by temperate glaciers (e.g., Cowan et al., 2010) than mild sub-polar glaciers (e.g., Rosenblume and

Powell, 2019), which suggests that the "Wynyard Glacier" had a temperate thermal regime during the deposition of these facies associations. This interpretation is consistent with previous works (Ahmad, 1957; Carey and Ahmad, 1961; Clarke and Banks, 1975; Banks, 1981; Powell, 1990; Hand,1993; Henry et al., 2012; Reid et al., 2014).

In contrast, the lower-most 58 m of this succession, which overlies the basal unconformity, is dominantly composed of a muddy, massive diamictite (MDm). This facies association was likely deposited as a grounding zone wedge (GZW). GZWs are deposited in marine settings by ice streams (fast flowing areas of the glacier with their bases dominantly at their pressure melting point) of glaciers with cold sub-polar to polar thermal regimes, distributed (non-channelized, Darcian-flow dominated) subglacial meltwater systems, and ice shelves. The hypothetical glaciers with polar or varying thermal regimes have not been previously proposed for the Pennsylvanian-Permian glaciation of Tasmania.

The lack of non-glacigenic strata in this succession and similarities in depositional style and provenance between Sequence I and II most likely suggest that the succession of Wynyard Fm described in this paper was deposited during the same glacial interval and were not separated in time by an interglacial period. The subglacial erosional surface between the two sequences described in this manuscript are likely the result of fluctuations in the glacier's margin location within several kilometers up- or down-glacier (see discussion in section 3.6.2).

3.7.1. The Wynyard Glacier

In this discussion, the "Wynyard Glacier" refers to the glacier that was responsible for depositing the succession discussed this study, which was likely the same glacier for both Sequences I and II (see section 3.6.2). This discussion does not necessarily apply to other strata in the Wynyard Fm type section, that are likely stratigraphically above, or other Wynyard Fm localities.

Characteristics of the Wynyard Fm and its structural setting at this location can be used to infer the size of the "Wynyard Glacier". The glacier must have been sufficiently thick to become grounded on what was likely a basinal shelf below storm wave base. This suggests water depths were *at least* ~ 150 - 200 m (Peters and Loss, 2012). A marine-terminating glacier with a calving, tidewater margin, the glacier's margin may be stable at thicknesses that range from slightly thicker (by tens of meters) than the water depth (the glacier's density-determined "flotation thickness") to ~ 100 m thicker than the water depth (Ma et al., 2017). For example, if the continental shelf was 200 m below sea level, then the grounded margin of a marine ice-cliff would be stable if the glacier at its terminus was ~ 225 – 300 m thick. If the "Wynyard Glacier" was grounded on a continental shelf too deep to allow for the re-working of the sediment by waves, then the glacier margin must have exceeded ~ 200 m. In modern glaciers, a marine terminating glacier margin with thickness that exceed 200 m is more consistent with an outlet glacier of an ice sheet or large ice cap (e.g., ~ 400 m, Petermann Glacier, Greenland, Tinto et al. (2015) and ~ 800 m, Thwaites Glacier, Antarctica, Yu et al. (2019)) than a small ice sheet or ice cap (e.g., 30 – 90 m; southeastern Alaska, Brown et al (1982) or < 100 m, Svalbard, Fürst et al. (2017)).

The line of reasoning in the previous paragraph is based on some precarious assumptions, but the hypothesis that the "Wynyard Glacier" must have been relatively large is supported by the geometry of the Dundas Trough (Figure 3-1B). For the "Wynyard Glacier" to flow parallel to this structural element, the glacier must have been sufficiently thick and wide to fill and follow the topography of the Dundas Trough, which was likely 50 km wide, 200 – 500 m deep, and at least 100 km long. A width of 50 km is wider than the largest modern outlet glacier in Antarctica (Lambert Glacier, ~ 40 km wide), but is a similar width to many cross-shelf troughs that mark where ice streams (areas of fast-moving ice within ice sheets or large ice caps) eroded into the continental shelf (Livingstone et al., 2012; Batchelor and Dowdeswell, 2014). While Pleistocene ice streams are more often associated

with glaciers that have sedimentary substrates ("soft beds"), there is growing evidence that ice streams may also occur in glaciers underlain by bedrock ("hard beds"; Ó Cofaigh et al., 2014; Krabbendam et al., 2021), like the "Wynyard Glacier" initially was, and that the flow of some Pleistocene ice streams may have been influenced by bedrock structure (Livingstone et al., 2012). The proposed water depths of the depositional environments in the basal Wynyard Fm and the scale of the Dundas Trough structural element both suggest that the "Wynyard Glacier" was part of an ice center the size of an ice sheet or large ice cap. One could perhaps go as far as to reason that the "Wynyard Glacier" was an ice stream whose location was controlled by the structure and topography of the Dundas Trough.

The unique interpretation made in this study is the transition of the "Wynyard Glacier" from a relatively cold glacier thermal regime (cold sub-polar) at the base of this succession to a relatively warm glacier thermal regime (temperate) throughout the rest of the succession. The factors that drove this change in glacier thermal regime were likely not straightforward, especially if the Wynyard Fm was deposited at the margin of an ice sheet or large ice cap. While smaller glaciers may be dominantly temperate (warm-based), polar (cold-based), or subpolar (polythermal), larger ice caps and especially ice sheets are thermally complex ice bodies that end up having a patchwork of thermal regimes (e.g., Engelhardt, 2004; MacGregor et al., 2016). Variations in thermal regime throughout an ice sheet are the result of complex interactions between factors such as air temperature, local glacier thickness, geothermal heat flux, abundance of basal meltwater, mass balance, basal substrate, bed topography, and ice sheet history. In particular, categorizing the thermal regime, a term that combines ice temperature and basal hydraulic conditions, of ice streams is an ongoing and evolving area of study (e.g., Smith et al., 2013; Chu et al., 2018; Franke et al., 2021).

Geomorphic records from the Cenozoic can give insight into why and how large ice caps and ice sheets change their thermal regime. The landform records of Cenozoic ice sheets are notable for recording variations in glacier thermal regime through space and time (e.g., Dyke et al., 1992; Kleman and Glasser, 2007), but examples of cold-to-warm thermal regime transition are rare. Far more common are records of glaciers that transitioned from temperate (warm) landsystems and sedimentation to polar or subpolar (cold) systems (e.g., Lewis et al., 2007; Andreassen et al., 2014; Klages et al., 2015). This may be simply due to a preservation bias. Landform assemblages from temperate (warm) ice sheets are more common or more widespread on continental margins (Greenwood et al., 2021) and temperate glaciers tend to produce (Hodson et al., 1997) and deposit larger volumes of sediment. The geomorphic and sedimentary records of temperate glacier could bury, obscure, or their processes erode records of prior cold thermal regimes, so that the only records of cold thermal regimes we can easily observe are those that follow warm thermal regimes. In the sedimentary record, grounding zone wedge (GZW) deposition succeeded by more temperate glacial sedimentary systems (i.e., glaciofluvial, ice contact delta, etc.) have been identified in the Paleozoic Karoo Basin (Dietrich and Hofmann, 2019). Though in the Karoo example, repeated deposition of GZWs suggest that the thermal regime never transitioned to a fully temperate thermal regime.

So, while interesting and notable, the change in the glacial thermal regime indicated by changes in sedimentation style in the Wynyard Fm most likely does not reflect any abrupt warming. Rather, the change in thermal regime is more likely the result of changes that occurred during ice sheet retreat from the area. The preservation of a GZW in the sedimentary record is the result it being buried by, instead of eroded by, subsequent glaciers with temperate thermal regimes. The interpretation of this succession as a glacial retreat sequence does suggest that the glacier was shrinking overall.

3.7.2. Ice Age Context

The depositional settings and glacier characteristics inferred by this study do not stray far from our current, broad understanding of the Late Paleozoic Ice Age during the late Carboniferous and early Permian in southeast Gondwana. If the "Wynyard Glacier" was an ice sheet, centered somewhere to the modern south or southwest of Tasmania, the question stands whether and how the "Wynyard Glacier" was related to deposition of glacigenic sediments, especially in other parts of the Tasmanian Basin and in North Victoria Land (Cornamusini et al., 2017; Zurli et al., 2021).

3.8. Conclusions

The diamictite-rich, 415 m thick succession of the Wynyard Fm in its type section along the northwest coast of Tasmania is glacigenic, and was deposited in proglacial, glacier-proximal to glacier-distal, marine environments on a basinal shelf at water depths below storm wave base. Facies associations in this succession include muddy massive diamictite (MDm), sandy massive diamictite (SDm), and rhythmically laminated fine-grained facies (IsR). The MDm facies association was likely deposited as a subglacial and proglacial, glacier-proximal grounding zone wedge, the SDm facies association as part of a glacier-proximal grounding line fan or morainal bank, and the IsR facies association as a glacier-intermediate or glacier-distal cyclopelites. All facies associations contain mass transport and turbidite deposits that could have been driven by slope instability due to rapid deposition. This succession was likely deposited during a retreat phase of the "Wynyard Glacier", with some minor readvances over the area. The grounding line was likely always within kilometers of the measured sections. Deposition of these facies could have occurred over a relatively short period of time: grounding zone wedges are deposited on the scale of decades to centuries, grounding line fan and morainal bank deposits on the order of years or decades, and the cyclopelites on the order of years. The glacier likely shifted thermal regimes from cold subpolar (polythermal) during the

deposition of the MDm facies association at the base of the succession to temperate (warm) during the deposition of the SDm and IsR facies associations. This change in thermal regime was likely the result of physical changes to or shifts in the "Wynyard Glacier" that occurred as part of the glacier's overall retreat, and not some abrupt change in climate. The "Wynyard Glacier" likely flowed from south to north through the Dundas Trough in western Tasmania, probably as part of a large ice cap or ice sheet.

3.9. Conflict of Interest

The authors declare that the research was conducted in the absence of any commercial or financial relationships that could be construed as a potential conflict of interest.

3.10. Acknowledgments

This work was made possible with funding from the Geological Society of America's Graduate Student Research Grant program, P.E.O. Scholar Awards, University of Wisconsin – Milwaukee's RGI grants program, and National Science Foundation grants OISE-1559231 and OPP-1443557. Special thanks to Natural Resources Tasmania for their assistance with, and approval of, collection permits.

3.11. References

Alley, R. B., Anandakrishnan, S., Dupont, T. K., Parizek, B. R., and Pollard, D. (2007). Effect of sedimentation on ice-sheet grounding-line stability. Science, 315(5820), 1838-1841.

Allmendinger, R. W., Cardozo, N., & Fisher, D. M. (2011). Structural geology algorithms: Vectors and tensors. Cambridge University Press.

Alsop, G. I., & Weinberger, R. (2020). Are slump folds reliable indicators of downslope flow in recent mass transport deposits?. Journal of Structural Geology, 135, 104037.

Ahmad, N. (1957) The environment of the permian glacial sedimentation of Tasmania, with particular reference to the base of the Permian. Ph.D. dissertation, University of Tasmania.

Anandakrishnan, S., Catania, G. A., Alley, R. B., & Horgan, H. J. (2007). Discovery of till deposition at the grounding line of Whillans Ice Stream. Science, 315(5820), 1835-1838.

Andreassen, K., Winsborrow, M. C., Bjarnadóttir, L. R., & Rüther, D. C. (2014). Ice stream retreat dynamics inferred from an assemblage of landforms in the northern Barents Sea. Quaternary Science Reviews, 92, 246-257.

Baillie, P.W. (1985) 'Parmeener Super-Group' in Baillie, P.W. and Corbett, K.D. (eds.) Geological atlas 1:50000 series. Sheet 57 (7913N). Strahan, Explanatory Report of the Geological Survey, Tasmania Department of Mines, 31-34.

Banks, M.R., Loveday, J.L., and Scott, D.L. (1955) Permian varves from Wynyard, Tasmania. Papers and Proceedings of the Royal Society of Tasmania, 89, 203-218.

Banks, M.R. and Ahmad, N. (1962) The Permian system in western Tasmania. Papers and Proceeding of the Royal Society of Tasmanian, 96, 1-18.

Banks, M.R., and Clarke, M.J. (1987). 'Changes in the geography of the Tasmania Basin in the Late Paleozoic' in Mckenzie, G.D. (eds) Gondwana Six: Stratigraphy, Sedimentology, and Paleontology, Washington, DC, American Geophysical Union, Geophysical Monograph 41, 1-14.

Banks, M.R. (1962) 'Permian (Tasmania)' in Spry, A. and Banks, M.R. (eds) Geology of Tasmania, Journal of the Geological Society of Australia, 9, 189-216.

Banks, M.R. (1981) 'Late Paleozoic tillites of Tasmania' in M.J. Hardland and W.B. Harland (eds.) Earth's Pre-Pleistocene Glacial Record, 1st, Cambridge: Cambridge University Press, 495-501.

Batchelor, C. L., Dowdeswell, J. A., & Hogan, K. A. (2011). Late Quaternary ice flow and sediment delivery through Hinlopen Trough, Northern Svalbard margin: Submarine landforms and depositional fan. Marine Geology, 284(1-4), 13-27.

Batchelor, C. L. and Dowdeswell, J. A. (2014). The physiography of High Arctic cross-shelf troughs. Quaternary Science Reviews, 92, 68-96.

Batchelor, C. L. and Dowdeswell, J. A. (2015). Ice-sheet grounding-zone wedges (GZWs) on high-latitude continental margins. Marine Geology, 363, 65-92.

Bart, P. J., DeCesare, M., Rosenheim, B. E., Majewski, W., & McGlannan, A. (2018). A centuries-long delay between a paleo-ice-shelf collapse and grounding-line retreat in the Whales Deep Basin, eastern Ross Sea, Antarctica. Scientific Reports, 8(1), 1-9.

Benn, D. I., & Clapperton, C. M. (2000). Pleistocene glacitectonic landforms and sediments around central Magellan Strait, southernmost Chile: evidence for fast outlet glaciers with cold-based margins. Quaternary Science Reviews, 19(6), 591-612.

Benn, D. I., Warren, C. R., & Mottram, R. H. (2007). Calving processes and the dynamics of calving glaciers. Earth-Science Reviews, 82(3-4), 143-179.

Bennett, M. R., Waller, R. I., Glasser, N. F., Hambrey, M. J., & Huddart, D. (1999). Glacigenic clast fabrics: genetic fingerprint or wishful thinking?. Journal of Quaternary Science, 14(2), 125-135.

Bhattacharya, H. N. and Bhattacharya, B. (2015). Lithofacies architecture and palaeogeography of the late Paleozoic glaciomarine Talchir formation, Raniganj Basin, India. Journal of Palaeogeography, 4(3), 269-283.

Boulton, G. S. (1996). The origin of till sequences by subglacial sediment deformation beneath mid-latitude ice sheets. Annals of Glaciology, 22, 75-84.

Brown, C.S., Meier, M.F., Post, A. (1982) Calving speed of Alaska tidewater glaciers, with application to Columbia Glacier: a study of 15 iceberg-calving glaciers in Alaska establishes a relationship between calving speed and water depth at the terminus. Geological Survey Professional Paper 1258-C. United States Geological Survey, Alexandria, Virginia. Available at: https://dggs.alaska.gov/webpubs/usgs/p/text/p1258c.pdf

Cardozo, N., & Allmendinger, R. W. (2013). Spherical projections with OSXStereonet. Computers & Geosciences, 51, 193-205.

Carey, S.W. and Ahmad, N. (1961) 'Glacial Marine Sedimentation' in Raasch, G.O. (ed.) Geology of the Arctic: Proceedings of the First International Symposium on Arctic Geology, vol. 2. 1st. Toronto: University of Toronto Press, 865-894.

Carrivick, J. L., & Rushmer, E. L. (2009). Inter-and intra-catchment variations in proglacial geomorphology: an example from Franz Josef Glacier and Fox Glacier, New Zealand. Arctic, Antarctic, and Alpine Research, 41(1), 18-36.

Catuneanu, O., Wopfner, H., Eriksson, P. G., Cairncross, B., Rubidge, B. S., Smith, R. M. H., & Hancox, P. J. (2005). The Karoo basins of south-central Africa. Journal of African Earth Sciences, 43(1-3), 211-253.

Chen, B., Joachimski, M. M., Wang, X. D., Shen, S. Z., Qi, Y. P., & Qie, W. K. (2016). Ice volume and paleoclimate history of the Late Paleozoic Ice Age from conodont apatite oxygen isotopes from Naqing (Guizhou, China). Palaeogeography, Palaeoclimatology, Palaeoecology, 448, 151-161.

Chu, W., Schroeder, D. M., Seroussi, H., Creyts, T. T., & Bell, R. E. (2018). Complex basal thermal transition near the onset of Petermann Glacier, Greenland. Journal of Geophysical Research: Earth Surface, 123(5), 985-995.

Clarke, M.J. and Banks, M.R. (1975) 'The stratigraphy of the lower (Permo-Carboniferous) parts of the Parmeener Supergroup, Tasmania' in Campbell, K.S.W. (ed.) Gondwana Geology: Papers Presented at the Third Gondwana Symposium, Canberra, Australia, 1973, 453-467.

Clarke, M.J. and Forsyth, S.M. (1989) 'Late Carboniferous-Triassic' in Burnett, C.F. and Marten, E.L. (eds) Geology and Mineral Resources of Tasmania. Geological Society of Australia, Special Paper 15, 209-293.

Clarke, M.J. (1968) A reappraisal of a lower Permian type section Golden Valley, Tasmania. Geological Survey Record No. 7, Tasmania Department of Mines, 29 p.

Clarke, M.J. (1977) 'Paleontology' in Gee, R.D. (ed.) Geological atlas 1 mile series. Zone 7, Sheet 28 (8015N). Burnie, Explanatory Report of the Geological Survey, Tasmania Department of Mines, 53-54.

Collinson, J. W. and Kemp, N. R. (1983). Permian-Triassic sedimentary sequence in northern Victoria Land, Antarctica. Antarctic Earth Science, 221-225.

Cornamusini, G., Talarico, F. M., Cirilli, S., Spina, A., Olivetti, V., & Woo, J. (2017). Upper Paleozoic glacigenic deposits of Gondwana: stratigraphy and paleoenvironmental significance of a tillite succession in Northern Victoria Land (Antarctica). Sedimentary Geology, 358, 51-69.

Cowan, E. A., & Powell, R. D. (1990). Suspended sediment transport and deposition of cyclically interlaminated sediment in a temperate glacial fjord, Alaska, USA. Geological Society, London, Special Publications, 53(1), 75-89.

Cowan, E. A., Seramur, K. C., Powell, R. D., Willems, B. A., Gulick, S. P., and Jaeger, J. M. (2010) Fjords as temporary sediment traps: History of glacial erosion and deposition in Muir Inlet, Glacier Bay National Park, southeastern Alaska. Geological Society of America Bulletin, 122(7-8), 1067-1080.

Crompton, J. W., Flowers, G. E., Kirste, D., Hagedorn, B., & Sharp, M. J. (2015). Clay mineral precipitation and low silica in glacier meltwaters explored through reaction-path modelling. Journal of Glaciology, 61(230), 1061-1078.

Crowell, J.C. and Frakes, L.A. (1971) Late Paleozoic Glaciation of Australia. Geological Society of America Bulletin, 82(9), 2515-2540.

Cuffey, K. M., & Paterson, W. S. B. (2010). The physics of glaciers. 4th, Elsevier, Burlington, Massachusetts, USA, 702 p.

David, T.W.E. (1907) The Permo-Carboniferous glacial beds at Wynyard, near Table Cape, Tasmania. Australian Association for the Advancement of Science, XI, 274 – 279. Available at: https://www.biodiversitylibrary.org/item/50730

Demet, B. P., Nittrouer, J. A., Anderson, J. B., & Simkins, L. M. (2019). Sedimentary processes at ice sheet grounding-zone wedges revealed by outcrops, Washington State (USA). Earth Surface Processes and Landforms, 44(6), 1209-1220.

Dietrich, P., & Hofmann, A. (2019). Ice-margin fluctuation sequences and grounding zone wedges: The record of the Late Palaeozoic Ice Age in the eastern Karoo Basin (Dwyka Group, South Africa). The Depositional Record, 5(2), 247-271.

Domack, E. W., Burkley, L. A., Domack, C. R., & Banks, M. R. (1993). Facies analysis of glacial marine pebbly mudstones in the Tasmania Basin: Implications for regional paleoclimates during the late Paleozoic. In Findlay, R.H., Unrug, R, Banks, M.R., and Veevers, J.J. (eds) Gondwana Eight: Assembly, Evolution, and Dispersal, Preceedings of the 8th Gondwana Symposium, Hobard, Tasmania, Australia, June 1991, 471-484.

Dowdeswell, J. A., Hambrey, M. J., & Ruitang, W. (1985). A comparison of clast fabric and shape in Late Precambrian and modern glacigenic sediments. Journal of Sedimentary Research, 55(5), 691-704.

Dowdeswell, J. A., Whittington, R. J., & Marienfeld, P. (1994). The origin of massive diamicton facies by iceberg rafting and scouring, Scoresby Sund, East Greenland. Sedimentology, 41(1), 21-35.

Dowdeswell, J. A. and Fugelli, E. M. G. (2012). The seismic architecture and geometry of grounding-zone wedges formed at the marine margins of past ice sheets. Geological Society of America Bulletin, 124(11-12), 1750-1761.

Dowdeswell, J. A., Hogan, K. A., Arnold, N. S., Mugford, R. I., Wells, M., Hirst, J. P. P., & Decalf, C. (2015). Sediment-rich meltwater plumes and ice-proximal fans at the margins of modern and ancient tidewater glaciers: Observations and modelling. Sedimentology, 62(6), 1665-1692.

Dowdeswell, J. A., Canals, M., Jakobsson, M., Todd, B. J., Dowdeswell, E. K., & Hogan, K. A. (2016). The variety and distribution of submarine glacial landforms and implications for ice-sheet reconstruction. Geological Society, London, Memoirs, 46(1), 519-552.

Dyke, A.S., Morries, T.F., Green, D.E.C., England, J. (1992) Quaternary Geology of the Prince of Wales Island, Arctica Canada. Geological Survey of Cananda, Memoir 433.

Elliot, D. H. (2013). The geological and tectonic evolution of the Transantarctic Mountains: a review. Geological Society of London, Special Publications, 381(1), 7-35.

Engelhardt, H. (2004). Thermal regime and dynamics of the West Antarctic Ice Sheet. Annals of Glaciology, 39, 85-92.

Evans, D. J. and Ó Cofaigh, C. (2003). Depositional evidence for marginal oscillations of the Irish Sea ice stream in southeast Ireland during the last glaciation. Boreas, 32(1), 76-101.

Everard, J.L. (compiler) (2011) Digital Geological Atlas 1:25 000 Scale Series. Sheet 3846. Carver. Mineral Resources Tasmania.

Everard, J.L. and Calver, C.R. (compilers) (2011) Digital Geological Atlas 1:25 000 Scale Series. Sheet 3845. Wynyard. Mineral Resources Tasmania.

Eyles, C. H. (1988). A model for striated boulder pavement formation on glaciated, shallow-marine shelves; an example from the Yakataga Formation, Alaska. Journal of Sedimentary Research, 58(1), 62-71.

Eyles, C. H., & Lagoe, M. B. (1990). Sedimentation patterns and facies geometries on a temperate glacially-influenced continental shelf: the Yakataga Formation, Middleton Island, Alaska. Geological Society, London, Special Publications, 53(1), 363-386.

Eyles, N., Mory, A. J., & Backhouse, J. (2002). Carboniferous–Permian palynostratigraphy of west Australian marine rift basins: resolving tectonic and eustatic controls during Gondwanan glaciations. Palaeogeography, Palaeoclimatology, Palaeoecology, 184(3-4), 305-319.

Eyles, N., Eyles, C. H., Woodworth-Lynas, C., & Randall, T. A. (2005). The sedimentary record of drifting ice (early Wisconsin Sunnybrook deposit) in an ancestral ice-dammed Lake Ontario, Canada. Quaternary Research, 63(2), 171-181.

Farabee, M.J., Taylor, E.L. and Taylor, T.N. (1990) Correlation of Permian and Triassic palynomorph assemblages from the central Transantarctic Mountains, Antarctica. Review of palaeobotany and palynology, 65(1-4), 257-265.

Favier, L., Gagliardini, O., Durand, G. and Zwinger, T. (2012). A three-dimensional full Stokes model of the grounding line dynamics: effect of a pinning point beneath the ice shelf. The Cryosphere, 6(1), 101-112.

Fielding, C. R., Frank, T. D., and Isbell, J. L. (2008a). The late Paleozoic ice age—A review of current understanding and synthesis of global climate patterns. in Fielding, C. R., Frank, T. D., and Isbell, J. L. (eds) Resolving the late Paleozoic ice age in time and space, Special Paper 441, Geological Society of America, 343-354.

Fielding, C. R., Frank, T. D., Birgenheier, L. P., Rygel, M. C., Jones, A. T., & Roberts, J. (2008b). Stratigraphic imprint of the Late Palaeozoic Ice Age in eastern Australia: a record of alternating glacial and nonglacial climate regime. Journal of the Geological Society, 165(1), 129-140.

Fielding, C. R., Frank, T. D., Isbell, J. L., Henry, L. C., & Domack, E. W. (2010). Stratigraphic signature of the late Palaeozoic Ice Age in the Parmeener Supergroup of Tasmania, SE Australia, and inter-regional comparisons. Palaeogeography, Palaeoclimatology, Palaeoecology, 298(1-2), 70-90.

Frank, T. D., Shultis, A. I., & Fielding, C. R. (2015). Acme and demise of the late Palaeozoic ice age: A view from the southeastern margin of Gondwana. Palaeogeography, Palaeoclimatology, Palaeoecology, 418, 176-192.

Franke, S., Jansen, D., Beyer, S., Neckel, N., Binder, T., Paden, J., & Eisen, O. (2021). Complex basal conditions and their influence on ice flow at the onset of the Northeast Greenland Ice Stream. Journal of Geophysical Research: Earth Surface, 126(3), e2020JF005689.

Fürst, J.J., Gillet-Chaulet, F., Benham, T.J., Dowdeswell, J.A., Grabiec, M., Navarro, F., Pettersson, R., Moholdt, G., Nuth, C., Sass, B. and Aas, K. (2017) Application of a two-step approach for mapping ice thickness to various glacier types on Svalbard. The Cryosphere, 11(5), 2003-2032.

Gee, R.D. (1971) Geological atlas 1 mile series. Zone 7, Sheet 22 (8016S). Table Cape, Explanatory Report of the Geological Survey, Tasmania Department of Mines, 51 p.

Graly, J. A., Licht, K. J., Bader, N. A., & Bish, D. L. (2020). Chemical weathering signatures from Mt. Achernar Moraine, Central Transantarctic Mountains I: Subglacial sediments compared with underlying rock. Geochimica et Cosmochimica Acta, 283, 149-166.

Greenwood, S. L., Simkins, L. M., Halberstadt, A. R. W., Prothro, L. O., & Anderson, J. B. (2018). Holocene reconfiguration and readvance of the East Antarctic Ice Sheet. Nature Communications, 9(1), 1-12.

Greenwood, S. L., Simkins, L. M., Winsborrow, M. C., & Bjarnadóttir, L. R. (2021). Exceptions to bed-controlled ice sheet flow and retreat from glaciated continental margins worldwide. Science Advances, 7(3), eabb6291.

Gulline, A.B. and Bravo, A.P. (1977) in Gee, R.D. (ed.) Geological atlas 1 mile series. Zone 7, Sheet 28 (8015N). Burnie, Explanatory Report of the Geological Survey, Tasmania Department of Mines, 53-54.

Haldorsen, S. (1981). Grain-size distribution of subglacial till and its realtion to glacial scrushing and abrasion. Boreas, 10(1), 91-105.

Hambrey, M.J. and Glasser, N.F. (2012) Discriminating glacier thermal and dynamic regimes in the sedimentary record. Sedimentary Geology, 251, 1-33.

Hand, S.J. (1993) 'Paleogeography of Tasmania's Permo-Carboniferous glacigenic sediments' in Findlay, R.H., Unrug, R., Banks, M.R., and Veevers, J.J. (eds.) Gondwana Eight: Assembly, Evolution, and Dispersal, Proceedings of the 8th Gondwana Symposium, Rotterdam: A.A. Blakema, 459-469.

Hansom, J. D. (1983). Ice-formed intertidal boulder pavements in the sub-Antarctic. Journal of Sedimentary Research, 53(1), 135-145.

Hansom, J. D., Forbes, D. L., & Etienne, S. (2014). The rock coasts of polar and sub-polar regions. Geological Society, London, Memoirs, 40(1), 263-281.

Harris, W.K. and McGowran, B. (1971) Permian and reworked Devonian microfossils from the Troubridge Basin. Quarterly Geological Notes, 40(October 1971), 5–11.

Hart, J. K. (2017). Subglacial till formation: microscale processes within the subglacial shear zone. Quaternary Science Reviews, 170, 26-44.

Haughton, P., Davis, C., McCaffrey, W., and Barker, S. (2009). Hybrid sediment gravity flow deposits; classification, origin and significance. Marine and Petroleum Geology, 26, 1900-1918.

Henry, L.C., Isbell, J.L., Fielding, C.R., Domack, E.W., Frank, T.D., and Frasier, M.L. (2012) Proglacial deposition and deformation in the upper Carboniferous to lower Permian Wynyard Formation, Tasmania: A process analysis. Palaeogeography, Palaeclimatology, Palaeoecology, 315, 142-157.

Henstra, G. A., Grundvåg, S. A., Johannessen, E. P., Kristensen, T. B., Midtkandal, I., Nystuen, J. P., Rotevatn, A., Surlyk, F., Sæther, T., & Windelstad, J. (2016). Depositional processes and stratigraphic architecture within a coarse-grained rift-margin turbidite system: The Wollaston Forland Group, east Greenland. Marine and Petroleum Geology, 76, 187-209.

Hodson, A. J., Tranter, M., Dowdeswell, J. A., Gurnell, A. M., & Hagen, J. O. (1997). Glacier thermal regime and suspended-sediment yield: a comparison of two high-Arctic glaciers. Annals of Glaciology, 24, 32-37.

Howchin, W. (1912) Australian Glaciations. The Journal of Geology, 20(3), 193-227.

Isbell, J. L., Miller, M. F., Wolfe, K. L., Lenaker, P. A., Chan, M. A., & Archer, A. W. (2003). 'Timing of late Paleozoic glaciation in Gondwana: Was glaciation responsible for the development of Northern Hemisphere cyclothems?' in Chan, M.J. and Archer, A.W. (eds) Extreme depositional environments: mega end members in geologic time, Special Paper 370, Geological Society of America, 5-24.

Isbell, J.L., Henry, L.C., Gulbranson, E.L., Limarino, C.O., Fraiser, M.L., Koch, Z.J., Ciccioli, P.L. and Dineen, A.A. (2012) Glacial paradoxes during the late Paleozoic ice age: Evaluating the equilibrium line altitude as a control on glaciation. Gondwana Research, 22(1), pp.1-19.

Isbell, J.L., Vesely, F.F., Rosa, E.L., Pauls, K.N., Fedorchuk, N.D., Ives, L.R., McNall, N.B., Litwin, S.A., Borucki, M.K., Malone, J.E. and Kusick, A.R. (2021). Evaluation of physical and chemical proxies used to interpret past glaciations with a focus on the late Paleozoic Ice Age. Earth-Science Reviews, 103756.

Ives, L. R.W., & Isbell, J. L. (2021). A lithofacies analysis of a South Polar glaciation in the Early Permian: Pagoda Formation, Shackleton Glacier region, Antarctica. Journal of Sedimentary Research, 91(6), 611-635.

Jago, J.B. (1972) Geology of the Maydena Range. Papers and Proceedings of the Royal Society of Tasmania, 106, 45-56.

Kessler, T. C., Klint, K. E. S., Nilsson, B., and Bjerg, P. L. (2012). Characterization of sand lenses embedded in tills. Quaternary Science Reviews, 53, 55-71.

Kirkham, J. D., Hogan, K. A., Larter, R. D., Arnold, N. S., Nitsche, F. O., Golledge, N. R., & Dowdeswell, J. A. (2019). Past water flow beneath pine Island and Thwaites glaciers, west Antarctica. The Cryosphere, 13(7), 1959-1981.

Kitson, A.E. (1902) On the occurrence of glacial beds at Wynyard, near Table Cape, Tasmania. Proceedings of the Royal Society of Victoria, XV(1), 28 -35.

Klages, J.P., Kuhn, G., Graham, A.G., Hillenbrand, C.D., Smith, J.A., Nitsche, F.O., Larter, R.D. and Gohl, K. (2015) Palaeo-ice stream pathways and retreat style in the easternmost Amundsen Sea Embayment, West Antarctica, revealed by combined multibeam bathymetric and seismic data. Geomorphology, 245, 207-222.

Kleman, J., & Glasser, N. F. (2007). The subglacial thermal organisation (STO) of ice sheets. Quaternary Science Reviews, 26(5-6), 585-597.

Kurjanski, B., Rea, B. R., Spagnolo, M., Cornwell, D. G., Howell, J., & Archer, S. (2020) A conceptual model for glacigenic reservoirs: from landsystems to reservoir architecture. Marine and Petroleum Geology, 115, 104205.

Kyle, R. A. (1977). Palynostratigraphy of the Victoria Group of South Victoria Land, Antarctica. New Zealand Journal of Geology and Geophysics, 20(6), 1081-1102.

Lewis, A. R., Marchant, D. R., Ashworth, A. C., Hemming, S. R., & Machlus, M. L. (2007). Major middle Miocene global climate change: Evidence from East Antarctica and the Transantarctic Mountains. Geological Society of America Bulletin, 119(11-12), 1449-1461.

Limarino, C.O. and López-Gamundí, O.R. (2021) Late Paleozoic basins of South America: Insights and progress in the last decade. Journal of South American Earth Sciences, 107, 103150. Available at: https://doi.org/10.1016/j.jsames.2020.103150

Lindström, S. (1996) Late Permian palynology of Fossilryggen, Vestfjella, Dronning Maud Land, Antarctica. Palynology, 20(1), 15-48.

Livingstone, S. J., Cofaigh, C. Ó., Stokes, C. R., Hillenbrand, C. D., Vieli, A., & Jamieson, S. S. (2012). Antarctic palaeo-ice streams. Earth-Science Reviews, 111(1-2), 90-128.

Lowe, D. R. (1982). Sediment gravity flows; II, Depositional models with special reference to the deposits of high-density turbidity currents. Journal of Sedimentary Research, 52(1), 279-297.

López-Gamundí, O., Sterren, A. F., and Cisterna, G. A. (2016) Inter-and intratill boulder pavements in the Carboniferous Hoyada Verde Formation of West Argentina: An insight on glacial advance/retreat fluctuations in Southwestern Gondwana. Palaeogeography, Palaeoclimatology, Palaeoecology, 447, 29-41.

Lønne, I., & Nemec, W. (2011). The kinematics of ancient tidewater ice margins: criteria for recognition from grounding-line moraines. Geological Society of London, Special Publications, 354(1), 57-75.

Ma, Y., Tripathy, C.S., and Bassis, J.N. (2017) Bounds on the calving cliff height of marine terminating glaciers. Geophysical Research Letters, 44, 1369–1375, doi:10.1002/2016GL071560.

MacGregor, J.A., Fahnestock, M.A., Catania, G.A., Aschwanden, A., Clow, G.D., Colgan, W.T., Gogineni, S.P., Morlighem, M., Nowicki, S.M., Paden, J.D. and Price, S.F. (2016) A synthesis of the basal thermal state of the Greenland Ice Sheet. Journal of Geophysical Research: Earth Surface, 121(7), 1328-1350.

Mackiewicz, N. E., Powell, R. D., Carlson, P. R., & Molnia, B. F. (1984). Interlaminated ice-proximal glacimarine sediments in Muir Inlet, Alaska. Marine Geology, 57(1-4), 113-147.

Mantle, D.J., Kelman, A.P., Nicoll, R.S., and Laurie, J.R. (2010) Australian Biozonation Chart. Geoscience Australia, Canberra. Available at: https://d28rz98at9flks.cloudfront.net/70371/Australian_Biozonation_Chart_2010_Part1.pdf.

Martin, J. R., Redfern, J., Horstwood, M. S., Mory, A. J., & Williams, B. P. J. (2019). Detrital zircon age and provenance constraints on late Paleozoic ice-sheet growth and dynamics in Western and Central Australia. Australian Journal of Earth Sciences, 66(2), 183-207.

Masood, K. R., Taylor, T. N., Horner, T., & Taylor, E. L. (1994). Palynology of the Mackellar Formation (Beacon Supergroup) of East Antarctica. Review of Palaeobotany and Palynology, 83(4), 329-337.

McKay, R., Browne, G., Carter, L., Cowan, E., Dunbar, G., Krissek, L., Naish, T., Powell, R., Reed, J., Talarico, F., & Wilch, T. (2009). The stratigraphic signature of the late Cenozoic Antarctic Ice Sheets in the Ross Embayment. Geological Society of America Bulletin, 121(11-12), 1537-1561.

Meredith, A., Williams, S. E., Collins, A. S., Tetley, M. G., Mulder, J. A., Blades, M. L., Young, A., Armistead, S., Cannon, J., Zahirovic, S., and Müller, R. D. (2021) Extending Whole-Plate Tectonic Models into Deep Time: Linking the Neoproterozoic and the Phanerozoic. Earth Science Reviews, 103477. Gplates dataset available as "EarthByte Alternative Plate Reconstructions" at: https://www.earthbyte.org/gplates-2-3-software-and-data-sets/

Mineral Resources Tasmanian (2020, 9 September) 1:25,000 Scale Digital Geology of Tasmania. Digital Data, Mineral Resources Tasmania. Accessed October 2021. https://www.mrt.tas.gov.au/products/digital_data/125,000_geology_data_download

Montañez, I. P., & Poulsen, C. J. (2013). The Late Paleozoic ice age: an evolving paradigm. Annual Review of Earth and Planetary Sciences, 41, 629-656.

Mory, A. J., & Hocking, R. M. (2011). Permian, Carboniferous and Upper Devonian geology of the northern Canning Basin, Western Australia. À a field guide. Geology Survey of Western Australia, Department of Mines and Petroleum, Government of Western Australia, Record, 16.

Mulder, T., & Alexander, J. (2001). The physical character of subaqueous sedimentary density flows and their deposits. Sedimentology, 48(2), 269-299.

Müller, R.D., Cannon, J., Qin, X., Watson, R.J., Gurnis, M., Williams, S., Pfaffelmoser, T., Seton, M., Russell, S.H. and Zahirovic, S., (2018) GPlates: building a virtual Earth through deep time. Geochemistry, Geophysics, Geosystems, 19(7), 2243-2261. doi:10.1029/2018GC007584.

Nemec, W., Lønne, I., & Blikra, L. H. (1999). The Kregnes moraine in Gauldalen, west-central Norway: anatomy of a Younger Dryas proglacial delta in a palaeofjord basin. Boreas, 28(4), 454-476.

Nicoll, R.S., McKellar, J., Ayaz, S.A., Laurie, J.R., Esterle, J., Crowley, J., Woods, G., and Bodorkos, S. (2015) CA-IDTIMS Dating of Tuffs: Calibration of Palynostratigraphy and Stratigraphy of the Bowen and Galilee Basins: Extended Abstract, 7th Bowen Basin Symposium, Brisbane, Queensland.

Normington, V.J. (2017) Characterisation of late Palaeozoic glacigene sedimentary rocks of the Troubridge and Arckaringa basins and implications for palaeogeographic reconstructions of late Palaeozoic South Australia, Ph.D. Dissertation, University of Adelaide. Available at: https://hdl.handle.net/2440/130383

Ó Cofaigh, C., & Dowdeswell, J. A. (2001). Laminated sediments in glacimarine environments: diagnostic criteria for their interpretation. Quaternary Science Reviews, 20(13), 1411-1436.

Ó Cofaigh, C., Davies, B.J., Livingstone, S.J., Smith, J.A., Johnson, J.S., Hocking, E.P., Hodgson, D.A., Anderson, J.B., Bentley, M.J., Canals, M. and Domack, E. (2014) Reconstruction of ice-sheet changes in the Antarctic Peninsula since the Last Glacial Maximum. Quaternary Science Reviews, 100, 87-110.

Owen, G. (2003). 'Load structures: gravity-driven sediment mobilization in the shallow subsurface' in Van Rensbergen, P., Hillis, R.R., Maltman, A.J., Morley, C.K. (eds.) Subsurface Sediment Mobilization, Geological Society, London, Special Publication 216, 21 – 34.

Pauls, K.N., Isbell, J.L., Limarino, C.O., Alonso-Murauga, P.J., Malone, D.H., Schencman, L.J., Colombi, C.E. and Moxness, L.D. (2021). Constraining late paleozoic ice extent in the Paganzo basin of western Argentina: Provenance of the lower Paganzo group strata. Journal of South American Earth Sciences, 106, p.102899.

Peters, S. E., & Loss, D. P. (2012). Storm and fair-weather wave base: A relevant distinction? Geology, 40(6), 511-514.

Powell, R.D. and Cowan, E.A. (1986) 'Depositional processes at McBride Inlet and Riggs glacier'. in Anderson, P.G., Goldthwait, R.P., McKenzie, G.D. (eds.), Observed processes of glacial deposition in Glacier Bay, Alaska, Ohio State University, Institute of Polar Studies, Miscellaneous Publications, 256, pp. 140–156.

Powell, R. D. and Molnia, B. F. (1989). Glacimarine sedimentary processes, facies and morphology of the south-southeast Alaska shelf and fjords. Marine Geology, 85(2-4), 359-390.

Powell, R.D. (1990) Glacimarine processes at grounding-line fans and their growth to ice-contact deltas, Geological Society of London, Special Publications, 53(1), 53-73.

Powell, R., Krissek, L. A., & Van der Meer, J. (2000). Preliminary depositional environmental analysis of CRP-2/2A, Victoria Land Basin, Antarctica: palaeoglaciological and palaeoclimatic inferences. Terra Antartica, 7(3), 313-322.

Powell, R. D., & Cooper, J. M. (2002). A glacial sequence stratigraphic model for temperate, glaciated continental shelves. Geological Society, London, Special Publications, 203(1), 215-244.

Price, P.L. (1997) 'Permian to Jurassic Palynostratigraphic Nomenclature of the Bowen and Surat Basins', in P.M. Green (ed.) The Stuart and Bowen Basins, Southeast Queensland: Queensland Department of Mines and Energy, 137-178.

Prothro, L. O., Simkins, L. M., Majewski, W., & Anderson, J. B. (2018). Glacial retreat patterns and processes determined from integrated sedimentology and geomorphology records. Marine Geology, 395, 104-119.

Raymond, O.L., Liu, S., Gallagher, R., Zhang, W., Highet, L.M. (2012) Surface Geology of Australia 1:1 million scale dataset 2012 edition. Geoscience Australia, Canberra. Available at: http://pid.geoscience.gov.au/dataset/ga/74619

Reid, C.M., Forsyth, S.M., Clarke, M.J. and Bacon, C. (2014) 'The Parmeener Supergroup – late Carboniferous to Triassic' in Corbett, K.D., Quilty, K.D., and Calver, C.R. (eds.) Geological Evolution of Tasmania, 1st, Geological Society of Australia Special Publication 24, Geological Society of Australia (Tasmania Division), 363-384.

Robinson, D. E., Menzies, J., Wellner, J. S., & Clark, R. W. (2021). Subglacial sediment deformation in the Ross Sea, Antarctica. Quaternary Science Advances, 100029.

Rodrigues, M. C. N. d.L., Trzaskos, B., Alsop, G. I., & Vesely, F. F. (2020). Making a homogenite: An outcrop perspective into the evolution of deformation within mass-transport deposits. Marine and Petroleum Geology, 112, 104033.

Rosa, E.L.M and Isbell, J.L. (2021) 'Late Paleozoic Glaciation' in Alderton, D. and Elias, S.A. (eds) Encyclopedia of Geology, 2nd, Elsevier, 534-545

Rosenblume, J. A., & Powell, R. D. (2019). Glacial sequence stratigraphy of ANDRILL-1B core reveals a dynamic subpolar Antarctic Ice Sheet in Ross Sea during the late Miocene. Sedimentology, 66(6), 2072-2097.

Ruszczyńska-Szenajch, H. (1987) The origin of glacial rafts: detachment, transport, deposition. Boreas, 16(2), 101-112.

Rygel, M. C., Fielding, C. R., Frank, T. D., & Birgenheier, L. P. (2008). The magnitude of Late Paleozoic glacioeustatic fluctuations: a synthesis. Journal of Sedimentary Research, 78(8), 500-511.

Shackleton, C. S., Winsborrow, M. C., Andreassen, K., Lucchi, R. G., & Bjarnadóttir, L. R. (2020). Ice-margin retreat and grounding-zone dynamics during initial deglaciation of the Storfjordrenna Ice Stream, western Barents Sea. Boreas, 49(1), 38-51.

Simkins, L.M., Anderson, J.B., Greenwood, S.L., Gonnermann, H.M., Prothro, L.O., Halberstadt, A.R.W., Stearns, L.A., Pollard, D. and DeConto, R.M. (2017) Anatomy of a meltwater drainage system beneath the ancestral East Antarctic ice sheet. Nature Geoscience, 10(9), 691-697.

Simkins, L. M., Greenwood, S. L., & Anderson, J. B. (2018). Diagnosing ice sheet grounding line stability from landform morphology. The Cryosphere, 12(8), 2707-2726.

Smith, A. M., Jordan, T. A., Ferraccioli, F., & Bingham, R. G. (2013). Influence of subglacial conditions on ice stream dynamics: Seismic and potential field data from Pine Island Glacier, West Antarctica. Journal of Geophysical Research: Solid Earth, 118(4), 1471-1482.

Smith, T.W., Bernecker, T., Bodorkos, S., Gorter, J., Hall, L.S., Hill, T., Holmes, E., Kelman, A., Khider, K., Laurie, J., Lech, M., McKellar, J., Mory, A., Nicoll, R., Owens, R., Palu, T.J., Phillips, L., Stephenson, M., Wood, G. (2017) The impact of recalibrating palynological zones to the chronometric timescale: revised stratigraphic relationships in Australian and Triassic hydrocarbon-bearing basins. Poster Given at AAPG/SEG 2017 International Conference and Exhibition, London, England, October 15–18, 2017. Available at: https://www.searchanddiscovery.com/pdfz/documents/2017/51443smith/ndx_smith.pdf.html

Smith, J. A., Graham, A. G., Post, A. L., Hillenbrand, C. D., Bart, P. J., & Powell, R. D. (2019). The marine geological imprint of Antarctic ice shelves. Nature Communications, 10(1), 1-16.

Sobiesiak, M. S., Kneller, B., Alsop, G. I., & Milana, J. P. (2016). Internal deformation and kinematic indicators within a tripartite mass transport deposit, NW Argentina. Sedimentary Geology, 344, 364-381.

Sohn, Y. K. (1997). On traction-carpet sedimentation. Journal of Sedimentary Research, 67(3), 502-509.

Sohn, Y. K., Choe, M. Y., & Jo, H. R. (2002). Transition from debris flow to hyperconcentrated flow in a submarine channel (the Cretaceous Cerro Toro Formation, southern Chile). Terra Nova, 14(5), 405-415.

Soreghan, G. S., Soreghan, M. J., & Heavens, N. G. (2019). Explosive volcanism as a key driver of the late Paleozoic ice age. Geology, 47(7), 600-604.

Stephens, T. (1869) Remarks on the geological structures of part of the north west coast of Tasmania with special reference to the Tertiary marine beds near Table Cape. Proceedings of the Royal Society of Tasmania, 1868 – 1871, 5, 17-21.

Stewart, T. G. (1991). Glacial marine sedimentation from tidewater glaciers in the Canadian High Arctic. Glacial Marine Sedimentation, 95.

Talling, P. J., Masson, D. G., Sumner, E. J., & Malgesini, G. (2012). Subaqueous sediment density flows: Depositional processes and deposit types. Sedimentology, 59(7), 1937-2003.

Tinto, K. J., Bell, R. E., Cochran, J. R., & Münchow, A. (2015). Bathymetry in Petermann fjord from Operation IceBridge aerogravity. Earth and Planetary Science Letters, 422, 58-66.

Todd, S. P. (1989). Stream-driven, high-density gravelly traction carpets: possible deposits in the Trabeg Conglomerate Formation, SW Ireland and some theoretical considerations of their origin. Sedimentology, 36(4), 513-530.

Truswell, E.M. (1978) Palynology of the Permo-Carboniferous in Tasmania: and interim report. Bulletin of the Geological Survey of Tasmania, 56, 1-39.

Tulaczyk, S., Kamb, B., Scherer, R. P., & Engelhardt, H. F. (1998). Sedimentary processes at the base of a West Antarctic ice stream; constraints from textural and compositional properties of subglacial debris. Journal of Sedimentary Research, 68(3), 487-496.

Twelvetrees, W. H. (1905) Report on the north-west coast mineral deposits. Secretary for Mines Report, Tasmania, 9-59.

Veevers, J. J. (2006). Updated Gondwana (Permian–Cretaceous) earth history of Australia. Gondwana Research, 9(3), 231-260.

Warren, C. R., & Glasser, N. F. (1992). Contrasting response of South Greenland glaciers to recent climatic change. Arctic and Alpine Research, 24(2), 124-132.

Webb, J. A. and Spence, E. (2008). Glaciomarine Early Permian strata at Bacchus Marsh, central Victoria—the final phase of Late Palaeozoic glaciation in southern Australia. Proceedings of the Royal Society of Victoria, 120, 373-388.

Williams, P.R. and Lennox, P.G. (1989) 'Wynyard Tillite Correlate' in Seymour, D.B. (ed.) Geological atlas 1:50000 series. Sheet 36 (8015N). St Valentines, Explanatory Report of the Geological Survey, Tasmania Department of Mines, 27-29. Available at: https://www.mrt.tas.gov.au/mrtdoc/dominfo/download/ER8015S0/ER8015S.pdf

Winsemann, J., Asprion, U., Meyer, T., & Schramm, C. (2007). Facies characteristics of Middle Pleistocene (Saalian) ice-margin subaqueous fan and delta deposits, glacial Lake Leine, NW Germany. Sedimentary Geology, 193(1-4), 105-129.

Yu, H., Rignot, E., Seroussi, H., Morlighem, M., & Choi, Y. (2019). Impact of iceberg calving on the retreat of Thwaites Glacier, West Antarctica over the next century with different calving laws and ocean thermal forcing. Geophysical Research Letters, 46(24), 14539-14547.

Zellers, S. D. (1995). Foraminiferal sequence biostratigraphy and seismic stratigraphy of a tectonically active margin; the Yakataga Formation, northeastern Gulf of Alaska. Marine Micropaleontology, 26(1-4), 255-271.

Zieliński, T., & Van Loon, A. J. (1996). Characteristics and genesis of moraine-derived flowtill varieties. Sedimentary Geology, 101(1-2), 119-143.

Zurli, L., Cornamusini, G., Woo, J., Liberato, G. P., Han, S., Kim, Y., & Talarico, F. M. (2021). Detrital zircons from Late Paleozoic Ice Age sequences in Victoria Land (Antarctica): New constraints on the glaciation of southern Gondwana. GSA Bulletin. Available at: https://doi.org/10.1130/B35905.1

CHAPTER 4.
GLACIGENIC SEDIMENT PROVENANCE SHOULD BE DETERMINED THROUGH A "LOCAL FIRST" APPROACH

Submitted to *Nature Geoscience* by Ives, L.W.R., Isbell, J.L, and Licht, K.J.

Abstract

We propose that a "local first" approach should be applied to the interpretation of provenance indicators in glacigenic sediments, especially where the glacier flow path is poorly constrained and the records of potential source lithologies are incomplete. Provenance proxies, specifically U-Pb detrital zircon geochronology, of glacigenic sediments are commonly used to infer the size and distribution of past ice centers, which are in turn used to inform ancient climate reconstructions. Interpretations of these proxies often assume that similar provenance signals between glacigenic units of the same depositional age are evidence that they were deposited by the same glacier, even when those units are separated by sometimes thousands of kilometers of distance. This assumption is not appropriate for large ice masses as it does not acknowledge the fact that provenance proxies in glacial sediments are most likely to reflect proximal (within 100 km) sediment sources located along a specific flow path. In a "local first" approach, provenance indicators are first compared to local source lithologies. If the indicator cannot be attributed to proximal sources, only then should progressively distal sources be investigated. Applying a local first approach to sediment provenance in ancient glacial systems may result in significant revisions to paleo ice sheet reconstructions. The effectiveness of the local first approach is demonstrated here by comparing new U-Pb detrital zircon dates from the Permo-Carboniferous glacigenic Wynyard Fm with progressively distal source lithologies along the glacier's inferred flow path. The Wynyard Fm and source lithologies were compared using an inverse Monte-Carlo unmixing model (DZMix). All measured Wynyard Fm dates can be attributed to zircon sources within 33 km of the sample location along the glacier's flow path.

Introduction

Constraining the provenance of glacigenic sediments from ancient ice ages is a key tool in determining the size and distribution of ancient ice centers (e.g., [1,2]). The inferred characteristics of these ice centers are lynchpins in understanding ancient climates [3]. Recent publications have attempted to reconstruct Paleozoic ice sheet distributions using detrital zircon (DZ) U-Pb geochronology, including some studies that inferred continent-scale glacial sediment transport systems during the Paleozoic (e.g., [2,4]). These works assume that similar DZ provenance signals between geographically dispersed glacigenic sediments of equivalent depositional age are evidence that they were deposited by the same large mass (i.e., large glaciers such as ice sheets, and ice caps).

This assumption is not physically reasonable for glacial transport systems for largely two reasons. First, large ice masses generally radiate out from one or more central domes, thus flow is not uni-directional. Accordingly, glaciers cannot carry sediment from one edge of an ice sheet to another, as has been proposed in some models of LPIA provenance (e.g., [4]). Radially divergent flow patterns cross many potential combinations of source rocks within the footprint of a large ice mass, and sediments deposited in different parts of the same ice mass may not have similar provenance signals [5]. Second, the unique ways in which glaciers entrain, transport, and deposit sediments differ significantly from other sedimentary transport systems, such as continent-scale fluvial drainages (e.g., [6]). Glacial processes are more likely to create and deposit sediments dominated by proximal sources than sources thousands of kilometers up-glacier. Though the potential exists for glacially-transported sediments to be carried great distances, the relative abundance of a subglacially entrained sediment decreases exponentially down-glacier from its source and is most likely to be detectable within 100 km of a point-source [7-10].

We propose that a "local" null hypothesis is the most appropriate way to approach future interpretations of provenance indicators in glacigenic sediments, including DZ. Such an approach is especially useful in the ancient (pre-Pleistocene) record where glacier flow paths are poorly constrained, and hundreds of millions of years of deposition and erosion of intermediary sedimentary units means the rock record is incomplete. In this approach, provenance indicators should first be compared to potential bedrock and contemporaneously unlithified sediment sources along the glacier's proposed flow path (if known) adjacent to the target sample's location. If the provenance indicator cannot be attributed to sources within these spatial constraints, then progressively more distal sources may be considered. DZ is a good provenance indicator to use as a case study of this "local first" approach because DZ dates can more easily be attributed to specific sources than other geochemical or petrographic provenance indicators.

In this paper, we demonstrate the effectiveness of a local first approach by testing whether the DZ populations in sandstone samples collected from a Permo-Carboniferous glaciomarine succession in Tasmania (Wynyard Fm) could have been derived from local lithologies along the glacier's inferred flow path. Newly measured DZ dates from the Wynyard Fm (N = 2, n = 592) were compared to DZ dates from pre-Permian western Tasmanian lithologies (N = 59, n = 2015) using an inverse Monte Carlo unmixing model (DZMix [11]).

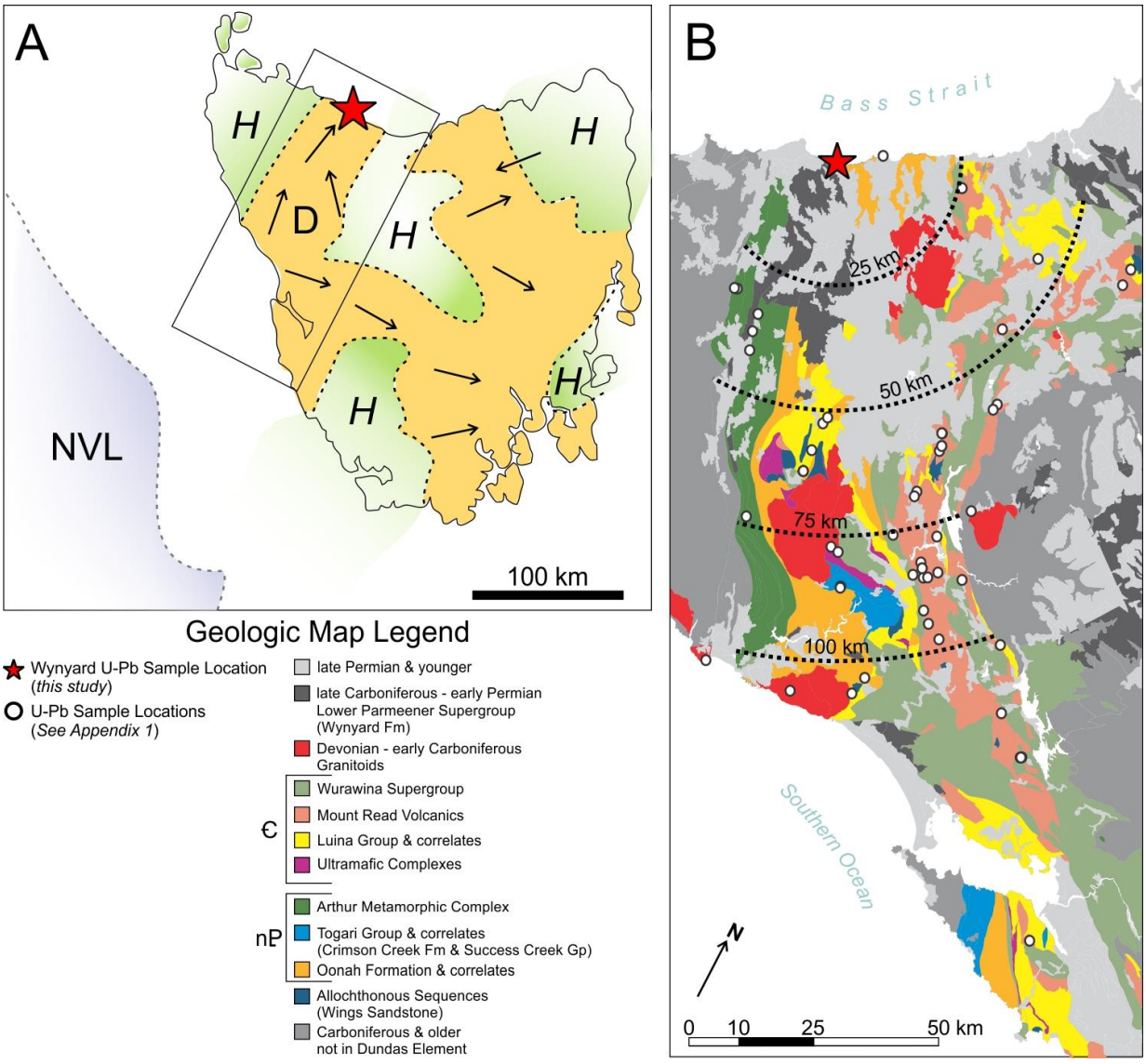

Figure 4-1. Geologic and paleogeographic context for the Wynyard Fm, Tasmania. The red star on all maps shows the location of the Wynyard Fm samples. A. Paleogeographic map of Tasmania during the deposition of the Wynyard Fm and correlates. Orange areas indicate the modern limits of the Wynyard Fm and correlates (both at the surface and in the subsurface) and are proposed paleotopographic lows. "D" notes the Dundas Trough. Areas labeled as "H" are paleotopographic highs. Arrows indicate ice paleoflow directions. The black box shows the extent of map 1B. The shaded area labeled NVL shows the approximate position of North Victoria Land during this time. Map after Hand [13], Henry, et al. [16], Elliot [31], and Reid [14]. B. Geologic map of pre-Permian units in the Dundas Trough [32]. Dashed lines show distances from the Wynyard Fm site.

Geologic Context

The Wynyard Fm and its correlates across Tasmania make up the basal strata of the Parmeener Supergroup in the Tasmanian Basin [12]. These successions are mostly confined to structural and paleotopographic lows within the Tasmanian Basin [13,14]. The Wynyard Fm crops out at the northern edge of one of these lows known as the Dundas Trough (Fig. 4- 1A). The Dundas Trough extends across mainland Tasmania's western side from its southern to northern coasts, and paleo flow directions associated with the Wynyard Fm indicate that the glacier flowed north through it (Fig. 4- 1A).

The Wynyard Fm is an appropriate example with which to test the local first approach primarily because the sediments were deposited in an ice-proximal setting by an ice mass that was actively eroding and transporting sediment subglacially [15,16]. The samples used in this study were deposited as part of sandy, sub-aqueous grounding-line fan systems (Fig. 4- 2). These sediments would have been sourced directly from subglacial materials and deposited in a proglacial environment near the ice margin. This depositional environment ensures that the zircons tested in this study were transported subglacially (by the ice and/or subglacial drainage systems) directly before deposition. Additionally, the paleo flow path of the Wynyard glacier is relatively well constrained and there are many "high-n" DZ data for source rocks along its proposed flow path.

The provenance of the Wynyard Fm is not well characterized and identifying the source of these sediments would help clarify the distribution and size of ice centers during the LPIA. Based on flow directions, the Wynyard Fm is proposed to have been deposited by an ice mass centered in North Victoria Land (NVL), Antarctica [17]. In contrast, prior provenance work has demonstrated that most Wynyard Fm clast lithologies are attributable to pre-Permian source rocks in western Tasmania [13,18].

The DZ dates of Permian glacigenic rocks in NVL do not have the same provenance as the Wynyard Fm [19] (Supplementary Figure 1).

Wynyard Fm zircon U-Pb measurements

Two moderately well-sorted, fine- to medium-grained sandstone samples were collected from the lower Wynyard Formation (n = 2, N = 592; Fig. 4- 2A). The samples were collected 75 m and 145 m above the Wynyard Fm's basal unconformity. Sample preparation was performed by staff at the Arizona LaserChron Center [20,21].

The Wynyard Fm zircon dates range from 319 Ma to 3075 Ma (Fig. 4- 3). The analyses from both samples were combined for this study because they have similar date populations that are not significantly different from one another when measurement uncertainties are accounted for (Supplementary Figure 2).

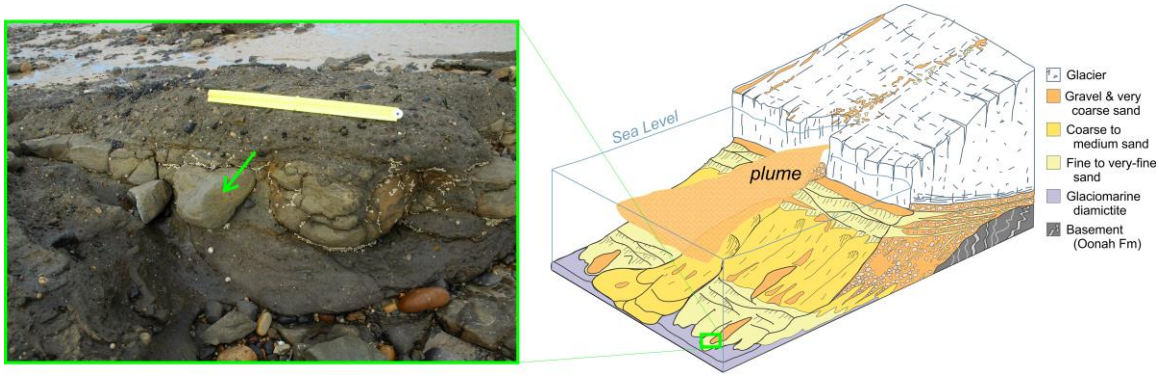

Figure 4-2. A. Photograph of a fine-grained sandstone in Wynyard Fm , similar to the samples used for detrital zircon analysis in this study, indicated by the green arrow. The ruler in the photo is 0.5 m long. **B.** Diagram showing the proposed ice-contact depositional setting of the Wynyard Fm. The green box indicates the approximate depositional setting of the sand body in A. Figure digitized from Lønne [33].

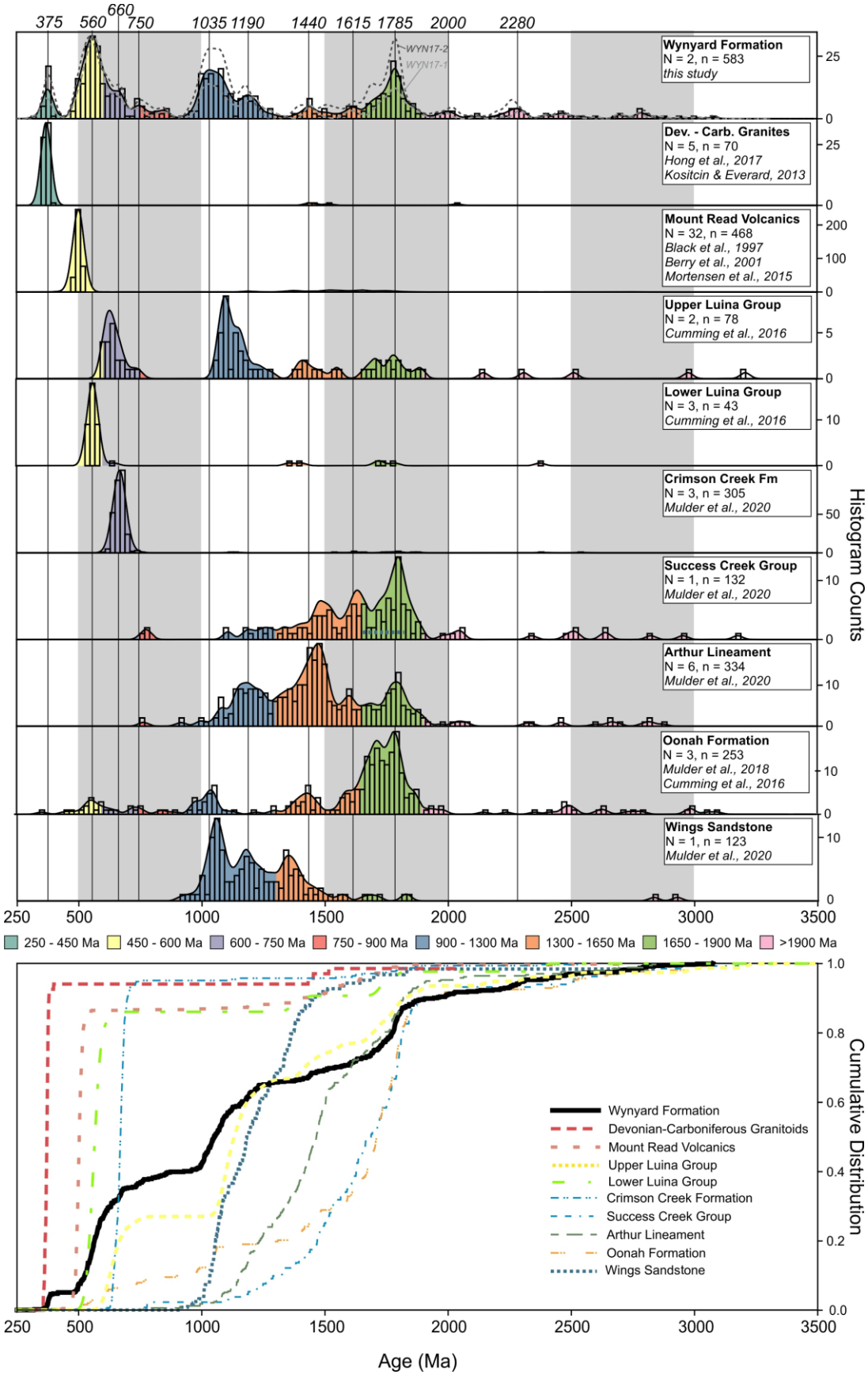
375
560
660
750
1035
1190
1440
1615
1785
2000
2280
WYN17-2
WYN17-1
Wynyard Formation
N = 2, n = 583
this study
Dev. - Carb. Granites
N = 5, n = 70
Hong et al., 2017
Kositcin & Everard, 2013
Mount Read Volcanics
N = 32, n = 468
Black et al., 1997
Berry et al., 2001
Mortensen et al., 2015
Upper Luina Group
N = 2, n = 78
Cumming et al., 2016
Lower Luina Group
N = 3, n = 43
Cumming et al., 2016
Crimson Creek Fm
N = 3, n = 305
Mulder et al., 2020
Success Creek Group
N = 1, n = 132
Mulder et al., 2020
Arthur Lineament
N = 6, n = 334
Mulder et al., 2020
Oonah Formation
N = 3, n = 253
Mulder et al., 2018
Cumming et al., 2016
Wings Sandstone
N = 1, n = 123
Mulder et al., 2020
Histogram Counts
250 - 450 Ma
450 - 600 Ma
600 - 750 Ma
750 - 900 Ma
900 - 1300 Ma
1300 - 1650 Ma
1650 - 1900 Ma
>1900 Ma
Cumulative Distribution
Wynyard Formation
Devonian-Carboniferous Granitoids
Mount Read Volcanics
Upper Luina Group
Lower Luina Group
Crimson Creek Formation
Success Creek Group
Arthur Lineament
Oonah Formation
Wings Sandstone
Age (Ma)

Figure 4-3. Relative and cumulative distributions of detrital zircon U-Pb dates for the Wynyard Fm and Dundas source lithologies used in this study. Relative distribution plots show Kernel Density Estimates (KDE) and histograms for each lithology. KDEs were calculated with a fixed 20 Ma bandwidth and plots normalized to the height of each graph, and histograms plotted with a 20 Ma bin sizes. The scale for each histogram is shown on the right-hand y-axis of each graph. Fill colors indicate distinct age ranges that represent natural groupings of Wynyard Fm detrital zircon ages. Vertical lines through the graphs highlight Wynyard Fm KDE peaks, ages of which are noted at the top of the graph. The lower plot shows the cumulative distribution function (CDF) for each lithology. Made using detritalPy v. 1.3.18 [34].

Unmixing model

The relative proportion of Dunas Trough source lithologies contributing to the Wynyard Fm DZ were modeled using an inverse Monte Carlo approach (DZMix) [11]. This approach used our new data from the Wynyard and detrital zircon U-Pb dates for potential source lithologies in the Dundas Trough that were collected from the literature (Fig. 4- 3; Supplementary Data 1; Table 4-1). Preference was given to recently measured, high n datasets.

The unmixing model was applied to DZ ages between 400 Ma and 2000 Ma. The older ages were excluded because they make up a very minor component of both the Wynyard Fm and source lithologies and were likely not consistently measured in source datasets with $n < 300$ [22]. Younger ages were excluded because the only source for those dates is Devonian - Carboniferous granites [23,24] whose presence can be inferred without the use of a model (Fig. 4- 3). The model ran 10,000 iterations where the date distribution of each potential source rock was randomly weighted so that the weights were summed to 100%. The weighted distributions were summed together. The resulting, mixed DZ date distributions were then compared to the Wynyard Fm using three methods:

1. two-sample K-S test D statistic (compares cumulative distribution functions, CDFs),
2. two-sample Kuiper test V statistic (compares CDFs), and
3. the cross-correlation coefficient (R^2, compares kernel density estimates, KDEs).

The 100 best-fit models (top 1%) from each comparison method were retained and are reported in Fig. 4- 4.

Five versions of the model were run, comparing the Wynyard Fm DZ dates with source lithologies that occur within 25 km, 35 km, 50 km, 75 km, and 100 km of the Wynyard Fm site (Fig. 4- 1; Fig. 4- 4). Sources within 25 km include the Arthur Metamorphic Complex[25] and Oonah Fm[26,27]. The 35 km added the Upper and Lower Luina Gp[27], the 50 km model added the Mount Read Volcanics[28-30], the 75 km model added the Wings Sandstone[25], and the 100 km model added the Crimson Creek Fm[25] and Success Creek Gp[25].

Zircon population comparisons

The DZMix models were able to account for all DZ dates in the Wynyard Fm using source lithologies within 35 km, 50 km, 75 km, and 100 km of the Wynyard Fm site (Fig. 4- 1B; Fig. 4- 4). The 25 km model was not able to account for all Wynyard Fm DZ dates (Fig. 4- 1B). All four of the successful DZMix model runs have overlapping mean fit parameter values (V, D, and R2), indicating that none of these model runs are a better fit than the others (Fig. 4- 4D). The successful DZMix models all identified the Luina Group as the principal source for the Wynyard Fm DZ (Fig. 4- 4), whereas the unsuccessful model (25 km) does not.

None of the models produced a perfect fit for the Wynyard Fm. This is likely because the relative abundance of DZ dates in the combined source populations used for this study (Fig. 4- 3) does not reflect the natural variability of these populations throughout the Dundas Trough.

Model results indicate that the Upper and Lower Luina Gp are the primary sources for DZs in the Wynyard Fm, and that other Dundas Trough sources are needed to account for DZ dates not in the Luina Gp (Fig. 4- 4A-C). Presently, the closest occurrence of the Luina Gp to the Wynyard Fm sample location along a paleo flowpath is ~33 km (Fig. 4- 1). Therefore, the model results indicate

that all of the sampled Wynyard Fm DZs could have been sourced from Dundas Trough within ~33 km of the Wynyard Fm depositional site.

Towards a "local first" approach

The mechanics of glacier erosion and transport make it more likely that glacigenic sediments, on average, are derived from proximal (tens of kilometers) rather than distal (> 100 km) bedrock sources. These mechanisms should be considered in the characterization of glacigenic sediment provenance. Where constraints on glacier size and flow paths are limited, like in ancient glacial systems, a conservative approach to provenance should be taken where local lithologies are considered as potential sources before distal sources. This approach can also be used to identify non-local DZ sources through a process of elimination. If provenance indicators cannot be attributed to proximal sources, then progressively more distal sources should be considered.

A local first approach may be challenging in regions where DZ data for potential sources are often not available. This study was possible in Tasmania because of the abundance of high-quality, high-n DZ measurements from many of the potential source lithologies and the detailed study of the Permo-Carboniferous glaciation in Tasmania. Even so, the analyses in this study are limited by the lack of high-n datasets from several likely zircon-rich Dundas Trough lithologies, such as the Wurawina Supergroup (Fig. 4- 1).

Despite the challenges, approaching glacigenic sediment provenance in this way has the potential to deepen our understanding of ancient icehouse intervals like the Permo-Carboniferous. The rich literature on sediment transport and provenance in Holocene and late Pleistocene glacial systems makes it clear that considering local sources before distal sources is the prudent approach. As we begin to understand the extent to which glaciations in the distant past were asynchronous and

dynamic, this more nuanced basis for interpreting sedimentary provenance, and particularly DZ geochronology, should help in teasing out their complex histories.

Figure 4-4. Results from the DZMix models. The CDF and KDE graphs show the 100 best-fit results of the: A. K-S test *D* statistic comparison, B. Kuiper test *V* statistic comparison, and C. K-S test *D* statistic comparisons. The relative contribution plots show the predicted percent contribution of each source lithology based on the results from the 35 km, 50 km, 75 km, and 100 km models. D. The mean fit parameter values for each model vs. distance from the Wynyard Fm sample site. Values towards the top of the plot indicate a better model fit.

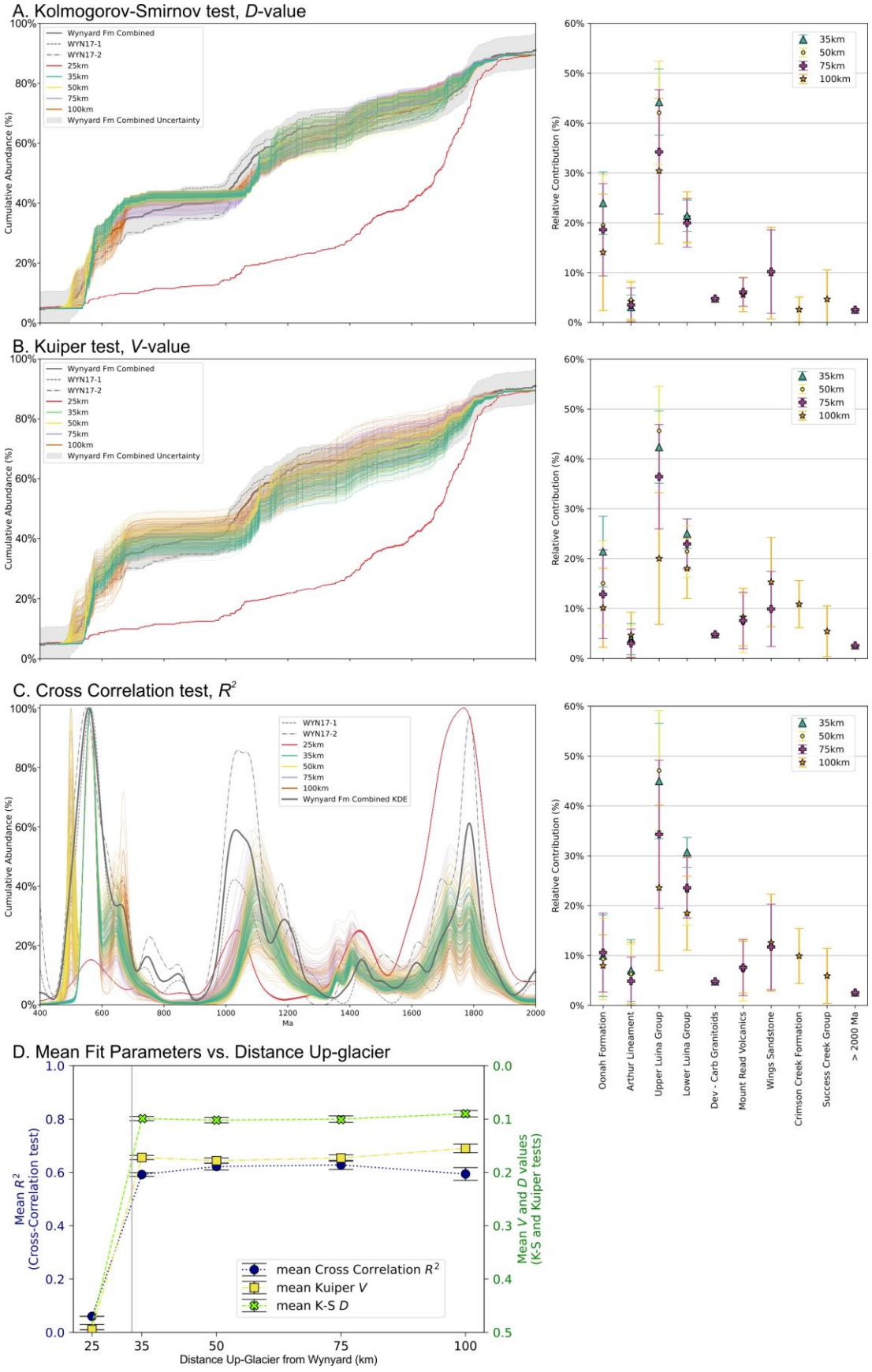
A. Kolmogorov-Smirnov test, D-value
B. Kuiper test, V-value
C. Cross Correlation test, R²
D. Mean Fit Parameters vs. Distance Up-glacier
Cumulative Abundance (%)
Relative Contribution (%)
Wynyard Fm Combined
WYN17-1
WYN17-2
25km
35km
50km
75km
100km
Wynyard Fm Combined Uncertainty
Wynyard Fm Combined KDE
Ma
Oonah Formation
Arthur Lineament
Upper Luina Group
Lower Luina Group
Dev - Carb Granitoids
Mount Read Volcanics
Wings Sandstone
Crimson Creek Formation
Success Creek Group
> 2000 Ma
Mean R² (Cross-Correlation test)
Mean V and D values (K-S and Kuiper tests)
mean Cross Correlation R²
mean Kuiper V
mean K-S D
Distance Up-Glacier from Wynyard (km)

Main References

1 Martin, J. R. R., J.; Horstwood, M.S.A.; Mory, A.J.; Williams, B.P.J. Detrital zircon age and provenance constraints on late Paleozoic ice-sheet growth and dynamics in Western and Central Australia. *Australian Journal of Earth Sciences*, doi:DOI: 10.1080/08120099.2019.1531925 (2019).

2 Griffis, N. P. *et al.* Isotopes to ice: Constraining provenance of glacial deposits and ice centersin west-central Gondwana. *Palaeogeography, Palaeoclimatology, Palaeoecology* **531**, 108745, doi:https://doi.org/10.1016/j.palaeo.2018.04.020 (2019).

3 Isbell, J. L. *et al.* Glacial paradoxes during the late Paleozoic ice age: Evaluating the equilibrium line altitude as a control on glaciation. *Gondwana Research* **22**, 1-19, doi:10.1016/j.gr.2011.11.005 (2012).

4 Craddock, J. P. *et al.* Detrital zircon provenance of Permo-Carboniferous glacial diamictites across Gondwana. *Earth Science Reviews* **192**, 285-316 (2019).

5 Licht, K. J. & Hemming, S. R. Analysis of Antarctic glacigenic sediment provenance through geochemical and petrologic applications. *Quaternary Science Reviews* **164**, 1-24 (2017).

6 Lawton, T. F., Blakey, R. C., Stockli, D. F. & Liu, L. Late Paleozoic (Late Mississippian–Middle Permian) sediment provenance and dispersal in western equatorial Pangea. *Palaeogeography, Palaeoclimatology, Palaeoecology* **572**, doi:https://doi.org/10.1016/j.palaeo.2021.110386 (2021).

7 Salonen, V. P. Glacial transport distance distributions of surface boulders in Finland. *Bulletin-Geological survey of Finland* **338** (1986).

8 Clark, P. U. Subglacial sediment dispersal and till composition. *The Journal of Geology* **95**, 527-541 (1987).

9 Larson, P. C. & Mooers, H. D. Glacial indicator dispersal process: a conceptual model. *Boreas* **33**, 238-249 (2008).

10 Hooke, R. L., Cummings, D. I., Lesemann, J.-E. & Sharpe, D. R. Genesis of dispersal plumes in till. *Canadian Journal of Earth Science* **50**, 847 - 855, doi:https://doi.org/10.1139/cjes-2013-0018 (2013).

11 Sundell, K. & Saylor, J. Unmixing detrital geochronology age distributions. *Geochemistry, Geophysics, Geosystems* **18**, 2872-2886 (2017).

12 Clarke, M. J. *et al.* in *Geology and mineral resources of Tasmania; Geological Society of Australia Special Publication* Vol. 15 (ed C F; Martin Burrett, E L) 293-338 (1989).

13 Hand, S. J. in *Gondwana Eight: Assembly, evolution and dispersal* (eds R. H. Findlay, R. Unrug, M. R. Banks, & J. J. Veevers) 459-469 (A.A. Balkema, 1993).

14 Reid, C. M. F., S.M.; Clarke, M.J.; Bacon, C. in *Geological Evolution of Tasmania Special Publications* (ed K.D.; Quilty Corbett, P.G.; Calver, C.R.; Davidson, G.) 363-384 (Geological Society of Australia, 2014).

15 Powell, R. D. in *Glacimarine Environments: processes and sediments* Vol. 53 (eds J. A. Dowdeswell & J. D. Scourse) 53-73 (Geological Society Special Publication, 1990).

16 Henry, L. C. *et al.* Proglacial deposition and deformation in the Upper Carboniferous to Lower Permian Wynyard Formation, Tasmania: A process analysis. *Palaeogeography, Palaeoclimatology, Palaeoecology* **315-316**, 142-157 (2012).

17 Veevers, J. J. Updated Gondwana (Permian–Cretaceous) earth history of Australia. *Gondwana Research* **9**, 231-260, doi:10.1016/j.gr.2005.11.005 (2006).

18 Banks, M. R. in *Earth's Pre-Pleistone Glacial Record.* (eds M.J. Hambrey & W.B. Harland) 495-501 (Cambridge University Press, 1981).

19 Zurli, L. *et al.* Detrital zircons from Late Paleozoic Ice Age sequences in Victoria Land (Antarctica): New constraints on the glaciation of southern Gondwana. *Geological Society of America Bulletin*, doi:https://doi.org/10.1130/B35905.1 (2021).

20 Gehrels, G. E., Valencia, V. A. & Ruiz, J. Enhanced precision, accuracy, efficiency, and spatial resolution of U-Pb ages by laser ablation-multicollector-inductively coupled plasma-mass spectrometry. *Geochem. Geophys. Geosys.*, 1-13 (2008).

21 Gehrels, G. E. & Pecha, M. Detrital zircon U-Pb geochronology and Hf isotope geochemistry of Paleozoic and Triassic passive margin strata of western North America. *Geosphere* **10**, 49-65 (2014).

22 Pullen, A., Ibañez-Mejia, M., Gehrel, G. E., Ibañez-Mejia, J. C. & Pecha, M. What happens when n = 1000? Creating large-ngeochronological datasets with LA-ICP-MS forgeologic investigations. *Journal of Analytical Atomic Spectrometry* **29**, 971-980 (2014).

23 Hong, W. *et al.* Geochronological, geochemical and Pb isotopic compositions ofTasmanian granites (southeast Australia): Controls on petrogenesis,geodynamic evolution and tin mineralisation. *Gondwana Research* **46**, 124-140, doi:https://doi.org/10.1016/j.gr.2017.03.009 (2017).

24 Kositcin, N. & Everard, J. L. New SHRIMP U–Pb zircon ages from Tasmania: July 2012-June 2013. (Geoscience Australia, Canberra, 2013).

25 Mulder, J. A. *et al.* Neoproterozoic opening of the Pacific Ocean recorded by multi-stage rifting in Tasmania, Australia. *Earth-Science Reviews* **201** (2020).

26 Mulder, J. A., Berry, R. F., Halpin, J. A., Meffre, S. & Everard, J. L. Depositional age and correlation of the Oonah Formation: refining the timing of Neoproterozoic basin formation in Tasmania. *Australian Journal of Earth Sciences* **65**, 391-407 (2018).

27 Cumming, G. V., Everard, J. L. & Meffre, S. Tasmanian Geological Survey Record UR2016/04Age constraints and provenance of the Mount Bischoff inlier and the Luina Group: evidence from LA-ICPMS U-Pb dating of detrital zircon (Mineral Resources Tasmania, 2016).

28 Black, L. P. *et al.* Dating Tasmania's Oldest Geological Events. *Australian Geological Survey Organisation Record* **15**, 57 (1997).

29 Berry, R. F., Jenner, G. A., Meffre, S. & Tubrett, M. N. A North American provenance for Neoproterozoic to Cambrian sandstones in Tasmania? *Earth and Planetary Science Letters* **192**, 207-222 (2001).

30 Mortensen, J. K., Gemmell, J. B., McNeill, A. W. & Friedman, R. M. High-Precision U-Pb Zircon Chronostratigraphy of the Mount Read Volcanic Belt in Western Tasmania, Australia: Implications for VHMS Deposit Formation. *Economic Geology* **110**, 445-468 (2015).

31 Elliot, D. H. in *Antarctic Palaeoenvironments and Earth-Surface Processes* (eds M. J. Hambrey *et al.*) 7-35 (Geological Society, London, Special Publications, 381, 2013).

32 Green, D. C. *et al.* (Mineral Resources Tasmania, 2012).

33 Lønne, I. Sedimentary facies and depositional architecture of ice-contact glaciomarine systems. *Sedimentary Geology* **98**, 13-43 (1995).

34 Sharman, G. R., Sharman, J. R. & Sylvester, Z. detritalPy: A Python-based toolset for visualizing and analysing detrital geo-thermochronologic data. *The Depositional Record* **4**, 202-215, doi:https://doi.org/10.1002/dep2.45 (2018).

Acknowledgments

This work was made possible with funding from the Geological Society of America's Graduate Student Research Grant program, P.E.O. Scholar Awards, University of Wisconsin – Milwaukee's RGI grants program, and National Science Foundation grants OISE-1559231 and OPP-1443557. Special thanks to Natural Resources Tasmania for their assistance with, and approval of, collection permits.

Methods

Wynyard Formation U-Pb measurement methods

Zircons derived from the Wynyard Fm ranged in size from 50 – 180 μm (silt – fine sand). Grain imaging was performed with a backscatter electron detector system using a Hitachi S3400 scanning electron microscope to ensure analysis of zircon and to avoid inclusions and fractures. Grains were selected for measurement with the intention of creating a dataset from representative grain sizes. Spots were selected using Chromium Offline Targeting. U–Pb isotopic analyses were conducted by LA-ICPMS using a Teledyne Photon Machines Analyte G2 laser connected to a Thermo Scientific Element 2 mass spectrometer. Analyses used a 20 μm diameter laser beam fired at 7 Hz for 10s. U–

Pb ages were calculated with E2agecalc[35]. For dates < 950 Ma, the $^{206}Pb/^{238}U$ ages were used and for dates > 950 Ma the $^{206}Pb/^{207}Pb$ ages were used. A relative discordance filter was applied to dates > 700 Ma. Concordance values are calculated as $\left(\frac{^{206}Pb/^{238}U}{^{206}Pb/^{207}Pb}\right) * 100$. For filtered dates, any analyses that were > 20% discordant or > 5% reverse discordant were not considered. Results are shown in Appendix B.

Supplementary Discussion 1: Comparing Wynyard Fm to Antarctic Equivalents

The Permian glacigenic Lanterman Fm in North Victoria Land, Antarctica and the Wynyard Fm likely do not share detrital zircon (DZ) provenance sources (Supplementary Figure 1).

The DZ dates < 1500 Ma for both datasets are similar, but none of the peak ages overlap. This is reasonable, considering that both West Tasmania and North Victoria Land experienced similar geologic histories along the Panthalassan margin of east Gondwana during those times. The igneous and volcanic rocks related to the Ross-Delamerian Orogeny (~ 625 – 480 Ma; [36,37]) are common in both the Wynyard Fm and Lanterman Fm DZ date populations. Both populations also have significant populations with dates between ~ 1300 – 900. These populations are common in Proterozoic and early Paleozoic sedimentary rocks in both North Victoria Land and West Tasmania (Zurli et al., 2021; Mulder et al., 2020).

The major difference between these datasets are the > 2000 Ma dates. Those populations are completely different between the two locations.

Supplementary Data 1: Descriptions of West Tasmanian Source Lithologies

West Tasmanian Terrane

The eastern and western sides of Tasmania have distinct geologic histories, and were assembled during the middle Devonian [38]. The Western Tasmanian Terrane (WTT) was tectonically active from the Neoproterozoic through the middle Devonian, and includes sedimentary strata and igneous rocks, most of which were metamorphosed and tectonically deformed during that time [25,39,40]. The WTT can be broken up into four regions with overlapping, but distinct, lithologies and geologic histories: the Rocky Cape, Dundas, Sheffield, and Tyennian elements (Supplementary Figure 3). The Arthur Lineament Metamorphic Zone separates the Rocky Cape and Dundas elements. King Island (located north-west of mainland Tasmania) is not included in this discussion because there are no Tasmanian Basin sediments on King Island, and the island does not appear to be along any Permo-Carboniferous glacier transport paths.

The Dundas Element and the Arthur Lineament likely made up topographic lows during the Permo-Carboniferous (the "Dundas Trough"), and much of the Rocky Cape Element and northern and southern Tyennian Element, and Sheffield Element were topographic highs [13,14]. The paleoflow directions associated with the Wynyard Fm and its correlates indicate that the Wynyard glacier likely flowed north through the Dundas Trough [13,41].

"Classic" Tasmanian U-Pb DZ ages from Black, et al. [42] and Black, et al. [43] were not available from the Geoscience Australia geochronology database at the time this manuscript was prepared, and were therefore not included in our analyses.

Devonian-Carboniferous Granitoids

The Devonian-Carboniferous Granitoids of the WTT were emplaced as part of the Lachlan Orogen, and are part of a Silurian to early Carboniferous granite belt that spans most of the eastern

Gondwana margin (east Australia to North Victoria Land region of Antarctica) [23,38,43]. These intrusions are scattered throughout western Tasmania (including in each WTT element), and intrude almost all other lithologies present in WTT.

The zircon U-Pb ages used to represent this source terrane in this study are from the Meredith, Pine Hill, White Heemskirk, and Pieman Heads Granites (Supplementary Figure 3) including data from LA-ICP-MS from Hong, et al. [23] (N = 4, n = 44) and SHRIMP ages from Kositcin and Everard [24] (N = 1, n = 26). $^{238}U/^{206}Pb$ ages were used for Devonian-Carboniferous ages for both datasets, and $^{207}Pb/^{206}Pb$ were used for inherited zircons in the Kositcin and Everard [24] dataset. The data reported by Hong et al. (2017) were filtered for concordance using methods described in Halpin et al. (2014). The SHRIMP ages from Kositcin and Everard [24] have discordance values ranging from -39% to +18%. Kositcin and Everard [24] described the measured zircons from the coarse-grained Meredith Granite as predominantly euhedral to subhedral with external morphologies ranging from prismatic to elongate, aspect ratios range from 1:1 to 1:6, and long axes are ~70–350μm.

These ages are strongly clustered around 375 Ma, with a few Proterozoic zircons that are likely inherited from the host rock [38].

Mount Read Volcanics

The Mount Read Volcanics are a complex of metamorphosed middle to late Cambrian, predominantly submarine, rhyolitic to basaltic volcanic and shallow intrusive rocks that are intercalated with volcaniclastic units [30]. Clastic units in this complex can contain metasedimentary grains, likely derived from local Meso-Neoproterozoic basement [44].

The ages used in this study to represent the Mount Read Volcanics are from a diverse range of lithologies and are reported in Mortensen, et al. [30] (N = 19, n = 101), Berry, et al. [29] (N = 5, n = 63), and Black, et al. [28] (N = 8, n = 304). Works that have measured U-Pb ages of zircons from Mount

Read Volcanics units have primarily focused on determining the depositional/formational ages of the volcanic and igneous lithologies through high-resolution methods, such as SHRIMP [28] and CA-TIMS [30], while the Berry, et al. [29] targeted inherited zircons, which were measured with LA-ICP-MS.

Mortensen, et al. [30] reported $^{238}U/^{206}Pb$, $^{207}Pb/^{206}Pb$, and $^{207}Pb/^{235}U$ ages. The $^{238}U/^{206}Pb$ was used for this study. Age uncertainty is reported as ± 2σ. Percent discordance was reported and ages were excluded with concordance values of <80 and >105. The zircons in this study had a "generally similar" appearance – pale pink, clear, stubby, euhedral prisms with simple terminations. Faint igneous zoning was visible in some grains, and no inherited cores were observed. Grain sizes were not reported. A wide variety of lithologies were used that are representative of the Mount Read volcanics, including volcaniclastics, volcanics, and igneous rocks.

Berry, et al. [29] focused on the non-Cambrian-aged zircons in Mount Read Volcanic sandstones, and reported $^{238}U/^{206}Pb$ and $^{207}Pb/^{206}Pb$ ages. Age uncertainty is reported as ± 2σ. Concordance was not calculated in the original study. For this study, we applied the same concordance filter that was applied to the Wynyard data. The percent concordance of these ages was calculated as $\left(\left[\frac{\frac{238U}{206Pb}\,\text{age}}{\frac{207Pb}{206Pb}\,\text{age}}\right]\cdot 100\right)$. Ages were excluded with concordance values of <80 and >105, and the "best age" was selected for each measurement by the age with the lowest ± 2σ value. According to the methods section of Berry, et al. [29], approximately ~20% of the zircons extracted from these sandstones were first cycle, euhedral zircons**, which were excluded from the study**. This study used the fine sand fraction (63 – 125 μm) of the samples, after crushing was performed with a mortar and pestle. Analyses targeted the cores of the zircon grains. Only 3 of the zircons analyzed in this study showed evidence of zoning, and fractured grains were rare.

Black, et al. [28] reported $^{238}U/^{206}Pb$ ages. Age uncertainty is reported as ±1 standard error. Percent discordance was reported only for anomalously old ages (>~1000 Ma). Some grains had multiple spots measured. Measured zircons were dominantly elongate, euhedral, and rhythmically zoned with rare subhedral faces. Some grains had discordant and/or poorly luminescent cores, that may have been recycled, and were not targeted for this study. No physical size information was reported for the zircons. The lithologies used in this study included both phaneritic and porphyritic lithologies.

Luina Group

The Luina Group is a succession of Neoproterozoic - early Cambrian lithwacke sandstones, volcaniclastic siltstones, mudstones, chert, and minor amounts of dolostone lithologies that are intercalated with mafic volcanics [27,45]. The Luina Group and its correlates outcrop in the Dundas and Sheffield elements.

The only record of DZ ages in the Luina Group come from Cumming, et al. [27] (N = 5, n = 122). U-Pb ages were measured using LA-ICPMS. The $^{238}U/^{206}Pb$, $^{207}Pb/^{206}Pb$, and $^{207}Pb/^{235}U$ ages were reported. Ages are reported as ±1 standard error. In the original study, a "preferred age" was selected for each analysis based on the degree of discordance, the amount of common Pb, and the age of the zircons. Specific descriptions of zircon sizes and shapes are not provided by the authors, but general descriptions appear in the discussions. Younger zircons from volcaniclastic units are described in the text as euhedral to sub-euhedral.

Within the Luina Group, DZ ages were measured in the Halls Formation, Deep Creek Volcanics, and Crescent Spur Sandstone. The Lower Luina Gp includes the Deep Creek Volcanics (N=2, n = 26) and the Halls Fm (N = 1, n = 17) DZ age population strongly clustered 560 Ma. The Crescent Spur Fm is the Upper Luina Gp (N = 2, n = 78) has major peaks at 630 Ma and 1095 Ma dispersed ages between 900 – 1900 Ma. The authors note that the Crescent Spur Sandstone has DZ with

similar ages distribution to the Wings Sandstone between 1000 – 2000 Ma, which are otherwise very rare in Tasmania [42].

Arthur Lineament

The Arthur Lineament (also known as the Arthur Metamorphic Complex) is a narrow, northeast-southwest trending, Cambrian-aged (Tyennan Orogeny), high-strain metamorphic belt composed of metasedimentary and mafic metaigneous lithologies [46,47]. Metamorphic grade within the zone is most often amphibolite grade, with the maximum grade reaching the amphibolite/metamorphic transition [47]. This zone effectively marks the boundary between the Dundas and Rocky Cape elements.

U-Pb DZ ages used to represent these lithologies come from Neoproterozoic metasediments of the Bowry Fm, Bird Phyllite, and Keith Schist, and were measured by Mulder, et al. [25] (N = 6, n = 334). These U-Pb ages were measured using LA-ICP-MS, following techniques described by Meffre et al. (2008) and Halpin, et al. [48]. The $^{207}Pb/^{206}Pb$ ages were used for grains older than 1500 Ma and $^{206}Pb/^{238}U$ ages were used for younger grains. All ages were uncorrected for common Pb unless otherwise stated. Discordant ages were filtered using the protocol of Spencer et al. (2016). The sizes, shapes, and morphologies of zircon grains were not described in this study.

Crimson Creek Formation

The Crimson Creek Formation is an up to 5-km-thick Cryogenian – Ediacaran clastic succession that mainly consists of volcaniclastic, lithwacke turbidites composed of immature, mafic-volcanic fragments with subordinate amounts of mudstone and siltstone, all of which is interrelated with mafic basalt flows and sills [49]. This succession overlies the Oonah Fm and the Success Creek Fm in the Dundas Element and is a lateral equivalent of the Togari Group. The U-Pb ages from the Crimson Creek Fm used in this study are from Mulder, et al. [25] (N = 3, n = 305), and were collected

only from the Red Rock Member. Methods are the same as those reported in the Arthur Lineament section of this appendix. The ages of DZ in the Crimson Creek Fm strongly cluster around 665 Ma.

Success Creek Group

The Success Creek Group is also a Cryogenian – Ediacaran succession that underlies an erosional contact with the Crimson Creek Fm [25,50]. The Dalcoath Fm makes up the base of the Success Creek Group, and is mainly composed of quarzitic meta-sandstone and -siltstones, likely deposited in a shallow marine to tidal setting. These sandstones fine upwards into the Renison Bell Fm, which includes shale, siltstones, dolostones, and minor sandstones. The DZ U-Pb ages for the Success Creek Group are from a sample of metasandstone (likely Dalcoath Fm?) reported in Mulder, et al. [25] (N = 1, n = 132). Methods are the same as those reported in the Arthur Lineament section of this appendix. Most ages in this sample range between 1000 – 1900 Ma, with a major peak at ~1780 Ma.

Oonah Formation

The Oonah Formation (also known locally as the Burnie Fm and Badger Head Group) is a Cryogenian-aged turbidite succession [26,49]. The Oonah Fm is very common throughout the Dundas Element, and some correlates can be found in the Arthur Metamorphic Complex [49]. At the site of this study, along the north coast of Tasmania, the Oonah Fm underlies an angular unconformity with the Wynyard Fm. Additionally, the Oonah Fm along the north coast was intruded prior to lithification by minor, mafic igneous bodies [49,51,52]. The main U-Pb zircon age population in the Oonah Fm is 1600 – 1800 Ma, with a major peak at ~1790 Ma. Though the intrusions were emplaced around ~733 Ma [26], zircons within the intrusions were likely recycled from older, sedimentary units, and have an age distribution similar to the host rock [53]. In this study, the DZ population of the Oonah Fm is represented by measurements from Cumming, et al. [27] (N = 2, n = 117) and Mulder, et al. [26] (N = 1, n = 136). Methods for the Cumming et al. (2016) datasets are

described under the Luina Group section of this appendix, and the methods for the Mulder et al. (2018) dataset are described the Forest Conglomerate (Togari Group) section of this appendix.

Wings Sandstone (Allochthonous Sequence)

The Wings Sandstone is a thick, fault-bounded succession of fine- to medium-grained massive quartz arenite that is exposed as part of a likely allochthonous sequence emplaced during the middle Cambrian as part of the Tyennan Orogeny [29,39,42,49]. The U-Pb ages for the Wings Sandstone used in this study are from Mulder et al. (2020) (N=1, n = 123). The methods for the Mulder et al. (2018) dataset are described the Arthur Lineament section of this appendix.

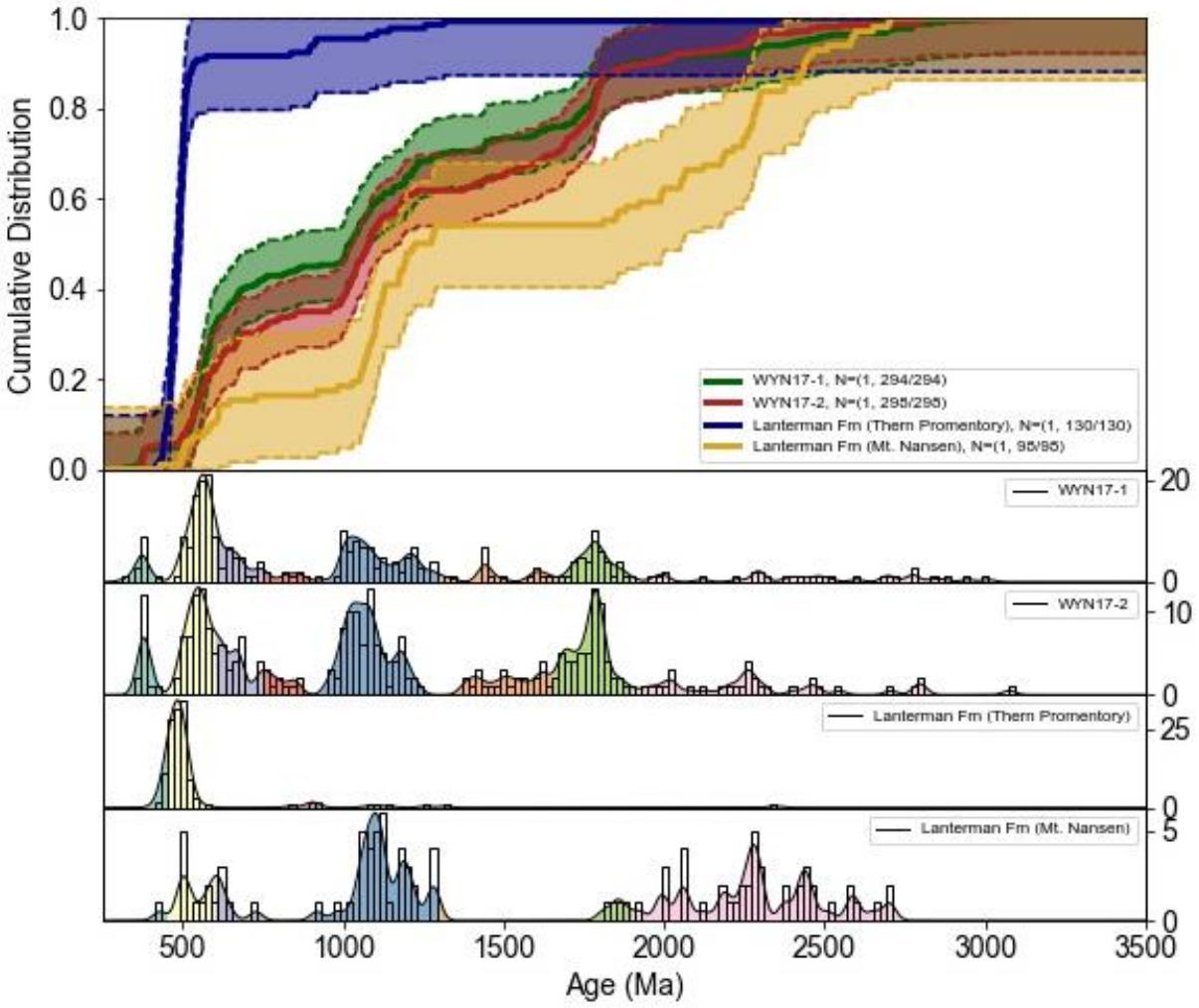

Supplementary Figure 4-1. Cumulative distribution functions (with 95% confidence interval plotted) and kernel density functions of the both the separate and combined Wynyard Fm and Lanterman Fm (North Victoria Land Permian glacigenic sediments) detrital zircon date populations. Plots made and confidence intervals calculated using detritalPy v. 1.3.18 [34]

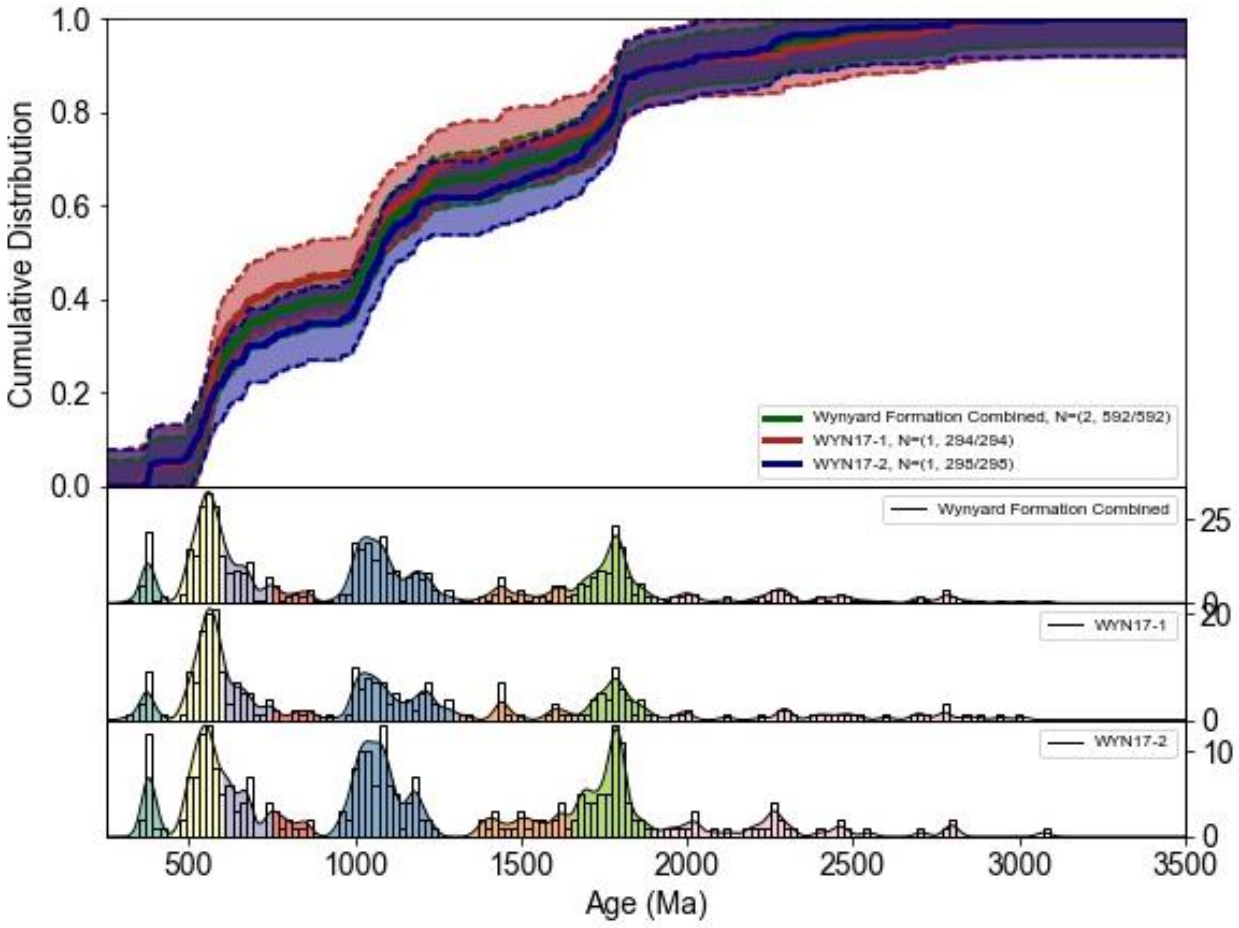

Supplementary Figure 4-2. Cumulative distribution functions (with 95% confidence interval plotted) and kernel density functions of the both the separate and combined Wynyard Fm detrital zircon date populations. Plots made and confidence intervals calculated using detritalPy v. 1.3.18 [34].

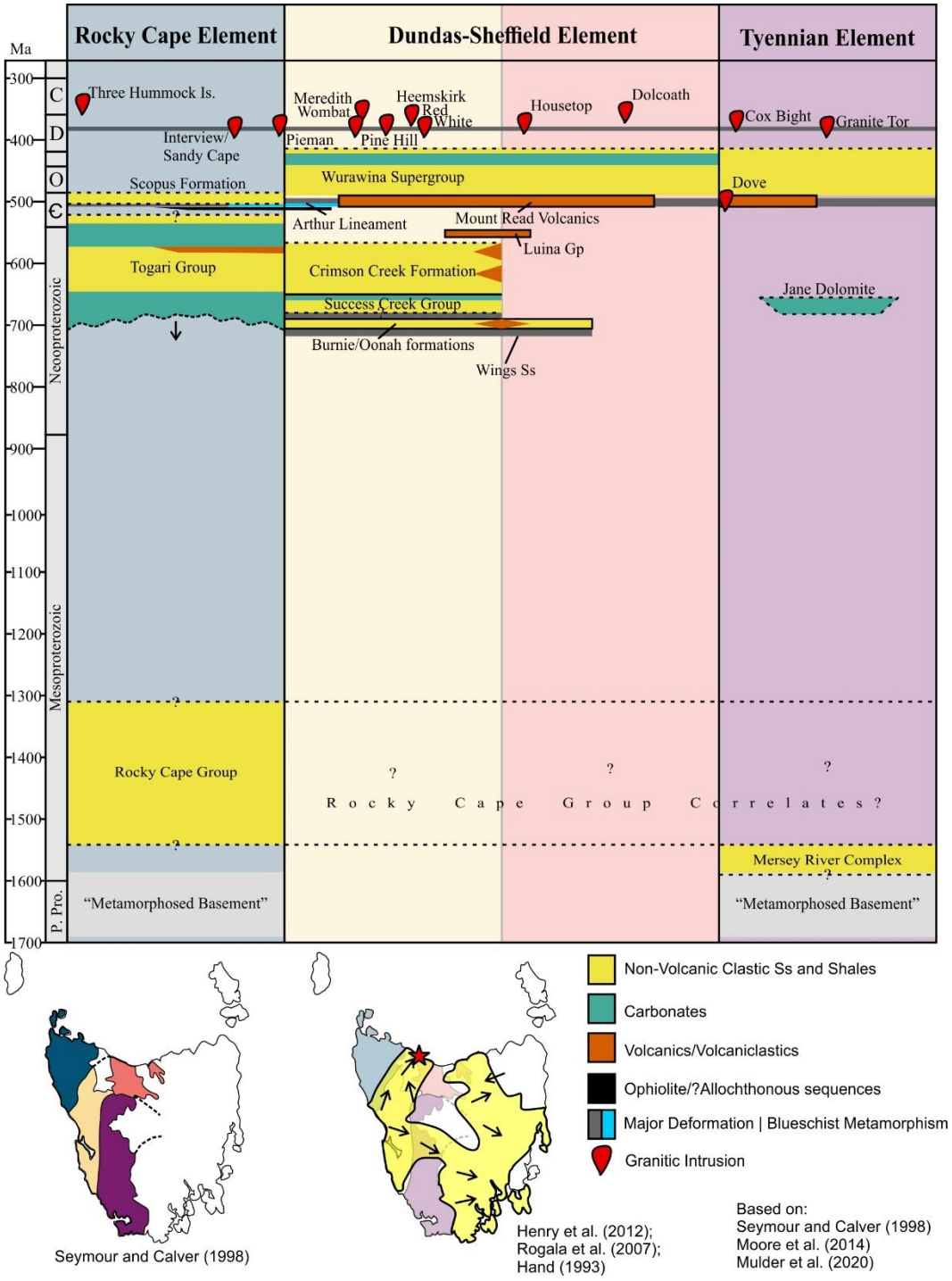

Supplementary Figure 4-3. Time – Space Diagram of the Western Tasmanian structural elements.[13,16,25,40,41,54]

Additional References

35 Pullen, A., Ibañez-Mejia, M., Gehrel, G. E., Giesler, D. & Pecha, M. Optimization of a Laser Ablation-Single Collector-Inductively Coupled Plasma-Mass Spectrometer (Thermo Element 2) for Accurate, Precise, and Efficient Zircon U-Th-Pb Geochronology. *Geochemistry, Geophysics, Geosystems* **19**, doi:10.1029/2018GC007889 (2018).

36 Foden, J., Elburg, M. A., Dougherty-Page, J. & Burtt, A. The timing and duration of the Delamerian Orogeny: correlation with the Ross Orogen and implications for Gondwana assembly. *The Journal of Geology* **114**, 189-210 (2006).

37 Paulsen, T. S., Deering, C., Sliwinski, J., Bachmann, O. & Guillong, M. Detrital zircon ages from the Ross Supergroup, north Victoria Land, Antarctica: Implications for the tectonostratigraphic evolution of the Pacific-Gondwana margin. *Gondwana Research* **35**, 79-96 (2016).

38 Black, L. P. *et al.* Controls on Devonian–Carboniferous magmatism in Tasmania, based on inherited zircon age patterns, Sr, Nd and Pb isotopes, and major and trace element geochemistry. *Australian Journal of Earth Sciences* **57**, 933-968 (2010).

39 Berry, R. F. B., S.W. The pre-Carboniferous geology of Tasmania. *Episodes* **35**, 195-204 (2012).

40 Moore, D. H. B., P.G.; Hall, M. Fragmented Tasmania: the transition from Rodinia to Gondwana. *Australian Journal of Earth Sciences*, 1-35, doi:DOI: 10.1080/08120099.2014.966757 (2015).

41 Rogala, B., James, N. P. & Reid, C. M. Deposition of Polar carbonates during interglacial highstands on an Early Permian shelf, Tasmania. *Journal of Sedimentary Research* **77**, 587-606 (2007).

42 Black, L. P., Calver, C. R., Seymour, D. B. & Reed, A. SHRIMP U–Pb detrital zircon ages from Proterozoic and Early Palaeozoic sandstones and their bearing on the early geological evolution of Tasmania. *Australian Journal of Earth Sciences* **51**, 885-900 (2004).

43 Black, L. P., McClenaghan, M. P., Korsch, R. J., Everard, J. L. & Foudoulis, C. Significance of Devonian–Carboniferous igneousactivity in Tasmania as derived from U–Pb SHRIMP datingof zircon. *Australian Journal of Earth Sciences* **52**, 807-829 (2005).

44 McPhie, J. & Allen, R. L. Facies Architecture of Mineralized Submarine Volcanic Sequences: Cambrian Mount Read Volcanics, Western Tasmania. *Economic Geology* **87**, 584-596 (1992).

45 Everard, J. L. & Calver, C. R. in *Geological Evolution of Tasmania Geological Society of Australia Special Publication* (eds K.D. Corbett, P.G. Quilty, & C.R. Calver) 110-141 (Geological Society of Australia, 2014).

46 Holm, O. H. & Berry, R. F. Structural history of the Arthur Lineament, northwest Tasmania: an analysis of critical outcrops. *Australian Journal of Earth Sciences* **2002**, 167-185 (2002).

47 Corbett, K. D. *et al.* in *Geological Evolution of Tasmania Geological Society of Australia Special Publications* (eds K.D. Corbett, P.G. Quilty, & C.R. Calver) 95-240 (Geological Society of Australia, 2014).

48 Halpin, J. A. *et al.* Authigenic monazite and detrital zircon dating from the Proterozoic Rocky Cape Group, Tasmania: Links to the Belt-Purcell Supergroup, North America. *Precambrian Research* **250**, 50-67 (2014).

49 Calver, C. R., Everard, J. L., Berry, R. F., Bottrill, R. S. & Seymour, D. B. in *Geological Evolution of Tasmania* Vol. Special Publication 24 (eds K.D. Corbett, P.G. Quilty, & C.R. Calver) 34-94 (Geological Society of Tasmania, 2014).

50 Morrison, G. W. *Stratigraphy and sedimentology of the Renison Mine Sequence* Ph.D. thesis, James Cook University, (1982).

51 Gee, R. D. in *The Geology of Western Tasmania—A Symposium.*

52 Crook, K. A. Tectonic implications of some field relations of the Adelaidean Cooee Dolerite Tasmania. *Journal of the Geological Society of Australia* **26**, 353-361 (1979).

53 Turner, N. J., Black, L. P. & Kamperman, M. Dating of Neoproterozoic and Cambrian orogeniesin Tasmania. *Australian Journal of Earth Sciences* **45**, 789-806 (1998).

54 Seymour, D. B. & Calver, C. R. in *Proceedings of the 14th Australian Geological Conventions.* 399.

Table 4-1. Detrital Zircon U-Pb Age Data Sources

Target Group	Lithology Name and/or Lithology	Stratigraphic Age	U-Pb Measurement Type	N	Latitude	Longitude	Sample Name	Source
Wynyard Formation	Wynyard Formation	Permo-Carboniferous	LA-ICP-MS	294	-41.015657	145.787801	WYN17-1	this study
Wynyard Formation	Wynyard Formation	Permo-Carboniferous	LA-ICP-MS	298	-41.011554	145.782597	WYN17-2	this study
Dev - Carb Granitoid	Meredith Granite	Mid to Late Devonian	LA-ICP-MS	14	-41.645000	145.359000	WT12WH73	Hong et al., 2017
Dev - Carb Granitoid	Pine Hill Granite	L. Devonian	LA-ICP-MS	14	-41.859000	145.508000	WT131414	Hong et al., 2017
Dev - Carb Granitoid	White Heemskirk Granite	L. Devonian - E. Carbon.	LA-ICP-MS	8	-41.845000	145.104000	WT12WH20	Hong et al., 2017
Dev - Carb Granitoid	Pieman Heads Granite	E. Carboniferous	LA-ICP-MS	8	-41.719000	144.937000	WT12WH11	Hong et al., 2017
Dev - Carb Granitoid	Meredith Granite	M-L Devonian	SHRIMP	26	-41.659851	145.369629	R017895	Kositcin and Everard, 2013
Wurawina SuperGp	Stitt Quartzite	L. Cambrian - E. Ordovician	LAM-ICP-MS	20	-41.76465108	145.5232752	B-130628	Berry et al., 2001
Wurawina SuperGp	Stitt Quartzite	L. Cambrian - E. Ordovician	LAM-ICP-MS	4	-41.680843	145.519787	B-130590	Berry et al., 2001
Mt Read Volcanics	Noddy Creek Rhyolite	M.-L. Cambrian	SHRIMP	48	-42.472157	145.405472	96220032	Black et al., 1997
Mt Read Volcanics	Bonds Range Porphyry	M.-L. Cambrian	SHRIMP	29	-41.558480	145.9083235	95220013	Black et al., 1997
Mt Read Volcanics	Mount Jukes Lava	M.-L. Cambrian	SHRIMP	24	-42.161710	145.5827238	95220028	Black et al., 1997
Mt Read Volcanics	Minnow Keratophyre	M.-L. Cambrian	SHRIMP	47	-41.470951	146.3344694	95220023	Black et al., 1997
Mt Read Volcanics	Winterbrook Lava	M.-L. Cambrian	SHRIMP	24	-41.438657	146.0005508	95220025	Black et al., 1997
Mt Read Volcanics	Tyndall Group ignimbrite	M.-L. Cambrian	SHRIMP	49	-41.557174	145.7458828	95220026	Black et al., 1997
Mt Read Volcanics	Lobster Creek Volcanics	M.-L. Cambrian	SHRIMP	55	-41.169661	146.0546816	95220022	Black et al., 1997
Mt Read Volcanics	Beulah Granite	M.-L. Cambrian	SHRIMP	28	-41.452393	146.3706845	95220024	Black et al., 1997
Mt Read Volcanics	Gog Greywacke	M.-L. Cambrian	LAM-ICP-MS	9	-41.353141	146.1608034	B-134329	Berry et al., 2001
Mt Read Volcanics	Gog Greywacke	M.-L. Cambrian	LAM-ICP-MS	8	-41.546351	146.568363	B-134308	Berry et al., 2001
Mt Read Volcanics	Animal Creek Greywacke	M.-L. Cambrian	LAM-ICP-MS	7	-41.630787	145.6229763	B-130600	Berry et al., 2001
Mt Read Volcanics	Animal Creek Greywacke	M.-L. Cambrian	LAM-ICP-MS	9	-41.636060	145.6120585	B-130598	Berry et al., 2001
Mt Read Volcanics	Sticht Range Fm	M.-L. Cambrian	LAM-ICP-MS	30	-41.958133	145.6569764	B-134362	Berry et al., 2001
Mt Read Volcanics	Pegmatitic gabbro	M.-L. Cambrian	CA-TIMS	5	-41.905160	145.248292	07M-02	Mortensen et al., 2015
Mt Read Volcanics	dacite	M.-L. Cambrian	CA-TIMS	4	-41.722746	145.622156	07M-05	Mortensen et al., 2015
Mt Read Volcanics	dacite	M.-L. Cambrian	CA-TIMS	5	-41.783027	145.585705	07M-07	Mortensen et al., 2015

Mt Read Volcanics	Kershaw Pumice Fm	M.-L. Cambrian	CA-TIMS	9	-41.778469	145.545303	07M-06	Mortensen et al., 2015
Mt Read Volcanics	Hercules Pumice Fm	M.-L. Cambrian	CA-TIMS	5	-41.751117	145.556084	315R-150	Mortensen et al., 2015
Mt Read Volcanics	Hercules Pumice Fm	M.-L. Cambrian	CA-TIMS	4	-41.833164	145.510658	08M-03	Mortensen et al., 2015
Mt Read Volcanics	Hercules Pumice Fm	M.-L. Cambrian	CA-TIMS	6	-41.762121	145.553070	120R-1414	Mortensen et al., 2015
Mt Read Volcanics	K lens porphyry	M.-L. Cambrian	CA-TIMS	8	-41.762121	145.553070	120R-1320	Mortensen et al., 2015
Mt Read Volcanics	White Spur Fm (rhyolite)	M.-L. Cambrian	CA-TIMS	5	-41.782107	145.555918	112R-668	Mortensen et al., 2015
Mt Read Volcanics	White Spur Fm (rhyolite)	M.-L. Cambrian	CA-TIMS	5	-41.894333	145.516000	WSP-5-12	Mortensen et al., 2015
Mt Read Volcanics	Que-Hellyer Volcanics	M.-L. Cambrian	CA-TIMS	5	-41.577547	145.730974	HED011-893	Mortensen et al., 2015
Mt Read Volcanics	Southwell Subgroup	M.-L. Cambrian	CA-TIMS	4	-41.583574	145.720515	HED02-73	Mortensen et al., 2015
Mt Read Volcanics	Southwell Subgroup	M.-L. Cambrian	CA-TIMS	4	-41.577547	145.730974	HED11-256	Mortensen et al., 2015
Mt Read Volcanics	Mt. Cripps Subgroup	M.-L. Cambrian	CA-TIMS	4	-41.556901	145.745576	07M-24	Mortensen et al., 2015
Mt Read Volcanics	Central Volcanic Complex	M.-L. Cambrian	CA-TIMS	5	-42.071537	145.585433	08M-09	Mortensen et al., 2015
Mt Read Volcanics	Central Volcanic Complex	M.-L. Cambrian	CA-TIMS	5	-42.162448	145.587041	07M-21	Mortensen et al., 2015
Mt Read Volcanics	Central Volcanic Complex	M.-L. Cambrian	CA-TIMS	8	-42.162060	145.584084	07M-22	Mortensen et al., 2015
Mt Read Volcanics	Range porphyr	M.-L. Cambrian	CA-TIMS	5	-41.563097	145.892847	07M-25	Mortensen et al., 2015
Mt Read Volcanics	Murchison granite	M.-L. Cambrian	CA-TIMS	5	-41.816814	145.635854	07M-09	Mortensen et al., 2015
Luina Group	Deep Creek Volcanics	Neopro. - E. Cambrian	LA-ICP-MS	12	-41.495282	145.374414	R018210	Cumming et al., 2016
Luina Group	Deep Creek Volcanics	Neopro. - E. Cambrian	LA-ICP-MS	14	-41.495282	145.374414	R018213	Cumming et al., 2016
Luina Group	Halls Formation	Neopro. - E. Cambrian	LA-ICP-MS	17	-41.495282	145.374414	R018218	Cumming et al., 2016
Luina Group	Crescent Spur Sandstone	Neopro. - E. Cambrian	LA-ICP-MS	50	-41.495282	145.374414	R018223	Cumming et al., 2016
Luina Group	Crescent Spur Sandstone	Neopro. - E. Cambrian	LA-ICP-MS	29	-41.468348	145.416808	R018272	Cumming et al., 2016
Arthur Lineament	Bowry Formation	Neoproterozoic	LA-ICP-MS	18	-41.219454	145.404646	R005453	Mulder et al., 2020
Arthur Lineament	Bowry Formation	Neoproterozoic	LA-ICP-MS	70	-41.248346	145.377329	R005458	Mulder et al., 2020
Arthur Lineament	Bowry Formation	Neoproterozoic	LA-ICP-MS	69	-41.519111	145.189739	G408136	Mulder et al., 2020
Arthur Lineament	Bird Phyllite (quartzite)	Neoproterozoic	LA-ICP-MS	21	-41.135701	145.414288	R005005	Mulder et al., 2020
Arthur Lineament	Bird Phyllite (Quartzite)	Neoproterozoic	LA-ICP-MS	36	-41.132322	145.408415	R005006	Mulder et al., 2020
Arthur Lineament	Keith Schist	Meso-Neoproterozoic	LA-ICP-MS	120	-41.195764	145.436811	R005432	Mulder et al., 2020
Crimson Creek Fm	Red Rock Member	Neoproterozoic	LA-ICP-MS	118	-41.891101	145.296794	SY016	Mulder et al., 2020
Crimson Creek Fm	Red Rock Member	Neoproterozoic	LA-ICP-MS	98	-41.711572	145.732019	G407255	Mulder et al., 2020
Crimson Creek Fm	Red Rock Member	Neoproterozoic	LA-ICP-MS	89	-41.719060	145.338708	G407256	Mulder et al., 2020

Success Creek Group	Dalcoath Formation?	Neoproterozoic	LA-ICP-MS	132	-41.720557	145.336385	SM17-46	Mulder et al., 2020
Togari Group	Forest Conglomerate	Neoproterozoic	LA-ICP-MS	184	-41.212543	144.905278	R004296	Mulder et al., 2018
Oonah Formation	Oonah Formation	Neoproterozoic	LA-ICP-MS	34	-41.434449	145.472318	R018036	Cumming et al., 2016
Oonah Formation	Oonah Formation	Neoproterozoic	LA-ICP-MS	83	-41.428819	145.490066	R018029	Cumming et al., 2016
Oonah Formation	Oonah Formation	Neoproterozoic	LA-ICP-MS	136	-41.046114	145.901832	BF1406	Mulder et al., 2018
Allocthonous	Wings Sandstone	?Neopro.or ?Cambrian	LA-ICP-MS	123	-42.687728	146.242078	73-116	Mulder et al., 2020
North Victoria Land	Lanterman	Permian	LA-ICP-MS	130	-74.562900	161.996000	04-01-15C10	Zurli et al., 2021
North Victoria Land	Lanterman	Permian	LA-ICP-MS	95	-74.464600	162.524000	22-11-15C5	Zurli et al., 2021

CHAPTER 5. CONCLUSIONS

The Late Paleozoic Ice Ae (LPIA; ~ 374 - 256Ma) is the longest Phanerozoic global icehouse interval. Geologic records of the LPIA are preserved in "near-field" settings that directly record the physical and environmental effects of extensive glaciation in the southern hemisphere (Isbell et al., 2012, 2021; Fielding et al., 2008b), and in "far-field" settings that indirectly record the effects of these glaciations (Gastaldo et al., 1996; Montañez and Soreghan, 2006; Fielding et al., 2008b; Montañez and Poulsen, 2013; Frank et al., 2015). Because wide-spread glaciation can have a significant influence on both regional and global climate and geology, constraining glacier behavior during the LPIA is critical to understanding the geologic and climatic records from that period. Constraining the characteristics of LPIA glaciers is essential to developing a global-scale understanding of this key climatic event in Earth's history, its impacts on the evolution of life, and the extent it can be used to predict future climate change. Reconstructing and relating the physical characteristics of glaciers (physical characteristics and distribution) to global climate trends (timing) through their sedimentary records is not a straightforward task. The works presented in this dissertation demonstrate that the best way to address these challenges, and build an accurate, nuanced understanding of global glaciations during the LPIA, is to begin on the local scale and build outward.

5.1. Outcomes of Stated Project Objectives

Objective 1: Characterize the types of glaciations (physical characteristics and extent) in South Polar regions during the LPIA

The sedimentology-based works in this dissertation (Chapters 2 & 3) contribute new perspectives to the understanding of South Polar glaciations during the LPIA by describing and interpreting glacigenic sedimentary rocks that had not been previous assessed in this way (Chapter 2; Pagoda Fm,

Transantarctic Basin) or had not been the topic of detailed study for more than 60 years (Chapter 3, Wynyard Fm, Tasmanian Basin). Though the interpretations of depositional environments made in these works broadly agree with the stated predictions (hypotheses 1.1 and 1.2), the novelty of these studies is in the interpretations of sequence stratigraphy, of details of the inferred depositional environments, and of glacier thermal regimes or hydrological conditions during deposition. Detailed studies and interpretations such as these, if performed at many point in a region or basin, will lead to more nuanced understanding of both the heterogeneity and broad trends within LPIA glaciogenic sedimentary systems.

Hypothesis 1.1: In the Shackleton Glacier Region of the Transantarctic Basin, LPIA glacigenic strata were deposited in a basin-marginal, marine setting by a warm-based glacier (Isbell et al., 2008a) and not in a terrestrial setting (e.g., Miller, 1989). This study also tests the basin vs. basin-marginal lithofacies model for glacigenic deposition in the Transantarctic Basin suggested by Isbell et al. (2008). This hypothesis proposes that basin-margin successions are thin (< 100 m) and contain lithofacies that are more likely to be deformed and have evidence for subglacial deposition and deformation, and that basinal successions are thicker (~400 m), have little-to-no evidence for subglacial processes, and are more likely to contain marine diamictites. The data and analysis presented in Chapter 2 supports all parts of hypothesis 1.1. The Pagoda Fm in the Shackleton Glacier Region of the Transantarctic Basin was deposited by a glacier with a temperate or mild subpolar thermal regime in a subaqueous, basin-marginal setting. The basin-margin lithofacies model proposed by Isbell et al. (2008) is consistent with the observations of the Pagoda Fm in the Shackleton Glacier Region.

Beyond the hypothesis: Pagoda Formation (Transantarctic Basin)

- The Pagoda Fm was described at four locations in the Shackleton Glacier Region of Antarctica during the 2017 – 2018 austral summer.

- The dominant lithology in the Pagoda Fm at those locations is a massive, sandy, clast-poor diamictite.

- Depositional processes governing these diamictites were subaqueous glacial processes in a **marine or brackish setting**; likely a combination of mass transport, iceberg rain-out, iceberg scouring, plume sedimentation, and subglacial till deposition.

- Current-transported sands and stratified diamictites in the Pagoda Fm were deposited as part of **grounding-line fan systems**.

- All glacigenic sediments in the Pagoda Fm at these locations were **likely deposited during the retreat phase of a single glacial sequence**.

- Glacier flow directions and trends in Pagoda Fm thicknesses in the Shackleton Glacier area support the hypothesis that **an ice center was present toward the Panthalassan margin of East Antarctica (Marie Byrd Land) during the LPIA**.

*Hypotheses 1.2: Glacigenic sediments in the Tasmanian Basin were deposited by multiple advances of temperate glaciers (Hand, 1993; Henry et al., 2012). Specifically, the Wynyard Fm was deposited by north-flowing glaciers, sourced from the south and east, that occupied a 40 km-wide, NNE-SSW trending bedrock valley (Dundas Trough).*The data presented in Chapter 3 are principally consistent with this hypothesis. Flow directions derived from subglacial striae, in addition to current transport directions, in the Wynyard Fm at its type section are consistent with glacier motion that follows the trend of the Dundas Trough. Most of the sediments in the succession described in this study were likely deposited by glaciers with temperate thermal regimes, but initial sedimentation is most likely associated with a polar thermal regime in the same glacier. Strata in the lower 415 m of the Wynyard Fm were likely deposited during a single retreat phase of the "Wynyard Glacier", with some minor readvances over the area. This interpretation of a single retreat cycle does not prohibit multiple glacial-interglacial cycles from being present in the Wynyard Fm farther up section in the type locality, or in other parts of the Tasmanian Basin.

Beyond the hypothesis: Wynyard Formation (Tasmanian Basin)

- The basal 415 m of the Wynyard Fm in its type section was described for this study.
- In this succession, the basal Wynyard Fm was deposited in **glacier-proximal to glacier-distal, marine environments on a continental shelf at water depths below storm wave base.**
- Facies associations in this succession include muddy massive diamictite (MDm), sandy massive diamictite (SDm), and rhythmically laminated fine-grained facies (IsR). The MDm facies association was likely deposited as a **subglacial and proglacial, glacier-proximal grounding zone wedge**, the SDm facies association as part of a **proglacial, glacier-**

proximal grounding line fan or morainal bank, and the IsR facies association as a **proglacial, glacier-intermediate or glacier-distal cyclopelites**.

- All facies associations contain mass transport and turbidite deposits that could have been driven by **slope instability due to rapid deposition**.

- **Deposition of these facies could have occurred over a relatively short period of time**: grounding zone wedges are deposited on the scale of decades to centuries, grounding line fan and morainal bank deposits on the order of years or decades, and the cyclopelites on the order of years.

- The lack of wave reworked sediments and dimensions of the Dundas Trough suggest that the Wynyard Glacier was at least ~ 200 m thick and ~ 50 km wide. These dimensions suggest that **the "Wynyard Glacier" was most likely an outlet glacier or ice stream draining a large ice cap or ice sheet**.

- The shift in depositional environment from grounding zone wedges (DMm facies association) to a grounding line fan or morainal bank (SDm facies association) suggests a change in glacier thermal and/or hydrologic regime. Change in Wynyard Glacier's thermal or hydrologic regime was likely the result of physical changes to or shifts in the Wynyard Glacier that occurred as part of the glacier's overall retreat, and ***not*** **some abrupt change in climate.**

Objective 2: Infer the extent of glaciers contributing to sedimentation in polar basins through provenance studies

Hypothesis 2.1: Glaciers contributing to deposits in the Tasmanian Basin could have come from ice centers nucleated in North Victoria Land (Antarctica), eastern Australia, or locally Measured flow directions in Tasmania, Antarctica, and mainland Australia indicate glacier motion both into the Tasmanian basin from either the north (Australia) or the south (Antarctica), and out of the Tasmanian Basin, to the north and east. The conclusion of this dissertation is that the proposed methods (detrital zircon provenance) were not appropriate to address the question of where the Wynyard Glacier ice center was nucleated. Sediment transport directions in the Wynyard Formation (Chapter 3) strongly suggest that this ice center was located to the south of Tasmania's modern (and Pennsylvanian-Permian) location (e.g., Banks, 1962; Hand, 1993). The motivation for this study was to test that long-standing hypothesis using detrital zircon geochronology as a powerful provenance technique that could potentially show distal sources from Antarctica. Instead, we confirmed the flow-path hypothesis for the Wynyard Fm by showing that all of the DZ in the Wynyard Fm could be sourced from the Dundas Trough.

This hypothesis and the proposed methods for addressing it were formulated based on how detrital zircon provenance is typically approached in Paleozoic glacigenic sedimentary systems. Such works assume that similar detrital zircon provenance signals between geographically dispersed glacigenic units of equivalent depositional age are evidence that both sedimentary units were deposited by the same large mass (i.e., large glaciers such as ice sheets and ice caps). Essentially, this "traditional" approach treats the processes that govern sediment transport by ice the same as those that govern sediment transport and provenance in large-scale fluvial systems. That assumption is not reasonable for glaciers for multiple reasons that are discussed in Chapter 4. What those reasons boil down to are that while glaciers can transport sediment over thousands of kilometers, they also entrain additional sediment along their flow paths, so that glacigenic sediments are most likely to have

provenance signatures that dominantly reflect lithologies entrained within 100 km of where that sediment was deposited.

In Chapter 4, we demonstrated that all measured detrital zircon dates from the Wynyard Fm can be attributed to zircon sources that occur within 33 km of the sample location along the glacier's flow path (the Dundas Trough). Therefore, while the detrital zircon provenance signature of the Wynyard Fm also supports the hypothesis that the Wynyard Glacier flowed north through the Dundas Trough, this information does not impart insight into where the ice center was nucleated.

5.2. Reconciling local records with global trends

The research question that was outlined in the proposal for this dissertation, and stated in Chapter 1, is: "To what extent can the physical characteristics, size, distribution, and timing of LPIA glaciers in high-latitude Gondwanan basins be constrained, and how does this knowledge inform our understanding of regional and global climate change during that time?"

In the cases of the strata examined in this study "that time" refers to the ~14 Myr between the latest Carboniferous (Gzhelian; beginning ~ 304 Ma) and the early Permian (Sakmarian; ending ~ 290 Ma). Globally, this is an interval (sometimes referred to as "Glacial III" or "P1") with the most prolific glacial deposits, preserved in basins across Gondwana, including in western Australia, eastern Australia, Tasmania, Antarctica, South Africa, central Africa, the Falklands (Malvinas), and southeastern South America (López-Gamundí, 1997; Isbell et al., 2003; Fielding et al., 2008a, 2008b). This apparent increase in the volume of glacigenic sediment coincided with a major interpreted decrease in atmospheric pCO_2 from ~ 400 ppm to possibly < 200 ppm (Fielding et al., 2008b; Richey et al., 2020) and the deposition of major low-latitude cyclothems driven by up to ~ 120 m of cyclic sea level change (e.g., Rygel et al., 2008). For reference, modern pCO_2 is around 415 ppm and was around 180 ppm at the end of the Last Glacial Maximum (~ 20 ka; Clark et al., 2009). Geologic

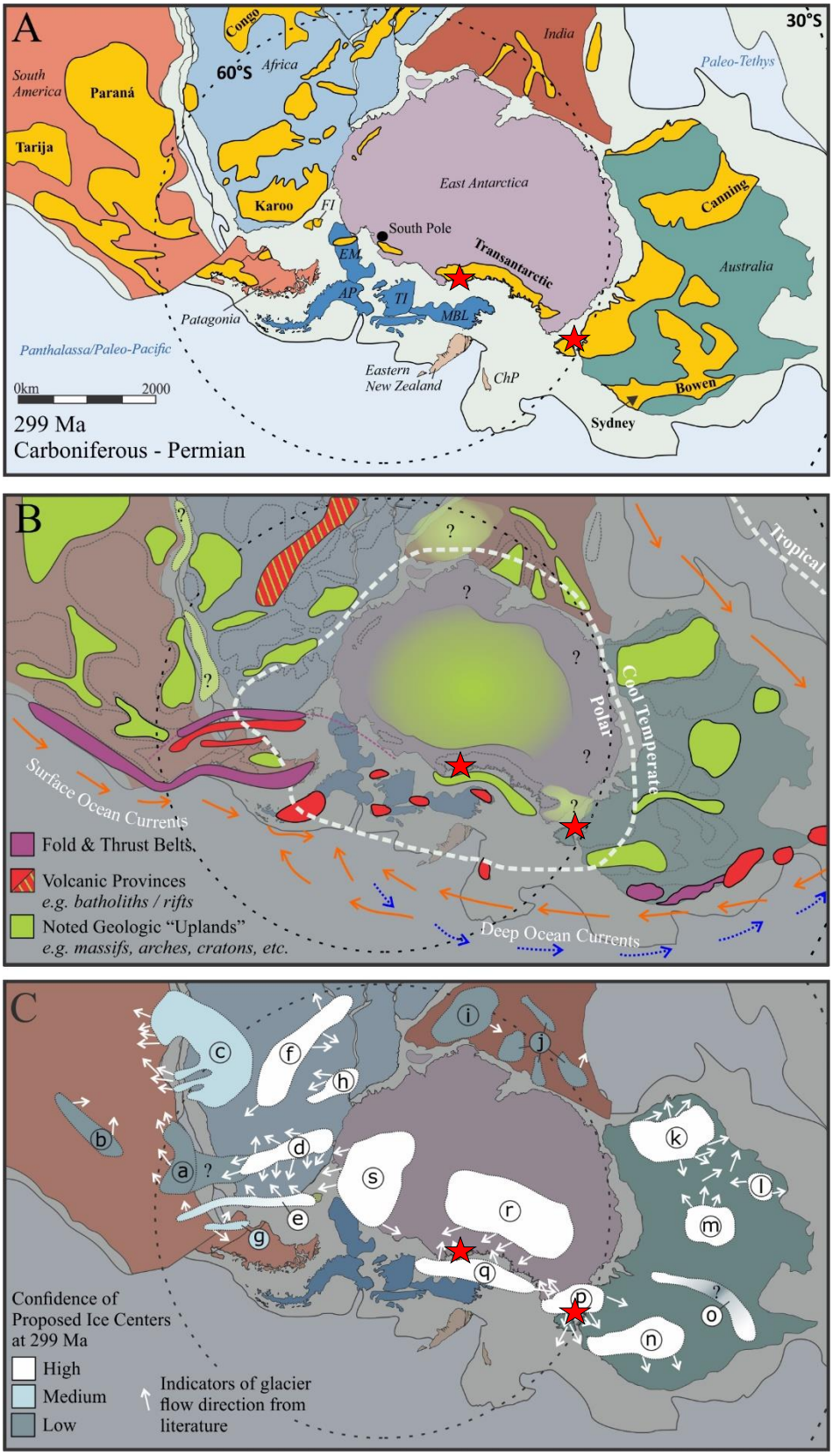
A
30°S
60°S
Congo
Africa
India
Paleo-Tethys
South America
Paraná
Tarija
Karoo
FI
East Antarctica
South Pole
Transantarctic
EM
AP
TI
MBL
Patagonia
Canning
Australia
Panthalassa/Paleo-Pacific
Eastern New Zealand
ChP
Bowen
Sydney
0km
2000
299 Ma
Carboniferous - Permian
B
Tropical
Cool Temperate
Polar
Surface Ocean Currents
Deep Ocean Currents
Fold & Thrust Belts
Volcanic Provinces
e.g. batholiths / rifts
Noted Geologic "Uplands"
e.g. massifs, arches, cratons, etc.
C
a
b
c
d
e
f
g
h
i
j
k
l
m
n
o
p
q
r
s
Confidence of
Proposed Ice Centers
at 299 Ma
High
Medium
Low
Indicators of glacier
flow direction from
literature

Figure 5-1. Paleogeographic reconstructions of Gondwana near the Pennsylvanian-Permian Boundary. All maps are south-polar projections. Stars indicates the approximate location of the Shackleton Glacier area and Wynyard Fm type section. Continent distributions are based on Lawver et al. (2011) and copied from (Isbell et al. 2012), and south pole position is from Meredith et al. (2021). **A.** Yellow regions indicate the modern extent of sedimentary basins containing late Paleozoic Ice Age strata. Abbreviations include: Falkland Islands/Malvinas (FI), Ellsworth Mountain block (EM), Antarctic Peninsula (AP), Thurston Island (TI), Marie Byrd Land (MBL), and the Challenger Plateau/western New Zealand (ChP). Basins adapted from Isbell et al. (2012). **B.** Map of climate and geologic conditions that likely would have controlled the distribution of glaciers. General climatic zones are from Boucot et al. (2013). Ocean current reconstructions are from Jones et al. (2006) and Frank et al. (2015), where solid, orange arrows indicate relatively warm surface waters and dashed, blue arrows indicate colder deep waters. The general distribution of topographic highs, in the form of contemporaneous fold-and-thrust belts, substantial batholiths, and "uplands" that had significant influence on the regional sediment dispersal (López-Gamundí et al. 1994; Veevers and Tewari 1995; Catuneanu et al. 2005; Veevers 2006; Ramos 2008; Pangaro and Ramos 2012; Wopfner 2012; Elliot 2013; Ramos and Naipauer 2014; Ramos et al., 2014). **C.** Proposed positions of glacial centers during the early Permian based on flow directions and position of basins and "highlands". Illustrated ice centers are not meant to represent the whole possible extent of each proposed glacier, but where proposed glaciers were likely to be nucleated. The arrows reflect field measurements of flow directions reported in the studies cited for each ice center. However, flow directions of glaciers are highly variable, both spatially and temporally, and the true flow paths of these ancient ice centers were likely much more variable than the arrows on this map. Confidence is based on abundance of available lithologic data, and both relative and absolute ages. Ice centers are as follows: a. Uruguay, b. Asunsción, c. Windhoek/ Koakoveld Highlands, d. Cargonian Highlands, e. Cape-Ventana Fold, f. East African Thermal Rise, g. Patagonian Western Magmatic Arc, h. Zimbabwe, i. Madagascar-SW India, j. Chotanagpur & Chhattisgarh, k. Pilabra-Yilgarn, l. Kimberly, m. Arunta-Musgrave, n. Bowen-Gunnedah-Sydney, o. Galilee, p. Wilson, r. East Antarctic, s. Ellsworth. References for ice centers in Figure 2-2 captions.

evidence and climate models show that southwestern, Panthalassan Gondwana during this time was very cold (with average land and ocean surface temperatures barely exceeding 0 °C in the summer and plunging below 20 °C in the winter), seasonally wet (~ 1 mm/day of precipitation in the summer on average), and had mountainous coastlines (Gibbs et al., 2002; Fielding et al., 2006; Lowry et al., 2014); all characteristics that favor the growth of glaciers (Lowry et al., 2014). Models of global climate during the early Permian with low pCO_2 suggest that the southwest coast of Gondwana was the recipient of relatively warm wind and ocean currents from temperate latitudes during the summer months (Gibbs et al., 2002; Fig. 5-1B). Since average summer surface air temperatures in these regions likely did not exceed 0° C, this moist air would have resulted in the ample precipitation of snow in southwestern Gondwana during the summer months (Gibbs et al., 2002; Lowry et al., 2014). Precipitation was likely more substantive in the coastal, mountainous areas that likely existed along the Panthalassan margin, outboard of either the Transantarctic or Tasmanian basins (Elliot, 2013). Climate models also predict that similar high-precipitation patterns

may have persisted in the Panthalassan ranges during the colder months, at the same time temperatures plunged well below freezing (Gibbs et al., 2002). Quaternary analogs to the southwestern Gondwanan margin, in terms of climate, topographic, and latitudinal setting, would be the Scandinavian and northern Cordilleran ice sheets.

How do the glacial strata of the Transantarctic and Tasmanian basins fit into this global and regional context? In Chapter 1, the idea was introduced that high-latitude glaciers will have the longest-lived glacial episodes during icehouse events compared to their temperate-latitude counterparts, and that glaciers at high-latitudes do not reflect climate primarily by their presence or absence, but rather by their thermal regime and extent. Additionally, based on our understanding of glaciations in polar regions during the Cenozoic ice age, polar regions likely experienced numerous glacial-interglacial cycles during the 14 Myr "icehouse" that began in the Gzhelian (Pennsylvanian) and ended in the Sakmarian (Permian). Therefore, we might expect that the Transantarctic and Tasmanian basins contain strata representing multiple glacial-interglacial cycles with different extents, durations, and possibly thermal regimes, like the Quaternary strata in the northern North Sea (e.g., Ottensen et al., 2018; Hjelstuen and Sejrup, 2021) and the Gulf of Alaska (Zellers and Lagoe, 1994).

This type of succession is not what was observed in the strata of the Transantarctic or Tasmanian basins. Instead, what is preserved at the successions examined in this study appears to represent only glacial retreat cycles. In both cases, the retreating glaciers have dominantly warm (mild subpolar to temperate) thermal regimes. The thermal regime of the higher-latitude glacier (Pagoda Fm, Transantarctic Basin, Chapter 2) appears to have been colder (mild subpolar) than the lower-latitude glacier (Wynyard Fm, Tasmanian Basin, Chapter 3), whose sedimentary record represents a dominantly temperate thermal regime. In the case of the Shackleton Glacier Region, this limited record is likely due the area being located on a basin margin, and accommodation being limited. In

the Tasmanian Basin, uncertainty around the structure and thickness of the Wynyard Fm type section limits how the trends observed in this study are related to the glacigenic strata in the rest of the basin, or indeed to other strata in the 6 km-long outcrop.

More generally, the depositional histories of LPIA glacigenic strata in the Transantarctic and Tasmanian basins fit with broad climate trends during the late Pennsylvanian and early Permian. If the interpretations of the relative ages of the biostratigraphy is correct, the deglaciation of the Transantarctic Basin occurred after the Tasmanian Basin. This trend is consistent with the Transantarctic Basin being closer to the paleogeographic south pole than the Tasmanian Basin. In large parts of both basins, the glacigenic strata are conformably overlain by fine-grained lithofacies that contain evidence for continued cold, polar postglacial conditions; the Woody Island and correlates in the Tasmanian Basin (Fielding et al., 2010) and the Mackellar Fm and correlates in the southern sub-basins on the Transantarctic Basin (Miller and Isbell, 2010). All these trends are consistent with what one might predict for glaciations in similar geologic and climatic settings.

5.3. Future Directions

To build on the work presented in this dissertation, additional studies focusing on local paleoenvironments in the Transantarctic, Tasmanian, and other neighboring basins are needed to try to better piece together the history of the southwestern coast of Gondwana during the Permo-Carboniferous. While the provenance of glacigenic sediment could be enlightening, provenance studies should use a local first approach, while employing multiple provenance techniques (e.g., Garzanti, 2016) and accounting for provenance biases between grain sizes and transport histories. The efficacy of the local-first hypothesis should also be tested in other basins and additional parts of the Tasmanian Basin.

While stratigraphy and sedimentology of glacigenic strata are essential to understanding the LPIA, more tools and perspectives could be brought to bear on the future studies of these rocks. More work and thought should also be put towards understanding the tectonic and geologic drivers for the existence of relatively low accommodation basins like the early Transantarctic and Tasmanian, which do not have clear drivers behind their inception. Tools such as thermochronology could be used to understand the timing of denudation and uplift of the glaciated landscape prior to, during, and after glaciations are thought to have occurred.

5.4. References

Boucot, A.J.; Xu, C., Scotese, C.R., and Morley, R.J., 2013, Phanerozoic Paleoclimate: An Atlas of Lithologic Indicators of Climate: SEPM Concepts in Sedimentology and Paleontology, v. No. 11.

Catuneanu, O., Wopfner, H., Eriksson, P.G., Cairncross, B., Rubidge, B.S., Smith, R.M.H., and Hancox, P.J., 2005, The Karoo basins of south-central Africa: Journal of African Earth Sciences, v. 43, p. 211-253.

Clark, P.U., Dyke, A.S., Shakun, J.D., Carlson, A.E., Clark, J., Wohlfarth, B., Mitrovica, J.X., Hostetler, S.W. and McCabe, A.M. (2009). The last glacial maximum. Science, 325(5941), 710-714.

Crespin, I. (1947). Foraminifera in the Permian Rocks of Australia. Australia Bureau of Mineral Resources Bulletin, 15, Paleontology Series, 5, 1-31.

Elliot, D. H. (2013). The geological and tectonic evolution of the Transantarctic Mountains: a review. Geological Society, London, Special Publications, 381(1), 7-35.

Fielding, C.R., Frank, T.D., Birgenheier, L.P., Rygel, M.C., Jones, A.T., and Roberts, J., 2008a, Stratigraphic record and facies associations of the late Paleozoic ice age in eastern Australia (New South Wales and Queensland), *in* Fielding, C.R., Frank, T., and Isbell, J.L., eds., Resolving the Late Paleozoic Ice Age in Time and Space: Boulder, Geological Society of America, Special Paper 441, p. 41-57.

Fielding, C.R., Frank, T.D., and Isbell, J.L., eds., 2008b, Resolving the Late Paleozoic Ice Age in Time and Space: Boulder, CO, Geological Society of America, Special Publication 441, 354 p.

Fielding, C. R., Frank, T. D., Isbell, J. L., Henry, L. C., & Domack, E. W. (2010). Stratigraphic signature of the late Palaeozoic Ice Age in the Parmeener Supergroup of Tasmania, SE Australia, and inter-regional comparisons. Palaeogeography, Palaeoclimatology, Palaeoecology, 298(1-2), 70-90.

Frank, T.D., Shultis, A.I., and Fielding, C.R., 2015, Acme and demise of the late Palaeozoic ice age: A view from the southeastern margin of Gondwana: Palaeogeography Palaeoclimatology Palaeoecology, v. 418, p. 176-192.

Garzanti, E. (2016). From static to dynamic provenance analysis—Sedimentary petrology upgraded. Sedimentary Geology, 336, 3-13.

Gibbs, M. T., Rees, P. M., Kutzbach, J. E., Ziegler, A. M., Behling, P. J., & Rowley, D. B. (2002). Simulations of Permian climate and comparisons with climate-sensitive sediments. The Journal of Geology, 110(1), 33-55.

Hjelstuen, B. O., & Sejrup, H. P. (2021). Latitudinal variability in the Quaternary development of the Eurasian ice sheets—Evidence from the marine domain. Geology, 49(3), 346-351.

Isbell, J. L., Lenaker, P. A., Askin, R. A., Miller, M. F., & Babcock, L. E. (2003). Reevaluation of the timing and extent of late Paleozoic glaciation in Gondwana: Role of the Transantarctic Mountains. Geology, 31(11), 977-980.

Jones, A.T., Frank, T.D., and Fielding, C.R., 2006, Cold climate in the eastern Australian mid to late Permian may reflect cold upwelling waters: Palaeogeography, Palaeoclimatology, Palaeoecology, v. 237, p. 370-377.

López-Gamundí, O.R., Espejo, I.S., Conaghan, P.J., Powell, C.M., and Veevers, J.J., 1994, Southern South America: Memoir - Geological Society of America, v. 184, p. 281-329.

López Gamundí, O. R., 1997. Glacial-postglacial transition in the late Paleozoic basins of Southern South America. In: Martini, I. P. (Ed.), Late glacial and postglacial environmental changes: Quaternary, Carboniferous-Permian, and Proterozoic, Oxford, U.K., Oxford University Press, 147–168.

Lowry, D. P., Poulsen, C. J., Horton, D. E., Torsvik, T. H., & Pollard, D. (2014). Thresholds for Paleozoic ice sheet initiation. Geology, 42(7), 627-630.

Miller, M. F., & Isbell, J. L. (2010). Reconstruction of a high-latitude, postglacial lake: Mackellar Formation (Permian), Transantarctic Mountains. Late Paleozoic glacial events and postglacial transgressions in Gondwana, 468, 193-207.

Montañez, I. P., & Poulsen, C. J. (2013). The Late Paleozoic ice age: an evolving paradigm. Annual Review of Earth and Planetary Sciences, 41, 629-656.

Ottesen, D., Batchelor, C. L., Dowdeswell, J. A., & Løseth, H. (2018). Morphology and pattern of Quaternary sedimentation in the North Sea Basin (52–62 N). Marine and Petroleum Geology, 98, 836-859.

Pangaro, F., and Ramos, V.A., 2012, Paleozoic crustal blocks of onshore and offshore central Argentina: New pieces of the southwestern Gondwana collage and their role in the accretion of Patagonia and the evolution of Mesozoic south Atlantic sedimentary basins: Marine and Petroleum Geology, v. 37, p. 162-183.

Ramos, V.A., 2008, Patagonia: a Paleozoic continent adrift?: Journal of South American Earth Sciences, v. 26, p. 235-251.

Ramos, V.A.C., F.; Naipauer, M.; Pazos, P.J., 2014, A provenance study of the Paleozoic Ventania System (Argentina): Transient complex sources from Western and Eastern Gondwana.: Gondwana Research, v. 26, p. 719-740.

Richey, J. D., Montañez, I. P., Goddéris, Y., Looy, C. V., Griffis, N. P., & DiMichele, W. A. (2020). Influence of temporally varying weatherability on CO 2-climate coupling and ecosystem change in the late Paleozoic. Climate of the Past, 16(5), 1759-1775.

Rygel, M. C., Fielding, C. R., Frank, T. D., & Birgenheier, L. P. (2008). The magnitude of Late Paleozoic glacioeustatic fluctuations: a synthesis. Journal of Sedimentary Research, 78(8), 500-511.

Veevers, J.J., and Tewari, R.C., 1995, Gondwana master basin of Peninsular India between Tethys and the interior of the Gondwanaland province of Pangea: Memoir Geological Society of America Memoir 187, p. 72.

Veevers, J.J., 2006, Updated Gondwana (Permian–Cretaceous) earth history of Australia: Gondwana Research, v. 9, p. 231-260.

Wopfner, H., 2012, Late Palaeozoic-Early Triassic deposition and climates between Samfrau and Tethys; a review: Geological Society Special Publications, v. 376, p. 5-32, 29.

Zellers, S. D., & Lagoe, M. B. (1994). Stratigraphic and seismic analysis of offshore Yakataga Formation sections, Northeast Gulf of Alaska. In 1992 Proceedings, International Conference on Arctic Margins: Anchorage, Alaska, September 1992 (Vol. 94, No. 40, p. 111). US Department of the Interior, Minerals Management Service, Alaska Outer Continental Shelf Region.

APPENDICIES

Appendix A: Site Descriptions and Flow Directions

A.1. Mt. Munson

The Pagoda Fm at Mt. Munson is ~5 m thick, and is an example of (Isbell et al. 2008c)'s Basin Margin FA. This observation contradicts those of Coates (1985), who described a 30 m-deep, steep-sided channel filled with Pagoda Fm sediments. A thorough, on-the-ground investigation of this site found that the "channel" described by Coates was more likely a significant debris-shoot/talus slope with boulders of diamictite up to 5m-wide. None of the boulders of diamictite or other sedimentary lithologies within the talus slope were unequivocally *in situ* and could not be traced laterally. A near-vertical fault that runs through Mt. Munson (Miller et al. 2010) may have created conditions that could account for Coates' observations of channel walls.

At Mt. Munson, the massive diamictite of the Pagoda Fm overlies striated and polished Queen Maud granitoids and has a sharp upper contact with the Mackellar Fm. Striations on the underlying bedrock are oriented both north-south and east-west. The vergence of folds within a slump within the Mackellar Fm at this location include measurements of 109°, 104°, and 114° (Table 2-2). Current-transport directions from asymmetrical ripples in the Lower Mackellar Fm indicated flow towards 157° ± 28.5° just above the contact with the Pagoda Fm and 109° ± 20.0° for up to 48 m above the Mackellar Fm's lower contact.

A.2. Mt. Butters

Five sedimentary sections were measured on the Mt. Butters Massif, four at site MB-17 and one at site MBSE-17 (Table 2-4; Fig. 2- 10). MB-17, and MBSE-17 are located ~2 km apart, MB-17 is located north of MBSE-17. Massive diamictites are the dominant facies in the Pagoda Fm at both sites, but the upper Pagoda Fm is comprised of different current-transported facies at each location.

At each location, the Pagoda Fm is underlain by Queen Maud granitoids (Borg 1983) and has a sharp upper contact with the Mackellar Fm. At both sites, the lowest 5 m of the Mackellar Fm contain out-sized clasts of similar composition to those within the Pagoda Fm diamictites. All sites described at Mt. Butters are examples of Isbell et al. (2004)'s Basin Margin FA. In the Shackleton Glacier Area, including locations on the Mt. Butter's massif, the Pagoda Fm is absent and Mackellar Fm laps directly on to basement rocks (La Prade 1970; Isbell et al. 1997a; Isbell 1999). Based on the thickness of the Pagoda Fm sections described at the Mt. Butters Massif both in this paper, La Prade (1970), Coates (1985), and Isbell (1999) the relief on the Maya Erosional Surface within the Massif was on the order of 100 – 200m.

A.2.1. MB-17A and MB-17B

These sections describe the basal 5 -7 m of the Pagoda Fm at MB-17 consisted of the Basal Fine-Grain-Dominated FA (Fig. 2- 6). The surface of the basement at site MB-17 underlying these facies dips uniformly towards 262° (strike 352°) with a dip angle of 11° (Table 2-2). Symmetrical ripple crests in these units are oriented at 346° ± 6.0° indicating that the orientation of wave energy in this lake environment locally paralleled the coast (Table 2-2, Fig. 2- 11). The internal slickenlines in the over-compacted portion of the BFG4 facies are oriented 006° - 186°.

A.2.2. MB-17C and D

Section MB-17C was measured through the bulk of the Pagoda Fm at this site (Fig. 2- 10). This section contains ~73 m of Massive Diamictite FA, overlain by ~10 m of Heterolitic Agglomeration Facies Association. The vergence of soft-sediment deformation features within the massive diamictite indicate transport directions within the diamictite. Near the base of section MB-17C (12 – 20 m), shear planes of sand "pods" indicate shear directions toward ~220° - 256° (Table 2-2). Shear planes beneath a thick, mass-transport deposit toward the top of the section (~58 m) indicate shear

directions range from 191° – 243° (Table 2-2). Within the Heterolitic Agglomeration FA current transport orientations are scattered. The transport directions of asymmetrical ripples are scattered around north, ranging from 055° - 236°, with a Fisher mean orientation toward 325° (Table 2-2). Cross beds in this facies are more tightly clustered toward the west, ranging from 221° - 356°. Two wide grooves interpreted as iceberg keel marks (Fig. 2- 10) at the top of the Mixed Heterolithic FA in this section have a Fisher mean lineation of 253° - 073° (Table 2-2). All grooves (N = 5) shallow toward the west.

A.2.3. MBSE-17

Section MBSE-17 was measured at a separate locale than the previous four Mt. Butters sites. The Pagoda Fm here is ~75 m thick. The Pagoda Fm overlies striated and polished granitoids and has a sharp contact with the overlying Mackellar Fm. The massive diamictite FA at the base of the Pagoda Fm is ~55 m thick here. The Pagoda Fm at this site also includes ~10 m inter-bedded stratified diamictite and discontinuous, sorted material that has been extensively deformed, which underlies an erosional contact with cross-bedded, channelized sands (CBS). Striations on the underlying granite are oriented ~314° - 134°. Large (~5 m long) thrust faults within the massive diamictite have vergence towards 263°, parallel to the paleoslope. Current transport directions in the CBS facies are towards 208°± 29°.

A.3. Reid Spur

The section measured and described at Reid Spur (RSP-18) contains ~60 m of Pagoda Fm. The base of this section was not exposed in outcrop, but isopach maps of the region suggest that the thickness of the Pagoda Fm here is ~100 m (Isbell et al. 1997b). The basement lithologies are likely metasandstones and schists of the Beardmore Group (Fig. 2- 1B). The upper contact of the Pagoda Fm at Reid Spur is sharp with the overlying Mackellar Fm. The Massive Diamictite FA in this

section does not contain any sand "pods" or other indicators of soft-sediment deformation. This is the only succession to contain the Laminated Sands FA. The current direction within the turbidites of the Laminated Sands FA is towards 176°± 29° (Table 2-2). Current transport directions in the overlying Mackellar include 261°, 241°, 211°, and 281° (Table 2-2).

A.4. Flow Directions – Transantarctic Basin

A table containing flow directions from glacigenic strata in the Transantarctic Basin has not been published since Coates (1985). Table A1 is such a table, incorporating work that has been published since 1985. Summary tables are necessary in addition to maps, especially in polar regions, because due to the proximity to the pole, the apparent orientation of flow directions on maps can vary dramatically with the map projection. Flow directions from table A1 are shown in Figure A1.

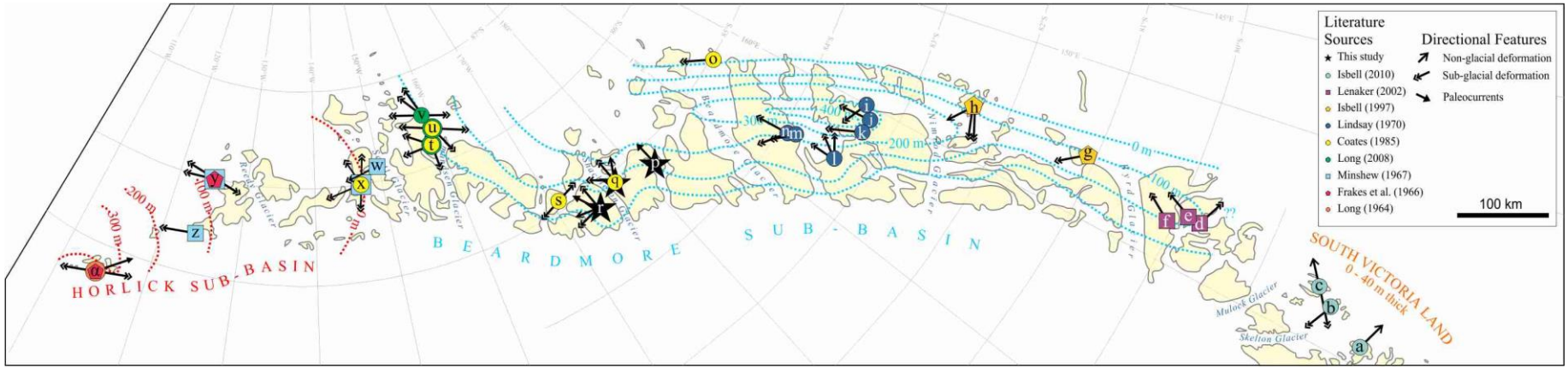

Figure- A1. Glacial transport directions from the literature and this study in the Pagoda Fm and equivalents in South Victoria Land, Beardmore Sub-basin, and Horlick Sub-basin. Directions are described in Table 4. Directions are from Long (1964b); Frakes et al. (1966); Minshew (1967); Lindsay (1970a); Coates (1985); Isbell et al. (1997b); Lenaker (2002); Long et al. (2008-2009); Isbell (2010), and this study. Isopachs are from Isbell et al. (2008c). Note how the orientation of north varies throughout the map area.

Table A1. Glacial transport directions from the literature and this study in the Pagoda Fm and equivalents in South Victoria Land, Beardmore Sub-basin, and Horlick Sub-basin. Directions are plotted in Figure 13. The orientation of magnetic/geographic north varies considerably with proximity to pole. Therefore, making direct comparisons between directional measurements is not advised. Transport direction of bi-directional features (striae) typically inferred from flow directions in adjacent or overlying strata. Data at Mt. Munson from Isbell (unpublished) are previously unpublished measurements that were collected during the 1995 field season, and from Mt. Weaver were measured during the 2017-2018 field season by Ives. This table includes data from Long (1964a); Frakes et al. (1966); Minshew (1967); Lindsay (1970a); Coates (1985); Isbell et al. (1997b); Lenaker (2002); Isbell (2010).

* = measured from figure, not reported in text

Point	Location	Study	Flow Orientation	Sedimentary Structure
a	Kennar Valley	Isbell (2010)	252° (toward), N=8	Large-scale thrust sheets
b	Mt. Metschel	Isbell (2010)	126° (toward), N=11	Deforming bed transport
c	Mt. Ritchie	Isbell (2010)	063° (toward), N=4 307° (toward), N=5	Deforming bed transport Large-scale thrust sheets
d	Colosseum Ridge CR2	Lenaker (2002)	294°	Striated clast pavement
e	Colosseum Ridge CR4	Lenaker (2002)	206°	Striated clast pavement
f	Haven Ridge	Lenaker (2002)	218°	Striated surface
g	Wallabies Nun.	Isbell (1997)	145˚	Striated clast pavement marks
h	Geologist's Range Mt Csejtey Sullivan Nunatak Arrowhead Nun.	Isbell (1997)	 074˚ 068˚ 129˚	 Striae on basement Striae on basement Grooves on mass transport
i	Moore Mtns Section P	Lindsay (1970)	114°	Soft-sediment grooves
j	Section V	Lindsay (1970)	184° ± 2°, N=3	Striated, Polished, Grooved surface
k	Section N	Lindsay (1970)	*156°	Grooved surface
l	Mt. Miller	Lindsay (1970) Section K	182° ± 5° (oldest) 148° ± 4° (younger) 123° ± 6° (younger)	Grooves in basement Striae Striae
m	Mt. Mackellar Section I	Lindsay (1970)	*132°	Grooved surface
n	Mt. Mackellar Sections ABCD	Lindsay (1970)	188°, 123°	Pebble fabrics and boulder pavements
o	Buckley Island	Coates (1985)	144°	Grooves and striae on Alexandra Fm
p	Reid Spur	this study	176˚	Mean current direction in grounding-line fan
q	Mt. Butters *locations combined on map*	Coates (1985) this study	180° 186° 215°, 205° 131°, 136°	Elongate hump on granite surface Slickenside lineation in facies BFG4 iceberg keel gouges Striae on granitic basement

r	Mt. Munson	this study	180°	Striae on polished granite
		this study (1997)	095°	Striae on granite (N= 8)
s	Mt. Smithson	Coates (1985)	*262°, *251°	Grooves in tillite, craig and tail structures
t	Crown Mountain	Coates (1985)	*180°	Striae on metavolcanic bedrock
	Section 16	Long et al. (2008)	130°, 090°	Fabrics of elongate pebbles and boulders at base
u	Roaring Valley	Long et al. (2008)	115°	Grooves on bedrock
	Kutschin Peak	Coates (1985)	*155°	Striae on basement with beveling upstream
v	Crack Bluff Sections 12 & 13	Long et al. (2008)	110°, 150°. 165°	Striae, grooves, crescent marks, & r. moutonnée
w	Mt. Blackburn	Minshew (1967)	075°	roche moutonnée, nail and chatter marks on bedrock
x	Watson	Coates (1985)	160°	Orientation if roche moutonnée
	Escarpment		156°, 189°	Striae on basement
		Minshew (1967)	075°, 070°	roche moutonnée, nail and chatter marks on bedrock
y	Tillite Spur	Minshew (1967)	089°	
	Wisconsin Range	Frakes et al. (1966)	*288°	Striae on bedrock and boulder pavements
z	Mt. LeSchack	Minshew (1967)	086° ± 35	Plucked surfaces, nail markings, clast fabrics
α	Discovery Ridge	Frakes et al. (1966)	*255°	Straited & plucked boulders, bedrock gouges & striae
			*227°	Paleocurrent directions (cross beds)
	Discovery Ridge & other locals	Long (1964b)	075°	Grooves and striae from “many levels”

--- Non glacial flow directions plotted on Fig. 2- 13 Map --

r	Mt. Munson	this study	109°	Slump vergence
		this study (1997)	157°	Current ripples 0 – 4 m above Mackellar Base
		this study (1997)	109˚	Current ripple 4- 48 m above Mackellar Base

Appendix B. Detrital Zircon U-Pb Data

Table 0-1. WYN17-1 detrital zircon U-Pb geochronologic analyses

WYN17-1. U-Pb geochronologic analyses.																			
							Isotope ratios						Apparent ages (Ma)						
Analysis	U	206Pb	U/Th	206Pb*	±	207Pb*	±	206Pb*	±	error	206Pb*	±	207Pb*	±	206Pb*	±	Best age	±	Conc
	(ppm)	204Pb		207Pb*	(%)	235U*	(%)	238U	(%)	corr.	238U*	(Ma)	235U	(Ma)	207Pb*	(Ma)	(Ma)	(Ma)	(%)
-WYN17-1 Spot 158	246	15608	24.9	14.8011	1.1	0.8915	2.0	0.0957	1.7	0.83	589.4	9.4	647.2	9.6	854.2	23.1	589.4	9.4	91.1
-WYN17-1 Spot 37	188	5341	2.1	19.6808	2.9	0.3549	3.1	0.0507	1.0	0.32	318.7	3.1	308.4	8.3	231.2	67.9	318.7	3.1	103.3
-WYN17-1 Spot 175	191	7726	1.6	18.9669	2.0	0.4108	2.5	0.0565	1.5	0.61	354.5	5.2	349.5	7.3	315.9	44.7	354.5	5.2	101.5
-WYN17-1 Spot 149	751	1032	2.4	9.9713	1.8	0.7898	2.3	0.0571	1.4	0.59	358.2	4.7	591.1	10.2	1628.6	34.2	358.2	4.7	60.6
-WYN17-1 Spot 221	155	27038	1.9	18.3623	1.5	0.4425	2.0	0.0590	1.4	0.70	369.3	5.1	372.0	6.4	389.1	32.8	369.3	5.1	99.3
-WYN17-1 Spot 29	514	18969	2.8	18.5554	1.2	0.4397	2.0	0.0592	1.6	0.79	370.7	5.6	370.0	6.1	365.6	27.1	370.7	5.6	100.2
-WYN17-1 Spot 31	216	21549	2.5	18.6469	1.1	0.4384	1.6	0.0593	1.2	0.75	371.4	4.5	369.1	5.1	354.5	24.2	371.4	4.5	100.6
-WYN17-1 Spot 8	407	6722	3.6	15.9346	2.9	0.5133	3.3	0.0593	1.6	0.49	371.7	5.9	420.7	11.5	699.0	61.9	371.7	5.9	88.3
-WYN17-1 Spot 154	441	30606	2.2	18.6185	1.1	0.4421	1.8	0.0597	1.4	0.79	374.0	5.1	371.8	5.5	357.9	24.5	374.0	5.1	100.6
-WYN17-1 Spot 202	497	37994	2.4	17.9996	1.1	0.4590	1.7	0.0600	1.3	0.75	375.3	4.7	383.6	5.5	433.7	25.3	375.3	4.7	97.8
-WYN17-1 Spot 108	416	59771	1.2	18.7468	1.1	0.4417	2.1	0.0601	1.7	0.84	376.2	6.3	371.5	6.5	342.4	25.8	376.2	6.3	101.3
-WYN17-1 Spot 243	328	20690	1.7	18.5647	1.3	0.4477	2.0	0.0603	1.5	0.76	377.5	5.7	375.7	6.4	364.4	30.2	377.5	5.7	100.5
-WYN17-1 Spot 220	262	14286	2.4	18.5964	1.2	0.4473	1.9	0.0604	1.5	0.77	377.8	5.4	375.4	6.0	360.6	27.4	377.8	5.4	100.6
-WYN17-1 Spot 233	390	32276	2.5	18.6572	1.4	0.4551	2.3	0.0616	1.8	0.80	385.4	6.9	380.8	7.2	353.3	30.5	385.4	6.9	101.2
-WYN17-1 Spot 77	242	7077	0.9	18.7228	1.1	0.4904	1.6	0.0666	1.2	0.75	415.7	4.9	405.2	5.4	345.3	24.1	415.7	4.9	102.6
-WYN17-1 Spot 255	227	7134	1.3	18.0015	1.0	0.6034	1.7	0.0788	1.4	0.81	489.0	6.4	479.4	6.5	433.5	22.3	489.0	6.4	102.0
-WYN17-1 Spot 85	150	17637	1.3	17.7817	1.3	0.6132	1.9	0.0791	1.4	0.73	490.9	6.6	485.6	7.4	460.8	29.3	490.9	6.6	101.1
-WYN17-1 Spot 256	98	4001	2.0	18.6148	1.2	0.5907	1.9	0.0798	1.5	0.77	494.8	7.0	471.3	7.1	358.4	27.1	494.8	7.0	105.0
-WYN17-1 Spot 305	218	60707	2.0	17.2644	1.5	0.6389	2.1	0.0800	1.5	0.71	496.4	7.1	501.7	8.2	525.9	31.9	496.4	7.1	98.9
-WYN17-1 Spot 248	302	31148	3.4	16.9746	1.1	0.6500	1.8	0.0801	1.4	0.79	496.4	6.7	508.5	7.1	562.9	23.6	496.4	6.7	97.6
-WYN17-1 Spot 112	102	47771	1.9	17.2502	1.0	0.6399	2.0	0.0801	1.7	0.87	496.7	8.3	502.3	7.9	527.7	21.9	496.7	8.3	98.9
-WYN17-1 Spot 203	61	5286	2.3	18.2604	2.6	0.6047	3.1	0.0801	1.7	0.54	496.8	8.0	480.2	11.8	401.6	57.7	496.8	8.0	103.5
-WYN17-1 Spot 106	385	168352	2.3	17.7018	1.1	0.6255	1.7	0.0803	1.3	0.75	498.2	6.0	493.3	6.5	470.8	24.3	498.2	6.0	101.0
-WYN17-1 Spot 290	162	6992	1.8	17.6712	1.6	0.6408	2.1	0.0822	1.5	0.69	509.0	7.2	502.8	8.5	474.6	34.5	509.0	7.2	101.2
-WYN17-1 Spot 179	189	11944	2.0	17.1926	0.9	0.6592	1.9	0.0822	1.6	0.86	509.5	7.8	514.1	7.5	535.0	20.4	509.5	7.8	99.1
-WYN17-1 Spot 307	34	3526	25.4	18.3279	1.9	0.6299	2.4	0.0838	1.5	0.64	518.5	7.6	496.0	9.5	393.3	41.7	518.5	7.6	104.5
-WYN17-1 Spot 275	48	8653	2.4	17.6812	1.5	0.6575	2.2	0.0844	1.6	0.73	522.1	8.1	513.1	8.9	473.3	33.2	522.1	8.1	101.7
-WYN17-1 Spot 72	367	81556	1.9	17.1478	1.0	0.6788	1.6	0.0845	1.3	0.79	522.6	6.3	526.0	6.5	540.7	21.5	522.6	6.3	99.4
-WYN17-1 Spot 3	445	112336	2.7	17.0057	0.9	0.6852	1.7	0.0845	1.4	0.83	523.2	7.1	529.9	7.0	558.9	20.7	523.2	7.1	98.7
-WYN17-1 Spot 236	191	87576	1.8	16.6802	1.3	0.7001	2.1	0.0847	1.7	0.80	524.3	8.6	538.9	8.9	600.9	27.8	524.3	8.6	97.3
-WYN17-1 Spot 267	393	69047	2.2	17.2401	1.0	0.6807	2.0	0.0851	1.8	0.87	526.8	8.9	527.2	8.4	529.0	22.2	526.8	8.9	99.9
-WYN17-1 Spot 134	14	2047	1.4	18.8766	4.5	0.6218	4.7	0.0852	1.3	0.27	526.9	6.5	491.0	18.3	326.8	102.4	526.9	6.5	107.3
-WYN17-1 Spot 216	170	25274	1.9	17.4441	1.1	0.6790	1.8	0.0859	1.4	0.79	531.5	7.3	526.2	7.5	503.2	24.9	531.5	7.3	101.0
-WYN17-1 Spot 145	315	102607	2.0	17.1416	1.1	0.6921	1.9	0.0861	1.5	0.81	532.3	7.8	534.1	7.8	541.5	24.3	532.3	7.8	99.7
-WYN17-1 Spot 207	25	3283	2.4	17.6765	4.3	0.6717	4.6	0.0862	1.5	0.32	532.7	7.5	521.8	18.7	473.9	96.2	532.7	7.5	102.1
-WYN17-1 Spot 81	28	2831	57.6	19.0902	1.8	0.6221	2.3	0.0862	1.4	0.60	532.8	7.2	491.1	9.0	301.1	42.1	532.8	7.2	108.5
-WYN17-1 Spot 13	204	40770	2.5	17.2884	0.9	0.6890	1.4	0.0864	1.1	0.79	534.4	5.7	532.2	5.8	522.8	19.0	534.4	5.7	102.2
-WYN17-1 Spot 54	201	28955	3.6	17.0211	1.1	0.7005	1.7	0.0865	1.3	0.78	534.9	6.9	539.1	7.2	556.9	23.7	534.9	6.9	96.0

-WYN17-1 Spot 178	212	315522	9.1	16.8554	1.1	0.7084	1.6	0.0866	1.2	0.72	535.6	6.1	543.8	6.9	578.2	24.7	535.6	6.1	92.6
-WYN17-1 Spot 130	159	11996	2.8	17.7024	1.4	0.6758	1.8	0.0868	1.1	0.63	536.6	5.8	524.2	7.3	470.7	30.7	536.6	5.8	102.4
-WYN17-1 Spot 26	207	112011	2.4	17.1474	1.0	0.7050	1.4	0.0877	1.0	0.69	542.0	5.1	541.7	6.0	540.8	22.4	542.0	5.1	100.2
-WYN17-1 Spot 5	508	49657	1.5	17.2859	1.0	0.7011	1.8	0.0879	1.6	0.85	543.3	8.2	539.4	7.7	523.1	20.9	543.3	8.2	103.9
-WYN17-1 Spot 92	323	9231	2.4	17.5370	0.8	0.6912	1.5	0.0880	1.3	0.85	543.4	6.8	533.5	6.4	491.5	18.2	543.4	6.8	101.9
-WYN17-1 Spot 231	154	7125	0.7	17.5062	1.3	0.6933	2.1	0.0881	1.6	0.77	544.1	8.3	534.8	8.6	495.3	28.8	544.1	8.3	101.7
-WYN17-1 Spot 303	43	4888	1.7	17.4445	2.8	0.6974	3.3	0.0883	1.8	0.55	545.3	9.4	537.2	13.7	503.1	60.6	545.3	9.4	101.5
-WYN17-1 Spot 47	242	30416	2.7	16.9979	1.2	0.7176	2.0	0.0885	1.6	0.79	546.7	8.4	549.2	8.6	559.9	27.2	546.7	8.4	97.6
-WYN17-1 Spot 148	201	58249	2.9	17.0367	1.2	0.7179	1.9	0.0887	1.5	0.77	548.1	7.7	549.4	8.0	554.9	26.2	548.1	7.7	98.8
-WYN17-1 Spot 308	355	420946	2.4	17.3042	1.3	0.7071	2.3	0.0888	1.9	0.82	548.3	9.9	543.0	9.6	520.8	28.4	548.3	9.9	101.0
-WYN17-1 Spot 282	223	202600	2.5	17.1117	0.8	0.7162	1.8	0.0889	1.5	0.88	549.1	8.1	548.4	7.5	545.3	18.5	549.1	8.1	100.7
-WYN17-1 Spot 97	208	15437	2.5	16.8961	1.0	0.7274	1.7	0.0892	1.3	0.80	550.7	7.1	555.0	7.2	573.0	22.0	550.7	7.1	96.1
-WYN17-1 Spot 101	238	19438	8.8	17.1922	1.0	0.7157	1.5	0.0893	1.1	0.74	551.2	5.8	548.1	6.3	535.0	21.8	551.2	5.8	103.0
-WYN17-1 Spot 252	28	4596	4.3	17.6213	2.3	0.6985	2.7	0.0893	1.5	0.56	551.4	8.0	537.9	11.4	480.8	50.0	551.4	8.0	102.5
-WYN17-1 Spot 69	425	50042	7.5	17.0294	0.8	0.7255	1.7	0.0897	1.6	0.89	553.5	8.3	553.9	7.4	555.9	17.0	553.5	8.3	99.6
-WYN17-1 Spot 181	479	37820	3.0	16.8274	1.0	0.7371	2.0	0.0900	1.7	0.86	555.5	9.0	560.7	8.4	581.8	21.7	555.5	9.0	95.5
-WYN17-1 Spot 300	293	18284	18.8	17.1541	1.2	0.7244	2.0	0.0902	1.6	0.79	556.5	8.4	553.3	8.5	539.9	26.9	556.5	8.4	103.1
-WYN17-1 Spot 169	53	21433	2.0	17.0252	1.5	0.7318	2.1	0.0904	1.4	0.68	557.9	7.5	557.6	8.9	556.4	33.1	557.9	7.5	100.3
-WYN17-1 Spot 142	261	35824	2.1	16.9813	1.1	0.7340	1.8	0.0904	1.4	0.79	558.1	7.5	558.9	7.6	562.0	23.8	558.1	7.5	99.3
-WYN17-1 Spot 230	103	5651	1.9	17.6938	1.3	0.7050	1.8	0.0905	1.3	0.69	558.5	6.8	541.8	7.7	471.8	29.7	558.5	6.8	103.1
-WYN17-1 Spot 139	317	33384	5.9	17.0193	1.3	0.7347	1.9	0.0907	1.4	0.75	559.9	7.6	559.3	8.2	557.2	27.5	559.9	7.6	100.5
-WYN17-1 Spot 237	58	24935	0.6	17.4141	1.7	0.7196	2.2	0.0909	1.4	0.64	561.0	7.5	550.4	9.3	506.9	37.2	561.0	7.5	101.9
-WYN17-1 Spot 78	88	16635	1.6	17.0421	1.2	0.7360	2.0	0.0910	1.6	0.78	561.5	8.4	560.1	8.6	554.2	27.2	561.5	8.4	101.3
-WYN17-1 Spot 302	160	31747	7.0	17.0973	1.0	0.7338	1.8	0.0910	1.5	0.82	561.7	7.8	558.8	7.6	547.2	22.3	561.7	7.8	102.6
-WYN17-1 Spot 259	66	13491	3.7	17.1110	1.4	0.7343	2.0	0.0912	1.4	0.71	562.4	7.5	559.1	8.5	545.4	30.5	562.4	7.5	103.1
-WYN17-1 Spot 314	407	44553	3.5	17.0479	1.1	0.7385	1.9	0.0914	1.6	0.82	563.5	8.5	561.5	8.3	553.5	23.9	563.5	8.5	101.8
-WYN17-1 Spot 75	298	25257	5.6	16.9385	1.2	0.7438	2.0	0.0914	1.5	0.78	563.9	8.3	564.6	8.5	567.5	26.6	563.9	8.3	99.4
-WYN17-1 Spot 68	65	21484	4.5	16.8275	1.7	0.7507	2.5	0.0917	1.8	0.74	565.4	9.9	568.7	10.8	581.8	36.2	565.4	9.9	97.2
-WYN17-1 Spot 289	348	47235	11.6	16.8480	1.0	0.7506	1.8	0.0918	1.5	0.84	565.9	8.2	568.6	7.8	579.2	21.0	565.9	8.2	97.7
-WYN17-1 Spot 219	239	7246	3.1	17.1893	1.2	0.7363	2.0	0.0918	1.5	0.79	566.4	8.4	560.3	8.5	535.5	26.5	566.4	8.4	101.1
-WYN17-1 Spot 23	120	21181	0.9	16.8390	1.3	0.7524	2.1	0.0919	1.6	0.77	566.9	8.6	569.6	9.0	580.3	28.2	566.9	8.6	97.7
-WYN17-1 Spot 196	301	35248	5.6	16.9434	1.1	0.7529	1.9	0.0926	1.6	0.81	570.7	8.6	569.9	8.5	566.9	24.8	570.7	8.6	100.7
-WYN17-1 Spot 190	198	8073	3.7	17.3206	1.8	0.7368	2.2	0.0926	1.4	0.62	570.8	7.6	560.5	9.6	518.7	38.4	570.8	7.6	101.8
-WYN17-1 Spot 34	866	43093	20.5	16.7156	0.8	0.7664	1.5	0.0929	1.3	0.86	573.0	7.3	577.7	6.8	596.3	16.7	573.0	7.3	96.1
-WYN17-1 Spot 74	131	24968	3.3	17.1749	1.0	0.7463	1.8	0.0930	1.5	0.85	573.3	8.5	566.1	7.9	537.3	21.1	573.3	8.5	101.3
-WYN17-1 Spot 217	94	15798	1.2	16.9131	1.3	0.7582	1.9	0.0930	1.4	0.71	573.5	7.4	573.0	8.3	570.8	29.2	573.5	7.4	100.5
-WYN17-1 Spot 118	522	63881	2.2	16.9320	1.0	0.7583	2.2	0.0932	2.0	0.89	574.2	11.0	573.0	9.8	568.4	21.8	574.2	11.0	101.0
-WYN17-1 Spot 28	181	10612	78.2	17.2879	1.0	0.7447	1.6	0.0934	1.3	0.79	575.7	7.0	565.1	6.9	522.9	21.1	575.7	7.0	101.9
-WYN17-1 Spot 45	53	5918	148.0	17.5002	1.4	0.7359	2.0	0.0934	1.4	0.70	575.9	7.6	560.0	8.5	496.1	31.0	575.9	7.6	102.8
-WYN17-1 Spot 19	284	13570	4.5	17.2742	1.0	0.7462	1.9	0.0935	1.6	0.84	576.4	8.6	566.0	8.0	524.6	21.9	576.4	8.6	101.8
-WYN17-1 Spot 156	503	150030	4.8	16.6811	1.0	0.7747	1.8	0.0938	1.6	0.85	577.7	8.7	582.4	8.2	600.7	20.9	577.7	8.7	96.2
-WYN17-1 Spot 253	817	2457805	11.8	16.7794	1.1	0.7763	1.8	0.0945	1.5	0.79	582.2	8.1	583.4	8.2	588.0	24.3	582.2	8.1	99.0
-WYN17-1 Spot 161	280	24164	3.8	16.7826	1.2	0.7777	2.0	0.0947	1.7	0.82	583.3	9.4	584.2	9.1	587.6	25.3	583.3	9.4	99.3
-WYN17-1 Spot 246	226	9395	10.0	17.2421	1.2	0.7587	2.0	0.0949	1.6	0.80	584.6	8.9	573.3	8.7	528.7	25.9	584.6	8.9	102.0
-WYN17-1 Spot 56	229	26583	2.8	16.8543	1.3	0.7762	1.8	0.0949	1.2	0.67	584.6	6.6	583.3	7.9	578.4	28.7	584.6	6.6	101.1
-WYN17-1 Spot 239	360	32562	1.8	17.0295	1.2	0.7683	1.9	0.0949	1.4	0.76	584.7	7.9	578.8	8.2	555.8	26.3	584.7	7.9	101.0
-WYN17-1 Spot 227	418	44399	8.5	16.9093	1.1	0.7739	1.8	0.0950	1.5	0.81	584.8	8.4	582.0	8.2	571.3	23.3	584.8	8.4	102.4
-WYN17-1 Spot 283	315	21628	4.8	16.7583	0.9	0.7816	1.6	0.0950	1.3	0.83	585.3	7.3	586.4	7.0	590.7	18.7	585.3	7.3	99.1
-WYN17-1 Spot 278	88	20503	0.4	16.6172	1.4	0.7887	2.1	0.0951	1.6	0.74	585.6	8.7	590.4	9.4	609.0	30.2	585.6	8.7	96.1
-WYN17-1 Spot 58	55	6396	2.8	17.2354	1.8	0.7613	2.4	0.0952	1.6	0.66	586.2	8.7	574.7	10.4	529.6	39.0	586.2	8.7	102.0
-WYN17-1 Spot 312	341	36307	4.0	17.0542	0.9	0.7715	1.7	0.0955	1.4	0.83	587.8	7.7	580.6	7.3	552.7	20.3	587.8	7.7	101.2
-WYN17-1 Spot 123	304	34348	0.7	16.3078	1.1	0.8107	2.0	0.0959	1.7	0.83	590.5	9.5	602.9	9.3	649.5	24.4	590.5	9.5	90.9
-WYN17-1 Spot 287	349	136681	1.1	16.3602	1.6	0.8109	2.0	0.0963	1.2	0.62	592.4	7.1	602.9	9.2	642.7	34.2	592.4	7.1	92.2

-WYN17-1 Spot 260	435	53845	41.2	16.6804	1.2	0.8015	2.0	0.0970	1.6	0.82	596.8	9.4	597.7	9.1	600.8	25.1	596.8	9.4	99.3
-WYN17-1 Spot 90	514	60658	4.6	16.9126	0.9	0.7939	1.6	0.0974	1.4	0.85	599.3	7.9	593.4	7.3	570.9	18.7	599.3	7.9	105.0
-WYN17-1 Spot 143	243	14233	3.1	16.5824	1.1	0.8115	1.8	0.0976	1.4	0.78	600.5	8.2	603.3	8.3	613.6	24.8	600.5	8.2	97.9
-WYN17-1 Spot 234	295	15098	0.7	17.0144	1.1	0.7968	1.6	0.0984	1.2	0.74	604.8	7.0	595.0	7.3	557.8	23.7	604.8	7.0	101.6
-WYN17-1 Spot 184	360	513509	2.8	16.6169	1.1	0.8164	1.8	0.0984	1.5	0.82	605.2	8.7	606.1	8.4	609.1	22.7	605.2	8.7	99.4
-WYN17-1 Spot 280	359	26084	3.1	16.7611	1.1	0.8119	2.0	0.0987	1.7	0.85	607.0	9.7	603.5	9.0	590.4	22.8	607.0	9.7	102.8
-WYN17-1 Spot 21	478	106599	4.2	16.9917	1.1	0.8040	2.0	0.0991	1.7	0.85	609.3	9.8	599.1	9.1	560.7	23.2	609.3	9.8	101.7
-WYN17-1 Spot 98	56	3849	0.8	17.6151	1.9	0.7765	2.3	0.0992	1.3	0.56	610.0	7.4	583.5	10.0	481.7	41.3	610.0	7.4	104.5
-WYN17-1 Spot 137	312	90834	18.5	15.4488	0.8	0.8973	1.5	0.1006	1.3	0.84	617.8	7.6	650.3	7.4	764.6	17.7	617.8	7.6	80.8
-WYN17-1 Spot 116	701	67162	16.1	16.6563	0.9	0.8488	1.6	0.1026	1.3	0.83	629.5	7.9	624.0	7.4	604.0	19.2	629.5	7.9	104.2
-WYN17-1 Spot 268	136	20057	2.0	16.2065	0.9	0.8758	1.5	0.1030	1.3	0.82	631.9	7.7	638.7	7.3	662.9	18.8	631.9	7.7	95.3
-WYN17-1 Spot 40	191	102190	1.9	16.5486	0.8	0.8578	1.8	0.1030	1.5	0.88	631.9	9.3	628.9	8.3	618.0	18.2	631.9	9.3	102.3
-WYN17-1 Spot 131	123	9484	1.4	16.4862	1.4	0.8645	1.9	0.1034	1.3	0.67	634.4	7.7	632.6	9.0	626.1	30.3	634.4	7.7	101.3
-WYN17-1 Spot 250	142	108199	0.6	16.4435	0.9	0.8767	1.5	0.1046	1.2	0.82	641.3	7.6	639.2	7.2	631.8	18.4	641.3	7.6	101.5
-WYN17-1 Spot 254	256	84180	2.7	15.5934	1.1	0.9257	1.8	0.1047	1.4	0.79	642.1	8.7	665.4	8.8	745.0	23.7	642.1	8.7	86.2
-WYN17-1 Spot 281	128	6332	2.2	16.3538	1.3	0.8838	2.0	0.1049	1.5	0.73	642.9	8.9	643.0	9.4	643.5	28.9	642.9	8.9	99.9
-WYN17-1 Spot 24	327	43729	3.7	15.7321	1.1	0.9266	1.9	0.1058	1.6	0.83	648.1	9.7	665.8	9.2	726.2	22.3	648.1	9.7	89.2
-WYN17-1 Spot 39	617	72929	2.6	16.4761	1.2	0.8931	2.1	0.1068	1.7	0.81	653.9	10.6	648.0	10.0	627.5	26.1	653.9	10.6	104.2
-WYN17-1 Spot 205	236	13031	1.6	15.7551	1.3	0.9489	1.9	0.1085	1.5	0.75	663.9	9.2	677.5	9.6	723.1	27.3	663.9	9.2	91.8
-WYN17-1 Spot 297	524	40424	4.0	16.0496	1.0	0.9319	2.0	0.1085	1.7	0.86	664.2	10.7	668.6	9.7	683.7	21.5	664.2	10.7	97.1
-WYN17-1 Spot 71	127	130630	2.7	15.8296	1.3	0.9458	2.0	0.1086	1.5	0.77	664.8	9.6	675.9	9.8	713.1	27.1	664.8	9.6	93.2
-WYN17-1 Spot 225	286	32602	2.2	15.9375	1.0	0.9433	1.7	0.1091	1.3	0.80	667.4	8.5	674.6	8.3	698.7	21.4	667.4	8.5	95.5
-WYN17-1 Spot 133	161	17400	1.4	15.7471	1.1	0.9606	1.7	0.1098	1.4	0.79	671.3	8.7	683.6	8.6	724.2	22.7	671.3	8.7	92.7
-WYN17-1 Spot 88	309	40444	2.5	15.9681	0.9	0.9512	1.6	0.1102	1.3	0.80	673.9	8.1	678.7	7.8	694.6	19.9	673.9	8.1	97.0
-WYN17-1 Spot 271	157	92776	2.4	16.1721	1.1	0.9430	2.1	0.1106	1.7	0.84	676.5	11.1	674.4	10.2	667.5	24.3	676.5	11.1	101.4
-WYN17-1 Spot 121	305	19746	5.7	15.6834	0.9	0.9763	1.5	0.1111	1.2	0.81	679.1	7.9	691.7	7.6	732.8	18.7	679.1	7.9	92.7
-WYN17-1 Spot 93	304	24224	5.3	15.8044	0.9	0.9838	1.7	0.1128	1.4	0.84	689.1	9.2	695.6	8.4	716.5	19.1	689.1	9.2	96.2
-WYN17-1 Spot 64	191	79359	5.3	15.9478	1.0	0.9899	1.8	0.1145	1.5	0.85	699.1	10.2	698.6	9.1	697.3	20.5	699.1	10.2	100.3
-WYN17-1 Spot 194	137	17357	3.4	15.4637	1.1	1.0494	2.0	0.1177	1.6	0.82	717.6	10.9	728.6	10.2	762.6	23.7	717.6	10.9	94.1
-WYN17-1 Spot 128	492	22210	4.1	15.2583	1.2	1.0831	2.1	0.1199	1.7	0.80	730.0	11.6	745.1	11.0	790.7	25.9	730.0	11.6	92.3
-WYN17-1 Spot 35	119	10243	9.1	15.4796	1.3	1.0730	1.7	0.1205	1.1	0.64	733.6	7.7	740.2	9.1	760.4	28.3	733.6	7.7	96.5
-WYN17-1 Spot 57	252	11875	4.2	15.1101	1.4	1.1076	2.1	0.1214	1.6	0.75	738.8	10.8	757.0	11.0	811.2	28.7	738.8	10.8	91.1
-WYN17-1 Spot 113	264	25488	4.1	15.7899	0.9	1.0743	2.1	0.1231	1.8	0.89	748.2	13.0	740.8	10.9	718.4	20.0	748.2	13.0	104.1
-WYN17-1 Spot 306	315	42108	1.1	15.6257	0.9	1.1005	2.1	0.1248	1.9	0.89	758.0	13.3	753.6	11.1	740.6	20.0	758.0	13.3	102.3
-WYN17-1 Spot 189	122	35792	1.8	15.3016	1.2	1.1291	1.9	0.1254	1.5	0.78	761.3	10.8	767.3	10.4	784.8	25.1	761.3	10.8	97.0
-WYN17-1 Spot 265	177	111475	12.2	14.1592	1.1	1.3055	1.9	0.1341	1.6	0.83	811.4	11.9	848.2	10.8	945.7	21.5	811.4	11.9	85.8
-WYN17-1 Spot 199	387	276719	3.4	14.3651	1.0	1.3053	2.0	0.1360	1.8	0.88	822.3	13.8	848.0	11.7	916.1	20.2	822.3	13.8	89.8
-WYN17-1 Spot 159	135	30933	1.2	14.6759	1.1	1.2994	1.9	0.1384	1.5	0.80	835.4	12.0	845.5	11.0	871.9	23.7	835.4	12.0	95.8
-WYN17-1 Spot 201	100	30331	2.2	14.1780	1.0	1.3788	1.9	0.1418	1.5	0.83	855.1	12.3	879.9	11.0	943.0	21.5	855.1	12.3	90.7
-WYN17-1 Spot 115	57	11017	3.1	14.3718	1.3	1.3701	1.9	0.1429	1.4	0.74	860.9	11.1	876.2	11.0	915.1	25.9	860.9	11.1	94.1
-WYN17-1 Spot 264	221	29616	1.5	14.5670	1.1	1.3698	2.0	0.1448	1.7	0.85	871.6	14.0	876.1	11.9	887.3	22.3	871.6	14.0	98.2
-WYN17-1 Spot 73	245	32561	1.4	14.2911	1.0	1.4319	1.7	0.1485	1.4	0.83	892.4	12.1	902.3	10.4	926.7	20.0	926.7	20.0	96.3
-WYN17-1 Spot 129	62	21453	2.4	13.9177	1.1	1.4577	1.9	0.1472	1.6	0.84	885.3	13.4	913.0	11.6	980.8	21.5	980.8	21.5	90.3
-WYN17-1 Spot 87	96	33303	2.3	13.8463	1.1	1.6834	1.7	0.1691	1.2	0.74	1007.3	11.7	1002.3	10.7	991.3	23.0	991.3	23.0	101.6
-WYN17-1 Spot 105	132	49718	2.4	13.7913	0.9	1.6092	1.6	0.1610	1.3	0.81	962.5	11.5	973.8	9.9	999.4	18.7	999.4	18.7	96.3
-WYN17-1 Spot 204	166	25088	1.6	13.7809	1.1	1.6520	2.0	0.1652	1.7	0.82	985.6	15.1	990.3	12.7	1000.9	23.0	1000.9	23.0	98.5
-WYN17-1 Spot 114	209	9381	2.6	13.7730	1.6	1.6258	2.0	0.1625	1.2	0.59	970.5	10.7	980.2	12.7	1002.1	33.2	1002.1	33.2	96.9
-WYN17-1 Spot 4	235	113167	1.9	13.7621	1.0	1.6865	1.6	0.1684	1.2	0.76	1003.3	11.5	1003.4	10.3	1003.7	21.2	1003.7	21.2	100.0
-WYN17-1 Spot 36	65	18163	1.3	13.7417	1.2	1.6555	1.7	0.1651	1.2	0.70	984.9	10.7	991.6	10.7	1006.7	24.6	1006.7	24.6	97.8
-WYN17-1 Spot 157	218	21310	2.8	13.7286	1.1	1.6338	1.5	0.1627	1.0	0.70	972.0	9.4	983.3	9.4	1008.6	21.7	1008.6	21.7	96.4
-WYN17-1 Spot 173	239	61100	5.6	13.7217	0.9	1.6768	1.5	0.1669	1.2	0.81	995.3	11.5	999.8	9.7	1009.6	18.1	1009.6	18.1	98.6
-WYN17-1 Spot 240	234	24176	6.4	13.7206	0.9	1.7951	1.9	0.1787	1.6	0.87	1059.9	15.9	1043.7	12.2	1009.8	18.5	1009.8	18.5	105.0
-WYN17-1 Spot 291	206	11136	2.6	13.7200	1.1	1.6705	2.1	0.1663	1.8	0.85	991.7	16.7	997.4	13.5	1009.9	22.6	1009.9	22.6	98.2

-WYN17-1 Spot 32	73	23952	1.2	13.7153	1.1	1.7130	1.6	0.1705	1.1	0.69	1014.7	10.2	1013.4	10.1	1010.6	23.1	1010.6	23.1	100.4
-WYN17-1 Spot 285	125	15527	1.8	13.6889	0.9	1.7945	1.5	0.1782	1.2	0.79	1057.3	11.8	1043.5	9.9	1014.5	18.7	1014.5	18.7	104.2
-WYN17-1 Spot 309	71	14272	1.7	13.6702	1.3	1.7220	2.0	0.1708	1.5	0.75	1016.6	14.1	1016.8	12.8	1017.3	26.8	1017.3	26.8	99.9
-WYN17-1 Spot 127	351	45061	3.2	13.6149	0.8	1.7567	1.9	0.1735	1.7	0.91	1031.6	16.1	1029.6	12.1	1025.5	16.1	1025.5	16.1	100.6
-WYN17-1 Spot 172	197	59079	3.7	13.6091	1.2	1.7238	1.7	0.1702	1.3	0.73	1013.3	11.7	1017.5	11.0	1026.3	23.7	1026.3	23.7	98.7
-WYN17-1 Spot 165	185	39717	1.6	13.5999	1.2	1.7182	1.7	0.1695	1.3	0.74	1009.6	11.9	1015.3	11.1	1027.7	23.6	1027.7	23.6	98.2
-WYN17-1 Spot 95	326	31447	5.5	13.5816	1.0	1.7720	1.6	0.1746	1.3	0.77	1037.5	12.1	1035.2	10.6	1030.4	21.0	1030.4	21.0	100.7
-WYN17-1 Spot 136	364	97697	3.3	13.5522	0.8	1.8052	1.5	0.1775	1.2	0.83	1053.4	12.1	1047.3	9.8	1034.8	16.8	1034.8	16.8	101.8
-WYN17-1 Spot 76	365	291031	4.3	13.5331	0.8	1.7561	1.5	0.1724	1.3	0.85	1025.5	12.4	1029.4	10.0	1037.6	16.4	1037.6	16.4	98.8
-WYN17-1 Spot 144	112	22911	3.1	13.5203	1.0	1.7462	1.6	0.1713	1.3	0.80	1019.3	12.3	1025.7	10.6	1039.6	19.9	1039.6	19.9	98.0
-WYN17-1 Spot 62	193	32317	7.3	13.4913	1.2	1.8461	2.0	0.1807	1.6	0.81	1070.9	15.9	1062.0	13.1	1043.9	23.7	1043.9	23.7	102.6
-WYN17-1 Spot 52	164	22968	2.7	13.4710	0.9	1.8856	1.6	0.1843	1.4	0.83	1090.5	13.6	1076.1	10.9	1047.0	18.5	1047.0	18.5	104.2
-WYN17-1 Spot 104	67	20452	2.1	13.4673	1.4	1.8485	2.0	0.1806	1.4	0.72	1070.4	14.1	1062.9	13.0	1047.5	27.6	1047.5	27.6	102.2
-WYN17-1 Spot 187	227	37474	2.9	13.4596	0.9	1.8542	1.7	0.1811	1.5	0.86	1072.9	14.6	1064.9	11.4	1048.7	17.9	1048.7	17.9	102.3
-WYN17-1 Spot 44	377	81709	1.7	13.4480	1.0	1.8053	1.9	0.1762	1.6	0.85	1045.9	15.2	1047.4	12.1	1050.4	19.8	1050.4	19.8	99.6
-WYN17-1 Spot 42	347	141607	2.8	13.4459	0.9	1.8690	1.4	0.1823	1.1	0.78	1079.8	10.8	1070.2	9.2	1050.7	17.5	1050.7	17.5	102.8
-WYN17-1 Spot 11	441	66868	3.3	13.4185	0.9	1.7895	1.8	0.1742	1.6	0.87	1035.4	15.4	1041.6	12.0	1054.8	18.3	1054.8	18.3	98.2
-WYN17-1 Spot 258	139	12470	1.6	13.3860	1.0	1.8683	1.6	0.1815	1.2	0.77	1075.0	12.1	1069.9	10.5	1059.7	20.4	1059.7	20.4	101.4
-WYN17-1 Spot 170	57	250866	1.9	13.3529	1.1	1.9179	1.9	0.1858	1.5	0.82	1098.7	15.4	1087.3	12.4	1064.7	21.6	1064.7	21.6	103.2
-WYN17-1 Spot 61	384	124084	1.7	13.3400	1.0	1.8744	2.2	0.1814	2.0	0.89	1074.8	19.4	1072.1	14.6	1066.6	20.4	1066.6	20.4	100.8
-WYN17-1 Spot 214	414	38318	2.8	13.3230	1.1	1.9346	1.8	0.1870	1.5	0.80	1105.2	14.9	1093.1	12.3	1069.2	22.4	1069.2	22.4	103.4
-WYN17-1 Spot 86	238	85720	3.3	13.2967	1.1	1.8624	1.6	0.1797	1.2	0.76	1065.2	12.1	1067.8	10.7	1073.2	21.1	1073.2	21.1	99.3
-WYN17-1 Spot 82	197	64665	2.2	13.2894	1.2	1.9314	1.7	0.1862	1.2	0.71	1101.0	12.5	1092.0	11.6	1074.3	24.4	1074.3	24.4	102.5
-WYN17-1 Spot 160	179	24929	2.2	13.2387	0.9	1.8278	1.7	0.1756	1.4	0.84	1042.8	13.5	1055.5	11.0	1081.9	18.0	1081.9	18.0	96.4
-WYN17-1 Spot 195	189	10825	2.1	13.2367	0.9	1.8650	2.0	0.1791	1.8	0.90	1062.2	17.4	1068.8	13.1	1082.3	17.7	1082.3	17.7	98.1
-WYN17-1 Spot 206	388	4972036	4.7	13.2266	1.0	1.7773	1.7	0.1706	1.3	0.78	1015.2	12.2	1037.2	10.8	1083.8	20.8	1083.8	20.8	93.7
-WYN17-1 Spot 293	91	30692	2.1	13.2086	1.2	1.8559	1.9	0.1779	1.5	0.78	1055.3	14.9	1065.5	12.9	1086.5	24.3	1086.5	24.3	97.1
-WYN17-1 Spot 223	46	14782	2.5	13.1992	1.2	1.7856	2.0	0.1710	1.5	0.77	1017.7	14.3	1040.2	12.7	1087.9	24.8	1087.9	24.8	93.5
-WYN17-1 Spot 120	131	18337	2.0	13.1635	0.8	1.9011	1.3	0.1816	1.1	0.82	1075.6	10.9	1081.5	8.9	1093.4	15.4	1093.4	15.4	98.4
-WYN17-1 Spot 174	258	37316	2.5	13.1154	0.9	1.9796	1.6	0.1884	1.3	0.84	1112.6	13.5	1108.6	10.6	1100.7	17.1	1100.7	17.1	101.1
-WYN17-1 Spot 269	241	114377	5.0	13.1022	0.9	1.9026	1.6	0.1809	1.2	0.80	1071.7	12.3	1082.0	10.4	1102.7	18.9	1102.7	18.9	97.2
-WYN17-1 Spot 152	541	53257	14.2	13.0389	1.0	1.9278	1.8	0.1824	1.4	0.82	1080.0	14.4	1090.8	11.8	1112.4	20.0	1112.4	20.0	97.1
-WYN17-1 Spot 147	278	35274	7.5	12.9720	0.9	1.9576	1.6	0.1843	1.3	0.81	1090.2	12.9	1101.1	10.6	1122.6	18.4	1122.6	18.4	97.1
-WYN17-1 Spot 168	170	23988	2.4	12.9626	1.1	1.9841	1.6	0.1866	1.2	0.74	1103.0	12.1	1110.1	10.9	1124.1	21.8	1124.1	21.8	98.1
-WYN17-1 Spot 132	239	15149	1.2	12.9587	0.9	2.0828	1.6	0.1958	1.3	0.82	1152.9	13.4	1143.1	10.6	1124.7	17.7	1124.7	17.7	102.5
-WYN17-1 Spot 262	141	15720	1.8	12.9395	1.0	1.9767	2.0	0.1856	1.7	0.86	1097.4	17.4	1107.6	13.5	1127.6	20.2	1127.6	20.2	97.3
-WYN17-1 Spot 59	309	67856	22.7	12.7847	0.8	2.1167	1.6	0.1964	1.4	0.87	1155.7	15.1	1154.3	11.3	1151.6	15.8	1151.6	15.8	100.4
-WYN17-1 Spot 50	89	12934	2.1	12.7705	1.4	2.1960	1.8	0.2035	1.2	0.66	1194.0	13.1	1179.8	12.7	1153.8	27.0	1153.8	27.0	103.5
-WYN17-1 Spot 218	185	54207	2.3	12.7582	0.9	2.0537	1.8	0.1901	1.6	0.86	1122.0	16.0	1133.5	12.3	1155.7	18.0	1155.7	18.0	97.1
-WYN17-1 Spot 84	145	35617	2.4	12.7209	0.9	2.1356	1.6	0.1971	1.3	0.82	1159.8	13.5	1160.4	10.8	1161.5	17.8	1161.5	17.8	99.9
-WYN17-1 Spot 176	266	36823	8.8	12.6265	1.1	2.2254	1.7	0.2039	1.3	0.77	1196.1	14.4	1189.1	11.9	1176.3	21.4	1176.3	21.4	101.7
-WYN17-1 Spot 224	142	86164	1.8	12.5666	1.0	2.2046	1.8	0.2010	1.4	0.81	1180.8	15.5	1182.5	12.3	1185.7	20.2	1185.7	20.2	99.6
-WYN17-1 Spot 276	127	19723	1.9	12.5228	1.3	2.2165	1.9	0.2014	1.4	0.73	1182.8	15.3	1186.3	13.5	1192.5	26.0	1192.5	26.0	99.2
-WYN17-1 Spot 274	139	14221	1.7	12.5205	1.0	2.2892	1.9	0.2080	1.6	0.86	1218.0	18.3	1209.0	13.5	1192.9	19.1	1192.9	19.1	102.1
-WYN17-1 Spot 80	433	32716	1.1	12.5125	1.0	2.3592	2.1	0.2142	1.9	0.88	1251.1	21.1	1230.3	15.1	1194.1	19.8	1194.1	19.8	104.8
-WYN17-1 Spot 235	249	149193	1.9	12.5120	1.0	2.2550	1.9	0.2047	1.6	0.86	1200.6	17.7	1198.4	13.3	1194.3	19.3	1194.3	19.3	100.5
-WYN17-1 Spot 146	111	50727	1.4	12.4779	1.1	2.1798	1.7	0.1974	1.3	0.76	1161.1	14.0	1174.6	12.1	1199.6	22.2	1199.6	22.2	96.8
-WYN17-1 Spot 30	131	111081	2.2	12.4043	0.9	2.2629	1.6	0.2037	1.3	0.82	1195.0	14.4	1200.8	11.3	1211.3	18.2	1211.3	18.2	98.7
-WYN17-1 Spot 153	293	69118	9.2	12.3846	1.1	2.2424	1.6	0.2015	1.3	0.77	1183.4	13.7	1194.4	11.6	1214.4	20.8	1214.4	20.8	97.4
-WYN17-1 Spot 198	123	268302	1.3	12.3799	1.1	2.2968	1.6	0.2063	1.1	0.72	1209.2	12.3	1211.3	11.1	1215.2	21.5	1215.2	21.5	99.5
-WYN17-1 Spot 99	60	29402	2.2	12.3657	1.3	2.2499	1.8	0.2019	1.3	0.72	1185.3	13.9	1196.8	12.6	1217.4	24.6	1217.4	24.6	97.4
-WYN17-1 Spot 294	187	1526316	1.5	12.3459	1.0	2.3136	1.8	0.2073	1.5	0.83	1214.2	16.6	1216.5	12.9	1220.5	20.0	1220.5	20.0	99.5
-WYN17-1 Spot 245	29	19038	1.7	12.3010	1.4	2.3876	2.4	0.2131	1.9	0.81	1245.3	21.6	1238.9	16.9	1227.7	27.4	1227.7	27.4	101.4

-WYN17-1 Spot 229	294	61576	1.7	12.2879	0.8	2.2980	1.4	0.2049	1.1	0.81	1201.5	12.5	1211.7	10.0	1229.8	16.2	1229.8	16.2	97.7
-WYN17-1 Spot 67	110	26659	1.0	12.2867	0.8	2.2702	1.5	0.2024	1.3	0.86	1188.1	14.1	1203.1	10.7	1230.0	15.2	1230.0	15.2	96.6
-WYN17-1 Spot 126	168	141099	2.8	12.2716	1.1	2.4040	1.8	0.2141	1.5	0.81	1250.4	16.6	1243.8	12.9	1232.4	20.8	1232.4	20.8	101.5
-WYN17-1 Spot 0	298	96110	4.0	12.1691	1.0	2.2737	1.4	0.2008	1.0	0.71	1179.4	10.8	1204.2	10.0	1248.9	19.5	1248.9	19.5	94.4
-WYN17-1 Spot 186	35	31250	2.9	12.0296	1.2	2.4402	2.0	0.2130	1.5	0.79	1244.7	17.5	1254.5	14.2	1271.4	23.7	1271.4	23.7	97.9
-WYN17-1 Spot 171	238	6094	3.0	12.0110	3.1	2.1826	3.6	0.1902	1.9	0.52	1122.5	19.6	1175.5	25.2	1274.4	60.2	1274.4	60.2	88.1
-WYN17-1 Spot 313	93	25242	2.1	12.0033	0.9	2.4382	1.5	0.2123	1.2	0.80	1241.3	13.4	1253.9	10.7	1275.6	17.6	1275.6	17.6	97.3
-WYN17-1 Spot 96	128	15126	1.8	11.9159	1.0	2.6505	2.0	0.2292	1.7	0.87	1330.1	20.7	1314.8	14.6	1289.9	18.8	1289.9	18.8	103.1
-WYN17-1 Spot 103	53	24952	1.6	11.7921	0.9	2.6921	1.8	0.2303	1.5	0.87	1336.3	18.4	1326.3	13.0	1310.2	16.9	1310.2	16.9	102.0
-WYN17-1 Spot 33	67	23820	2.7	11.6301	0.9	2.6401	1.8	0.2228	1.6	0.86	1296.6	18.4	1311.9	13.5	1337.0	18.2	1337.0	18.2	97.0
-WYN17-1 Spot 200	83	9073	1.6	11.0753	1.1	3.1945	2.4	0.2567	2.2	0.90	1473.0	28.7	1455.8	18.8	1430.8	20.6	1430.8	20.6	102.9
-WYN17-1 Spot 242	34	24614	1.9	11.0512	1.4	3.0357	2.1	0.2434	1.7	0.78	1404.5	21.0	1416.7	16.4	1435.0	25.8	1435.0	25.8	97.9
-WYN17-1 Spot 182	234	38167	2.1	11.0329	1.2	2.9832	1.6	0.2388	1.1	0.70	1380.5	14.2	1403.3	12.4	1438.2	22.2	1438.2	22.2	96.0
-WYN17-1 Spot 298	267	38932	1.4	11.0205	1.1	3.1519	1.9	0.2520	1.6	0.83	1449.0	20.6	1445.5	14.8	1440.3	20.5	1440.3	20.5	100.6
-WYN17-1 Spot 292	60	15890	0.7	11.0034	1.4	3.0210	2.2	0.2412	1.7	0.76	1392.9	20.7	1412.9	16.5	1443.3	26.8	1443.3	26.8	96.5
-WYN17-1 Spot 277	58	83497	2.1	11.0017	1.2	3.0106	1.8	0.2403	1.4	0.75	1388.4	17.4	1410.3	14.1	1443.6	23.1	1443.6	23.1	96.2
-WYN17-1 Spot 288	193	61733	2.2	10.9836	1.1	3.1933	1.8	0.2545	1.5	0.79	1461.6	19.0	1455.5	14.2	1446.7	21.2	1446.7	21.2	101.0
-WYN17-1 Spot 244	390	146311	2.1	10.8766	1.1	3.2034	1.7	0.2528	1.4	0.79	1452.9	17.9	1458.0	13.4	1465.3	20.2	1465.3	20.2	99.2
-WYN17-1 Spot 9	113	110389	1.6	10.6990	0.9	3.3154	1.4	0.2574	1.1	0.77	1476.4	13.9	1484.7	10.7	1496.5	16.6	1496.5	16.6	98.7
-WYN17-1 Spot 215	244	274596	2.5	10.2375	0.8	3.4983	1.5	0.2599	1.2	0.82	1489.1	16.1	1526.8	11.7	1579.5	15.8	1579.5	15.8	94.3
-WYN17-1 Spot 177	153	633259	2.0	10.1341	0.8	3.8289	1.5	0.2815	1.2	0.83	1599.1	17.7	1598.8	12.1	1598.4	15.5	1598.4	15.5	100.0
-WYN17-1 Spot 18	170	409212	3.2	10.1239	0.7	3.7687	1.4	0.2768	1.3	0.88	1575.4	17.6	1586.1	11.4	1600.3	12.4	1600.3	12.4	98.4
-WYN17-1 Spot 162	346	450887	7.5	10.0878	0.9	3.9709	1.6	0.2906	1.3	0.81	1644.8	18.4	1628.3	12.8	1607.0	17.3	1607.0	17.3	102.4
-WYN17-1 Spot 284	25	5538	1.1	9.9807	1.5	3.9435	2.2	0.2856	1.6	0.74	1619.4	23.5	1622.7	18.1	1626.9	28.1	1626.9	28.1	99.5
-WYN17-1 Spot 22	247	199332	0.7	9.9599	0.8	3.8920	1.7	0.2813	1.5	0.89	1597.7	21.6	1612.0	13.9	1630.7	14.8	1630.7	14.8	98.0
-WYN17-1 Spot 238	99	49733	1.7	9.8542	1.0	3.9644	1.8	0.2835	1.5	0.82	1608.7	20.9	1626.9	14.5	1650.5	19.1	1650.5	19.1	97.5
-WYN17-1 Spot 241	161	45540	1.7	9.6656	1.0	3.5098	1.7	0.2461	1.4	0.80	1418.6	17.3	1529.4	13.5	1686.3	18.9	1686.3	18.9	84.1
-WYN17-1 Spot 49	205	304273	0.8	9.6069	0.8	3.5736	1.5	0.2491	1.3	0.85	1433.8	16.6	1543.7	12.0	1697.5	14.7	1697.5	14.7	84.5
-WYN17-1 Spot 222	231	89928	1.7	9.5131	0.9	4.2785	1.5	0.2953	1.2	0.79	1668.1	17.4	1689.2	12.4	1715.6	16.9	1715.6	16.9	97.2
-WYN17-1 Spot 38	335	106022	1.5	9.4882	0.9	4.3121	1.9	0.2969	1.6	0.87	1675.8	24.2	1695.7	15.6	1720.4	17.4	1720.4	17.4	97.4
-WYN17-1 Spot 125	616	1480876	5.0	9.4824	0.9	4.0687	2.0	0.2799	1.8	0.90	1591.1	25.6	1648.1	16.5	1721.5	16.4	1721.5	16.4	92.4
-WYN17-1 Spot 270	283	27247	1.3	9.4727	0.9	4.1731	2.1	0.2868	1.9	0.90	1625.6	27.0	1668.7	17.0	1723.4	16.4	1723.4	16.4	94.3
-WYN17-1 Spot 111	270	250269	2.4	9.4289	0.9	4.5534	1.6	0.3115	1.4	0.85	1748.2	21.3	1740.8	13.6	1731.9	15.9	1731.9	15.9	100.9
-WYN17-1 Spot 257	363	33354	1.8	9.4281	0.8	4.2266	1.6	0.2891	1.4	0.87	1637.2	20.6	1679.2	13.5	1732.1	15.2	1732.1	15.2	94.5
-WYN17-1 Spot 135	43	5357	1.9	9.4007	1.0	4.5314	1.8	0.3091	1.5	0.84	1736.2	23.4	1736.7	15.3	1737.4	18.3	1737.4	18.3	99.9
-WYN17-1 Spot 43	170	36468	1.9	9.3595	0.9	4.5836	1.5	0.3113	1.2	0.82	1747.0	19.1	1746.3	12.6	1745.4	15.7	1745.4	15.7	100.1
-WYN17-1 Spot 91	261	39096	2.3	9.3399	1.0	4.7001	1.8	0.3185	1.5	0.82	1782.5	23.0	1767.3	15.1	1749.3	19.1	1749.3	19.1	101.9
-WYN17-1 Spot 247	120	50411	2.2	9.3229	1.0	4.3961	1.5	0.2974	1.2	0.77	1678.3	17.2	1711.6	12.5	1752.6	17.7	1752.6	17.7	95.8
-WYN17-1 Spot 180	99	20104	1.1	9.3068	1.0	4.3307	1.6	0.2924	1.3	0.79	1653.7	18.8	1699.2	13.5	1755.8	18.4	1755.8	18.4	94.2
-WYN17-1 Spot 107	140	22457	3.8	9.2526	0.9	4.8247	1.7	0.3239	1.4	0.83	1808.8	22.0	1789.2	14.2	1766.4	17.4	1766.4	17.4	102.4
-WYN17-1 Spot 263	41	319544	1.9	9.2381	1.0	4.7825	1.7	0.3206	1.3	0.79	1792.5	21.0	1781.8	14.3	1769.3	19.1	1769.3	19.1	101.3
-WYN17-1 Spot 232	142	37664	2.5	9.2341	0.9	4.6818	1.4	0.3137	1.0	0.76	1758.8	15.8	1764.0	11.3	1770.1	16.1	1770.1	16.1	99.4
-WYN17-1 Spot 151	66	92370	1.8	9.1958	1.1	4.6886	1.9	0.3128	1.6	0.82	1754.7	23.9	1765.2	15.8	1777.7	19.5	1777.7	19.5	98.7
-WYN17-1 Spot 89	503	209635	2.4	9.1919	0.7	4.8805	1.7	0.3255	1.5	0.90	1816.6	23.9	1798.9	14.2	1778.5	13.5	1778.5	13.5	102.1
-WYN17-1 Spot 16	265	246332	3.0	9.1771	0.8	4.8302	1.4	0.3216	1.2	0.84	1797.7	18.9	1790.2	12.0	1781.4	14.1	1781.4	14.1	100.9
-WYN17-1 Spot 2	365	12503	1.3	9.1765	1.0	3.7744	1.9	0.2513	1.7	0.87	1445.2	21.7	1587.3	15.5	1781.5	17.4	1781.5	17.4	81.1
-WYN17-1 Spot 138	151	481080	3.6	9.1762	0.9	4.7965	1.6	0.3194	1.3	0.82	1786.6	19.9	1784.3	13.1	1781.6	16.1	1781.6	16.1	100.3
-WYN17-1 Spot 261	87	32725	1.3	9.1709	1.0	4.7013	1.5	0.3128	1.2	0.78	1754.7	18.2	1767.5	12.8	1782.6	17.5	1782.6	17.5	98.4
-WYN17-1 Spot 15	272	58055	1.8	9.1637	1.0	4.7279	1.6	0.3144	1.2	0.78	1762.1	19.0	1772.2	13.3	1784.1	18.1	1784.1	18.1	98.8
-WYN17-1 Spot 273	176	35908	1.4	9.1449	1.0	4.6352	2.0	0.3076	1.7	0.86	1728.7	26.3	1755.6	16.8	1787.8	18.7	1787.8	18.7	96.7
-WYN17-1 Spot 296	322	39038	5.2	9.1341	0.9	4.6486	1.7	0.3081	1.5	0.86	1731.3	22.3	1758.0	14.3	1790.0	15.9	1790.0	15.9	96.7
-WYN17-1 Spot 70	150	101761	2.2	9.1291	0.8	4.7792	1.7	0.3166	1.5	0.88	1773.0	23.0	1781.3	14.2	1791.0	14.7	1791.0	14.7	99.0
-WYN17-1 Spot 79	105	28521	2.0	9.1110	0.9	4.7144	1.7	0.3117	1.4	0.84	1748.9	21.4	1769.8	14.0	1794.6	16.6	1794.6	16.6	97.5

-WYN17-1 Spot 299	174	30050	2.6	9.0773	1.4	4.4322	2.1	0.2919	1.6	0.77	1651.1	23.5	1718.4	17.4	1801.3	24.6	1801.3	24.6	91.7
-WYN17-1 Spot 183	204	160727	4.4	9.0654	1.0	4.8153	1.7	0.3167	1.3	0.80	1773.8	20.5	1787.6	14.0	1803.7	18.3	1803.7	18.3	98.3
-WYN17-1 Spot 266	92	25766	2.1	9.0437	0.9	4.7571	1.8	0.3122	1.6	0.88	1751.3	24.1	1777.4	15.0	1808.1	15.7	1808.1	15.7	96.9
-WYN17-1 Spot 210	136	101858	0.9	9.0380	1.1	4.8363	1.8	0.3172	1.4	0.78	1775.8	21.4	1791.2	14.9	1809.2	20.3	1809.2	20.3	98.2
-WYN17-1 Spot 301	147	89237	2.4	9.0102	0.9	4.8317	1.7	0.3159	1.4	0.85	1769.6	22.0	1790.4	14.1	1814.8	16.3	1814.8	16.3	97.5
-WYN17-1 Spot 213	114	4402779	2.6	8.9791	0.7	4.8761	1.4	0.3177	1.2	0.86	1778.4	18.4	1798.1	11.6	1821.1	12.9	1821.1	12.9	97.7
-WYN17-1 Spot 272	71	8260	1.3	8.9450	1.3	5.0525	1.9	0.3279	1.4	0.72	1828.3	21.9	1828.2	16.3	1828.0	24.3	1828.0	24.3	100.0
-WYN17-1 Spot 209	153	193528	12.1	8.9365	0.9	5.2157	1.6	0.3382	1.4	0.84	1878.0	22.3	1855.2	13.9	1829.7	16.2	1829.7	16.2	102.6
-WYN17-1 Spot 197	166	17827	1.8	8.8787	0.9	5.0812	1.7	0.3273	1.4	0.84	1825.5	22.3	1833.0	14.2	1841.5	16.4	1841.5	16.4	99.1
-WYN17-1 Spot 212	118	53392	0.9	8.8057	1.0	5.1834	1.6	0.3312	1.2	0.79	1844.1	19.9	1849.9	13.4	1856.4	17.5	1856.4	17.5	99.3
-WYN17-1 Spot 20	162	28395	2.8	8.7997	0.7	5.2878	1.4	0.3376	1.2	0.85	1875.2	18.9	1866.9	11.7	1857.6	13.2	1857.6	13.2	100.9
-WYN17-1 Spot 228	128	24106	2.5	8.7909	1.1	5.2576	1.8	0.3354	1.5	0.79	1864.3	23.5	1862.0	15.6	1859.4	20.1	1859.4	20.1	100.3
-WYN17-1 Spot 63	44	19085	2.0	8.7551	1.2	5.3875	2.1	0.3422	1.7	0.82	1897.4	27.7	1882.9	17.6	1866.8	21.1	1866.8	21.1	101.6
-WYN17-1 Spot 102	62	26836	9.4	8.6807	1.0	5.3993	1.6	0.3401	1.3	0.80	1887.0	20.7	1884.7	13.6	1882.2	17.2	1882.2	17.2	100.3
-WYN17-1 Spot 166	404	98765	5.4	8.5741	0.8	5.4831	1.6	0.3411	1.3	0.85	1892.0	21.8	1898.0	13.4	1904.4	14.8	1904.4	14.8	99.3
-WYN17-1 Spot 122	87	31230675	2.0	8.2894	0.9	5.8322	1.8	0.3508	1.5	0.86	1938.4	25.7	1951.2	15.4	1964.8	16.0	1964.8	16.0	98.7
-WYN17-1 Spot 110	467	295768	3.3	8.1753	1.0	5.6527	1.9	0.3353	1.6	0.85	1864.1	26.3	1924.2	16.4	1989.5	17.6	1989.5	17.6	93.7
-WYN17-1 Spot 10	706	3286	3.4	8.1595	0.9	5.2035	2.0	0.3081	1.7	0.88	1731.2	26.3	1853.2	16.7	1993.0	16.4	1993.0	16.4	86.9
-WYN17-1 Spot 83	341	494883	2.9	8.1059	0.9	6.0576	1.7	0.3563	1.5	0.86	1964.5	24.9	1984.2	14.9	2004.7	15.6	2004.7	15.6	98.0
-WYN17-1 Spot 41	128	271904	2.2	7.6041	0.9	6.8705	1.7	0.3791	1.5	0.85	2072.0	26.3	2094.9	15.4	2117.4	16.0	2117.4	16.0	97.9
-WYN17-1 Spot 249	122	20030	1.7	7.1386	1.0	8.0274	1.7	0.4158	1.4	0.83	2241.3	27.3	2234.1	15.7	2227.5	16.7	2227.5	16.7	100.6
-WYN17-1 Spot 100	158	378206	3.4	6.8971	0.8	8.5567	1.6	0.4282	1.4	0.87	2297.7	26.6	2292.0	14.4	2286.9	13.4	2286.9	13.4	100.5
-WYN17-1 Spot 51	301	218513	1.5	6.8871	0.8	7.8249	1.6	0.3910	1.4	0.87	2127.6	25.3	2211.1	14.4	2289.4	13.5	2289.4	13.5	92.9
-WYN17-1 Spot 211	302	213782	1.1	6.8834	1.1	8.2873	1.9	0.4139	1.5	0.80	2232.8	28.5	2262.9	17.1	2290.3	19.5	2290.3	19.5	97.5
-WYN17-1 Spot 12	150	61307	1.8	6.8718	0.8	8.6379	1.5	0.4307	1.2	0.83	2308.9	23.9	2300.6	13.5	2293.2	14.1	2293.2	14.1	100.7
-WYN17-1 Spot 1	222	259716	7.3	6.7951	0.9	8.6271	1.6	0.4254	1.4	0.83	2284.7	26.3	2299.4	15.0	2312.5	15.8	2312.5	15.8	98.8
-WYN17-1 Spot 192	36	19104	1.0	6.5284	1.0	9.1870	1.5	0.4352	1.2	0.78	2329.0	23.4	2356.8	14.1	2380.9	16.5	2380.9	16.5	97.8
-WYN17-1 Spot 124	336	98665	2.5	6.4527	0.9	8.8777	1.7	0.4157	1.4	0.85	2240.7	27.4	2325.5	15.5	2400.8	15.2	2400.8	15.2	93.3
-WYN17-1 Spot 193	83	37260	1.3	6.3679	0.9	9.0372	1.6	0.4176	1.4	0.85	2249.4	26.1	2341.8	14.9	2423.3	14.7	2423.3	14.7	92.8
-WYN17-1 Spot 310	372	24522	2.8	6.2543	1.0	9.0490	1.9	0.4106	1.6	0.85	2217.9	29.8	2343.0	17.1	2453.8	16.8	2453.8	16.8	90.4
-WYN17-1 Spot 17	215	32250	5.6	6.1752	1.0	10.2092	2.0	0.4574	1.8	0.88	2428.2	35.8	2453.9	18.7	2475.2	16.3	2475.2	16.3	98.1
-WYN17-1 Spot 25	196	448060	3.7	6.1201	0.9	10.3312	1.5	0.4588	1.2	0.82	2434.1	25.2	2464.9	14.0	2490.4	14.4	2490.4	14.4	97.7
-WYN17-1 Spot 141	225	133206	1.3	6.0186	0.7	10.6352	1.3	0.4644	1.1	0.84	2459.1	22.3	2491.8	12.1	2518.5	12.0	2518.5	12.0	97.6
-WYN17-1 Spot 109	475	668409	2.7	5.7328	0.9	10.3003	1.7	0.4285	1.4	0.84	2298.8	27.7	2462.1	15.7	2599.9	15.4	2599.9	15.4	88.4
-WYN17-1 Spot 286	310	1041879	42.4	5.4310	1.1	13.1043	1.7	0.5164	1.3	0.78	2683.9	28.9	2687.2	15.9	2689.7	17.5	2689.7	17.5	99.8
-WYN17-1 Spot 155	68	39193	1.4	5.4168	1.1	12.9080	1.7	0.5073	1.4	0.80	2645.2	30.0	2673.0	16.4	2694.0	17.4	2694.0	17.4	98.2
-WYN17-1 Spot 251	79	36599	2.0	5.3484	1.0	13.2124	1.7	0.5127	1.3	0.79	2668.3	29.4	2694.9	16.1	2715.0	17.1	2715.0	17.1	98.3
-WYN17-1 Spot 53	100	26534	3.1	5.1652	0.9	13.0425	1.5	0.4888	1.1	0.77	2565.5	24.0	2682.7	13.8	2772.3	15.3	2772.3	15.3	92.5
-WYN17-1 Spot 6	75	48796	3.4	5.1570	0.9	13.4832	1.6	0.5045	1.3	0.82	2633.2	29.2	2714.1	15.5	2774.9	15.2	2774.9	15.2	94.9
-WYN17-1 Spot 66	35	11719	1.7	5.1561	0.9	15.1678	2.0	0.5675	1.8	0.90	2897.4	42.1	2825.8	19.1	2775.2	14.5	2775.2	14.5	104.4
-WYN17-1 Spot 295	145	158413	1.6	4.9688	1.0	14.5693	1.9	0.5253	1.6	0.85	2721.5	35.1	2787.5	17.6	2835.7	15.7	2835.7	15.7	96.0
-WYN17-1 Spot 119	266	2472205	21.0	4.8550	0.9	15.3876	1.5	0.5421	1.3	0.83	2792.1	28.5	2839.5	14.5	2873.4	14.0	2873.4	14.0	97.2
-WYN17-1 Spot 226	249	110428	2.3	4.6417	1.0	16.7245	1.7	0.5633	1.4	0.83	2880.1	33.5	2919.2	16.6	2946.2	15.6	2946.2	15.6	97.8
-WYN17-1 Spot 208	84	146820	2.4	4.4642	0.9	17.7736	1.6	0.5757	1.4	0.83	2931.2	31.9	2977.6	15.7	3009.0	14.7	3009.0	14.7	97.4
-WYN17-1 Spot 7	917	428	7.6	6.0407	1.9	2.1115	2.8	0.0925	2.1	0.74	570.6	11.5	1152.6	19.5	2512.4	31.8	2512.4	31.8	22.7
-WYN17-1 Spot 149	751	1032	2.4	9.9713	1.8	0.7898	2.3	0.0571	1.4	0.59	358.2	4.7	591.1	10.2	1628.6	34.2	358.2	4.7	60.6
-WYN17-1 Spot 150	19	2018	2.7	18.9191	2.9	0.6868	3.2	0.0943	1.4	0.44	580.8	7.9	530.8	13.4	321.7	66.4	580.8	7.9	180.5
-WYN17-1 Spot 304	28	1815	4.9	19.3845	1.8	0.6635	2.6	0.0933	1.8	0.71	575.1	9.9	516.7	10.4	266.2	41.6	575.1	9.9	216.1

Table 0-2. WYN17-2 detrital zircon U-Pb geochronologic analyses

WYN17-2. U-Pb geochronologic analyses.																			
							Isotope ratios						Apparent ages (Ma)						
Analysis	U	206Pb	U/Th	206Pb*	±	207Pb*	±	206Pb*	±	error	206Pb*	±	207Pb*	±	206Pb*	±	Best age	±	Conc
	(ppm)	204Pb		207Pb*	(%)	235U*	(%)	238U	(%)	corr.	238U*	(Ma)	235U	(Ma)	207Pb*	(Ma)	(Ma)	(Ma)	(%)
-WYN17-2 Spot 34	366	86904	1.3	17.8736	0.9	0.4471	1.7	0.0580	1.5	0.85	363.3	5.2	375.2	5.4	449.3	20.2	363.3	5.2	96.8
-WYN17-2 Spot 282	275	367365	1.9	18.3061	1.0	0.4442	1.6	0.0590	1.2	0.77	369.6	4.4	373.2	5.0	396.0	23.2	369.6	4.4	99.0
-WYN17-2 Spot 90	100	45184	2.5	18.4037	1.7	0.4472	2.3	0.0597	1.5	0.68	373.9	5.6	375.3	7.2	384.0	37.8	373.9	5.6	99.6
-WYN17-2 Spot 64	204	34303	2.6	18.1153	1.2	0.4561	1.9	0.0600	1.5	0.77	375.3	5.5	381.6	6.2	419.4	27.8	375.3	5.5	98.4
-WYN17-2 Spot 255	310	30908	2.7	18.2892	1.1	0.4522	1.9	0.0600	1.5	0.81	375.7	5.6	378.8	6.0	398.0	24.9	375.7	5.6	99.2
-WYN17-2 Spot 66	259	22602	2.9	18.4792	1.1	0.4481	1.8	0.0601	1.4	0.79	376.1	5.1	375.9	5.6	374.8	25.0	376.1	5.1	100.0
-WYN17-2 Spot 190	509	59691	2.4	18.3772	1.2	0.4528	1.9	0.0604	1.5	0.79	377.9	5.5	379.2	5.9	387.3	25.8	377.9	5.5	99.7
-WYN17-2 Spot 96	284	16227	3.0	18.7472	1.2	0.4447	1.5	0.0605	1.0	0.65	378.6	3.6	373.6	4.7	342.4	26.1	378.6	3.6	101.4
-WYN17-2 Spot 125	285	10896	2.5	18.6611	1.2	0.4476	1.8	0.0606	1.4	0.75	379.3	5.0	375.6	5.7	352.8	27.1	379.3	5.0	101.0
-WYN17-2 Spot 118	274	30736	3.2	18.4463	1.3	0.4551	2.1	0.0609	1.7	0.81	381.2	6.4	380.8	6.8	378.8	28.4	381.2	6.4	100.1
-WYN17-2 Spot 185	493	40520	3.2	18.4701	1.0	0.4548	1.9	0.0610	1.6	0.85	381.4	6.1	380.7	6.1	375.9	23.0	381.4	6.1	100.2
-WYN17-2 Spot 80	279	56003	2.0	18.2469	1.4	0.4619	2.0	0.0612	1.5	0.75	382.6	5.7	385.6	6.6	403.2	30.3	382.6	5.7	99.2
-WYN17-2 Spot 79	484	10421	3.2	15.4995	2.8	0.5449	3.2	0.0613	1.6	0.50	383.4	6.0	441.6	11.4	757.7	58.3	383.4	6.0	86.8
-WYN17-2 Spot 225	638	80960	2.5	18.5316	1.0	0.4587	1.6	0.0617	1.3	0.81	385.8	4.9	383.3	5.1	368.5	21.4	385.8	4.9	100.6
-WYN17-2 Spot 21	656	3360196	1.9	18.0032	1.1	0.4826	1.8	0.0630	1.4	0.77	394.1	5.3	399.9	5.9	433.3	25.1	394.1	5.3	98.6
-WYN17-2 Spot 170	261	9395	2.5	18.4424	1.2	0.4980	2.0	0.0666	1.6	0.80	415.9	6.4	410.3	6.7	379.3	26.8	415.9	6.4	109.6
-WYN17-2 Spot 181	155	31219	1.7	17.3977	1.3	0.6145	1.9	0.0776	1.3	0.72	481.6	6.2	486.4	7.2	509.0	28.7	481.6	6.2	94.6
-WYN17-2 Spot 294	269	27004	1.6	17.1143	1.1	0.6315	1.8	0.0784	1.4	0.79	486.7	6.5	497.0	6.9	545.0	23.6	486.7	6.5	89.3
-WYN17-2 Spot 194	180	11849	1.5	17.7364	1.5	0.6152	2.3	0.0792	1.8	0.77	491.1	8.4	486.8	9.0	466.5	33.1	491.1	8.4	105.3
-WYN17-2 Spot 183	257	15676	3.0	18.0193	1.0	0.6153	1.8	0.0804	1.5	0.82	498.8	7.1	486.9	7.0	431.3	23.2	498.8	7.1	115.7
-WYN17-2 Spot 292	240	6778	1.6	16.0529	1.5	0.6909	2.0	0.0805	1.4	0.68	499.0	6.5	533.3	8.3	683.3	31.1	499.0	6.5	73.0
-WYN17-2 Spot 97	403	22793	1.6	17.8054	0.9	0.6254	1.5	0.0808	1.2	0.81	500.9	5.7	493.2	5.7	457.8	19.4	500.9	5.7	109.4
-WYN17-2 Spot 86	290	17874	1.3	17.4865	1.1	0.6380	1.8	0.0810	1.4	0.79	501.8	6.7	501.1	7.0	497.8	23.9	501.8	6.7	100.8
-WYN17-2 Spot 201	126	48874	1.9	17.3222	1.4	0.6536	2.4	0.0821	2.0	0.82	508.9	9.6	510.7	9.6	518.5	30.1	508.9	9.6	98.1
-WYN17-2 Spot 273	406	49352	2.1	17.5766	1.1	0.6444	1.9	0.0822	1.5	0.81	509.1	7.4	505.0	7.5	486.4	24.5	509.1	7.4	104.7
-WYN17-2 Spot 143	500	16506	2.8	17.7809	0.9	0.6405	1.5	0.0826	1.3	0.83	511.8	6.3	502.6	6.1	460.9	19.0	511.8	6.3	111.1
-WYN17-2 Spot 213	854	21768	4.5	17.0262	0.9	0.6714	1.8	0.0829	1.6	0.87	513.6	7.8	521.5	7.4	556.2	19.1	513.6	7.8	92.3

-WYN17-2 Spot 91	203	97829	0.8	17.4568	1.5	0.6553	2.1	0.0830	1.5	0.69	514.0	7.3	511.7	8.6	501.5	33.8	514.0	7.3	102.5
-WYN17-2 Spot 14	673	23903	2.5	16.7737	1.1	0.6892	2.1	0.0839	1.7	0.84	519.2	8.6	532.3	8.5	588.8	24.1	519.2	8.6	88.2
-WYN17-2 Spot 81	144	12346	65.2	17.2227	1.4	0.6732	2.0	0.0841	1.4	0.72	520.7	7.2	522.7	8.1	531.2	30.3	520.7	7.2	98.0
-WYN17-2 Spot 31	341	82798	2.4	16.8844	1.2	0.6896	2.0	0.0845	1.6	0.79	522.8	7.9	532.5	8.2	574.5	26.2	522.8	7.9	91.0
-WYN17-2 Spot 234	206	11641	2.5	17.2558	1.2	0.6812	1.8	0.0853	1.4	0.76	527.7	7.1	527.5	7.6	527.0	26.4	527.7	7.1	100.1
-WYN17-2 Spot 216	284	12091	2.4	17.2560	1.3	0.6848	2.0	0.0857	1.5	0.75	530.3	7.6	529.7	8.2	527.0	28.6	530.3	7.6	100.6
-WYN17-2 Spot 196	144	203321	1.2	16.8620	1.2	0.7050	1.9	0.0863	1.4	0.77	533.4	7.4	541.8	7.8	577.4	25.8	533.4	7.4	92.4
-WYN17-2 Spot 207	485	53918	1.9	17.3198	1.2	0.6876	1.8	0.0864	1.3	0.75	534.3	6.8	531.4	7.3	518.8	25.6	534.3	6.8	103.0
-WYN17-2 Spot 162	216	10492	3.0	17.7497	1.1	0.6720	1.6	0.0865	1.2	0.75	535.1	6.3	521.9	6.6	464.8	23.7	535.1	6.3	115.1
-WYN17-2 Spot 92	132	27717	3.0	16.7220	1.4	0.7154	1.9	0.0868	1.4	0.71	536.6	7.1	547.9	8.2	595.4	29.4	536.6	7.1	90.1
-WYN17-2 Spot 100	307	22283	18.6	17.6556	1.1	0.6783	1.7	0.0869	1.3	0.78	537.1	6.7	525.7	6.9	476.5	23.3	537.1	6.7	112.7
-WYN17-2 Spot 56	215	19121	3.0	17.0094	1.1	0.7042	1.7	0.0869	1.2	0.72	537.2	6.2	541.3	7.0	558.4	25.0	537.2	6.2	96.2
-WYN17-2 Spot 154	343	75443	2.8	17.5149	1.0	0.6840	1.7	0.0869	1.3	0.79	537.3	6.7	529.2	6.8	494.2	22.5	537.3	6.7	108.7
-WYN17-2 Spot 163	358	46281	2.4	17.4371	1.3	0.6873	1.8	0.0870	1.3	0.72	537.5	6.8	531.2	7.6	504.0	28.3	537.5	6.8	106.6
-WYN17-2 Spot 259	141	6493	230.2	16.9679	1.4	0.7176	2.1	0.0883	1.6	0.77	545.8	8.6	549.2	9.1	563.7	29.9	545.8	8.6	96.8
-WYN17-2 Spot 248	353	36595	3.6	16.8764	1.3	0.7241	2.0	0.0887	1.5	0.76	547.7	8.1	553.1	8.7	575.5	28.9	547.7	8.1	95.2
-WYN17-2 Spot 28	288	29641	1.5	17.0915	0.9	0.7161	1.5	0.0888	1.2	0.78	548.5	6.2	548.3	6.3	547.9	20.4	548.5	6.2	100.1
-WYN17-2 Spot 263	157	41134	1.5	16.6733	1.1	0.7366	1.8	0.0891	1.4	0.77	550.3	7.2	560.4	7.6	601.7	24.3	550.3	7.2	91.4
-WYN17-2 Spot 38	170	46618	2.4	16.9565	1.3	0.7261	1.9	0.0893	1.4	0.73	551.6	7.4	554.2	8.2	565.2	28.5	551.6	7.4	97.6
-WYN17-2 Spot 24	1149	613689	380.6	16.7697	0.9	0.7364	1.7	0.0896	1.5	0.87	553.2	7.9	560.3	7.4	589.3	18.7	553.2	7.9	93.9
-WYN17-2 Spot 232	452	96842	21.5	17.0686	1.2	0.7244	1.9	0.0897	1.5	0.78	553.9	7.8	553.3	8.0	550.8	25.4	553.9	7.8	100.5
-WYN17-2 Spot 300	222	48194	2.7	16.7065	1.1	0.7436	1.9	0.0901	1.5	0.82	556.4	8.1	564.5	8.1	597.4	23.4	556.4	8.1	93.1
-WYN17-2 Spot 16	30	3558	98.2	17.4137	2.1	0.7165	2.5	0.0905	1.4	0.55	558.7	7.5	548.6	10.7	506.9	46.4	558.7	7.5	110.2
-WYN17-2 Spot 70	252	56557	6.3	17.1069	1.1	0.7300	1.8	0.0906	1.4	0.79	559.2	7.6	556.6	7.7	545.9	24.4	559.2	7.6	102.4
-WYN17-2 Spot 72	234	62363	1.6	16.7104	1.2	0.7474	1.8	0.0906	1.3	0.72	559.2	6.9	566.7	7.7	597.0	26.8	559.2	6.9	93.7
-WYN17-2 Spot 242	138	29566	2.2	16.6684	1.6	0.7493	2.5	0.0906	1.9	0.76	559.2	10.1	567.8	10.8	602.4	34.8	559.2	10.1	92.8
-WYN17-2 Spot 224	252	13805	1.8	16.8550	1.3	0.7435	2.0	0.0909	1.5	0.74	561.1	7.9	564.5	8.7	578.3	29.3	561.1	7.9	97.0
-WYN17-2 Spot 48	75	13299	0.5	16.9478	1.2	0.7422	1.8	0.0913	1.3	0.73	563.1	7.2	563.7	7.9	566.3	27.0	563.1	7.2	99.4
-WYN17-2 Spot 12	271	22689	128.6	16.8393	1.4	0.7490	2.1	0.0915	1.6	0.75	564.5	8.5	567.6	9.1	580.3	29.9	564.5	8.5	97.3
-WYN17-2 Spot 36	188	101232	1.0	16.7727	1.3	0.7586	2.1	0.0923	1.7	0.78	569.2	9.0	573.2	9.3	588.9	28.7	569.2	9.0	96.7
-WYN17-2 Spot 18	218	24126	17.7	16.7925	0.9	0.7603	1.5	0.0926	1.2	0.81	571.1	6.5	574.2	6.4	586.3	18.7	571.1	6.5	97.4
-WYN17-2 Spot 63	396	29718	8.7	16.9963	1.0	0.7558	1.8	0.0932	1.5	0.82	574.5	8.3	571.6	8.0	560.1	22.7	574.5	8.3	102.6
-WYN17-2 Spot 30	412	82312	7.4	16.8450	1.0	0.7632	1.8	0.0933	1.4	0.81	574.9	7.9	575.8	7.8	579.6	22.3	574.9	7.9	99.2

-WYN17-2 Spot 46	1144	138251	12.2	16.9688	0.9	0.7619	1.6	0.0938	1.4	0.84	578.0	7.5	575.1	7.1	563.6	19.2	578.0	7.5	102.6
-WYN17-2 Spot 133	304	123615	6.1	16.7906	1.1	0.7702	2.0	0.0938	1.7	0.85	578.1	9.3	579.9	8.8	586.6	23.1	578.1	9.3	98.6
-WYN17-2 Spot 62	341	119140	1.8	16.1507	1.2	0.8010	1.8	0.0939	1.3	0.73	578.4	7.3	597.4	8.1	670.3	26.3	578.4	7.3	86.3
-WYN17-2 Spot 271	320	8781	5.1	16.9945	1.1	0.7714	1.8	0.0951	1.5	0.79	585.8	8.1	580.6	8.1	560.3	24.6	585.8	8.1	104.5
-WYN17-2 Spot 13	413	51982	1.4	16.9332	0.7	0.7772	1.5	0.0955	1.3	0.87	587.9	7.4	583.9	6.7	568.2	16.3	587.9	7.4	103.5
-WYN17-2 Spot 27	567	54743	8.0	16.7669	1.1	0.8009	2.0	0.0974	1.7	0.84	599.4	9.5	597.3	8.9	589.6	23.1	599.4	9.5	101.7
-WYN17-2 Spot 175	221	22267	7.4	16.7488	1.3	0.8064	2.2	0.0980	1.7	0.78	602.7	9.7	600.5	9.8	592.0	29.2	602.7	9.7	101.8
-WYN17-2 Spot 32	170	4466	0.7	14.4204	2.7	0.9372	3.1	0.0981	1.4	0.47	603.0	8.3	671.4	15.2	908.1	56.3	603.0	8.3	66.4
-WYN17-2 Spot 120	130	12320	0.8	16.6912	1.3	0.8124	2.0	0.0984	1.6	0.77	604.9	8.9	603.8	9.1	599.4	27.6	604.9	8.9	100.9
-WYN17-2 Spot 94	97	38484	118.4	16.5788	1.4	0.8242	2.0	0.0991	1.4	0.70	609.4	8.0	610.4	9.0	614.0	30.5	609.4	8.0	99.2
-WYN17-2 Spot 0	401	96812	8.4	16.5725	0.9	0.8280	1.7	0.0996	1.5	0.86	611.9	8.5	612.5	7.8	614.9	18.6	611.9	8.5	99.5
-WYN17-2 Spot 58	348	40108	5.1	16.2030	0.8	0.8529	1.3	0.1003	1.1	0.82	616.0	6.4	626.3	6.2	663.4	16.4	616.0	6.4	92.9
-WYN17-2 Spot 200	102	5395	16.6	14.0240	2.4	0.9860	3.2	0.1003	2.1	0.66	616.4	12.4	696.7	16.2	965.3	49.5	616.4	12.4	63.8
-WYN17-2 Spot 277	380	23072	8.4	16.9081	1.3	0.8185	2.0	0.1004	1.5	0.74	616.9	8.6	607.2	9.1	571.4	29.1	616.9	8.6	108.0
-WYN17-2 Spot 19	436	999349	2.6	16.4480	1.0	0.8482	1.6	0.1012	1.3	0.81	621.6	7.9	623.7	7.7	631.2	20.6	621.6	7.9	98.5
-WYN17-2 Spot 68	380	115614	4.8	16.9937	1.0	0.8227	1.6	0.1014	1.3	0.79	622.8	7.7	609.5	7.5	560.4	22.1	622.8	7.7	111.1
-WYN17-2 Spot 110	348	32127	2.8	16.4434	0.9	0.8631	1.8	0.1030	1.5	0.86	631.8	9.1	631.8	8.3	631.8	19.0	631.8	9.1	100.0
-WYN17-2 Spot 288	511	213357	4.7	16.0673	1.2	0.8842	2.7	0.1031	2.4	0.88	632.4	14.2	643.3	12.7	681.4	26.5	632.4	14.2	92.8
-WYN17-2 Spot 267	150	47905	4.8	16.0886	1.2	0.8838	1.7	0.1032	1.3	0.73	633.0	7.7	643.0	8.3	678.5	25.5	633.0	7.7	93.3
-WYN17-2 Spot 131	380	39979	31.6	16.3086	1.1	0.9108	1.7	0.1078	1.3	0.78	659.8	8.3	657.5	8.2	649.5	22.9	659.8	8.3	101.6
-WYN17-2 Spot 173	317	37120	2.9	16.5153	1.0	0.9019	1.5	0.1081	1.1	0.76	661.6	7.0	652.7	7.1	622.3	20.6	661.6	7.0	106.3
-WYN17-2 Spot 220	159	30723	3.3	16.0978	1.1	0.9262	1.7	0.1082	1.4	0.78	662.2	8.5	665.6	8.5	677.3	23.1	662.2	8.5	97.8
-WYN17-2 Spot 55	267	38098	4.1	15.8423	1.1	0.9474	1.6	0.1089	1.2	0.74	666.4	7.6	676.7	8.0	711.4	23.0	666.4	7.6	93.7
-WYN17-2 Spot 20	311	33842	1.6	15.8696	1.0	0.9526	1.9	0.1097	1.6	0.85	670.9	10.5	679.5	9.6	707.8	21.8	670.9	10.5	94.8
-WYN17-2 Spot 150	282	66371	3.0	16.3329	1.0	0.9276	1.9	0.1099	1.6	0.84	672.4	10.1	666.4	9.2	646.3	22.2	672.4	10.1	104.0
-WYN17-2 Spot 252	357	49551	4.6	15.9308	0.9	0.9512	1.6	0.1100	1.3	0.82	672.5	8.5	678.7	8.1	699.5	20.0	672.5	8.5	96.1
-WYN17-2 Spot 51	501	25891	40.4	15.9533	0.8	0.9505	1.9	0.1100	1.7	0.90	672.9	10.8	678.4	9.3	696.6	17.5	672.9	10.8	96.6
-WYN17-2 Spot 50	535	64665	3.2	16.1581	1.3	0.9396	2.3	0.1102	1.9	0.83	673.7	12.0	672.7	11.1	669.3	27.0	673.7	12.0	100.6
-WYN17-2 Spot 296	198	103910	3.8	15.7570	1.1	0.9694	1.8	0.1108	1.4	0.80	677.6	9.1	688.1	8.9	722.9	22.4	677.6	9.1	93.7
-WYN17-2 Spot 7	485	41007	3.5	15.7844	0.9	0.9740	1.8	0.1116	1.6	0.87	681.8	10.4	690.5	9.2	719.2	19.1	681.8	10.4	94.8
-WYN17-2 Spot 289	292	49321	3.1	14.9483	1.2	1.1111	1.9	0.1205	1.4	0.76	733.5	10.0	758.7	10.2	833.7	25.9	733.5	10.0	88.0
-WYN17-2 Spot 230	179	58908	3.2	15.1528	1.1	1.1001	1.9	0.1209	1.5	0.80	736.0	10.5	753.4	10.1	805.3	24.1	736.0	10.5	91.4
-WYN17-2 Spot 278	282	47590	11.1	15.2488	0.9	1.0992	1.7	0.1216	1.4	0.84	739.8	10.0	752.9	9.1	792.0	19.5	739.8	10.0	93.4
-WYN17-2 Spot 211	222	18054	6.0	14.8306	1.3	1.1461	2.2	0.1233	1.8	0.83	749.7	13.1	775.4	12.1	850.1	26.0	749.7	13.1	88.2

-WYN17-2 Spot 244	368	63237	5.0	14.8337	1.1	1.1608	1.7	0.1249	1.3	0.78	758.9	9.5	782.3	9.3	849.7	22.0	758.9	9.5	89.3
-WYN17-2 Spot 258	457	51361	0.5	15.0173	1.1	1.1547	1.7	0.1258	1.3	0.77	764.0	9.5	779.5	9.3	824.0	22.8	764.0	9.5	92.7
-WYN17-2 Spot 88	367	74485	4.4	14.9686	1.1	1.1590	1.8	0.1259	1.4	0.78	764.3	10.1	781.5	9.8	830.9	23.6	764.3	10.1	92.0
-WYN17-2 Spot 115	622	110357	8.1	15.2225	1.2	1.1707	2.1	0.1293	1.7	0.82	783.9	12.7	787.0	11.5	795.6	25.0	783.9	12.7	98.5
-WYN17-2 Spot 95	212	21752	0.6	15.2614	1.1	1.1913	1.8	0.1319	1.4	0.79	798.8	10.7	796.6	10.0	790.3	23.4	798.8	10.7	101.1
-WYN17-2 Spot 117	36	5572	1.1	15.2115	1.7	1.1969	2.3	0.1321	1.6	0.68	799.9	11.7	799.2	12.7	797.2	35.6	799.9	11.7	100.3
-WYN17-2 Spot 57	236	100560	3.7	14.4356	1.0	1.3097	1.7	0.1372	1.3	0.81	828.7	10.3	850.0	9.5	906.0	20.2	828.7	10.3	91.5
-WYN17-2 Spot 212	31	4193	0.6	15.0460	1.9	1.2853	2.4	0.1403	1.5	0.60	846.5	11.5	839.2	13.8	820.1	40.1	846.5	11.5	103.2
-WYN17-2 Spot 262	327	94426	4.6	14.4194	1.2	1.3477	1.7	0.1410	1.2	0.71	850.3	9.6	866.6	9.9	908.3	24.6	850.3	9.6	93.6
-WYN17-2 Spot 107	312	46132	4.2	14.2587	1.0	1.3720	1.8	0.1419	1.5	0.85	855.6	12.4	877.0	10.7	931.4	19.7	855.6	12.4	91.9
-WYN17-2 Spot 176	214	38409	4.2	14.0943	1.1	1.3889	1.9	0.1420	1.6	0.83	856.2	12.7	884.2	11.4	955.1	22.1	955.1	22.1	89.6
-WYN17-2 Spot 285	95	58264	2.6	14.0627	1.0	1.5675	2.0	0.1599	1.7	0.87	956.5	15.1	957.4	12.2	959.7	20.1	959.7	20.1	99.7
-WYN17-2 Spot 159	271	25338	1.8	14.0562	1.1	1.5002	1.9	0.1530	1.5	0.80	917.8	13.0	930.5	11.5	960.7	23.0	960.7	23.0	95.5
-WYN17-2 Spot 158	150	22575	3.8	13.9462	1.1	1.4735	1.8	0.1491	1.4	0.79	895.9	11.5	919.6	10.6	976.7	22.2	976.7	22.2	91.7
-WYN17-2 Spot 191	44	5286	2.3	13.8861	1.4	1.6354	2.0	0.1648	1.4	0.73	983.3	13.1	983.9	12.5	985.5	27.8	985.5	27.8	99.8
-WYN17-2 Spot 124	89	26461	1.8	13.8326	1.1	1.5646	1.8	0.1570	1.4	0.81	940.3	12.5	956.3	11.0	993.3	21.3	993.3	21.3	94.7
-WYN17-2 Spot 209	552	245414	5.3	13.8318	0.9	1.6613	1.6	0.1667	1.3	0.83	994.1	12.3	993.9	10.2	993.4	18.1	993.4	18.1	100.1
-WYN17-2 Spot 141	73	9621	6.2	13.8137	1.6	1.4687	2.5	0.1472	1.9	0.76	885.3	15.9	917.6	15.2	996.1	33.1	996.1	33.1	88.9
-WYN17-2 Spot 60	224	26162	2.8	13.8133	1.0	1.6937	1.6	0.1698	1.2	0.79	1010.7	11.6	1006.2	10.0	996.1	19.5	996.1	19.5	101.5
-WYN17-2 Spot 85	96	48816	1.1	13.7811	1.0	1.7216	1.7	0.1721	1.4	0.82	1023.9	13.3	1016.6	11.0	1000.9	19.6	1000.9	19.6	102.3
-WYN17-2 Spot 222	318	69248	1.7	13.7508	1.0	1.6337	1.6	0.1630	1.3	0.79	973.4	11.5	983.3	10.1	1005.3	19.9	1005.3	19.9	96.8
-WYN17-2 Spot 179	796	94442	4.7	13.7259	0.9	1.7048	1.9	0.1698	1.7	0.87	1010.9	15.7	1010.3	12.3	1009.0	19.0	1009.0	19.0	100.2
-WYN17-2 Spot 249	422	144924	4.3	13.7254	1.1	1.6671	2.4	0.1660	2.1	0.88	990.2	19.2	996.1	15.0	1009.1	22.4	1009.1	22.4	98.1
-WYN17-2 Spot 195	104	24591	3.1	13.7173	1.0	1.7782	1.6	0.1770	1.3	0.79	1050.5	12.4	1037.5	10.6	1010.3	20.3	1010.3	20.3	104.0
-WYN17-2 Spot 160	182	18280	5.5	13.7020	1.0	1.6933	1.6	0.1684	1.3	0.80	1003.0	12.2	1006.0	10.5	1012.6	20.0	1012.6	20.0	99.1
-WYN17-2 Spot 303	144	57101	3.8	13.7020	1.4	1.6728	2.1	0.1663	1.5	0.75	991.8	14.2	998.3	13.1	1012.6	27.6	1012.6	27.6	97.9
-WYN17-2 Spot 149	271	15665	2.5	13.6687	1.1	1.7680	2.0	0.1753	1.7	0.83	1041.5	16.0	1033.8	13.1	1017.5	22.9	1017.5	22.9	102.4
-WYN17-2 Spot 250	277	24716	3.9	13.6536	1.1	1.6953	1.9	0.1679	1.5	0.81	1000.8	13.9	1006.8	11.9	1019.7	22.1	1019.7	22.1	98.1
-WYN17-2 Spot 302	148	18236	1.8	13.6339	1.0	1.7685	1.7	0.1749	1.4	0.80	1039.3	13.0	1034.0	11.0	1022.6	20.8	1022.6	20.8	101.6
-WYN17-2 Spot 223	159	17415	5.1	13.6190	1.0	1.8151	1.7	0.1794	1.4	0.80	1063.5	13.4	1050.9	11.2	1024.9	20.6	1024.9	20.6	103.8
-WYN17-2 Spot 247	136	20543	2.0	13.6143	1.0	1.8121	1.8	0.1790	1.5	0.82	1061.6	14.2	1049.9	11.6	1025.6	20.7	1025.6	20.7	103.5
-WYN17-2 Spot 22	375	25774	5.3	13.6012	0.8	1.7485	3.0	0.1726	2.9	0.96	1026.2	27.5	1026.6	19.5	1027.5	17.0	1027.5	17.0	99.9
-WYN17-2 Spot 293	139	177060	3.2	13.5973	1.1	1.6852	2.0	0.1663	1.6	0.83	991.5	14.9	1002.9	12.5	1028.1	22.4	1028.1	22.4	96.4
-WYN17-2 Spot 265	400	112541	6.7	13.5519	1.0	1.7912	1.9	0.1761	1.6	0.86	1045.8	15.4	1042.2	12.1	1034.8	19.4	1034.8	19.4	101.1
-WYN17-2 Spot 93	235	24445	3.0	13.5427	1.1	1.7356	1.8	0.1705	1.5	0.82	1015.1	14.2	1021.8	11.8	1036.2	21.2	1036.2	21.2	98.0

-WYN17-2 Spot 121	50	54784	2.3	13.5322	1.4	1.7105	1.7	0.1679	1.0	0.56	1000.8	8.9	1012.5	10.9	1037.8	28.5	1037.8	28.5	96.4
-WYN17-2 Spot 44	172	72459	2.0	13.5291	1.0	1.7948	1.4	0.1762	1.0	0.74	1046.1	10.0	1043.6	9.2	1038.2	19.3	1038.2	19.3	100.8
-WYN17-2 Spot 40	489	177747	56.2	13.5280	1.0	1.6658	1.8	0.1635	1.5	0.82	976.2	13.6	995.6	11.6	1038.4	21.2	1038.4	21.2	94.0
-WYN17-2 Spot 67	153	48306	3.2	13.5116	1.1	1.8018	1.6	0.1766	1.2	0.76	1048.6	12.0	1046.1	10.7	1040.9	21.6	1040.9	21.6	100.7
-WYN17-2 Spot 59	315	114818	75.3	13.5091	1.1	1.8096	1.9	0.1774	1.5	0.80	1052.6	14.5	1048.9	12.2	1041.2	22.5	1041.2	22.5	101.1
-WYN17-2 Spot 286	501	55625	10.5	13.5076	0.9	1.8213	1.7	0.1785	1.4	0.85	1058.8	13.9	1053.1	10.9	1041.4	17.7	1041.4	17.7	101.7
-WYN17-2 Spot 306	121	112910	4.5	13.4939	1.1	1.7571	2.0	0.1720	1.6	0.83	1023.3	15.5	1029.8	12.7	1043.5	21.8	1043.5	21.8	98.1
-WYN17-2 Spot 114	377	26488	3.5	13.4652	0.9	1.8531	1.5	0.1810	1.2	0.82	1072.7	12.3	1064.5	10.0	1047.8	17.6	1047.8	17.6	102.4
-WYN17-2 Spot 215	357	45661	2.7	13.4163	1.0	1.7841	1.6	0.1737	1.3	0.80	1032.4	12.5	1039.7	10.7	1055.2	19.9	1055.2	19.9	97.8
-WYN17-2 Spot 119	164	28741	2.7	13.4120	1.1	1.8785	1.6	0.1828	1.2	0.73	1082.3	11.9	1073.5	10.8	1055.8	22.2	1055.8	22.2	102.5
-WYN17-2 Spot 8	439	609376	3.2	13.3941	1.2	1.8109	2.2	0.1760	1.9	0.85	1045.0	18.2	1049.4	14.6	1058.5	23.8	1058.5	23.8	98.7
-WYN17-2 Spot 108	458	25805	1.6	13.3767	1.2	1.6830	2.3	0.1634	1.9	0.85	975.4	17.5	1002.1	14.5	1061.1	24.5	1061.1	24.5	91.9
-WYN17-2 Spot 309	112	85999	2.8	13.3693	1.4	1.7724	1.9	0.1719	1.3	0.70	1022.8	12.6	1035.4	12.3	1062.2	27.4	1062.2	27.4	96.3
-WYN17-2 Spot 126	492	314456	24.5	13.3566	0.7	1.9519	1.9	0.1892	1.8	0.92	1116.9	18.0	1099.1	12.8	1064.1	14.9	1064.1	14.9	105.0
-WYN17-2 Spot 156	355	41657	4.5	13.3102	0.9	1.9695	1.7	0.1902	1.5	0.86	1122.5	15.1	1105.1	11.6	1071.1	17.8	1071.1	17.8	104.8
-WYN17-2 Spot 145	191	94800	3.6	13.3087	1.1	1.8679	1.9	0.1804	1.6	0.81	1069.0	15.3	1069.8	12.6	1071.4	22.4	1071.4	22.4	99.8
-WYN17-2 Spot 314	190	50200	6.0	13.3055	0.8	1.8946	1.5	0.1829	1.3	0.84	1082.8	12.6	1079.2	9.9	1071.8	16.1	1071.8	16.1	101.0
-WYN17-2 Spot 87	289	247314	3.2	13.2891	1.0	1.7534	1.6	0.1691	1.2	0.76	1007.0	11.4	1028.4	10.4	1074.3	21.0	1074.3	21.0	93.7
-WYN17-2 Spot 205	312	46439	3.8	13.2760	1.1	1.8401	2.1	0.1773	1.7	0.83	1051.9	16.7	1059.9	13.6	1076.3	23.0	1076.3	23.0	97.7
-WYN17-2 Spot 25	336	25992	1.4	13.2695	0.9	1.9132	1.3	0.1842	0.9	0.72	1089.9	9.2	1085.7	8.6	1077.3	17.9	1077.3	17.9	101.2
-WYN17-2 Spot 301	132	53106	1.3	13.2556	1.0	1.8648	1.9	0.1794	1.6	0.84	1063.5	15.4	1068.7	12.4	1079.4	20.4	1079.4	20.4	98.5
-WYN17-2 Spot 197	236	53823	4.6	13.2393	0.9	1.8673	1.6	0.1794	1.3	0.83	1063.6	13.2	1069.6	10.8	1081.8	18.4	1081.8	18.4	98.3
-WYN17-2 Spot 166	312	2062047	2.1	13.2385	0.9	1.9099	1.6	0.1835	1.3	0.81	1085.8	13.1	1084.5	10.8	1082.0	19.0	1082.0	19.0	100.4
-WYN17-2 Spot 146	525	57750	3.1	13.2384	0.8	1.7501	1.4	0.1681	1.2	0.81	1001.7	10.8	1027.2	9.3	1082.0	16.9	1082.0	16.9	92.6
-WYN17-2 Spot 135	210	25501	2.0	13.2357	1.0	1.8385	1.6	0.1766	1.2	0.75	1048.2	11.4	1059.3	10.3	1082.4	20.7	1082.4	20.7	96.8
-WYN17-2 Spot 47	24	8988	7.3	13.2081	1.5	1.8279	2.0	0.1752	1.3	0.67	1040.6	12.6	1055.5	12.9	1086.6	29.2	1086.6	29.2	95.8
-WYN17-2 Spot 26	117	8177	2.4	13.1923	1.1	1.8742	1.6	0.1794	1.2	0.72	1063.7	11.4	1072.0	10.7	1089.0	22.4	1089.0	22.4	97.7
-WYN17-2 Spot 287	269	62188	3.5	13.1792	1.2	1.8442	2.0	0.1764	1.5	0.78	1047.0	14.8	1061.4	13.0	1090.9	24.8	1090.9	24.8	96.0
-WYN17-2 Spot 229	189	50039	1.5	13.1725	1.0	1.9002	1.6	0.1816	1.3	0.80	1075.8	12.9	1081.2	10.8	1092.0	19.6	1092.0	19.6	98.5
-WYN17-2 Spot 188	258	22307	4.1	13.1327	1.3	1.8393	2.0	0.1753	1.6	0.77	1041.1	14.9	1059.6	13.3	1098.0	25.9	1098.0	25.9	94.8
-WYN17-2 Spot 147	119	46478	2.0	13.1002	1.0	2.0210	1.5	0.1921	1.2	0.76	1132.7	12.1	1122.6	10.3	1103.0	19.6	1103.0	19.6	102.7
-WYN17-2 Spot 270	144	242123	1.1	13.0902	1.0	1.8146	1.8	0.1724	1.5	0.83	1025.1	14.3	1050.7	11.9	1104.5	20.2	1104.5	20.2	92.8

-WYN17-2 Spot 99	72	45885	4.2	13.0872	1.1	1.9416	2.0	0.1844	1.6	0.84	1090.8	16.4	1095.6	13.1	1105.0	21.5	1105.0	21.5	98.7
-WYN17-2 Spot 123	181	410666	0.7	13.0519	0.9	2.0378	1.7	0.1930	1.5	0.87	1137.5	15.6	1128.2	11.8	1110.4	17.4	1110.4	17.4	102.4
-WYN17-2 Spot 128	193	20746	1.3	13.0339	1.1	1.9669	1.6	0.1860	1.2	0.74	1099.7	12.0	1104.2	10.8	1113.1	21.5	1113.1	21.5	98.8
-WYN17-2 Spot 298	375	45992	11.1	12.9992	1.0	2.0047	1.9	0.1891	1.6	0.86	1116.4	16.7	1117.1	12.8	1118.5	19.2	1118.5	19.2	99.8
-WYN17-2 Spot 76	321	57877	14.4	12.9928	1.0	2.0432	1.6	0.1926	1.2	0.77	1135.5	12.6	1130.0	10.7	1119.4	20.0	1119.4	20.0	101.4
-WYN17-2 Spot 9	672	128153	1.5	12.9653	0.9	2.1077	1.8	0.1983	1.5	0.87	1166.1	16.3	1151.3	12.1	1123.7	17.1	1123.7	17.1	103.8
-WYN17-2 Spot 168	289	73983	2.8	12.8773	1.2	2.1551	2.2	0.2014	1.8	0.83	1182.6	19.5	1166.7	15.0	1137.2	24.0	1137.2	24.0	104.0
-WYN17-2 Spot 5	1015	2140332	21.5	12.7865	1.0	2.1940	1.9	0.2036	1.6	0.84	1194.4	17.4	1179.2	13.3	1151.3	20.6	1151.3	20.6	103.7
-WYN17-2 Spot 148	305	36875	2.0	12.7391	1.0	2.2056	1.5	0.2039	1.1	0.75	1196.1	11.9	1182.8	10.2	1158.6	19.2	1158.6	19.2	103.2
-WYN17-2 Spot 89	236	103164	2.1	12.7314	1.1	2.1405	2.0	0.1977	1.6	0.82	1163.1	17.2	1162.0	13.7	1159.8	22.8	1159.8	22.8	100.3
-WYN17-2 Spot 43	257	38424	1.5	12.7163	1.1	2.2214	2.1	0.2050	1.8	0.86	1201.9	20.1	1187.8	14.9	1162.2	21.5	1162.2	21.5	103.4
-WYN17-2 Spot 69	363	197868	2.5	12.6329	1.0	1.9418	1.8	0.1780	1.5	0.84	1056.0	14.5	1095.6	11.9	1175.3	19.0	1175.3	19.0	89.9
-WYN17-2 Spot 235	551	77975	14.1	12.6177	0.9	2.1558	1.8	0.1974	1.5	0.86	1161.2	16.5	1166.9	12.5	1177.6	18.1	1177.6	18.1	98.6
-WYN17-2 Spot 180	94	18326	2.4	12.6039	0.9	2.2312	1.6	0.2040	1.3	0.82	1197.0	14.2	1190.9	11.1	1179.8	17.7	1179.8	17.7	101.5
-WYN17-2 Spot 116	215	47897	3.3	12.6028	1.0	2.1368	1.8	0.1954	1.5	0.83	1150.5	16.0	1160.8	12.6	1180.0	20.0	1180.0	20.0	97.5
-WYN17-2 Spot 52	825	194701	2.0	12.5789	0.7	2.2291	1.5	0.2034	1.3	0.88	1193.8	14.4	1190.2	10.5	1183.7	14.2	1183.7	14.2	100.9
-WYN17-2 Spot 239	250	57280	1.9	12.5780	1.1	2.2579	1.8	0.2061	1.4	0.78	1207.8	15.1	1199.3	12.4	1183.9	21.8	1183.9	21.8	102.0
-WYN17-2 Spot 71	113	32761	2.3	12.5507	1.0	2.1832	1.4	0.1988	1.1	0.74	1169.0	11.4	1175.7	10.0	1188.1	19.1	1188.1	19.1	98.4
-WYN17-2 Spot 122	257	19216	1.8	12.5236	0.8	2.2622	1.5	0.2056	1.2	0.84	1205.2	13.5	1200.6	10.3	1192.4	15.9	1192.4	15.9	101.1
-WYN17-2 Spot 152	336	63588	7.6	12.4973	1.0	2.3070	1.8	0.2092	1.5	0.84	1224.5	17.1	1214.4	13.0	1196.5	19.7	1196.5	19.7	102.3
-WYN17-2 Spot 165	106	250954	2.7	12.3794	1.2	2.2470	1.8	0.2018	1.3	0.75	1185.2	14.3	1195.9	12.3	1215.2	22.8	1215.2	22.8	97.5
-WYN17-2 Spot 144	85	9694	1.9	12.3122	1.0	2.4441	2.1	0.2183	1.8	0.87	1273.1	21.3	1255.7	15.3	1225.9	20.5	1225.9	20.5	103.9
-WYN17-2 Spot 214	123	22268	2.1	12.2836	0.9	2.2906	1.6	0.2042	1.2	0.80	1197.6	13.5	1209.4	11.0	1230.5	18.4	1230.5	18.4	97.3
-WYN17-2 Spot 202	164	117572	1.6	11.3992	0.9	2.5408	1.7	0.2101	1.4	0.83	1229.6	15.4	1283.8	12.1	1375.6	17.9	1375.6	17.9	89.4
-WYN17-2 Spot 174	237	48737	1.7	11.3574	1.0	2.9206	1.6	0.2407	1.2	0.78	1390.2	15.3	1387.3	11.9	1382.7	19.1	1382.7	19.1	100.5
-WYN17-2 Spot 112	102	11691	1.7	11.2641	1.0	2.9480	1.7	0.2409	1.3	0.78	1391.6	16.2	1394.3	12.6	1398.5	20.0	1398.5	20.0	99.5
-WYN17-2 Spot 217	377	14385	3.2	11.1950	2.2	2.4192	2.6	0.1965	1.4	0.54	1156.5	14.8	1248.3	18.7	1410.3	42.0	1410.3	42.0	82.0
-WYN17-2 Spot 1	154	30311	2.4	11.1826	0.9	3.0629	1.5	0.2485	1.2	0.79	1430.8	15.8	1423.5	11.9	1412.4	18.1	1412.4	18.1	101.3
-WYN17-2 Spot 251	194	45941	1.5	11.0848	1.1	2.9404	1.8	0.2365	1.4	0.80	1368.5	17.6	1392.4	13.5	1429.2	20.2	1429.2	20.2	95.7
-WYN17-2 Spot 101	137	91261	1.6	11.0403	1.1	3.0898	1.7	0.2475	1.3	0.75	1425.6	16.2	1430.2	12.9	1436.9	21.1	1436.9	21.1	99.2

-WYN17-2 Spot 106	279	60274	1.2	10.8872	1.1	3.1915	1.7	0.2521	1.3	0.78	1449.4	17.2	1455.1	13.1	1463.5	20.0	1463.5	20.0	99.0
-WYN17-2 Spot 4	116	42176	0.8	10.8277	0.9	3.2898	1.4	0.2585	1.1	0.78	1481.9	14.4	1478.6	10.8	1473.9	16.3	1473.9	16.3	100.5
-WYN17-2 Spot 281	64	94664	2.4	10.7166	1.0	3.2707	2.0	0.2543	1.7	0.87	1460.7	22.5	1474.1	15.4	1493.4	18.5	1493.4	18.5	97.8
-WYN17-2 Spot 203	92	61089	2.5	10.6398	1.1	3.3262	1.9	0.2568	1.6	0.84	1473.4	21.5	1487.2	15.2	1507.0	20.0	1507.0	20.0	97.8
-WYN17-2 Spot 155	185	27442	3.3	10.6352	1.1	3.5271	1.9	0.2722	1.6	0.81	1551.8	21.4	1533.3	15.1	1507.8	21.2	1507.8	21.2	102.9
-WYN17-2 Spot 243	120	61704	1.7	10.5946	1.0	3.3242	1.8	0.2555	1.5	0.84	1467.0	19.3	1486.8	13.8	1515.1	18.3	1515.1	18.3	96.8
-WYN17-2 Spot 137	379	84310	1.1	10.4773	1.1	3.6970	1.7	0.2811	1.2	0.73	1596.7	17.3	1570.7	13.3	1536.0	21.3	1536.0	21.3	103.9
-WYN17-2 Spot 275	115	34185	3.0	10.4337	0.9	3.4058	1.7	0.2578	1.4	0.85	1478.8	18.7	1505.7	13.1	1543.9	16.8	1543.9	16.8	95.8
-WYN17-2 Spot 113	108	293866	2.3	10.3258	1.0	3.6558	1.9	0.2739	1.6	0.85	1560.6	21.9	1561.8	14.8	1563.4	18.3	1563.4	18.3	99.8
-WYN17-2 Spot 276	254	98744	1.1	10.2918	1.1	3.6715	1.8	0.2742	1.4	0.78	1561.9	19.0	1565.2	14.0	1569.6	20.5	1569.6	20.5	99.5
-WYN17-2 Spot 140	399	69420	2.3	10.1324	0.8	3.5201	1.8	0.2588	1.6	0.90	1483.7	21.3	1531.7	14.0	1598.8	14.2	1598.8	14.2	92.8
-WYN17-2 Spot 206	272	533450	1.8	10.0878	0.8	3.8468	1.4	0.2816	1.1	0.81	1599.3	16.1	1602.6	11.3	1607.0	15.2	1607.0	15.2	99.5
-WYN17-2 Spot 187	141	50186	1.1	10.0401	1.1	3.7420	1.9	0.2726	1.5	0.80	1554.0	20.6	1580.4	14.9	1615.8	20.6	1615.8	20.6	96.2
-WYN17-2 Spot 134	72	36497	1.3	10.0230	0.9	3.8804	1.5	0.2822	1.1	0.77	1602.4	16.3	1609.6	12.0	1619.0	17.5	1619.0	17.5	99.0
-WYN17-2 Spot 279	115	853986	2.3	9.9765	1.2	3.8967	2.0	0.2821	1.6	0.81	1601.8	23.4	1613.0	16.4	1627.6	22.1	1627.6	22.1	98.4
-WYN17-2 Spot 65	99	57158	10.8	9.9693	1.2	3.8685	1.8	0.2798	1.3	0.76	1590.5	19.0	1607.1	14.4	1629.0	21.6	1629.0	21.6	97.6
-WYN17-2 Spot 246	254	46495	1.3	9.8671	1.3	4.1603	2.1	0.2979	1.7	0.80	1680.7	24.9	1666.2	17.2	1648.1	23.2	1648.1	23.2	102.0
-WYN17-2 Spot 98	405	204110	4.6	9.7704	1.0	4.2814	1.5	0.3035	1.2	0.76	1708.8	17.3	1689.8	12.4	1666.3	18.1	1666.3	18.1	102.5
-WYN17-2 Spot 153	236	37620	2.6	9.7568	0.9	4.3399	1.7	0.3072	1.5	0.86	1727.1	22.0	1701.0	14.0	1668.9	16.0	1668.9	16.0	103.5
-WYN17-2 Spot 198	74	47976	1.8	9.7024	0.9	4.1489	1.8	0.2921	1.6	0.87	1651.9	22.8	1664.0	14.7	1679.3	16.4	1679.3	16.4	98.4
-WYN17-2 Spot 226	415	72632	1.7	9.6798	1.1	4.3088	1.9	0.3026	1.5	0.79	1704.3	22.5	1695.0	15.6	1683.6	21.2	1683.6	21.2	101.2
-WYN17-2 Spot 132	274	637645	2.8	9.6628	1.1	4.3510	1.4	0.3051	0.9	0.63	1716.3	13.1	1703.1	11.3	1686.8	19.6	1686.8	19.6	101.8
-WYN17-2 Spot 37	297	94978	5.1	9.6588	0.8	4.1171	1.7	0.2885	1.5	0.88	1634.2	21.1	1657.7	13.5	1687.6	14.3	1687.6	14.3	96.8
-WYN17-2 Spot 127	882	264662	8.5	9.6526	0.9	4.1960	1.6	0.2939	1.4	0.85	1660.9	20.4	1673.2	13.5	1688.8	16.1	1688.8	16.1	98.3
-WYN17-2 Spot 6	312	986671	2.2	9.6237	1.0	4.3021	2.0	0.3004	1.7	0.86	1693.3	25.4	1693.8	16.4	1694.3	19.0	1694.3	19.0	99.9
-WYN17-2 Spot 221	272	58519	2.9	9.6115	0.9	4.3948	1.8	0.3065	1.6	0.88	1723.4	23.9	1711.4	14.9	1696.6	15.7	1696.6	15.7	101.6
-WYN17-2 Spot 138	260	38753	5.1	9.6094	0.8	4.3663	1.7	0.3044	1.5	0.88	1713.3	23.1	1706.0	14.4	1697.0	15.1	1697.0	15.1	101.0
-WYN17-2 Spot 236	380	492268	3.0	9.5918	1.2	4.3179	1.8	0.3005	1.3	0.74	1693.8	19.9	1696.8	14.8	1700.4	22.3	1700.4	22.3	99.6
-WYN17-2 Spot 35	254	154794	2.4	9.5280	1.0	4.1562	1.8	0.2873	1.5	0.84	1628.2	21.4	1665.4	14.5	1712.7	17.7	1712.7	17.7	95.1
-WYN17-2 Spot 245	265	51042	2.1	9.5029	1.0	4.5246	1.5	0.3120	1.1	0.76	1750.4	17.5	1735.5	12.6	1717.5	18.2	1717.5	18.2	101.9
-WYN17-2 Spot 261	347	99279	2.2	9.4691	1.2	4.4734	2.0	0.3074	1.7	0.82	1727.7	25.5	1726.0	17.0	1724.1	21.3	1724.1	21.3	100.2
-WYN17-2 Spot 53	164	323109	2.1	9.4535	1.0	4.3434	1.6	0.2979	1.3	0.82	1681.0	19.9	1701.6	13.6	1727.1	17.5	1727.1	17.5	97.3
-WYN17-2 Spot 231	86	43250	3.9	9.4225	1.2	4.4520	2.1	0.3044	1.7	0.81	1713.0	25.8	1722.1	17.6	1733.1	22.8	1733.1	22.8	98.8

-WYN17-2 Spot 39	388	2252817	3.4	9.4162	0.9	4.0102	2.0	0.2740	1.7	0.88	1561.0	24.0	1636.3	15.9	1734.4	16.7	1734.4	16.7	90.0
-WYN17-2 Spot 253	354	104499	2.5	9.4057	0.9	4.5812	1.9	0.3127	1.6	0.87	1753.7	25.0	1745.9	15.6	1736.4	16.9	1736.4	16.9	101.0
-WYN17-2 Spot 11	482	287381	6.9	9.3568	0.8	4.7889	1.5	0.3251	1.2	0.84	1814.7	19.8	1783.0	12.5	1746.0	14.9	1746.0	14.9	103.9
-WYN17-2 Spot 83	473	366147	2.5	9.3461	0.8	4.7875	1.5	0.3247	1.3	0.83	1812.4	19.8	1782.7	12.7	1748.1	15.4	1748.1	15.4	103.7
-WYN17-2 Spot 33	187	704251	3.1	9.3104	0.8	4.5960	1.3	0.3105	1.0	0.78	1743.1	16.0	1748.5	11.2	1755.1	15.2	1755.1	15.2	99.3
-WYN17-2 Spot 161	258	143064	4.3	9.2849	0.9	4.8478	1.7	0.3266	1.4	0.83	1821.9	22.1	1793.2	14.1	1760.1	17.2	1760.1	17.2	103.5
-WYN17-2 Spot 136	68	19696	2.0	9.2707	1.2	4.7663	2.2	0.3206	1.8	0.84	1792.7	28.8	1779.0	18.5	1762.9	22.2	1762.9	22.2	101.7
-WYN17-2 Spot 171	356	142047	4.2	9.2543	0.9	4.7016	1.4	0.3157	1.1	0.76	1768.7	16.3	1767.5	11.6	1766.1	16.5	1766.1	16.5	100.1
-WYN17-2 Spot 291	191	2021591	2.4	9.2361	0.8	4.6380	1.6	0.3108	1.4	0.86	1744.8	21.5	1756.1	13.6	1769.7	15.0	1769.7	15.0	98.6
-WYN17-2 Spot 193	411	85781	3.1	9.2298	0.9	4.9482	1.5	0.3314	1.2	0.80	1845.1	19.5	1810.5	12.8	1771.0	16.7	1771.0	16.7	104.2
-WYN17-2 Spot 167	383	114388	2.1	9.2163	1.0	4.8384	1.7	0.3236	1.3	0.80	1807.1	20.9	1791.6	14.0	1773.6	18.2	1773.6	18.2	101.9
-WYN17-2 Spot 269	255	114028	2.8	9.2135	0.9	4.6643	1.7	0.3118	1.4	0.85	1749.6	22.2	1760.9	14.2	1774.2	16.2	1774.2	16.2	98.6
-WYN17-2 Spot 290	115	35935	2.4	9.1857	1.0	4.2503	1.7	0.2833	1.3	0.79	1607.9	19.0	1683.8	13.9	1779.7	18.9	1779.7	18.9	90.3
-WYN17-2 Spot 208	214	43282	2.0	9.1824	0.9	4.7712	1.8	0.3179	1.5	0.84	1779.4	23.2	1779.8	14.8	1780.3	17.2	1780.3	17.2	99.9
-WYN17-2 Spot 272	142	20724	1.7	9.1771	1.0	4.6902	1.7	0.3123	1.4	0.82	1752.1	22.0	1765.5	14.5	1781.4	17.9	1781.4	17.9	98.4
-WYN17-2 Spot 218	225	41682	2.2	9.1693	0.8	4.8467	1.7	0.3225	1.5	0.87	1801.7	23.2	1793.0	14.3	1783.0	15.5	1783.0	15.5	101.1
-WYN17-2 Spot 219	314	459201	2.6	9.1685	0.9	4.9243	1.4	0.3276	1.1	0.77	1826.7	17.5	1806.4	12.1	1783.1	16.7	1783.1	16.7	102.4
-WYN17-2 Spot 227	420	32457591	2.2	9.1657	1.0	4.8762	1.8	0.3243	1.5	0.83	1810.7	23.5	1798.2	15.0	1783.7	18.0	1783.7	18.0	101.5
-WYN17-2 Spot 192	166	29259	2.1	9.1632	0.9	4.8403	1.4	0.3218	1.1	0.77	1798.6	17.4	1791.9	12.1	1784.2	16.7	1784.2	16.7	100.8
-WYN17-2 Spot 311	128	147855	2.2	9.1603	1.1	4.9505	1.9	0.3290	1.5	0.81	1833.7	24.6	1810.9	16.0	1784.7	20.0	1784.7	20.0	102.7
-WYN17-2 Spot 109	156	49368	2.8	9.1561	1.0	4.8391	1.7	0.3215	1.4	0.82	1797.0	22.2	1791.7	14.5	1785.6	17.7	1785.6	17.7	100.6
-WYN17-2 Spot 29	177	47956	1.5	9.1499	1.0	4.7303	1.5	0.3140	1.2	0.77	1760.6	18.1	1772.6	12.9	1786.8	18.0	1786.8	18.0	98.5
-WYN17-2 Spot 54	353	351380	2.3	9.1333	0.9	4.9616	1.7	0.3288	1.5	0.86	1832.6	23.9	1812.8	14.7	1790.1	16.1	1790.1	16.1	102.4
-WYN17-2 Spot 74	228	169646	2.1	9.1282	1.1	4.8727	1.5	0.3227	1.1	0.71	1803.1	17.1	1797.6	12.8	1791.1	19.4	1791.1	19.4	100.7
-WYN17-2 Spot 78	206	149570	2.9	9.1141	0.7	4.8093	1.5	0.3180	1.4	0.88	1780.1	21.2	1786.5	13.0	1794.0	13.1	1794.0	13.1	99.2
-WYN17-2 Spot 102	141	127469	2.1	9.1141	0.9	4.8275	1.6	0.3192	1.3	0.82	1786.0	20.2	1789.7	13.2	1794.0	16.2	1794.0	16.2	99.6
-WYN17-2 Spot 10	131	53015	2.6	9.1074	0.9	4.8344	1.5	0.3195	1.3	0.82	1787.1	19.7	1790.9	13.0	1795.3	16.1	1795.3	16.1	99.5
-WYN17-2 Spot 256	266	75803	6.7	9.1039	1.0	4.7845	2.1	0.3160	1.8	0.89	1770.4	28.5	1782.2	17.4	1796.0	17.5	1796.0	17.5	98.6
-WYN17-2 Spot 23	170	236818	1.9	9.0962	0.9	4.7387	1.5	0.3128	1.2	0.80	1754.2	19.0	1774.1	12.9	1797.5	16.7	1797.5	16.7	97.6
-WYN17-2 Spot 42	282	181701	3.1	9.0894	0.9	4.7962	1.6	0.3163	1.3	0.84	1771.7	20.6	1784.2	13.4	1798.9	15.9	1798.9	15.9	98.5
-WYN17-2 Spot 164	92	51694	2.0	9.0848	1.1	4.7623	1.9	0.3139	1.6	0.82	1760.0	24.2	1778.3	16.1	1799.8	20.1	1799.8	20.1	97.8
-WYN17-2 Spot 268	350	224310	4.4	9.0654	0.9	4.7684	1.8	0.3136	1.6	0.88	1758.6	24.9	1779.3	15.4	1803.7	15.7	1803.7	15.7	97.5
-WYN17-2 Spot 204	250	56137	1.8	9.0572	1.5	4.8195	2.3	0.3167	1.8	0.78	1773.7	28.2	1788.3	19.6	1805.4	26.6	1805.4	26.6	98.2
-WYN17-2 Spot 307	141	64807	1.5	9.0295	1.0	4.7904	1.5	0.3138	1.2	0.76	1759.6	17.9	1783.2	12.8	1810.9	17.9	1810.9	17.9	97.2
-WYN17-2 Spot 77	264	68129	1.4	9.0248	1.3	5.0356	1.9	0.3297	1.4	0.74	1837.2	22.2	1825.3	16.0	1811.9	23.2	1811.9	23.2	101.4

-WYN17-2 Spot 264	162	228053	2.0	9.0248	1.0	4.6947	2.0	0.3074	1.7	0.85	1728.0	25.3	1766.3	16.4	1811.9	18.7	1811.9	18.7	95.4
-WYN17-2 Spot 257	126	76240	3.4	9.0209	1.0	4.8281	2.1	0.3160	1.8	0.87	1770.3	27.8	1789.8	17.4	1812.6	18.6	1812.6	18.6	97.7
-WYN17-2 Spot 15	483	84114	2.4	8.8803	0.8	5.0444	1.9	0.3250	1.6	0.89	1814.3	26.1	1826.8	15.7	1841.1	15.3	1841.1	15.3	98.5
-WYN17-2 Spot 84	332	46285	3.4	8.8794	0.9	5.2098	1.4	0.3357	1.1	0.78	1865.7	18.2	1854.2	12.3	1841.3	16.5	1841.3	16.5	101.3
-WYN17-2 Spot 169	98	22980	2.9	8.8050	1.1	4.6671	1.9	0.2982	1.6	0.82	1682.2	23.3	1761.4	16.0	1856.5	19.6	1856.5	19.6	90.6
-WYN17-2 Spot 299	431	654290	2.4	8.7637	1.2	5.3978	2.0	0.3432	1.6	0.80	1902.2	25.8	1884.5	16.9	1865.0	21.6	1865.0	21.6	102.0
-WYN17-2 Spot 82	151	128577	1.7	8.7072	1.0	5.1046	1.8	0.3225	1.5	0.83	1801.9	23.2	1836.9	15.1	1876.7	17.8	1876.7	17.8	96.0
-WYN17-2 Spot 177	389	105263	4.7	8.5895	0.8	5.3632	1.7	0.3343	1.5	0.87	1859.0	24.0	1879.0	14.6	1901.2	15.2	1901.2	15.2	97.8
-WYN17-2 Spot 297	88	92021	1.7	8.4055	1.0	5.3706	1.7	0.3275	1.4	0.82	1826.5	21.7	1880.2	14.3	1940.0	17.3	1940.0	17.3	94.1
-WYN17-2 Spot 157	298	28875	1.4	8.3273	1.0	5.9696	1.7	0.3607	1.4	0.82	1985.5	23.9	1971.4	14.9	1956.7	17.6	1956.7	17.6	101.5
-WYN17-2 Spot 228	382	183474	4.0	8.1794	1.0	6.1728	2.2	0.3663	1.9	0.89	2012.2	33.4	2000.6	18.9	1988.6	17.2	1988.6	17.2	101.2
-WYN17-2 Spot 274	43	16453	1.1	8.1385	0.9	5.8583	1.7	0.3459	1.5	0.86	1915.2	24.2	1955.1	14.8	1997.6	15.7	1997.6	15.7	95.9
-WYN17-2 Spot 105	272	144768	2.7	8.0284	0.9	6.4270	2.0	0.3744	1.8	0.90	2050.0	32.4	2036.0	18.0	2021.7	15.6	2021.7	15.6	101.4
-WYN17-2 Spot 130	202	73791	2.7	8.0110	0.9	6.2304	1.7	0.3622	1.5	0.84	1992.4	24.9	2008.7	15.2	2025.6	16.7	2025.6	16.7	98.4
-WYN17-2 Spot 254	88	58025	2.6	8.0001	0.9	6.2642	1.6	0.3636	1.3	0.81	1999.3	22.3	2013.5	14.1	2028.0	16.8	2028.0	16.8	98.6
-WYN17-2 Spot 139	160	34849	1.2	7.7725	1.3	6.1451	2.2	0.3466	1.7	0.78	1918.1	28.1	1996.7	18.9	2078.9	23.6	2078.9	23.6	92.3
-WYN17-2 Spot 313	184	51182	1.9	7.5525	0.9	7.2051	1.6	0.3948	1.4	0.85	2145.2	25.4	2137.1	14.7	2129.4	15.4	2129.4	15.4	100.7
-WYN17-2 Spot 172	45	18163	0.6	7.3269	1.1	7.2360	2.0	0.3847	1.6	0.81	2098.1	28.6	2140.9	17.5	2182.3	19.9	2182.3	19.9	96.1
-WYN17-2 Spot 210	647	430386	17.1	7.2142	0.9	7.5378	1.8	0.3946	1.6	0.87	2144.0	29.3	2177.5	16.6	2209.2	15.8	2209.2	15.8	97.0
-WYN17-2 Spot 103	644	189792	11.0	7.1974	0.8	8.3009	1.7	0.4335	1.4	0.86	2321.5	27.8	2264.4	15.0	2213.3	14.7	2213.3	14.7	104.9
-WYN17-2 Spot 49	175	23420	1.6	7.0614	1.1	7.9897	1.8	0.4094	1.4	0.80	2212.0	26.7	2229.9	16.1	2246.3	18.5	2246.3	18.5	98.5
-WYN17-2 Spot 142	260	74379	3.4	7.0364	0.8	8.2389	1.6	0.4206	1.4	0.85	2263.3	25.9	2257.6	14.4	2252.4	14.2	2252.4	14.2	100.5
-WYN17-2 Spot 186	69	26854	1.3	7.0320	1.1	8.0967	1.9	0.4131	1.5	0.81	2229.2	28.8	2241.9	17.0	2253.5	19.0	2253.5	19.0	98.9
-WYN17-2 Spot 199	232	287553	5.8	7.0019	1.1	8.1870	1.8	0.4159	1.4	0.78	2242.0	25.9	2251.9	16.0	2260.9	19.2	2260.9	19.2	99.2
-WYN17-2 Spot 3	236	38355	2.1	6.9855	1.0	8.5875	1.6	0.4353	1.2	0.78	2329.4	24.4	2295.2	14.6	2264.9	17.3	2264.9	17.3	102.8
-WYN17-2 Spot 182	182	65773	2.9	6.9379	0.8	8.1284	1.6	0.4092	1.4	0.86	2211.2	25.5	2245.4	14.3	2276.7	14.0	2276.7	14.0	97.1
-WYN17-2 Spot 295	44	83477	0.9	6.9365	1.3	8.1272	2.1	0.4090	1.6	0.77	2210.5	29.9	2245.3	18.7	2277.1	22.7	2277.1	22.7	97.1
-WYN17-2 Spot 45	106	57560	0.4	6.8218	0.9	8.2951	1.7	0.4106	1.5	0.85	2217.6	27.2	2263.8	15.5	2305.8	15.5	2305.8	15.5	96.2
-WYN17-2 Spot 238	662	52504	3.1	6.7976	0.8	8.0854	1.7	0.3988	1.5	0.88	2163.5	27.8	2240.6	15.6	2311.9	14.2	2311.9	14.2	93.6
-WYN17-2 Spot 312	400	30497	3.6	6.4535	0.9	9.7318	1.7	0.4557	1.4	0.85	2420.6	28.4	2409.7	15.3	2400.6	14.9	2400.6	14.9	100.8
-WYN17-2 Spot 237	146	55078	1.6	6.2659	1.0	10.4537	2.0	0.4753	1.7	0.87	2506.7	36.0	2475.8	18.5	2450.6	16.7	2450.6	16.7	102.3
-WYN17-2 Spot 280	267	433187	1.6	6.2469	1.0	10.4119	2.0	0.4719	1.7	0.86	2492.0	34.8	2472.1	18.1	2455.7	16.8	2455.7	16.8	101.5
-WYN17-2 Spot 283	121	120145	2.1	6.1568	1.2	10.8690	1.9	0.4856	1.5	0.80	2551.4	32.6	2512.0	18.0	2480.3	19.6	2480.3	19.6	102.9
-WYN17-2 Spot 304	145	147785	1.4	5.9196	0.8	9.4160	2.5	0.4044	2.3	0.95	2189.4	43.5	2379.4	22.6	2546.3	12.8	2546.3	12.8	86.0

-WYN17-2 Spot 111	354	33531	0.9	5.3768	1.0	13.2128	1.6	0.5155	1.3	0.77	2679.9	27.5	2695.0	15.3	2706.3	16.9	2706.3	16.9	99.0
-WYN17-2 Spot 240	54	2940275	1.5	5.1158	1.0	14.2094	1.9	0.5274	1.6	0.85	2730.7	36.2	2763.8	18.1	2788.0	16.4	2788.0	16.4	97.9
-WYN17-2 Spot 308	152	166929	2.2	5.0990	1.1	14.4634	1.8	0.5351	1.5	0.81	2763.0	33.3	2780.6	17.4	2793.4	17.6	2793.4	17.6	98.9
-WYN17-2 Spot 233	85	67759	2.3	5.0571	0.9	14.3338	1.6	0.5260	1.3	0.82	2724.4	28.4	2772.1	14.8	2806.9	14.7	2806.9	14.7	97.1
-WYN17-2 Spot 184	141	62377	1.6	4.2843	1.1	18.9383	1.6	0.5887	1.2	0.73	2984.3	28.6	3038.7	15.8	3074.9	17.8	3074.9	17.8	97.1
-WYN17-2 Spot 310	323	3617	4.3	12.7728	1.0	0.7657	2.0	0.0710	1.8	0.86	441.9	7.5	577.3	9.0	1153.4	20.5	441.9	7.5	38.3
-WYN17-2 Spot 129	237	13264	131.7	17.5676	1.3	0.7196	2.0	0.0917	1.5	0.74	565.7	7.9	550.4	8.4	487.6	29.7	565.7	7.9	116.0
-WYN17-2 Spot 17	55	2804	2.0	18.1164	1.6	0.6721	2.0	0.0883	1.3	0.62	545.7	6.6	522.0	8.2	419.3	35.2	545.7	6.6	130.2
-WYN17-2 Spot 73	7	788	37573.6	22.2480	12.5	0.5684	12.7	0.0918	1.8	0.15	566.0	10.0	457.0	46.7	NA	NA	566.0	10.0	123.8

CURRICULUM VITAE

PERSONAL INFORMATION

Libby R.W. Ives
Ph.D. Candidate

University of Wisconsin - Milwaukee
Department of Geosciences
P.O. Box 413
Milwaukee, WI 53201

EDUCATION

2021 **Ph.D.** Geosciences **University of Wisconsin – Milwaukee**

- **Dissertation**: South Polar View of Late Paleozoic Glaciation: Physical Sedimentology and Provenance of Glacial Successions in the Tasmanian and Transantarctic Basins
- **Adviser:** John L. Isbell

2016 **M.S.** Geology **Iowa State University**

- **Thesis:** Magnetic mineralogy and fabrics of small-scale glacial flutes, Múlajökull and Breiðamerkurjökull, Iceland
- **Advisers:** Neal R. Iverson and Thomas S. Hooyer

2013 **B.S.** Earth Science **Northern Michigan University**
minor: History *summa cum laude*

- **Senior Project:** Paleogeographic interpretation of the late Cambrian Groveland Mine stratigraphy, Dickinson County, Michigan.
- **Adviser:** Robert R. Regis

Additional Training

2020 – 2022	Graduate Certificate	Earth Data Analytics	UC-Boulder
2021	Geology Short Course	High-Resolution X-ray CT Facility	UT-Austin
2020	Workshop	Geo. Image Processing w/ Python	Nord. Sed. Res. Gp.
2020	Workshop	Introductory Storytelling	The Story Collider
2020	Short Course	How to Build Coupled Models	GSA Ann. Meeting
2020	Short Course	GeoSci & Soc, Teaching Workshop	GSA Ann. Meeting
2019	Short Course	Glacial Isostatic Adjustment	Gävle, Sweden
2018	Short Course	Summer School of Sedimentology	Neuquén, Argentina
2018	Semester Course	Glacial and Marine Envi. History	UNIS, Svalbard
2017	Short Course	U-Pb Geochronology	GSA Ann. Meeting
2014	Semester Course	Geology Field Camp	Black Hills, USA
2012	Short Course	Volcanology Field Camp	Kamchatka, Russia

ACADEMIC APPOINTMENTS

2019 – 2020	Distinguished Dissertator Fellow	Geosciences	UW – Milwaukee
2018 – 2019	Distinguished Graduate Fellow	Geosciences	UW – Milwaukee
2017 – 2018	Graduate Research Assistant	Geosciences	UW – Milwaukee
2015 – 2016	Graduate Research Assistant	Geology	Iowa State Univ.
2015	Graduate Teaching Assistant	Geology	Iowa State Univ.
2014 – 2014	Graduate Research Assistant	Geosciences	UW – Milwaukee

RELEVANT WORK EXPERIENCE

2021 – present	Student Trainee (Geology)	United States Geological Survey
2018 – 2020	Student/Project Geologist	Wisconsin Geological and Nat. History Survey
2020	Hydrologic and Soils Technician	United States Forest Service

TEACHING EXPERIENCE

Instructor of Record

2020 Stratigraphy and Sedimentology (Geo Sci 511) — UW – Milwaukee
4 cr. Lec/Lab, 23 students

Teaching Assistant

2015 Surficial Processes (GEOL 479) — Iowa State University
3 cr. Lec/Lab, 25 students

Mentoring and Supervision

2014 Miles Harbury and Emily Joynt, University of Wisconsin – Milwaukee
Undergraduate field and lab assistants for research on magnetic sedimentary fabrics in Icelandic glacial tills

PUBLICATIONS

Accepted

Ives, L.R.W. and Rawling, J.E. (in press) Pleistocene Geologic Map of Jefferson County, Wisconsin, 1:100,000. Wisconsin Geological and Natural History Survey.

Isbell, J.L.; Vesely, F.F.; Rosa, E.L.M; Pauls, K.N.; Fedorchuk, N.D.; Ives, L.R.W.; McNall, N.B., Litwin, S.A.; Borucki, M.K.; Malone, J.E.l Kusick, A.R. (2021) Evaluation of physical and chemical proxies used to interpret past glaciations with a focus on the late Paleozoic Ice Age. Earth Science Reviews, 103756. https://doi.org/10.1016/j.earscirev.2021.103756

Ives, L.R.W. and J.L. Isbell. (2021) A lithofacies analysis of a South Polar glaciation in the early Permian: Pagoda Formation, Shackleton Glacier region, Antarctica. Journal of Sedimentary Research, 91(6), 611-635. https://doi.org/10.2110/jsr.2021.004

Ives, L. R. W. and Iverson, N. R. (2019). Genesis of glacial flutes inferred from observations at Múlajökull, Iceland. GEOLOGY, 47(5), 387-390. https://doi.org/10.1130/G45714.1

In Prep

Ives, L.R.W., Isbell, J.L., and Licht, K.J. A "local first" approach to glacigenic sediment provenance demonstrated using U-Pb detrital zircon geochronology.

Ives, L.R.W. and J.L. Isbell. Contrasting styles of glacial sedimentation and glacier thermal regimes in the lower Wynyard Formation (Permo-Carboniferous, Tasmanian Basin)

GRANTS AND AWARDS

Fellowships

2019 – 2020	P.E.O. Scholar Award	P.E.O.	$ 15,000
2019 – 2020	Distinguished Dissertator Fellow	UW – Milwaukee	$ 16,500
2018 – 2019	Distinguished Graduate Fellow	UW – Milwaukee	$ 15,000
2015	U.S. Student Visiting Fellow	IRM	$ 500
2010 – 2013	Presidential Harden Scholar	NMU	Full-tuition

Grants

2020	Travel Award, SEPM 2020	NSF-ISGC-SEPM	$ 1,700
2020	Travel Award	SEPM	$ 300

GRANTS AND AWARDS, cont'd

2019	Travel Grant, GIA Training School	POLENET/NSF	$ 1,500
2019	Graduate School Conference Travel	UW – Milwaukee	$ 1,000
2019	Department Travel Award	UW – Milwaukee	$ 200
2018	Bighorn Basin Field Award	ExxonMobil/GSA	declined
2018	Summer School Travel Grant	IAS	$ 570
2018	A.L. Medlin Research Scholarship	GSA Energy Division	$ 1,500
2018	Research Grant	WI Geological Society	$ 400
2018	Graduate Student Grant	GSA	$ 1,900
2018	Tinker Research Grant	UWM CLACS	$ 4,750
2018	Student Travel Grant	North-Central GSA	$ 125
2014	Graduate Student Grant	GSA	$ 1,500
2011	Spooner Student Research Grant	NMU	$ 500

Scholarships

2020 – 2021	Chancellor's Scholarship	UW-Milwaukee	$ 1, 200
2019 – 2020	Chancellor's Scholarship	UW-Milwaukee	$ 1, 200
2018 – 2019	Chancellor's Scholarship	UW-Milwaukee	$ 1, 200
2018	Lukowicz Memorial Scholarship	UW-Milwaukee	
2018	American Federation of Mineralogical Soc.	--	$ 4,000
2018	Wisconsin Geological Society	--	$ 500
2017 - 2018	Chancellor's Scholarship	UW-Milwaukee	$ 1, 200
2014	Nelson Memorial Field Camp Scholarship	UW-Milwaukee	
2014	Graduate Field Work Scholarship	WI Geo Soc	
2013 – 2014	Chancellor's Scholarship	UW-Milwaukee	
2011 – 2013	Earth Science Award	Ishpeming R&M Club	

Awards

2013	Outstanding Graduating Senior	Northern Michigan University
2012	Volunteer of the Month (March)	Northern Michigan University

CONFERENCE ABSTRACTS

* = presenting author/ ° = postponed or canceled due to COVID

Carson, E.C.*, L.R.W. Ives, K.C. Stolzman, J.E. Rawling III (2021). Glacial lakes in the footprint of the southern Green Bay Lobe of the Laurentide Ice Sheet. GSA Connects 2021.

Carson, E.C.*, L.R.W. Ives, K.C. Stolzman, J.E. Rawling III (2021). Tracking the evolution of glacial lakes Yahara and Scuppernong, south-central Wisconsin, USA. Geological Society of America Annual North-Central and South-Central Joint Section Meeting.

° Ives, L.R.W., J.E. Rawling III, and K.C. Stolzman (2020). Landform assemblages, Quaternary stratigraphy, and preliminary Quaternary geologic map, Jefferson County, Wisconsin. Geological Society of America North-Central Section Meeting, Duluth, Minnesota, USA, May 18 -19, 2020. (cancelled due to COVID-19)

° Ives, L.R.W. and J.L. Isbell (2020). South Polar glaciation and the glacial-to-postglacial transition in the Permian: an example from the Pagoda Formation, Shackleton Glacier Region, Antarctica. International Sedimentary Geosciences Congress, Flagstaff, Arizona, USA, April 26-29, 2020.

Ives, L.R.W. and J.L. Isbell (2019). South Polar Glaciation during the Late Paleozoic: Observations from the Shackleton Glacier Region, Transantarctic Mountains. U.S. Interdisciplinary Antarctic Earth Sciences Meeting and Deep Field Camp Planning Workshop, Julian, California, USA, October 13-16, 2019.

ABSTRACTS, cont'd

Ives, L.R.W.* and N.R. Iverson (2019). Genesis of glacial flutes: a case study from Múlajökull, Iceland. International Symposium on Glacial Erosion and Sedimentation, Madison, Wisconsin, USA, May 12-17, 2019.

Ives, L.R.W.* and J.L. Isbell (2019). Preliminary sedimentology of the early Permian, glacigenic Pagoda Fm., Mt. Butters, Shackleton Glacier Region, Central Transantartic Mountains, Antarctica. DEEPDUST ICDP Workshop, Norman, Oklahoma, USA, March 6 – 10, 2019.

Isbell, J.L. and L.R.W.Ives* (2018). Antarctica, the heart of it all: a South Polar view of glaciation during the Late Paleozoic Ice Age. American Geophysical Union Fall Meeting, Washington, DC, USA, December 10 – 14, 2018.

Ives, L.R.W.* and J.L. Isbell. (2018). Preliminary sedimentological and stratigraphic analysis of the basal glacigenic Wynyard Formation (Wynyard, Tasmania, Australia). Geological Society of America, North-Central 52nd Annual Meeting, Ames, Iowa, USA, April 16-17, 2018.

Ives, L.R.W.* and J.L. Isbell. (2018). Preliminary sedimentological and stratigraphic analysis of the basal glacigenic Wynyard Formation (Wynyard, Tasmania, Australia). VII Simposio del Paleozoico Superior; Esquel, Chubut, Argentina, March 26-28, 2018.

Ives, L.R.W.*, T.S. Hooyer, N.R. Iverson, A. Schomaker (2014). Measuring fabrics of glacial flutes using anisotropy of magnetic susceptibility, Múlajökull, Iceland. Geological Society of America Annual Meeting, Vancouver, B.C., Canada, October 19-22, 2014. paper # 137-22.

Woodford, L.R.* and R.S. Regis (2013). Paleogeographic interpretation of the late Cambrian Groveland Mine stratigraphy, Dickinson County, Michigan. Geological Society of America North-Central Section, Kalamazoo, MI, USA, May 2-3, 2013. paper # 28-32.

INVITED PRESENTATIONS

2021	Distinguished Lecture	Museum of Discovery & Science, Ft. Lauderdale, FL
2018	Quaternary Group	University of Wisconsin – Madison
2018	Science Lecture Series	Shackleton Glacier Deep Field Camp

SERVICE

2021	Pod Organizer, UW - Milwaukee	URGE: Unlearning Racism in the Geosciences
2017-2020	Sed. Group Meetings Coordinator	University of Wisconsin – Milwaukee
2020	Technical Session Co-Chair	GSA2020
"T46. An Interdisciplinary View of Paleozoic Glaciations and Icehouse Climates: Sedimentology, Paleoclimate, Paleontology, Geochemistry, Geochronology, and Modeling."		
2019	Host, Special Lecture Tour	International Association of Sedimentologists
2018	Student Representative (Geoscience)	UW – Milwaukee Student Association
2018-19	President, Great Lakes Chapter	Association for Women Geoscientists
2011-13	President, Rock and Mineral Club	Northern Michigan University
2012-13	President, Gamma Theta Upsilon	Northern Michigan University
2011-13	Grader and Supervisor	Michigan Science Olympiad

REVIEWER FOR

Geology (1)
Journal of Quaternary Science (1)

FIELD RESEARCH EXPERIENCE

2020	Forest Soil Monitoring Surveys	Michigan, USA
2018-20	Glacial Geology Mapping and Core Collecting	Wisconsin, USA
2018	Sedimentology of Esquel and Valle Chico Fms	Patagonia, Argentina
2018	Sedimentology of Sierra de Tepuel	Patagonia, Argentina
2018-17	Sedimentology of Permian – Triassic strata	Shackleton Glacier, Antarctica

FIELD RESEARCH EXPERIENCE, cont'd	2017	Sedimentology of the Wynyard Fm	Tasmania, Australia
	2017	Sedimentology of Sierra de Tepuel	Patagonia, Argentina
	2014	Glacial geology of Breiðamerkurjökull	Iceland
	2014	Glacial geology of Múlajökull	Iceland
	2014	Glacial geology of Múlajökull	Iceland

OUTREACH AND VOLUNTEERING

In-person

2017 – present	Science Adviser/Character	"Dinosaurs of Antarctica"| Giant Screen Films
2021	Dinosaurs of Antarctica Panel	Clarke Planetarium, Salt Lake City, UT
2021	Dinosaurs of Antarctica Panel	Awesomecon, Washington, DC
2021	Les Cheneaux Geology Field Trip	Aldo Leopold Festival, Cedarville, MI
2021	Invited Lecture	Mackinaw Area Historical Society
2020 – 2021	Voices for Science Fellow	American Geophysical Union
2019 – 2020	Pen pal	Letters to a Pre-Scientist
2020	Science-A-Thon	Earth Science Women's Network
2020	7th Grade Classroom Visit	Learn 6 Campus, North Chicago, IL
2020	1st Grade Classroom Visit	Lake Bluff Elementary, Shorewood, WI
2019	Invited Lecture	P.E.O. Mankato, MN
2019	Invited Lecture	Kettle Moraine Geological Society
2019	Invited Lecture	Wisconsin Geological Society
2016	Mapping Ecological Communities	Little Traverse Conservancy
2014	Science Bag Assistant	University of Wisconsin – Milwaukee
2011- 2012	Assistant Coach, LEGO Robotics	Bothwell Middle School, Marquette, MI

Written

Ives, L.R.W. and P. Matheny. "Cryo-Adventures – The Glacial Isostatic Adjustment (GIA) Training School: Personal and Virtual Attendance", EGU Cryospheric Sciences Division Blog, October 4, 2019. LINK